Orthoclase is the second most abundant mineral grain in Cannon Beach sandstones, and averages 13 percent of all grains (Figure 78). The interior of most orthoclase grains is dusky or cloudy, reflecting a moderate to high amount of diagenetic alteration. Untwinned plagioclase is almost as common as orthoclase, averaging 12 percent of all detrital grains, and ranges from fresh to severely altered. Although untwinned plagioclase is usually indicative of a metamorphic terrain, the abundance of volcanic rock fragments and zoned plagioclase in other sedimentary units of the Tillamook embayment suggest that many point counts assigned to the untwinned plagioclase category could be zoned plagioclase grains broken into sizes too small to reveal zoning. Twinned plagioclase is second to untwinned plagioclase in abundance, contributing an average of 7 percent of all detrital grain types. Although most twinned plagioclase grains are albite twinned (Figure 78), rare Carlsbad twins are also present. Most twinned plagioclase grains are extremely altered to clay. The composition of select fresh feldspar grains, estimated using the Michel-Levy method (Kerr, 1979), ranges from An_{12} to An_{34} (oligoclase to andesine). Microcline feldspar is the least abundant feldspar in the Cannon Beach member, comprising only four percent of all grains. Like orthoclase, it has a dusky interior that is moderately to severely altered to clay. The mica group of minerals comprise two percent of detrital grains, and include both biotite and muscovite. Many mica plates are bent and deformed by compaction around other, more rigid framework grains.

The lithic suite of rock fragments includes metamorphic, sedimentary and igneous intrusive constituents and is dominated by mafic volcanic rock fragments, which account for an average of 12 percent of

all detrital grains. Although the presence of silicic volcaniclastic grains is indicated by the occurrence of volcanic chert, mafic volcanic rock fragments are much more abundant, and are typically moderately altered to reddish-brown smectitic (?) clays. Extremely altered mafic volcaniclastic fragments also occur, however, as distorted smectitic (?) and chloritic masses which have deformed to form pseudomatrix (Dickinson, 1970). Relatively fresh grains reveal that the mafic volcanic rock fragments are aphyric, and possess both intersertal and pilotaxitic flow textures.

Metamorphic rock fragments comprise 5 percent of all detrital grains and include quartzite, schist, and phyllite grains. Sedimentary lithic fragments follow in abundance, contributing only three percent of all detrital grains. The sedimentary lithic suite is dominated by siltstone fragments that have been plastically deformed into pseudomatrix. Because most of the Cannon Beach samples were collected from turbidite sandstone beds, the siltstone grains are probably intrabasinal rip-ups, transported a short distance within a turbidity current. Granitic rock fragments are the least common lithic type, contributing only two percent of all detrital grains and typically occur as intergrowths of quartz and potassium feldspar. Trace amounts of myrmekite were also found in a thin section from locality O-18 (northeast quarter sec. 33, T. 1 S., R. 10 W.).

Heavy Minerals

In order to better compare the sedimentary units of this study to one another and identify the provenances that contributed to the Cannon Beach strata, a detailed heavy mineral analysis was performed on four samples. Visual estimates of non-opaque heavy minerals were made and

compiled in Appendix VII. The results of this analysis reveal that the non-opaque heavy mineral population of the Cannon Beach member, which accounts for less than one percent of detrital grains, is dominated by epidote and garnet-group minerals, each comprising 30 percent of the non-opaque heavy mineral suite (Figure 79). These are followed by mica-group minerals (17 percent), zircon (14 percent), tourmaline-group minerals (five percent), amphibole-group minerals (three percent), orthopyroxenes (two percent), kyanite (one percent), and rutile (one percent).

The epidote-group is dominated by green epidote, which comprises 13 percent of all non-opaque heavy minerals. Clear epidote follows with 9 percent, clinozoisite with 7 percent, and zoisite with two percent. All epidote group minerals are very fresh and free of diagenetic alteration. Euhedral and abraded clear, pink, and red garnets comprise 15, 8, and 7 percent of the non-opaque heavy mineral suite in the Cannon Beach member, repectively. Euhedral and abraided zircon make up 22 percent of the non-opaque heavy mineral population. These rounded and abrasion-resistant grains are significant because they may indicate sediment recycling and derivation from older sedimentary rocks in the provenance.

Both green and brown biotite contribute 8 and 9 percent of the total, respectively (Figure 79). The amphibole-group of minerals in the Cannon Beach heavy mineral suite is dominated by green hornblende, which constitutes only 3 percent of all non-opaque heavy minerals, followed by brown hornblende, tremolite-actinolite, and glaucophane or riebeckite, which are all present in trace amounts. All amphibole-group minerals have characteristic serated or bladed terminations that may reflect

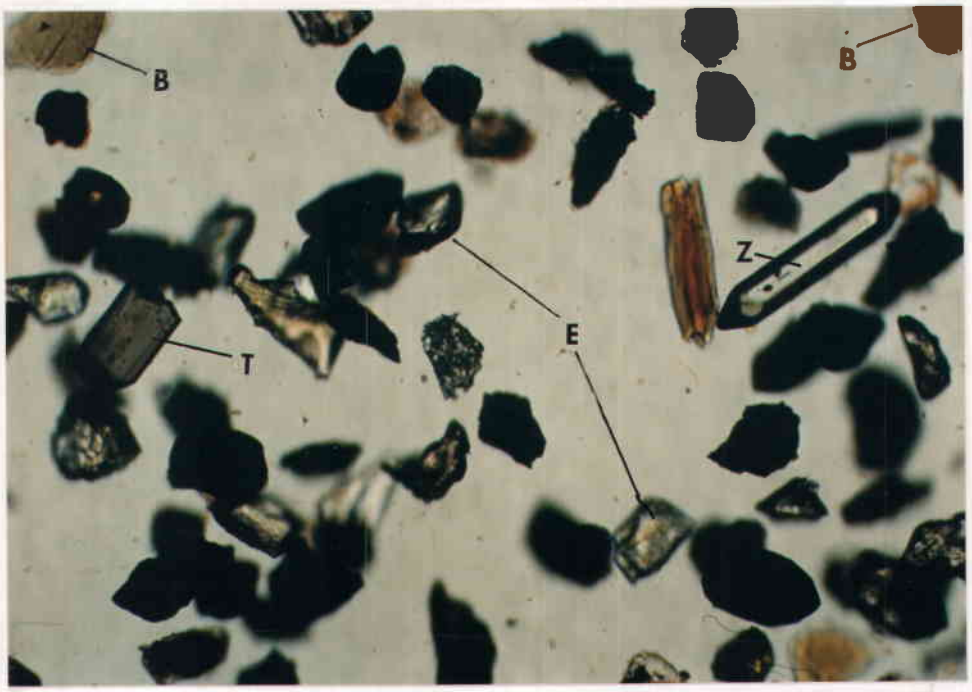

Figure 79. Photomicrograph of heavy minerals from the Cannon Beach member with zircon (Z), tourmaline (T), epidote (E), and biotite (B). Note the absence of hornblende relative to the shallow-marine sandstones of the Tillamook embayment. Field of view is 1.31 mm. Uncrossed nicols.

diagenetic etching along cleavage planes. Tourmaline-group minerals account for two percent of the heavy mineral suite and include euhedral schorlite (two percent) and elbaite (trace). Kyanite and rutile each comprise one percent of non-opaque heavy minerals, and trace amounts of apatite and monazite are also present.

Characteristic Heavy Mineral Assemblage of the Cannon Beach and Netarts Bay Members of the Astoria Formation

The non-opaque heavy mineral suites of the Cannon Beach member and the Netarts Bay member sandstones are very similar to one another but are distinct from the other shallow-marine sandstone units in the study area (Figure 80). The sandstones of these two outer shelf to slope deposits are both relatively enriched in zircon as well as biotite and garnet-group minerals, and impoverished in amphibole-group minerals. Although this pattern is not duplicated elsewhere in the various members of the Astoria Formation (Cooper, 1981), it is quite effective for distinguishing sandstones of the Netarts Bay and Cannon Beach members from the shalow-marine rock units in the thesis area.

It is possible that the distinctive heavy mineral suite of the Netarts Bay and Cannon Beach members may be the product of a change in the provenance. However, both super- and subjacent shelf sandstones (Grande Ronde sandstone interbed and Angora Peak member, Figure 80) have very similar heavy mineral compositions that may indicate that heavy mineral patterns in the Tillamook embayment were environmentally controlled. The deep slope deposits of the Cannon Beach and Netarts Bay members may be relatively enriched in biotite because this mineral was hydrodynamically unstable on the higher energy storm-wave dominated

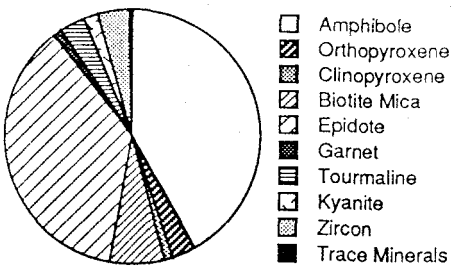

SANDSTONE OF WHALE COVE (4)

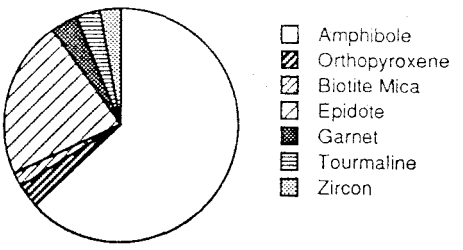

GRAND RONDE SANDSTONE INTERBED (1)

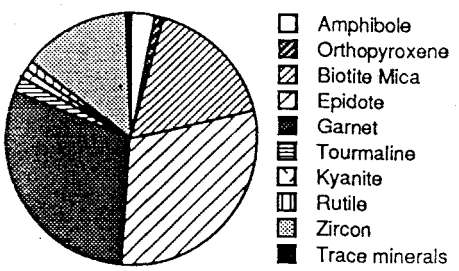

CANNON BEACH TURBIDITE SANDSTONE (4)

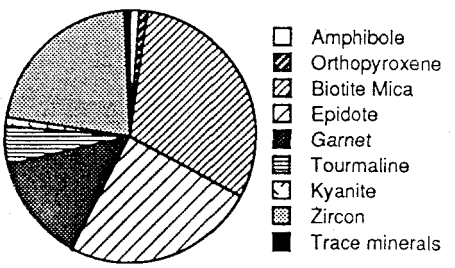

NETARTS BAY MEMBER (3)

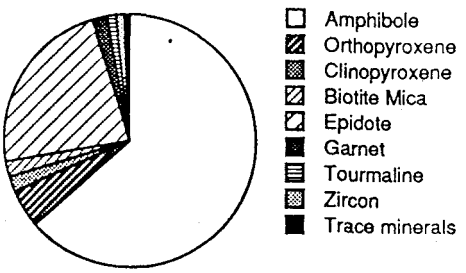

ANGORA PEAK MEMBER (6)

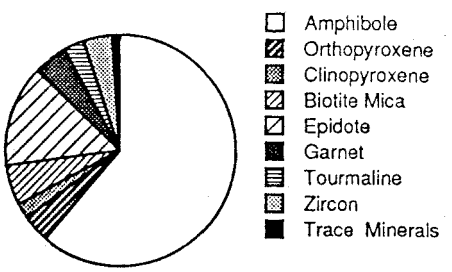

BEWLEY CREEK FM. (6)

Figure 80. Pie diagrams showing relative abundances of heavy minerals (3 and 4 phi) in sandstones of the study area. Diagrams illustrate the contrasting heavy mineral assemblage of the Cannon Beach and Netarts Bay members, which are enriched in garnet, zircon, and biotite relative to shelf sandstone units.

inner and middle shelf. Thus, they may have been preferentially transported to the lower energy outer shelf and slope depositional environment where they could settle. The absence of amphibole minerals from Netarts Bay and Cannon Beach member sandstones may be the result of selective removal of these relatively soft (hardness 6; Berry and Mason, 1959) minerals by previous extensive wave abrasion on a high-energy shelf. Therefore, as a result of removal of most amphiboles, the more resistant zircon and garnet-group minerals are represented in greater abundance in the deeper-marine sandstone deposits which source their sediment from the higher-energy inner shelf.

An alternative hypothesis to explain the unique heavy mineral population of the deeper marine sediments of the Netarts Bay and Cannon Beach members may be that the amphibole minerals were more sensitive to the effects of transgression. During transgression, hornblendes may have been selectively trapped in flooded estuaries and on the widened continental shelf. However, this hypothesis is difficult to reconcile with the increased relative abundance of the denser heavy minerals zircon and garnet in the Netarts Bay and Cannon Beach members.

A third hypothesis to explain heavy mineral differences between the deeper and shallower marine sandstones may be that different heavy mineral populations may characterize different parts of the continental shelf. This may be the product of contrasting sediment transport processes associated with inner shelf littoral drift currents (Kulm et al., 1975), and outer shelf and slope contour currents (Walker, 1984), both of which which may entrain sand with unique heavy mineral populations sourced from different provenances.

A fourth hypothesis is that the distinctive heavy mineral assemblages observed between rock units is the product of chance variations associated with random sampling of sedimentary units (Blatt et al., 1980).

Porosity

Porosity in the Cannon Beach member sandstones averages 12 percent. It occurs predominantly as reduced primary interparticle porosity, with many grains partially to completely coated by clay-rim cement. A late stage hematite cement follows in abundance, and clay coat and chlorite cements are present in only trace amounts. Porosity has also been reduced significantly by pseudomatrix, which is composed of altered volcanic clasts and siltstone fragments. Several thin sections show trace amounts of secondary solution porosity formed by leaching of select feldspar grains. A small amount of intragranular secondary porosity has also been produced through deformation of mica plates and solution of feldspar microlites in volcaniclastic grains.

Compositional and Textural Maturity

Textural and petrographic analyses indicate that sandstones of the Cannon Beach member in the thesis area are moderately to well-sorted (Appendix VI), composed of angular to subrounded grains, and contain moderate amounts of detrital clay matrix. According to the classification system of Folk (1951), these textural characteristics indicate that the Cannon Beach sandstones are texturally submature, suggesting rapid deposition and burial. A textural fabric of aligned micas and normal grading is present in several thin sections, consistent with turbidite sandstone origin.

The high percentage of volcanic, metamorphic, sedimentary, and intrusive igneous lithic fragments in Cannon Beach sandstones indicates that these strata are compositionally immature (Folk, 1951). This suggests that the chemically unstable rock fragments and minerals must have been quickly eroded and deposited under conditions where physical weathering processes were more significant than chemical weathering processes.

Diagenesis and Paragenetic Sequence

Many mineral and lithic grains of the Cannon Beach member sandstones have suffered diagenetic alteration. The grains most severely altered are the mafic volcanic clasts, many of which have been partially to completely altered to reddish-brown smectite (?) clay, or, more rarely, to chlorite clay. Throughout the burial history of the Cannon Beach member sandstones, alteration of iron-rich mafic volcanic grains may have liberated the ions neccessary to form early smectite (?) clay-rim cements and late hematite cement. In addition, heavily altered volcaniclastic grains and siltstone rip-ups were plastically deformed into pseudomatrix as they lost their rigidity during alteration and simultaneous compression with deeper burial. The effects of this deep burial are also reflected in the presence of bent mica flakes, many of which are deformed around brittle and more rigid quartz and feldspar grains.

The cores of most feldspar grains are slightly to moderately altered to clay, and potassium feldspars have suffered slightly greater alteration than plagioclase feldspars. A very small amount of secondary porosity (<1%) has been created in the interiors of select feldspar grains which have been completely dissolved. These relatively brittle

feldspar grains are free of the compaction effects attending burial, which suggests that their cores were dissolved after the unit was compacted or partially cemented.

Paragenetic Sequence

The diagenetic history of Cannon Beach member sandstones was characterized by early alteration of chemically unstable volcaniclastic grains during compaction attending burial. Smectite (?) and chlorite clay-rim cements precipitated as compaction and alteration continued and was accompanied by development of pseudomatrix as altered volcaniclastic and siltstone fragments were squeezed into pore spaces. A small amount of secondary porosity was created during compaction by deformation of mica flakes, some of which parted to create new pore space. After the point of maximum compaction, the cores of select feldspar grains were partially to completely dissolved, creating an extremely small amount of secondary porosity. Late in the diagenetic history, possibly accompanying uplift into the vadose zone, iron in pore fluids was oxidized to form the late telogenetic hematite cement.

The presence of clay-rim cements and pseudomatrix indicates that the depth of burial of the Cannon Beach member in the thesis area was moderate, perhaps ranging from 300 to 1800 meters (Figure 28; Galloway, 1979).

Age and Correlation

The age of the Cannon Beach member in the thesis area is Saucesian, based on Foraminifera collected at locality NNB-6A (northeast quarter sec. 4, T. 2 S., R. 10 W., section 4), and foram samples collected by

Cooper (1981) and Parke Snavely, Jr. of the U.S. Geological Survey (Wells, written communication, 1987; Plate I).

Foraminifera from site NNB-6A were sent to both H. Heitman of Unocal and W. Rau of the Washington State Department of Natural Resources for cross-check and paleontological age analysis. Heitman reported that the assemblage is definately Saucesian, and Rau reported that it was most likely Saucesian, and certainly no older. Age-diagnostic Foraminifera identified in this study include:

Angulogerina astoriensis
Bolvina marginata
Uvigerina obesa impolita
Florilus cf. F. incisum (Cushman)

(Heitman, written communication, 1989; Rau, written communication, 1988)

Although the maximum age of the Saucesian Cannon Beach member is only poorly constrained by the presence of Pillarian stage (lower Saucesian) Vertipecten fucanus (Moore, written communication, 1989) within the underlying Angora Peak member strata (Appendix V), the minimum age of the Cannon Beach member can be constrained by the age of the overlying low magnesium-low titanium R_2 Grouse Creek unit of the middle Miocene Grande Ronde Basalt at locality 4-88 (northwest quarter sec. 28, T. 1 S., R. 10 W.; see Columbia River Basalt section).

The Cannon Beach strata of the thesis area correlate with the Pillarian-Newportian Angora Peak, Youngs Bay and Wicklup Mountain member of the Astoria embayment, and possibly with the Angora Peak member of the Newport embayment (Cooper, 1981; Niem and Niem, 1985).

Depositional Environment

The lower Cannon Beach member of the Astoria Formation was deposited in a slope environment during a trangressive phase. This was marked by a thinning- and fining-upward sequence of interbedded turbidite sandstones and siltstones that culminated in deposition of middle to upper bathyal foram-bearing laminated claystones with rare very thin-bedded turbidite sandstone beds (Rau, written communication, 1989; Heitman, written communication, 1989; Figure 73). A previously undescribed overlying regressive phase is also present in the upper Cannon Beach member of the thesis area, however. It is a coarsening-upward sequence that passes from laminated claystones and rare thin-bedded turbidite sandstones, through a channelized interbedded and amalgamated turbidite sandstone-rich interval, ultimately to a bioturbated and laminated to cross-bedded sandstone section near the upper contact with the Grande Ronde Basalt (Figure 73). This shallowing-upward sequence within the Cannon Beach member is important because it may chronicle uplift within the Tillamook embayment that preceded eruption of columnar jointed and pillowed lava flows of the middle Miocene Grande Ronde Basalt.

The thick carbonaceous, micaceous, hemipelagic siltstone and laminated claystone beds of the Cannon Beach member probably represent deposits of a prodelta-slope environment seaward of an ancestral Columbia River (Balsley, 1982; Figure 12, described in the Smuggler Cove section). This river delivered fine-grained arkosic-lithic sediment to the coast. Suspended material may have been transported to the slope environment of the Cannon Beach member in mid-water column density-stratified turbid layers, capable of bypassing the shelf (Kulm

et al., 1975), or in low density turbidites generated on the shelf by direct discharge of mud-charged rivers (Stowe, 1986). Low density turbidites may also have been generated by resuspension of silt and clay during storm events (Stowe, 1986). The fining-upward sequence in the lower Cannon Beach member, which grades from thick-bedded turbidite sandstone-bearing carbonaceous siltstone to rare thin-bedded turbidite sandstone-bearing noncarbonaceous claystone, may reflect deepening of the basin of deposition, possibly indicative of regional subsidence that coincided with northward migration of the Angora Peak depocenter.

Petrographic analyses indicate that sand within turbidite beds of the Cannon Beach member are similar in composition to Angora Peak sandstones (Appendix V). Textural analyses reveal that the textural characteristics of sandstones from the Cannon Beach member plot among the shelf sandstones of this study on the grain size plots of Kulm et al. (1975) (see textural analysis section). This may indicate that these characteristics were inherited from the shelf environment, and support derivation from reworked inner to middle shelf deposits of the Angora Peak member. These sands were probably delivered to the slope within turbidity currents that passed through submarine canyon heads or channels cut into the shelf.

Depositional Environment of the Lower Cannon Beach Member

The fining- and thinning-upward sequence displayed by turbidite sandstone beds in the lower Cannon Beach member may represent a transition from outer shelf to deeper marine upper to middle bathyal sedimentation. Although it is tempting to place these strata within the depositional environment framework of a submarine fan, channelized slope, or submarine ramp facies context, significant departures from

these established depositional models suggest that the Cannon Beach strata of the thesis area were deposited under somewhat different conditions.

Contrasts to Submarine Fan Model

The sequence of Cannon Beach strata in the study area differs from the classic submarine fan model of Mutti and Ricci-Lucchi (Nilsen, 1978) Normark (1982), and Walker (1982; 1984). The submarine fan transgressive stratigraphic sequence which progresses from the sand-rich channelized inner fan to the sandy unchannelized amalgamated and interbedded turbidite sandstone interval of the supra-fan mid-fan region, is entirely absent from the relatively sandstone-poor Cannon Beach member. Furthermore, the mid-fan region, which is characterized by stacked thickening- and coarsening-upward cycles (Walker, 1984), has no analog in the Cannon Beach strata of the thesis area. Instead, lower Cannon Beach strata are characterized by a rapid facies change from the channelized shelf-slope break deposits of the Netarts Bay member, and the bioturbated shelf sandstones of the upper Angora Peak member, to a siltstone-dominated sequence containing some thick-bedded turbidite sandstone beds which fine and thin upward. Although these sedimentological characteristics are similar to the siltstone-rich lower submarine fan (Walker, 1984), they are entirely out of context if trying to fit Cannon Beach strata into the classic submarine fan depositional model.

The model of a submarine fan predicts that the fan is a deep-marine deposit, typically bathyal to abyssal, tethered to the shelf by a single submarine canyon (Stowe, 1986; Heller and Dickinson, 1985).

Stratigraphic evidence collected from the Cannon Beach member and the underlying Netarts Bay member, however, indicate that sand was supplied to the slope from the shelf by several different channels. In addition, Foraminifera collected from a thick laminated claystone interval, interpreted to reflect the deepest marine deposits of the Cannon Beach member (locality NNB-6A, southwest quarter sec. 4, T.2 S., R. 10 W.; Figure 9A), include both inner shelf and upper to middle bathyal forms (Rau, written communication, 1988; Heitman, written communication, 1989). While the mixed fauna in this sample indicate that turbidites may have been sourced from the inner shelf, the deeper upper to middle bathyal forams suggest a final depositional environment shallower than that predicted for the typical outer fan environment (Stowe, 1986).

Contrasts to the Submarine Ramp and Channelized Slope Model

The submarine ramp facies model of Heller and Dickinson (1985), and adjacent channelized slope and shelf facies model of Dott and Bird (1979), based on the Tyee and Elkton formations in southwestern Oregon, provide a closer, though still somewhat inadequate analog to the depositional setting of the lower Cannon Beach member.

As stated previously, field evidence supports the existence of several feeder channels cut into the shelf and slope that supplied sand to the Cannon Beach member (described in greater detail in the Netarts Bay member depositional environment section). A multiple feeder channel system connecting shelf to slope is a crucial aspect of both submarine ramp and channelized shelf and slope models. However, in contrast to the seacliff exposures in the type area near Cannon Beach which display numerous small sandstone-filled nested channels and thin-bedded

turbidite sandstone interbeds representative of a channelized turbidite slope facies similar to the Elkton formation (Cooper, 1981), no evidence for channelization exists in exposures of the lower Cannon Beach member in the thesis area. Thus, the model of Dott and Bird (1979), which predicts thin-bedded turbidites and lenticular sand bodies reflecting back-filled channels cut into shelf and upper slope, may not be a suitable analog.

The submarine ramp model of Heller and Dickinson (1985) can be applied to the lower Cannon Beach strata in that proximal and distal submarine ramps are supplied by multiple feeder channels, predominantly unchannelized, characterized by tabular turbidite sandstones adjacent to a channelized slope and shelf (represented by the Netarts Bay member deposits), and generally deposited in a relatively shallow-marine environment (lower to upper bathyal, or as shallow as the shelf slope break). However, the submarine ramp model analog for Cannon Beach strata breaks down when details of the characteristics predicted within proximal and distal submarine ramp deposits are compared to lower Cannon Beach sequence.

Both the proximal and distal submarine ramp described by Heller and Dickinson (1985) are much sandier, thicker, and wider-spread deposits than the lower Cannon Beach strata. The proximal ramp ranges from 80 to 90 percent sandstone and the distal ramp ranges from 60 to 80 percent turbidite sandstone. In contrast, the lower and most sandstone-rich part of the Cannon Beach member is less than 10 percent turbidite sandstone. Furthermore, the lower Cannon Beach member, with its thick siltstone interbeds, is more characteristic of distal submarine ramp deposits than proximal ramp deposits. This carries the important implication that the

amalgamated unchannelized turbidite sandstone-rich interval of the proximal ramp, predicted to occur between the channelized slope and deeper distal ramp (Heller and Dickinson, 1985), is absent from the stratigraphic sequence in the lower Cannon Beach strata in the thesis area.

A Depositional Model for the lower Cannon Beach Member

Although the submarine ramp model of Heller and Dickinson (1985) provides a superior analog to the lower Cannon Beach member than the classical submarine fan model, it fails to explain the overwhelmingly fine-grained nature of the Cannon Beach strata. A possible explanation is that the lower Cannon Beach strata represent deposits of a relatively clastic-starved slope environment caused by a subsidence and transgressive event within the Tillamook embayment which may have coincided with a shift of the Angora Peak delta or river-mouth coarse sediment source away from the Tillamook embayment.

Periods of transgression are marked by retention of continental detritus along shorelines in deltas and coastal plain-estuary complexes (Figure 81; Miall, 1985). While shelf aggradation rates during transgression are high, continental slopes tend to be sand-starved (Miall, 1985; Stowe, 1986). Submarine fans, and presumably submarine ramps, do not prograde during these periods because their feeder channel and canyon heads are established well below the depth at which sand can be delivered to them. Thus, the lower Cannon Beach strata may be a record of transgression-induced sand starvation, which could have been further augmented by a shift of the Angora Peak depocenter away from the Tillamook embayment. This shift is documented by paleontologic data

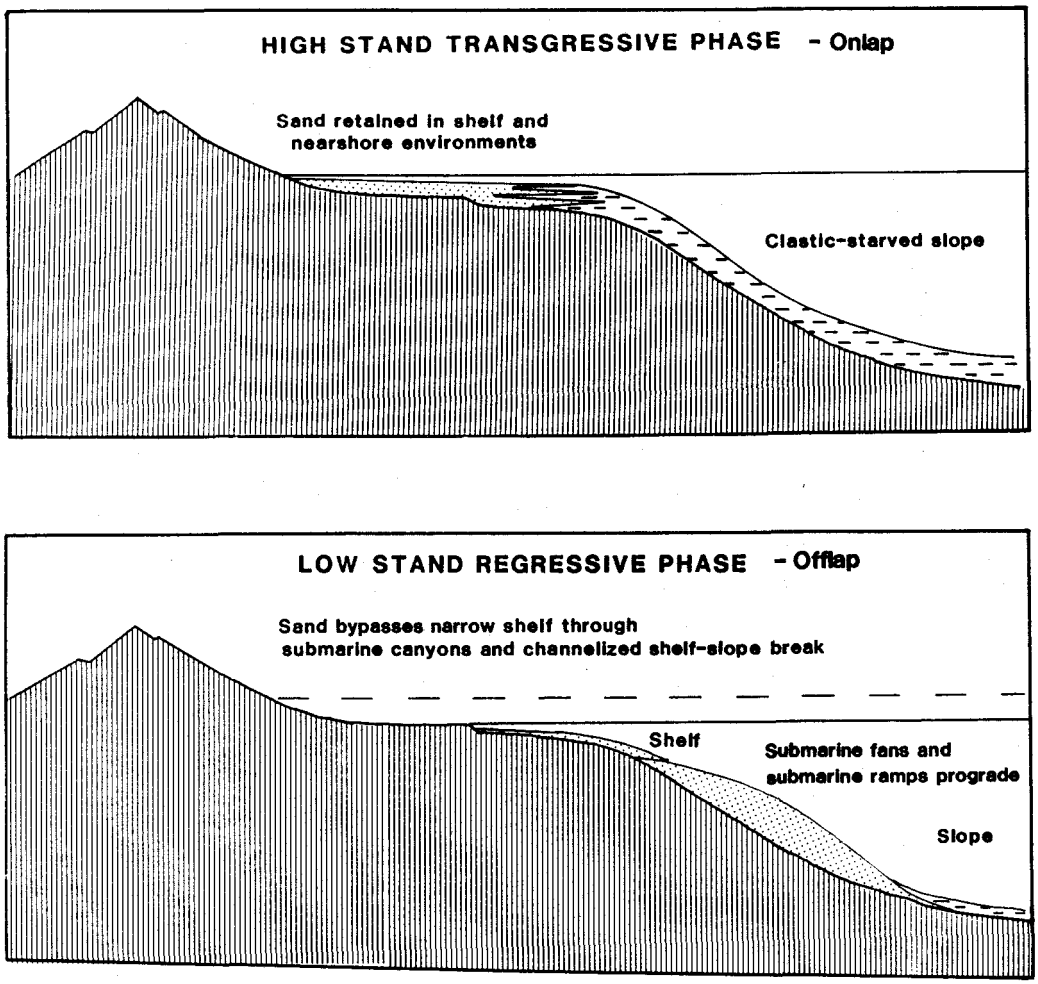

Figure 81. Diagram showing the relationship between shelf and slope sedimentation and changes in sea level. Modified after Miall (1985).

which indicate the presence of younger Angora Peak member delta and shelf deposits in the Astoria embayment to the north. These deposits contain both younger Newportian stage Patinopecten propatulus and older Pillarian stage Vertipecten fucanus (Cooper, 1981; Figure 10), compared to Angora Peak strata in the Tillamook embayment (excluding Cape Kiwanda) which include only the older Pillarian stage Vertipectin fucanus (Moore, personal communication, 1988).

Deprived of the sand required to develop the sand-rich proximal and distal facies of the submarine ramp by transgression and/or removal of a proximal depocenter, lower Cannon Beach strata contain relatively few turbidite sandstone beds, which thin and fine upward reflecting continued subsidence.

Depositional Environment of the Upper Cannon Beach Member

The upper Cannon Beach member of the thesis area is characterized by a coarsening-upward sequence that may represent shallowing of the basin of deposition from its upper to middle bathyal maxima. Laminated claystones with rare very thin-bedded turbidite sandstone interbeds, grade upward to rhythmicly interbedded turbidite sandstones with Bouma T_{c-e} and T_{d-e} sequences, and siltstones with some starved ripple laminae. These strata may have been deposited from relatively dilute overbank turbidity currents adjacent to a submarine channel, or from turbidites generated from outer shelf slumping events initiated by earthquakes or storm events (Stowe, 1986; Walker, 1984). This turbidite sandstone-rich interval is unlike the lower Cannon Beach of the study area which has thick siltstone interbeds, and may reflect marine regression coupled with increased delivery of sand to the slope as the continental shelf narrowed and the strand prograded.

Slightly higher in the section amalgamated turbidite sandstone packages are common, cut by both clastic dikes and rare nested channels (Figure 73). These features suggest further shallowing of the basin of deposition, and attest to rapid deposition in a channelized slope environment that was richly supplied by sand from the shelf (similar to upper Sutton Creek depositional environment in Figure 38). However, some extensively bioturbated sandstone beds are also present in this part of the section. These support a relatively shallow (upper slope to outer shelf) unrestricted marine environment characterized by periods of slow deposition, which allowed homogenization of sediment by infauna (Balsley, 1982).

The amalgamated turbidite and channelized interval in the upper Cannon Beach member is similar to the nested channel facies of the Eocene Elkton formation described by Dott and Bird (1979) and was recognized as such by Cooper (1981). Sea gullies connecting a sand-rich narrow shelf to the slope can form in water from 300 to 30 meters in depth. Sea gully channels are commonly incised or nested into one another and contain large intraclasts and clastic dikes similar to those observed in the upper Cannon Beach strata (Dott and Bird, 1979).

The uppermost Cannon Beach strata near the contact with the Grande Ronde Basalt (e.g. locality O-110, northeast quarter sec. 28, T.1 S, R. 10 W.) is characterized by arkosic-micaceous, carbonaceous, moderately to well-sorted, cross-bedded to parallel laminated and bioturbated sandstones. These deposits may represent shallowing of the basin of deposition to middle or inner shelf depths where bedforms were influenced by fair and storm weather waves.

A burrowed, laminated to cross-bedded, arkosic-micaceous, and partially volcaniclastic-rich sandstone bed exposed along the beach near the town of Cape Meares (locality 90-89, southwest quarter sec. 7, T. 1 S., R. 10 W.) occupies an anomalous stratigraphic position relative to both the Cannon Beach and Angora Peak members. Although it was previously mapped by Cooper (1981) in a sliver of Angora Peak member sandstone faulted into position against Cannon Beach strata (Cooper, 1981), its position at the base of a very large slide in sections 7 and 18 (T. 2 S., R. 10 W.) adds the possibility that this sandstone bed has slid down into its present position (Plate I). In this study the slide block hypothesis is favored. However, although the sandstone may have been derived from the underlying Angora Peak member, the discovery of shelf sandstones at the top of the Cannon Beach member near the contact with the Grande Ronde Basalt indicates that the anomalous sandstone could represent a block of upper Cannon Beach strata calved into this large slide.

Contact Relationships

In the northern part of its outcrop area the Cannon Beach member conformably overlies the Angora Peak member, and in the southern part conformably overlies the Netarts Bay member (Plate I). The contact with the Netarts Bay member is defined by an abrupt facies and lithological change from thick massive sandstones of the submarine canyon head and channelized shelf deposits to the siltstone-dominated lower Cannon Beach member. The contact between these two members is exposed only at one locality (Fiogure 63; locality NNB-38, southwest quarter sec. 10, T. 2 S., R. 10 W.) where medium- to coarse-grained massive sandstone of the

Netarts Bay member bearing large channel wall failure blocks are overlain and draped by laminated siltstones and very thin-bedded sandstones of the Cannon Beach member. Although the lower contact with the Angora Peak member is not exposed in the thesis area, a fining-upward sequence in the upper part of the Angora Peak member suggests that the contact with the Cannon Beach member is conformable and gradational.

The nonconformable upper contact between the Cannon Beach member and the Grande Ronde Basalt is well exposed at low tide at locality 71-88 (northwest quarter sec. 18, T. 1 S., R. 10 W.). In this sea cliff exposure, soft Cannon Beach mudstones have eroded back forming a deep notch at beach level under resistant pillowed high-magnesium N_2 Sentinel Bluff Unit flows of the Grande Ronde Basalt. Outcrop patterns and attitudes of both the Cannon Beach and Grande Ronde Basalt (Plates I and II) indicate that the upper part of the Cannon Beach member was removed by erosion and deeply incised prior to emplacement of the Grande Ronde Basalt flows, which presently fills topographic lows cut in Miocene Cannon Beach, Netarts Bay, and Angora Peak member strata.

COLUMBIA RIVER BASALT GROUP

Introduction

The sedimentary strata of the Tillamook embayment provide a record of the tumultuous geologic history of Oregon during the lower to middle Miocene, which was characterized by active subduction off the coast, and punctuated by episodes of explosive silicic volcanism within the Western Cascade arc (Niem and Niem, 1984). However, during the middle Miocene this dynamic geologic history seemed to rise to a cataclysmic crescendo when 300,000 km^3 of tholeiitic flood basalt of the Columbia River Basalt Group were erupted from large fissure systems in eastern Oregon and Washington (Reidel et al., 1982; Swanson et al., 1979). Over a period of approximately ten million years, basalt lava was episodicly extruded and these flows expanded to cover approximately 200,000 km^2 of Oregon, Washington, and western Idaho (Figure 82; Mangan et al., 1986). The most laterally extensive of the Columbia River Basalt Group flows, which include the Grande Ronde Basalt, Frenchman Springs member of the Wanapum Basalt, and the Pomona member of the Saddle Mountains Basalt, made it to the northwest Oregon and southwest Washington strandline via an ancestral Columbia River drainage system and represent the middle Miocene coastal basalts (Anderson et al., 1987; Beeson, et al., 1979). All three basalt units are exposed in the Astoria embayment (Beeson et al., 1979; Murphy, 1981; Peterson, 1984; Nelson, 1985; Niem and Niem, 1985; Rarey, 1986; Goalen, 1988; Mumford, 1989; Wells and Coe, 1985; Wells and Niem, 1987), and the former two, the Grande Ronde and Frenchman Springs basalts, are present within the Tillamook embayment in

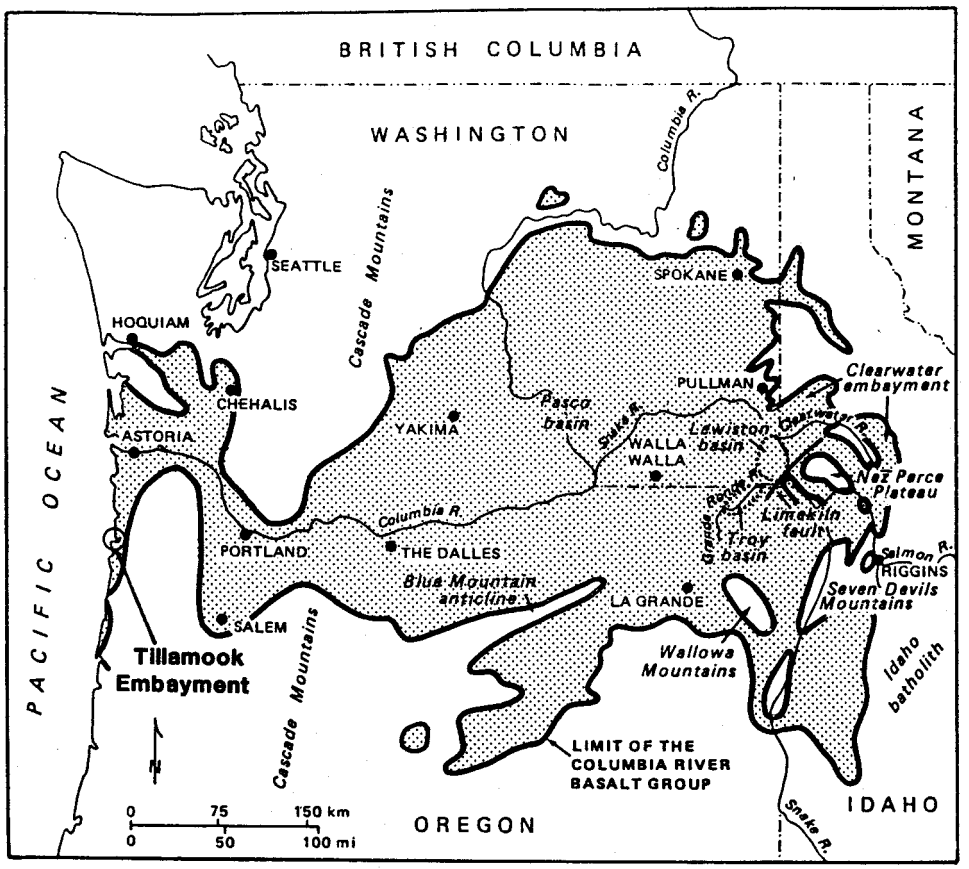

Figure 82. Outcrop area of the Columbia River Basalt Group. Modified from Anderson et al. (1987).

the present study area (Wells, personal communication, 1987; this study).

The section that follows briefly summarizes the nomenclature of the Columbia River Basalt Group, and focuses on the Grande Ronde and Frenchman Springs Basalts in particular. For a detailed discussion of Columbia River Basalt Group flows and intrusives (invasive flows) in the Astoria embayment of northwest Oregon, the reader is referred to Rarey (1986) and Goalen (1988).

Nomenclature

Columbia River Basalt Group

The earliest description of rocks of the Columbia River Basalt Group was made by Russell (1893), who, in 1901, first applied the name "Columbia River Basalt" to all basalts in the Pacific Northwest that were Miocene or older, thus encompasing a suite of rocks that ranged as old as Eocene. This same year, however, Merriam (1901) and Lindgren (1901) took a major step toward clarifying Pacific Northwest stratigraphy when they suggested that the term "Columbia River Basalt" be restricted only to middle to upper Miocene basalt flows. The stratigraphy was refined further when Waters (1961) proposed that only Miocene basalt flows within select parts of northern Oregon, eastern Idaho, and southern Washington be refered to as the Columbia River Basalt.

The contribution of Waters (1961) to refinement of Columbia River Basalt (CRB) stratigraphy was quite significant because he was the first to integrate field evidence, as well as petrographic and geochemical data to delineate groups of flows within the CRBs. These methods allowed

him to break the CRBs into two flow units which he termed the younger "Picture Gorge Basalt" and the older "Yakima Basalt". He also distinguished a post-early Pliocene package of flows, which he refered to as "Late Yakima flows". Building upon Waters' work, Wright et al. (1973) recognized eleven geochemical flow units within the CRBs based on MgO vs. SiO_2 variation diagrams, and further refined CRB stratigraphy by establishing a four unit nomenclature which included (from oldest to youngest) the Picture Gorge Basalt, and the lower, middle, and upper Yakima Basalts.

The stratigraphic framework of Wright et al. (1973) was extensively revised by Swanson et al. (1979) based on a detailed compilation of additional geochemical, field, K-Ar age, and paleomagnetic data collected from the CRBs (Figure 83). As a result of this synthesis, Swanson et al. (1979) elevated the CRBs to group status, and raised the Yakima Basalt to a subgroup level which contained (from oldest to youngest) the Grande Ronde, Wanapum, and Saddle Mountains basalts as formational units (Figure 83). The Picture Gorge Basalt was also raised to formational status and envisioned as contemporaneous with the Grande Ronde Basalt. Another formation, the Imnaha Basalt, was designated as the oldest unit in the CRB Group (Swanson et al., 1979; Figure 83).

Subsequent to its introduction as a formational unit, the Wanapum Basalt was broken into several members which included the Frenchman Springs Basalt member. The Frenchman Springs Basalt is one of the most laterally extensive packages of flows in the CRB group, and its 15,600 km^3 volume covers approximately 179,000 km^2 of Oregon and Washington (Beeson et al., 1985). The name was originally proposed by Mackin in 1961, who found that the Frenchman Springs member could be distinguished

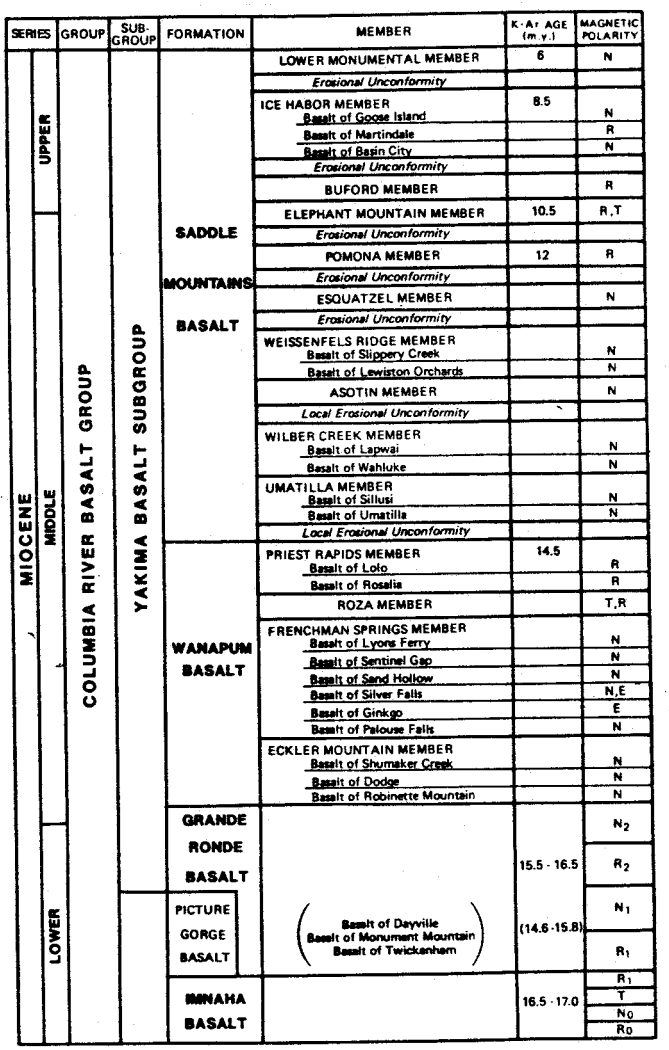

SERIES	GROUP	SUB-GROUP	FORMATION	MEMBER	K-Ar AGE (m.y.)	MAGNETIC POLARITY
MIOCENE UPPER	COLUMBIA RIVER BASALT GROUP	YAKIMA BASALT SUBGROUP	SADDLE MOUNTAINS BASALT	LOWER MONUMENTAL MEMBER	6	N
				Erosional Unconformity		
				ICE HABOR MEMBER	8.5	
				Basalt of Goose Island		N
				Basalt of Martindale		R
				Basalt of Basin City		N
				Erosional Unconformity		
				BUFORD MEMBER		R
				ELEPHANT MOUNTAIN MEMBER	10.5	R,T
				Erosional Unconformity		
				POMONA MEMBER	12	R
				Erosional Unconformity		
				ESQUATZEL MEMBER		N
				Erosional Unconformity		
				WEISSENFELS RIDGE MEMBER		
				Basalt of Slippery Creek		N
				Basalt of Lewiston Orchards		N
				ASOTIN MEMBER		N
				Local Erosional Unconformity		
				WILBER CREEK MEMBER		
				Basalt of Lapwai		N
				Basalt of Wahluke		N
				UMATILLA MEMBER		
				Basalt of Sillusi		N
				Basalt of Umatilla		N
				Local Erosional Unconformity		
MIDDLE			WANAPUM BASALT	PRIEST RAPIDS MEMBER	14.5	
				Basalt of Lolo		R
				Basalt of Rosalia		R
				ROZA MEMBER		T,R
				FRENCHMAN SPRINGS MEMBER		
				Basalt of Lyons Ferry		N
				Basalt of Sentinel Gap		N
				Basalt of Sand Hollow		N
				Basalt of Silver Falls		N,E
				Basalt of Ginkgo		E
				Basalt of Palouse Falls		N
				ECKLER MOUNTAIN MEMBER		
				Basalt of Shumaker Creek		N
				Basalt of Dodge		N
				Basalt of Robinette Mountain		N
LOWER			GRANDE RONDE BASALT		15.5 - 16.5	N_2
						R_2
			PICTURE GORGE BASALT	Basalt of Dayville, Basalt of Monument Mountain, Basalt of Twickenham	(14.6-15.8)	N_1
						R_1
			IMNAHA BASALT		16.5 - 17.0	R_1
						T
						N_0
						R_0

Figure 83. Stratigraphic nomenclature, age, and magnetic polarity for Columbia River Basalt Group. N= normal polarity; R= reversed polarity; T= transitional polarity; E= excursional polarity. From Beeson and Tolan (1985).

from other flows of the CRB group by characteristic stratigraphic position, intraflow structures, and the presence of large plagioclase phenocrysts and glomerocrysts (Beeson et al., 1985). Recently, Beeson et al. (1985) proposed an informal nomenclature for the Frenchman Springs member which includes six units identified by stratigraphic position, aerial extent, and major and trace element composition. These units (from oldest to youngest) include the Palouse Falls Unit, Ginkgo Unit (Tfs on Plate I), Silver Falls Unit, Sand Hollow Unit, Sentinal Gap Unit, and the Lyons Ferry Unit (Beeson et al., 1985; Figure 83; Plate I).

Underlying the Frenchman Springs member of the Wanapum Basalt in the thesis area is the Grande Ronde Basalt (Plate I) which makes up approximately 85% (275,000 km^3) of the entire CRB sequence and covers approximately 200,000 km^2 of Oregon and Washington (Mangan et al., 1986). Although the Grande Ronde Basalt was not broken into individual members during the nomeclatural revisions of Swanson et al. (1979), it was redefined as four magnetostratigraphic sub-units designated R_1, N_1, R_2, N_2 (Figure 83). Some of these magnetostratigraphic subtypes have been recognized in northwest Oregon (e.g. Murphy, 1981; Goalen, 1988; Niem and Niem, 1985; Anderson et al., 1987). In an effort to further refine the stratigraphy of the Grande Ronde Basalt, Mangan et al. (1986) compiled available geochemical data on MgO vs. TiO_2 and MgO vs. P_2O_5 chemical variation diagrams. Their study revealed that the Grande Ronde Basalt is composed of five geochemical subtypes, which could be further sudivided on the basis of the magnetostratigraphy of Swanson et al. (1979). Because cartographic subunits of the Grande Ronde Basalt have been established during the course of recent research efforts, Grande

Ronde nomenclature is presently under revision as select geochemical and magneto-stratigraphic units are being assigned informal unit names (Tolan, personal communication, 1989; Reidel et al., in prep). These informal units are further discussed in the next section.

The Middle Miocene Coastal Basalts of Northwest Oregon and Southwest Washington

The nomenclature and hypothesized origins of the middle Miocene basalts in northwest Oregon and southwest Washington have been the subject of controversy for the past several years. Early work by Warren et al. (1945) and Snavely et al. (1963) revealed some continuity and similar age relationship between the Miocene coastal basalts and the plateau-derived CRBs, however the presence of basalt dikes and sills along the coast lead them to the conclusion that the coastal basalts were erupted from local fissures on the west side of the ancestral Oregon coast range. In 1973, Snavely et al. also recognized coastal basalt sills and dikes with similar chemistry and petrography to associated CRB basalt flows, but concurred with Warren et al.'s interpretation that the coastal basalts were erupted locally. In their paper, Snavely et al. (1973) formalized nomenclature by assigning Miocene coastal basalt units the local names Depoe Bay Basalt, Cape Foulweather Basalt, and Basalt of Packsack Lookout, and pointed out that each unit had a unique geochemical and petrographic signature that could be used to distinguish each from the others. However, they also noted that the chemical and petrographic types of coastal basalts had analogs on the Columbia Plateau that were both the same age and in the same stratigraphic order. Thus, Snavely et al. (1973) recognized the

similarity between Miocene coastal basalt and Columbia Plateau basalt listed below:

Coastal Basalts	Columbia River Basalt Group
Basalt of Packsack Lookout	Pomona member of the Saddle Mountains Basalt
Cape Foulweather Basalt	Frenchman Springs member of the Wanapum Basalt
Depoe Bay Basalt	Grande Ronde Basalt

Recognizing the genetic relationships, but convinced of separate eruptive centers, Snavely et al. (1973) proposed three Plate tectonic scenarios that might account for the presence of the Miocene coastal basalts. For a summary of these the reader is referred to Goalen (1988) and Murphy (1981).

In 1979, Beeson et al. published a controversial hypothesis regarding the origin of the coastal Miocene basalts in western Oregon and Washington that has been the topic of heated debate ever since. They suggested that the coastal Miocene Basalt of Packsack Lookout, Cape Foulweather Basalt, and Depoe Bay Basalt represent distal flows of the Pomona, Wanapum, and Grande Ronde Basalts of the CRB Group, respectively, which flowed overland from fissures on the Columbia Plateau to the sea through low points in the Oregon and Washington coast range. Countering the field evidence for local coastal extrusion cited by Warren et al. (1945) and Snavely et al. (1973, 1980), however, Beeson et al. (1979) proposed that the submarine coastal sills and dikes were not generated from a local magma chamber and injected into Tertiary strata from below. Rather, Beeson et al. (1979) suggested that these basalts were emplaced through the process of autoinvasion, during which overland-flowing dense basalt lava injects downward into less dense unlithified, yielding, water-saturated strata. This provocative

emplacement scenario was modeled after the behavior of small-scale invasion of CRB into central Washington diatomaceous lacustrine sediments, which was first described by Schmincke (1967) and Byerly and Swanson (1978). Since the introduction of Beeson et al.'s (1979) hypotheses, they have been used to explain the occurrence of Miocene CRB flows, dikes, and sills in northwest Oregon and southwest Washington by several workers (e.g. Murphy, 1981; Peterson, 1984; Nelson, 1985; Niem and Niem, 1985; Rarey, 1986; Rarey and Niem, 1986; Wells and Coe, 1985; Wells and Niem, 1987; Goalen, 1988; Mumford, 1989; this study).

Through the extensive magnetostratigraphic and geochemical analyses and field mapping of previous workers in northwest Oregon and southwest Washington (e.g. Murphy, 1981; Peterson, 1984; Nelson, 1985; Niem and Niem, 1985; Rarey, 1986; Mangan et al., 1986; Goalen, 1988; Mumford, 1989; Wells et al., in prep; Wells and Coe, 1985), Grande Ronde, Frenchman Springs, and Pomona basalts of the CRB group have been mapped and described where they were formally designated Miocene submarine basalt units (e.g. Depoe Bay and Cape Foulweather basalts). In addition, these workers also distinguished four subtypes of Grande Ronde Basalt on the basis of their magnetic polarity and geochemical characteristics, which include (in stratigraphic order): magnetically reversed (R_2) low MgO-high TiO_2 flows, R_2 low MgO-low TiO_2 flows, normal (N_2) low MgO-low TiO_2 flows, and N_2 high MgO flows (Figure 84).

In the present study area previous workers have applied the coastal basalt "Depoe Bay" and "Cape Foulweather" nomenclature of Snavely et al. (1973) to Miocene basalt flows, sills, and dikes. Cooper (1981) mapped Depoe Bay Basalt near Cape Lookout and Cape Meares in the Tillamook embayment, and Wells et al. (1984) mapped both Depoe Bay and Cape

SCHEMATIC REPRESENTATION OF COLUMBIA RIVER BASALT FLOWS PRESENT IN CLATSOP COUNTY, NORTHWEST OREGON

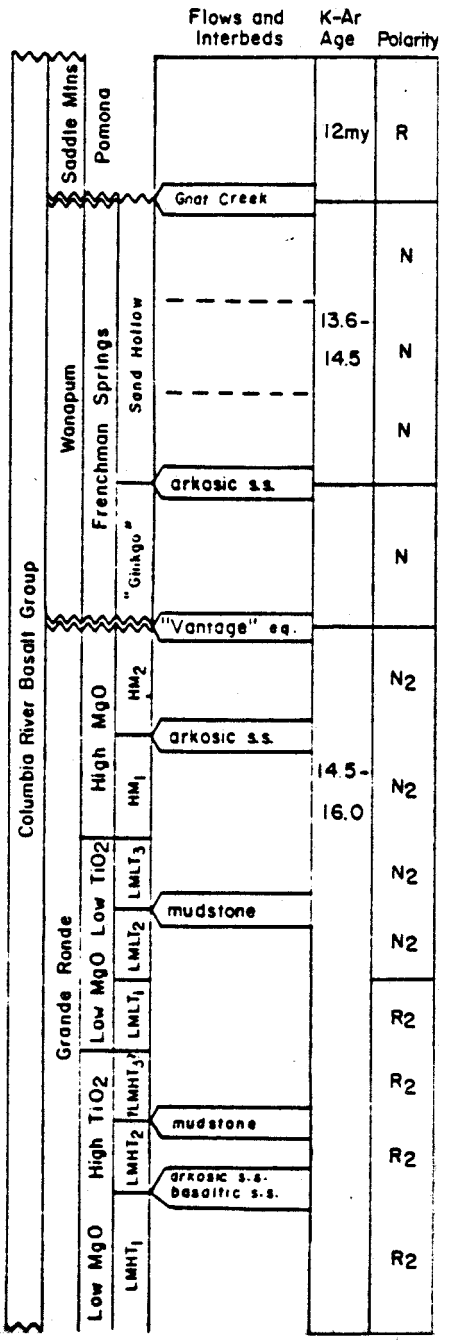

Figure 84. Clatsop County, northwest Oregon, Columbia River Basalt Group flows. General stratigraphic nomenclature after Swanson et al. (1979). Modified after Goalen (1988).

Foulweather Basalts in the same region. However, based on the mounting evidence supplied by previous workers studying Miocene basalts in the Astoria embayment of northwest Oregon and southwest Washington (e.g. Beeson et al., 1979; Beeson et al., 1985; Niem and Niem; 1985, Peterson, 1984; Nelson, 1985; Pfaff and Beeson, 1987; Wells and Niem, 1987; Wells and Niem, 1989; Wells and Coe, 1985; Goalen, 1988; Mumford, 1989) it is proposed in this study that the Miocene basalts of the Tillamook embayment also probably represent distal flows erupted from fissures on the Columbia Plateau, and that the nomenclature of these units be changed to correspond with the nomenclature of the CRB Group. Thus, on Plate I, the Depoe Bay Basalt and Cape Foulweather Basalts of Cooper (1981) and Wells et al. (1984) are informally reassigned to units of the Grande Ronde and Frenchman Springs Basalt, respectively.

Grande Ronde Basalt units in the Tillamook embayment have been assigned informal names on the basis of geochemical, petrographic, and magnetostratigraphic analyses and correlation to similar flow units within the Grande Ronde and Frenchman Springs basalts in eastern Oregon and Washington. The names correspond to the most recent nomenclature for Grande Ronde Basalt stratigraphy of Reidel et al. (in prep; Figure 85) and are (from oldest to youngest; Figure 86): the Grouse Creek Unit (R_2 Low magnesium-low titanium, Tgr_1 on Plate I), Winterwater Unit (N_2 Low magnesium-low titanium, Tgr_2 on Plate I), and Sentinal Bluff Unit (N_2 High magnesium, Tgr_3 on Plate I). Similarly, the Frenchman Springs member of the Wanpum basalt has also been assigned the informal unit name: "Ginkgo Unit" (Tfs on Plate I).

Proposed Informal Units of the Grande Ronde Basalt (Reidel et al., in prep.)

		Magnetic Polarity
Sentinel Bluff *	High Mgo	N_2
Slack Canyon		
Field Springs		
Winterwater *	Low TiO2 low MgO	
Umtanum		
Ortley		
Armstrong Canyon		
Meyer Ridge		R_2
Grouse Creek *	Low TiO2 low MgO	
Wapshilla Ridge		
Mount Horrible		
China Creek		N_1
Downey Gulch		
Center Creek		R_1
Rogersburg		
Teepee Butte		
Buckhorn Springs		

* Units mapped in the Tillamook embayment

Figure 85. Informal units of the Grande Ronde Basalt proposed proposed by Reidel et al. (in prep).

Schematic Representation of Columbia River Basalt Flows
in the Tillamook Embayment

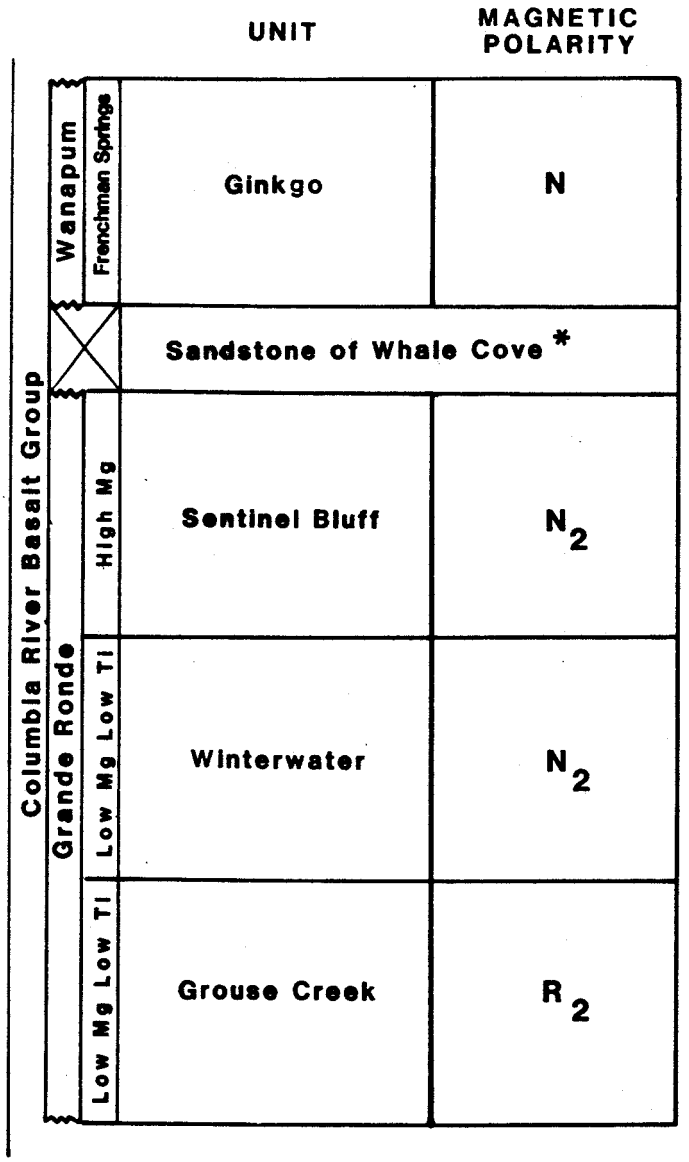

Figure 86. Units of the Columbia River Basalt Group present in the Tillamook embayment.
* Sedimentary units are not part of the Columbia River Basalt nomenclature (Swanson et al, 1979). This is a local coastal informal name used by Snavely et al. (1973) in the Newport embayment. It would equate with the Vantage sandstone interbed of the Ellensburg group of eastern Oregon and Washington.

Grande Ronde Basalt Chemistry and Normalizations

Through extensive compilation of Miocene coastal basalt and Columbia River basalt geochemical data, Snavely et al. (1973) designated compositional fields on silica variation diagrams that distinguish Grande Ronde (Depoe Bay Basalt), Frenchman Springs (Cape Foulweather Basalt), and Pomona (Basalt of Packsack Lookout) flows from one another and from other Columbia River Basalt Group flow units (coastal basalt nomenclature of Snavely et al., 1973, in parentheses). More recently, Mangan et al. (1986) compiled Grande Ronde Basalt geochemical data and found that it grouped into five recognizable subtypes, which they designated within compositional fields on their MgO vs. TiO_2 and MgO vs. P_2O_5 diagrams.

The diagrams of both Snavely et al. (1973) and Mangan et al. (1986) have been very helpful in previous studies of Grande Ronde Basalt in northwest Oregon (e.g. Murphy, 1981; Peterson, 1984; Nelson, 1985; Mangan et al., 1986; Rarey, 1986; Goalen, 1988; and Mumford, 1989), because the different geochemical subtypes of this rock unit are difficult to tell apart on the basis of hand sample or petrographic characteristics alone (Mangan et al., 1986; Goalen, 1988). For this reason, they are also used in this study to help determine which subunits of the Grande Ronde Basalt previously identified in northwest Oregon occur in the Tillamook embayment.

Major and trace element geochemical analysis of 23 basalt samples from the thesis area was performed by the lab of Dr. Peter Hooper at Washington State University, Pullman, on a Rugaku X-ray fluoresence

(XRF) machine (Appendix IX). These analyses were used in conjunction with magnetostratigraphic data to help assign the flows and dikes of Grande Ronde Basalt within the present study area to their respective subunits. However, it is very important to note that the geochemical analyses of major elements in this study were performed on a different XRF machine (Rugaku XRF vs. Phillips XRF) and against a different lab standard (international vs. CRB-1) than used in the analyses of previous workers (e.g. Snavely, 1973; Murphy, 1981; Peterson, 1984; Nelson, 1985; Rarey, 1986; Goalen, 1988; Mumford, 1989) who employed their data to help delineate fields which define CRB and northwest Oregon Grande Ronde Basalt subtypes on major element variation diagrams.

In order to more effectively utilize these diagnostic fields, an attempt was made to bring the geochemical data of this study into accord with that of previous studies such that all data could be plotted on the same major element variation diagrams for comparison. To accomplish this end, two sets of normalizations, one compensating for a change in XRF machine and the other to account for a change in lab standard, were carried out on the normalized water-free geochemical data furnished by Hooper's lab (Appendix IX-A).

International Basalt to CRB-1 Normalization Factor

The attempt to compensate for the change from the old CRB-1 standard to the new international basalt standard was modelled after a similar effort by Goalen (1988), who developed major-element normalization factors after he inadvertantly ran his samples against the international standard at Hooper's lab. Unfortunately, when his normalization factors were applied to the geochemical data set of this study, the data points plotted in erratic and inconsistent fields on the

diagrams of Snavely et al. (1973) and Mangan et al. (1986). Furthermore, many of the resulting Grande Ronde subtype assignments also contradicted magnetostratigraphic data collected from the same basalt flows. Dr. M. Beeson of Portland State University (personal communication, 1989) and T. Tolan of Westinghouse-Hanford, Washington Operations (personal communication, 1989) have also been frustrated in their efforts to develop a similar set of normalization factors, finding that the factors often generated confusing or even erroneous results. As a result of the findings of this study, and those of Beeson and Tolan, the international basalt standard to CRB-1 normalization factors were not used.

Rugaku XRF to Phillips XRF Normalization Factors

A set of normalization factors were furnished in 1988 to Dr. Niem from Terry Tolan of Westinghouse Hanford Company to compensate for the difference in analytical sensitivity resulting from the change in XRF equipment from the old Phillips XRF machine (on which many of the analyses used to construct Grande Ronde Basalt subunit diagrams were run) to the new Rugaku XRF machine at Washinton State University, Pullman (Table 1). These factors were calculated by Tolan through comparitive analysis of identical samples run on both machines. The normalized water-free geochemical results from Hooper's lab (Appendix IX-A) were recalculated with these factors and are listed in Appendix IX-B. The major oxide values that were normalized in this study are used in all the following major oxide diagrams.

Table 1

Major Oxide Normalization Factors Compiled by Westinghouse Hanford Company to Compensate for the Change from the Older Phillips X-Ray Fluorescence Machine to the New Rugaku XRF at Washington State University, Pullman.

OXIDE	SLOPE	STD ERROR	INTERCEPT	STD ERROR
SiO_2	0.86	0.04	7.18	0.72
Al_2O_3	0.68	0.05	5.43	0.34
FeO	0.94	0.03	0.75	0.47
MgO	0.91	0.05	0.53	0.42
CaO	0.91	0.04	0.68	0.42
Na_2O	0.29	0.09	1.58	0.28
K_2O	0.93	0.05	0.04	0.16
TiO_2	0.92	0.02	0.27	0.14
P_2O_5	0.80	0.01	0.05	0.02
MnO	0.73	0.04	0.06	0.01

Geochemistry of the Grande Ronde Basalt Flows within the Tillamook Embayment

The normalized geochemical analyses of this study are plotted on Snavely et al.'s (1973) silica variation diagrams in Figure 87 along with geochemical data provided by Wells (unpublished) and Snavely et al. (1973) from basalt samples they collected from the present study area (Appendix IXc; sample locations shown on Plate I). The fields on each major-oxide diagram outline major flow units of the Columbia River Basalt Group that have correlatives on the Oregon and Washington coast. With the exception of two samples from Frenchman Springs Basalt flows (CFW and SNB-162; discussed in a later section), samples from the Tillamook embayment consistently plot within or near the field designated for the Grande Ronde Basalt (Figure 87). Based on these findings, all samples within or near the Grande Ronde Basalt field are assigned to this rock unit.

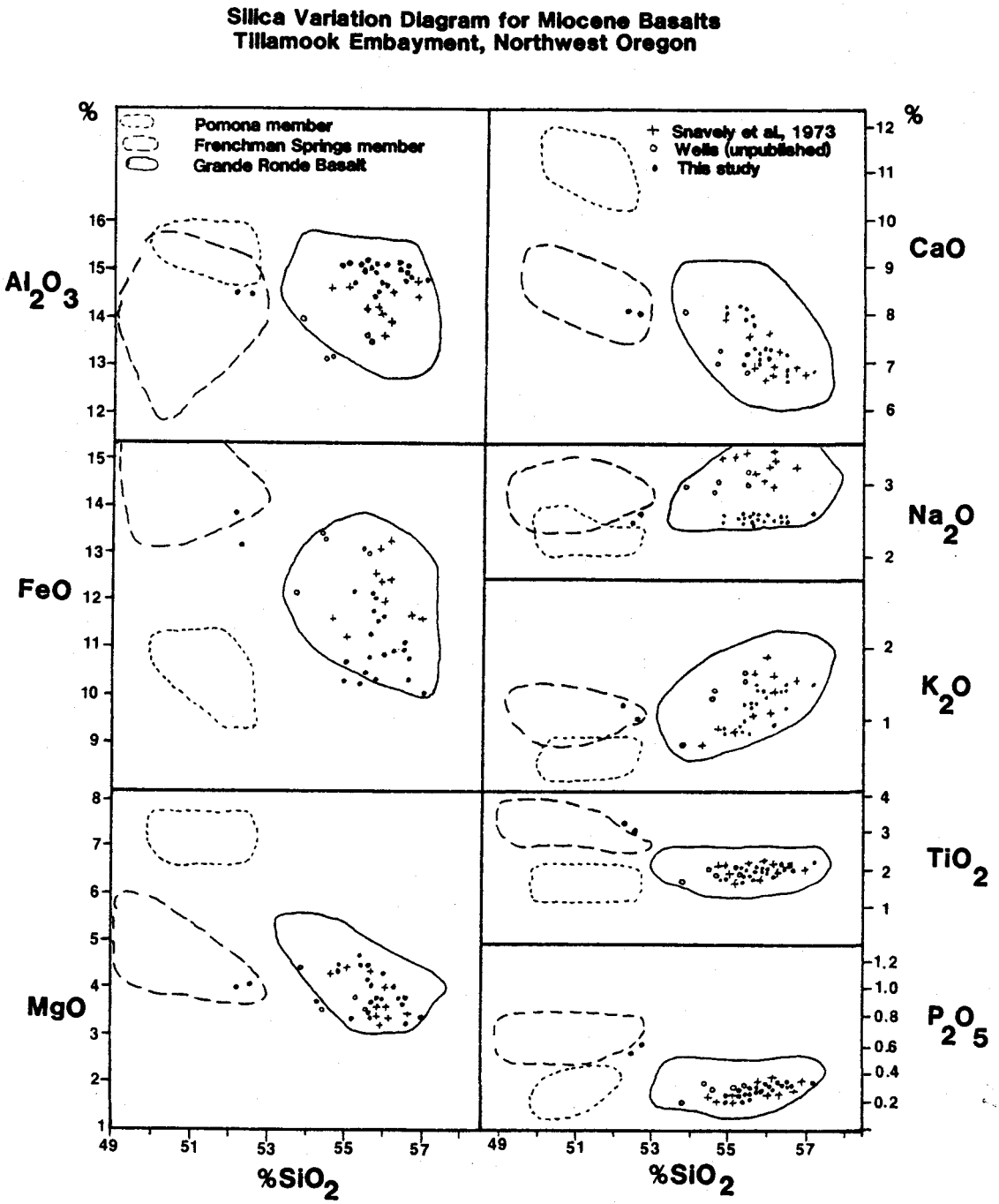

Figure 87. Silica variation diagram with fields defined for Miocene flows of the Pomona (Basalt of Packsack Lookout), Frenchman Springs (Cape Foulweather), and Grande Ronde (Depoe Bay) basalts. Plotted points represent samples collected from the thesis area. Figure and terminology modified after Snavely et al. (1973).

As an aid to determine which subtypes of the Grande Ronde Basalt occur in the Tillamook embayment, geochemical data were also plotted on Mangan et al.'s (1986) MgO vs. TiO_2 and MgO vs. P_2O_5 diagrams, which are sectored into five fields that define different Grande Ronde geochemical subtypes (Figure 88). However, although previous workers studying the Grande Ronde Basalt in northwest Oregon (e.g. Mumford, 1989; Rarey, 1986; Goalen, 1988) have generally accepted Mangan et al.'s fields 1, 3, and 4 as representative of high magnesium Grande Ronde flows, and fields 2 and 5 as low magnesium Grande Ronde flows, T. Tolan (personal communication, 1989) recommended that this diagram be used with caution. Subsequent studies have shown that the predesignated fields of Mangan et al. (1986) are not always representative of the actual Grande Ronde subtype, and that corroborative data is sometimes needed to cross-check Grande Ronde subtype assignments (Tolan, personal communication, 1989).

For example, samples from the present study area with a magnesium weight percent of 4.1 or higher plot in inconsistent fields on Mangan et al.'s (1986) diagram (Figure 88). In Figure 88-A these points are scattered within and between fields 3 and 5, and in Figure 88-B they plot both within and between fields 4 and 5. In spite of these inconsistencies, however, the samples are assigned to the high magnesium Grande Ronde Basalt subtype on the basis of their respective magnesium and calcium-oxide weight percents described below.

According to Beeson and Tolan (personal communication, 1989) high magnesium Grande Ronde Basalts are generally distinguished from low magnesium Grande Ronde Basalt by having a magnesium-oxide weight percent that is greater than 4.0. However, they report that borderline cases can also be differentiated by their respective calcium-oxide weight

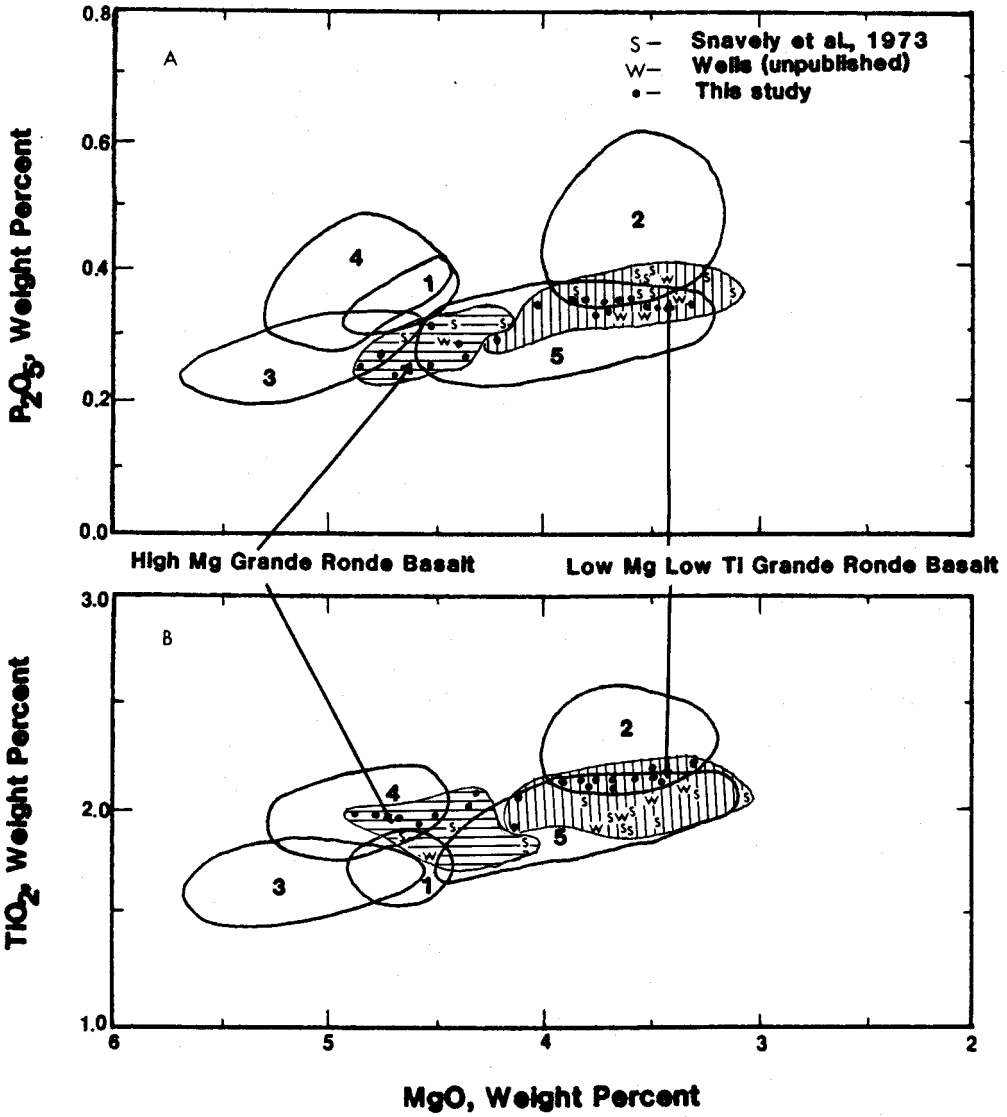

Figure 88. The high magnesium (horizontal lines) and low magnesium-low titanium (vertical lines) subtypes of Grande Ronde Basalt of the thesis area plotted against the geochemical fields of Grande Ronde Basalt defined by Mangan et al. (1986). Frenchman Springs Basalt samples not plotted. Modified after Mangan et al. (1986).

percents, which is typically near or above 8 weight % for high magnesium flows, and near 7 weight % for low magnesium Grande Ronde Basalt. Figure 89 illustrates the relationship between MgO and CaO weight percents for all samples used in this study, and sample data points are enclosed in high and low magnesium basalt fields. The calcium-oxide weight percent of samples assigned to the high magnesium Grande Ronde Basalt in this study range from 7.5 to 8.3, which supports assignment to the high magnesium Grande Ronde Basalt subtype.

All other basalt samples with an MgO weight percent lower than 4.1 plot predominately within field 5 of Figure 88-A and B, indicative of the low magnesium-low titanium Grande Ronde Basalt subtype (Mumford, 1989; Rarey, 1986; Goalen, 1988). Assignment to this subtype agrees with the typical titanium-oxide content for low magnesium flows of the Grande Ronde Basalt, which ranges as high as 2.2 weight percent (Tolan, personal communication, 1989). Although several points plot in field 2 (which is typical for high titanium flows; Goalen, 1988), or in the overlap zone between fields 2 and 5 of Figure 88, these samples still do not possess titanium values high enough to warrant assignment to the high titanium Grande Ronde subtype, which ranges from 2.25 to 2.60 weight percent titanium (Tolan, personal communication, 1989).

To verify the low magnesium-low titanium assignment of samples which plot within field 5 of Figure 88, they were checked against the magnetic polarity data of this study and the paleomagnetic data of Wells et al. (in press). Magnetic polarity is diagnostic because low magnesium-high titanium flows of the Grande Ronde Basalt are reversed (Tolan, personal communication, 1989; Swanson et al, 1979). Sample 5-88 of this study, which plots in field 2 on Figure 88-B with the highest

BLANK PAGE

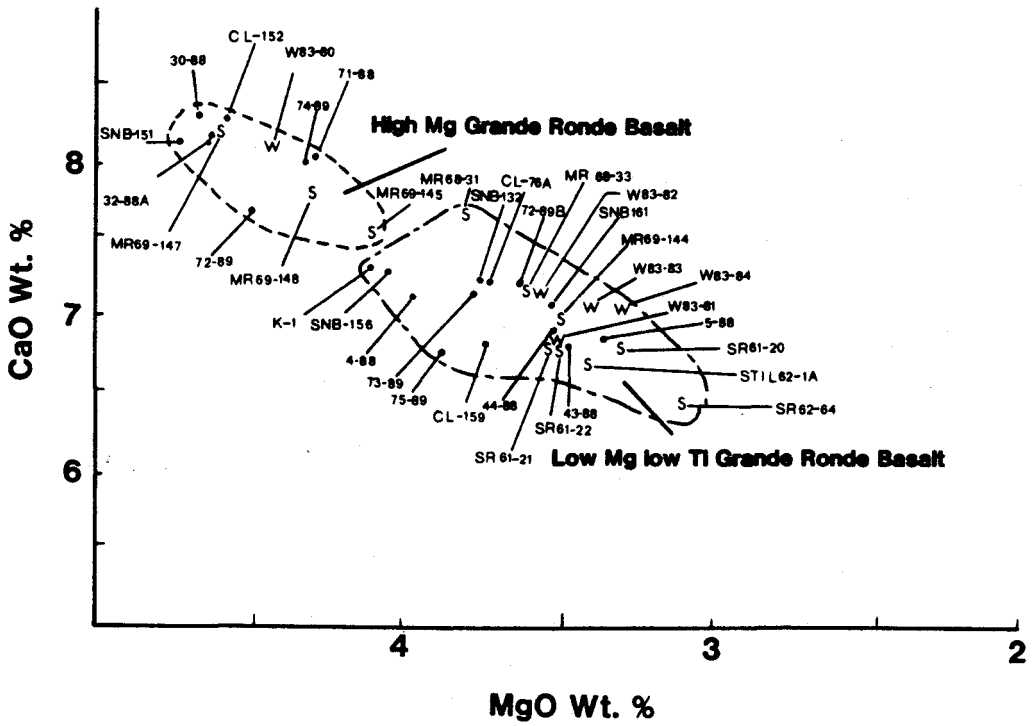

Figure 89. Diagram showing the relationship of MgO and CaO weight percent for Grande Ronde Basalt chemical subtypes in the thesis area. Point label conventions are the same as in Figure 88. Frenchman Springs samples not plotted.

overall titanium value, came from a flow that has a normal polarity (Appendix X). In addition, Wells et al. (in prep) found that the magnetic direction of basalt flows from which some of these samples were taken is typical of the Winterwater (N_2 low magnesium-low titanium) unit of the Grande Ronde Basalt (Appendix X). Although Wells et al. (in prep) also report the existence reversed flows in the Tillamook embayment, their magnetic inclination and declination are typical of R_2 low magnesium-low titanium Grande Ronde Basalt flows (Appendix X). Based on the sum of these data, the Tillamook embayment samples with magnesium weight percent below 4.1 are assigned to the low magnesium-low titanium Grande Ronde subtype.

On the basis of these analyses, two geochemical subtypes of Grande Ronde Basalt have been identified in the study area: the low magnesium-low titanium subtype and the high magnesium subtype. Further subdivision of Grande Ronde Basalt flows in the present study area has been achieved through magnetostratigraphy, and is described in the following section.

Magnetostratigraphy of Columbia River Basalts within the Tillamook Embayment

The magnetostratigraphy of Grande Ronde Basalt flows and dikes in the thesis area was established by bringing oriented basalt samples into the lab and measuring their polarity with a fluxgate magnetometer. However, additional polarity data was also provided by Wells et al. (in press) who performed paleomagnetic analyses on basalt cores drilled in Grande Ronde Basalt flows at several locations in the present study area. The magnetic polarity data of Wells et al. (in press) has been combined with data of this study, and both are used to determine the

magnetostratigraphy and subunits of Grande Ronde Basalts in the Tillamook embayment. The polarity data used in this study is listed in Appendix X and plotted on Plate I.

N_2 High Magnesium Sentinal Bluff Unit and N_2 Low Magnesium-Low Titanium Grouse Creek Unit of the Grande Ronde Basalt

The magnetic polarity of 55 oriented samples (Appendix X) collected from Grande Ronde Basalt flows and invasive dikes in the Tillamook embayment is normal (Plate I). Those samples with normal polarity that have been placed in the high magnesium category based on geochemical analyses are assigned in this study to the N_2 high magnesium subtype of the Grande Ronde Basalt, which corresponds to the Sentinal Bluff Unit in the new nomenclature of Reidel et al. (in prep; Tolan, personal communication, 1989). Paleomagnetic data (Appendix X) collected from cores drilled in the sea cliffs on the south side of Short Beach north of Oceanside in section 24 of T. 1 S., R. 11 W. (Wells' sites 5S132 and 5S151; Plate I) corroborate the presence of N_2 high magnesium Grande Ronde Basalt in the Tillamook embayment (Wells et al., in press).

Normally polarized samples placed in the low magnesium-low titanium category in this study (Figure 84) are assigned to the N_2 low magnesium-low titanium subtype, which corresponds to the Winterwater Unit of the Grande Ronde Basalt (Tolan, personal communication, 1989; Figure 85). Again, this assignment is corroborated by the paleomagnetic data of Wells et al. (in prep) from their sites DB3-DB6 and 5S125 (Plate I), which indicate that N_2 low magnesium-low titanium basalt of the Winterwater Unit are present in Cape Lookout State Park.

R_2 Low Magnesium-Low Titanium Grouse Creek Unit of the Grande Ronde Basalt

Seven samples from this study (4-88, 7-88, 16-88, 71-88, CL-77, 85-89, CL-152) and two paleomagnetic core sites (DB-1 and DB-2) of Wells et al. (in prep) have reversed polarity (Plate I; Appendix X). In the sequence of basalts north of the town of Netarts, three basalt samples (4-88, and 7-88, and 85-89) collected near the contact between the Cannon Beach member of the Astoria Formation and the Grande Ronde Basalt have a reversed magnetic polarity. In addition, two paleomagnetic core sites (DB-1 and DB-2) drilled within the coastal cliffs within and 100 m north of Maxwell Point in the northwest quarter of section 25, T.1 S., R. 11 W. (Plate I) have reversed magnetic polarities as well as magnetic inclination and declination characteristics typical of low magnesium flows of the Grande Ronde Basalt (Wells et al., in press; Appendix X). Given the low stratigraphic position of samples 4-88, 7-88, and 85-89 near the bottom of the Grande Ronde section, the diagnostic magnetic characteristics of samples DB-1, and DB-2, and the correspondence or proximity of these samples to samples with low magnesium-low titanium chemical composition, it is likely that these samples were taken from R-2 low magnesium-low titanium flows (Plate I).

Another reversed sample (16-88) occurs in a faulted seacliff exposure within a north-dipping sequence of basalt flows in section 24, T. 1 S., R. 11 W.. However, this sample was extracted near low magnesium-low titanium Grande Ronde basalt flows that Snavely et al. (1973) sampled and analyzed for major element composition (sample MR69-144; Appendix IX-C). Thus, sample 16-88 was probably collected from a series of R_2 low magnesium-low titanium Grande Ronde flows.

Using the revised Grande Ronde nomenclature of Reidel et al. (In prep.; Figure 85) these magnetically reversed basalts are assigned in this study to the Grouse Creek Unit of the Grande Ronde Basalt.

Anomalous Polarities in the Grande Ronde Basalt of the Tillamook Embayment

Three of the samples with reversed polarity (71-88, CL-77, and CL-152) have geochemical characteristics and occupy stratigraphic positions that make these polarities suspect. In the magnetostratigraphic investigation of this study the polarity of these samples has been ignored, and each sample has been assigned to a normally polarized unit. However, the criteria used to neglect the reversed polarity of samples 71-88, CL-77, and CL-152 is discussed below.

Reversed sample 71-88, collected on the north side of Cape Meares at the lower contact between the Grande Ronde Basalt and the Cannon Beach member of the Astoria Formation is enigmatic because major and trace element analysis indicates it was taken from a flow of the high magnesium Grande Ronde subtype, which was erupted during a period of normal magnetic polarity (Mangan et al., 1986; Goalen, 1988). Sample 71-88 was collected only 10 meters below sample 74-89, and is a normally polarized sample (Appendix X) of the high magnesium Grande Ronde Basalt (Appendix IX). The similar chemistry and close proximity between these two sample locations suggests that the magnetic polarity of sample 71-88 is not representative of the entire flow.

Within the southern basalt sequence near Cape Lookout State Park, two samples have an apparent reversed magnetic polarity (CL-77 and

CL-152, Appendix X). However, stratigraphic position and chemistry of CL-77 and CL-152 suggest that the polarity of these samples is not representative of the polarity of the flow from which they were collected. Reversed basalt sample CL-152 has a major-element chemistry that matches the high magnesium Grande Ronde subtype (Appendix IX), and was collected up section from locality CL-151 which has a normal polarity and the chemical composition of a high magnesium Grande Ronde Basalt flow. Because this polarity is out of stratigraphic order (no reversed Grande Ronde flows within or above high Mg N_2 flows; Figure 83) the polarity of CL-152 is anomalous, and probably not representative of the entire flow. Similarly, field mapping indicates that reversed sample CL-77 was collected from the same stratigraphic horizon as the basalt sample collected at site CL-76A, which is a N-2 low magnesium-low titanium Grande Ronde Basalt flow. As CL-77 is in an anomalous position for a reversed flow, and no reversed basalt flows have been found lower in the section within the entire southern basalt pile, the polarity of CL-77 is also probably not representative of the flow from which it was collected.

The anomalous polarities of these samples may be the result of lightening strikes, instrument error, or incorrect orientation of sample during collection.

Distribution

Flows of the erosionally-resistant Grande Ronde Basalt form the two mountains that flank the north and south ends of Netarts Bay (Plate I). Major element geochemistry and magnetostratigraphic analyses reveal that three subtypes of the Grande Ronde Basalt occur in the study area, and

include (in stratigraphic order): R_2 low magnesium-low titanium basalt of the Grouse Creek Unit (50-60 m thick); N_2 low magnesium-low titanium basalt of the Winterwater Unit (100-150 m thick); N_2 high magnesium basalt of the Sentinal Bluff Unit (90-120 m thick). These basalts have been broken out on Plate I as Tgr1, Tgr2, and Tgr3, respectively. Although vegetative cover is quite thick over most of the Grande Ronde Basalts, the best exposures of this volcanic unit can be found in rock quarrys, and dramatic coastal cliff exposures.

The R_2 low magnesium-low titanium Grouse Creek Unit flows cover approximately 2 square kilometers of the study area and crop out at the base of the basalt sequence north of Netarts Bay. The best exposures of this rock unit are found in the beach cliffs north of Oceanside Beach State Wayside in the northeast quarter of sec. 25, T. 1 S., R. 11 W..

The Grouse Creek Unit is overlain by the more laterally-extensive N_2 low magnesium-low titanium Winterwater Unit flows, which are present both north and south of Netarts Bay, and cover approximately 10 square kilometers of the study area. Spectacular exposures of these basalts can be seen within the 70 meter tall vertical cliffs on the south side of Cape Lookout. These cliffs are the best for distant viewing of Winterwater basalt flows, but are inaccessible for close outcrop examination. However, numerous rock quarrys are present within these flows, and their locations are indexed on Plate I. A Winterwater Unit dike is also present in the study area on the south flank of Cape Kiwanda (locality K-1, southwest quarter sec. 13, T. 4 S., R. 11 W.).

Overlying the Winterwater and Grouse Creek Units of the Grande Ronde Basalt are flows of the Sentinel Bluff Unit, which cover approximately five square kilometers of the present study area (Plate

I). It is well exposed within cliffs bordering the beach between Agate Beach and the coastal outfall of Short Creek (e.g. localities 32-88A and 30-88; southeast quarter sec. 24, T. 1 S., R. 11 W.), within the extreme southeast corner of sec. 13, T. 1 S., R. 11 W. (e.g. locality 17-88A) and on the north side of Cape Meares (e.g. localities 71-88 and 74-89). Southeast of Netarts Bay Sentinel Bluff flows of the Grande Ronde Basalt are perched near the top of the mountain between Winterwater flows and the Sandstone of Whale Cove. Good exposures of Sentinel Bluff Unit basalt are rare south of Netarts Bay, but found in the rock quarrys at localities CL-152 and SNB-151 (northeast quarter of sec. 29, T. 2 S., R. 10 W. and southwest quarter sec. 28, T.2 S., R. 10 W., respectively).

Lithology

Subaerial and submarine flows and breccias that compose the three subtypes of Grande Ronde Basalt (Grouse Creek, Winterwater, and Sentinel Bluff units) present in the Tillamook embayment are very hard to distinguish from one another on the basis of sample appearance and flow characteristics. As a result, unless specified, the following lithologic descriptions apply to undifferentiated Grande Ronde Basalt in the present study area.

Subaerial flows of Grande Ronde Basalt in the Tillamook embayment are typically aphanitic or aphyric to micro phyric, fairly fresh, and display crude to well-developed columnar jointing (colonnade), or hackly random joint patterns that may represent entablature (Figure 90). Although predominately vertical, columnar joints at one locality within the Sentinel Bluff Unit (N_2 high magnesium Grande Ronde Basalt) are oriented horizontally (northeast quarter sec. 24, T. 1 S., R. 11 W.).

Figure 90. Sea cliff exposure of two flows of high MgO Sentinel Bluff Unit of the Grande Ronde Basalt on the south side of the Cape Meares headland (southwest 1/4 sec. 13, T. 1 S., R. 11 W.). Base of section is a lava delta complex characterized by foreset-bedded pillow palagonite breccias (A) which grade upward to crudely columnar-jointed basalt (B). This is overlain by another lava delta with a foreset-bedded pillow palagonite complex (C) with columnar-jointed filled lava tube (D), and grades upward to close-packed pillows and columnar-jointed basalt flow (E).

Depending on position within an individual flow, vesicles may be absent to common, and are most abundant near the flow top, where they range in size from <1 mm to 4 cm in diameter. Vesicles and vugs are partially to completely filled with amygdaloidal banded chalcedony or zeolite minerals (natrolite?), but also are rarely encrusted with stubby black hematite (?) crystals. Although oxidized flow tops are generally rare, one is particularly well exposed between subaerial Sentinel Bluff flows in the 75 m high south-facing seacliff north of Cape Meares lighthouse (Snavely et al., 1973; this study). Most subaerial basalts are fresh to slightly weathered, and some have a thin (2mm - 3 cm thick) red to yellow iron oxide-rich weathering rind which is hematite and limonite-stained. Fresh Grande Ronde Basalt ranges from dark gray to black (N2 to N1 on GSA color chart).

Submarine flows of the Grande Ronde Basalt in the Tillamook embayment are also aphyric and aphanitic, but typically pillowed to brecciated, and range from deeply weathered to fresh. Pillows are poorly to well developed (Figure 91), and range from 0.5 to 2 meters in diameter. Although commonly closely packed (Carlisle, 1963) and nested, some are widely separated from one another by zones of altered brecciated basalt and altered basaltic glass matix within pillow palagonite complexes (Figure 90). Fresh pillows occasionally have slightly vesicular interiors and preserved glassy rinds, however the rinds are often commonly to extremely altered to clay. The interior of most pillows are randomly fractured to radially jointed, but these features are often masked by deeply weathered surfaces. Close-packed incipient pillows were described at Maxwell Point by Snavely et al. (1973; northeast quarter sec. 25, T. 1 S., R. 10 W.), and green chert

Figure 91. Sea cliff exposure of thick fine-grained shallow-marine hummocky cross-bedded arkosic sandstone interbed between two pillowed flows of high MgO Sentinel Bluff Unit of the Grande Ronde Basalt (locality 17-88). Top of lower flow is characterized by large closely packed nested pillows. Upper flow is also pillowed and contains two intersecting filled lava tubes with radial (A) and vertical (B) columnar joints.

occupies void spaces between these pillows near the top of the flow. Filled large lava tubes with characteristic war bonnet radial jointing are also present within pillowed sections, and vary from two meters to several tens of meters in length, and one to three meters in height. Because these thick elongate tubes are commonly columnar-jointed, they are very difficult to tell from subaerial columnar-jointed flows (Figure 91). At the end of Cape Lookout, cross-sections of very large filled lava tubes are exposed and characteristic radial war bonnet cooling joints have developed perpendicular to the vesicular tube walls, and define tubes that were up to 3 meters in diameter. The large lava-filled tubes are surrounded by a carapace of closely-packed lavas (e.g. Maxwell Point).

Some submarine flows of the Grande Ronde Basalt are present as pillow and breccia foreset complexes, and are well exposed on the south flank of Cape Lookout, and within the seacliffs to the north and south of Cape Meares Lighthouse (Snavely et al., 1973; this study; Figure 90). These foreset pillow palagonite complexes range from approximately 10 to 30 meters in thickness, and indicate a west to northwest direction of lava delta dispersal for the Grande Ronde Basalt. The forsets are composed of isolated dipping elongate pillows and filled mega-tubes in a basaltic breccia (Figure 90). These breccias are typically extremely diagenetically altered to green chloritic clays or soft reddish-orange iron oxides.

Submarine pillowed flows are generally more common in the west part of the study area, with columnar-jointed subaerial flows more common in to the east. However, within the cliff faces at Cape Meares and Cape

Lookout, some pillowed basalt and foreset breccia sequences lower in the flow form couplets with columnar-jointed upper parts (Figure 90).

Grande Ronde Invasive Dikes and Sills in the Tillamook Embayment

Several invasive dikes and sills of Grande Ronde Basalt have been mapped in the present study area (mechanism of invasion discussed in the depositional environment section). Those best exposed occur at locality K-1, on the southern flank of Cape Kiwanda, locality CL-75 (southwest quarter sec. 6, T. 3 S., R. 10 W.), and locality 72-89 (end of Cape Lookout). The dike at locality K-1 (Figure 92) is composed of Winterwater Unit basalt (N_2 low magnesium-low titanium basalt) (Appendices IX and X), injects into Angora Peak member sandstones, and is approximately 2.5 meters thick. This dike is dark gray (N-1), and horizontally jointed, with joints oriented perpendicular to cooling surfaces. The contact surfaces of the dike are glassy, reflecting rapid quenching, and bounding sandstones, though baked, are undisturbed. Wave action has preferentially eroded the Angora Peak member sandstones surrounding this dike so that it stands out as a low wall of basalt that trends parallel to the south side of Cape Kiwanda, tracable to the southwest toward Haystack Rock (Plate I) for 75 meters before it is obscured by the ocean surface. At the eastern terminous of the dike, the basalt is severely sheared by a fault zone (Figure 92).

The invasive dike at locality CL-75 is quite different in character and composition from the one at K-1, and is composed of Sentinel Bluff Unit basalt (N_2 high magnesium Grande Ronde Basalt; Appendix IX). At CL-75, surrounding Angora Peak member sandstones are extensively brecciated adjacent to severely brecciated and fragmented altered

Figure 92. Three meter wide invasive basalt dike of N_2 low MgO-low TiO_2 Winterwater unit of the Grande Ronde Basalt in Angora Peak member sandstone at Cape Kiwanda in seacliff (locality K-1). Dike is horizontally jointed and sheared in fault zone. Arrow points to notebook for scale.

basalt. Several irregular small finger- or pod-like intrusions (approximately 6 cm thick tapering to 0) on the fringe of the dike inject into sandstone breccia zones. The interior of the dike is partially pillowed, and like the surrounding sandstone, is extensively brecciated. The bedding of sandstone 10 m on either side of both the dike and sedimentary breccia zone is slightly deformed. This dike has the characteristics of a peperite formed by steam blasting and fragmentation into soft water-saturated sediments.

The invasive sill at locality 72-89 forms a wave-cut bench at the end of Cape Lookout and, like CL-75, is also composed of Sentinel Bluff Unit basalt (Appendix IX; Figure 93). The sill has intruded along the base of a sandstone interbed within the Winterwater basalt sequence, is at least 5 m thick, and has formed a peperite breccia on the underside of this sandstone unit (Figure 93). The lower part of the sandstone is profoundly disturbed, characterized by a basal chaotic mixture of structureless sediment and basalt caused by fluidization of sediment during emplacement of hot basalt lava (Kokelaar, 1982). A zone of contorted bedding overlies the peperite, and grades upward to a relatively undisturbed interval near the center of the bed. Where the sedimentary interbed has been removed by wave action, the top of the sill is extremely vesicular and may also be pillowed.

Sedimentary Interbeds within the Grande Ronde Basalt of the Tillamook Embayment

Sedimentary interbeds occur between several Grande Ronde Basalt flows throughout the study area, but are generally rare and tracable only over a short distance (Plate I). Although the dominant lithology of

Figure 93. Arkosic marine sandstone interbed between overlying pillowed N_2 low MgO-low TiO_2 Winterwater Unit and underlying invasive sill of high MgO Sentinel Bluff Unit basalt (locality 72-89 on wave-cut bench at extreme western end of Cape Lookout). Lower part of the sandstone bed is severely disrupted by peperitic sill which is composed of a mixture of sediment and fragmental basalt (at geologists feet). This mixture accounts for the light brown color of the top of the sill.

these interbeds is friable, fossilliferous to non-fossilliferous, well-sorted, arkosic-micaceous sandstone, rarer fossilliferous to carbonaceous mudstones and basalt cobble conglomerates have also been found between flows of the Grande Ronde Basalt in the Tillamook embayment. A brief synopsis of the major lithological characteristics of each sedimentary interbed follows.

Sandstones:

At locality 17-88 (southeast corner sec. 13, T. 1 S., R. 11 W.; Plate I), a particularly well exposed 10 meter thick sandstone bed occurs between a pillowed flows of N_2 high magnesium-low titanium Sentinal Bluff basalt (Figure 91). This sandstone is friable, light gray to buff, calcite concretionary, arkosic-micaceous, subhorizontally laminated, and baked at its upper contact by the overlying basalt flow. Grain size and petrographic analyses indicate that this sandstone is very fine-grained, micaceous-arkosic, well-sorted and composed of angular to subrounded grains (Appendix V; Appendix VI). Like other sandstone interbeds between Basalt flows of the Columbia River Basalt Group in the thesis area, this sandstone unit is relatively free of basalt fragments, which is remarkable given its occurrence between widespread pillow flows of the Grande Ronde Basalt. At locality 26-88 (northeast quarter sec. 32, T. 2 S., R. 10 W.) another thick (>5 meter) horizontally laminated marine sandstone interbed is exposed, which is compositionally and texturally similar to the sandstone at locality 17-88. The sedimentary unit at locality 26-88 rests on top of a pillowed flow of the Winterwater basalt which has a concentration of articulated molluscan fossils on its upper suface that include Spisula (Mactromeris) sp. cf. S. (M.) albaria, indicative of an open marine environment

ranging from intertidal to 110 m water depth (Moore, written communication, 1989; Appendix IV).

A fascinating two meter-thick package of hummocky cross-statified to ripple-laminated fine- to medium-grained sandstones with interbedded dark silty sandstone and siltstone is exposed on a wave cut bench at the end of Cape Lookout (locality 72-89; Figure 93). This interbed is baked on both its upper and lower surfaces, and small (< 50 cm thick) peperite dikes composed of sediment and Sentinel Bluff basalt mixtures invade the sediment from below (described in detail above). The upper contact of the sandstone bed with the overlying N_2 low magnesium-low titanium Winterwater Unit basalt flow is profoundly loaded and deformed, and a thin (<5 cm thick) baked zone has developed at the upper contact with this basalt.

Conglomerate:

A thin (< 50 cm thick) framework-supported fluvial (?) basalt cobble conglomerate occurs between an underlying subaerial and overlying submarine basalt flow of N_2 low magnesium-low titanium Winterwater basalt at locality 70-88 (center sec. 1, T. 3 S., R. 11 W., on Cape Lookout Road near the Cape Lookout trailhead parking lot). This deposit includes subrounded to rounded, poorly sorted cobbles up to 15 cm in diameter.

Mudstone:

Within a seacliff at locality 13-88 (northeast quarter sec. 24, T. 1 S., R. 11 W., approximately 500 m north of Lost Boy Cave), a 1.5 meter thick gastropod (cerithid ?) and oyster-bearing (Moore, written communication, 1989), carbonaceous, dark green siltstone occurs over a

pillowed flow of the Grouse Creek Unit, possibly separating this flow from pillowed high magnesium N_2 Sentinel Bluff Unit basalt. The mudstone contains abundant carbonized leaves and stems, and coarsens upward over approximately 1.5 m to a basaltic grit. The upper 8 cm of this deposit is severely baked.

Petrography

Seven basalt exposures representing all three subtypes of Grande Ronde Basalt in the Tillamook embayment were sampled for petrographic analysis. An effort was made to analyze basalt from subaerial and submarine flows, as well as dikes in the thesis area. As a result, five samples (43-88, 4-88, C1-159, SNB-151, 44-88) were collected from subaerial flows, one was collected from the interior of a basalt pillow (72-89B), and one from a basalt dike (K-1). Because the results from the petrographic analyses of this study generally support those of previous workers (e.g. Goalen, 1988; Mangan, 1986; Nelson, 1985; Murphy, 1981) who report that the individual subtypes of the Grande Ronde Basalt are petrographically similar, the petrographic characteristics of each subtype are discussed together in the following section, unless otherwise specified.

Plagioclase microlites comprise approximately 60 percent of Grande Ronde Basalt collected in the Tillamook embayment (Figure 94). These basalts are predominately characterized by randomly-oriented albite-twinned plagioclase laths in the groundmass which vary in length from 0.1 to 0.3 mm (Figure 94). Their composition, estimated from the Michel-Levy method (Kerr, 1979), ranges from andesine to labradorite (An_{48}-An_{55}), with labradorite being the most common plagioclase mineral.

Figure 94. Photomicrograph of N_2 low MgO-low TiO_2 Winterwater Unit basalt (locality 44-88) showing plagioclase laths partially encased in basaltic glass (extinct) and augite resulting in a subophitic to hyaloophitic texture. Blocky plagioclase micro phenocrysts, like the one pictured here, are characteristic of Winterwater flows (Beeson, personal communication, 1989). Field of view 3.3 mm. Crossed nicols.

Some microphenocrysts of plagioclase, which range from 0.75 to 1.2 mm in length, are also present in thin section, but are almost exclusively carlsbad-twinned. These are commonly zoned and sometimes possess a rim of gas or basaltic (tachylite or sideromelane) glass inclusions that marks the boundary between a rounded, stubby crystal core, and a compositionally different euhedral outer rim. These interesting microphenocrysts may represent changing pressure-temperature or composition conditions within the melt which resulted in partial resorption of the plagioclase crystal, and subsequent resumption of crystal growth under different chemical or physical (pressure-temperature) conditions. The terminations of plagioclase laths are commonly skeletal or ragged in thin sections that are characterized by glassy groundmass and hyaloophitic texture. Rare small glomerocrysts composed of plagioclase or intergrown plagioclase and augite crystals also occur in Grande Ronde basalt samples, and range up to 1.5 mm in diameter. Small but distinctive rare blocky microphenocrysts of plagioclase were observed only within thin sections cut from flows of the N_2 low magnesium-low titanium Grande Ronde subtype (K-1, 72-89B, CL-159, 43-88, and 44-88). According to M. Beeson (personal communication, 1989) these blocky phenocrysts are commonly found within Winterwater flows (low magnesium-low titanium N-2 Grande Ronde subtype), and are useful for distinguishing them from other Grande Ronde subtypes.

Augite microlites comprise an average of approximately 30 percent of each thin section (Figure 94), are fresh to slightly altered, and predominately occur as small (0.1-0.3 mm) subhedral crystals. More rarely, however, augite occurs as larger subhedral microphenocrysts which range from 1 to 1.5 mm in length. Within one sample (CL-159),

which is holocrystalline, both plagioclase and augite crystals of the groundmass tend to be larger, ranging up to 0.5 mm in length. These characteristics may indicate that the sample was collected from the internal part of a flow which had a longer cooling history. In most thin sections, plagioclase laths are partially encased by augite crystals, and thus have a subophitic texture (Figure 94). However, within samples containing a glassy groundmass, plagioclase microlites are partially enclosed within tachylite glass, and are thus hyalophitic.

The groundmass of most thin sections of Grande Ronde Basalt in the Tillamook embayment is composed, in part, of glass, which averages approximately ten percent of each specimen (Figure 46A). Glass is most prevalent in hypocrystalline samples K-1 and 72-89B, extracted from a rapidly quenched dike and basalt pillow, respectively. The most common type of glass is dark, turgid tachylite glass, which is often partially altered to smectitic (?) clays. Light brown sideromelane glass is also common in thin section. Within all thin sections, except holocrystalline sample CL-159, there are small regions that are characterized by abundant glass, and others that completely lack glass. Thus, it is important to note that the micro textural characteristics of Grande Ronde Basalt can significantly change over distances as short as those represented on the scale of a single thin section. Vesicles are commonly lined or partially filled with both sideromelane or tachylite glass. In places sideromelane has been extensively altered to radiating fibrous nontronite (?) or chlorophaeite (?).

Opaque minerals are fairly common in thin section, and are predominately composed of magnetite or ilmenite (Figure 94). Magnetite comprises approximately five to seven percent of the Grande Ronde Basalt

of the thesis area, and occurs as both octahedrons or as amorphous blebs. Rare fractures and voids in the basalt are also filled with sparry calcite cement and brownish green chlorophaeite. The palagonite foreset breccias of the study area were not sampled but detailed petrographic descriptions of similar CRB breccias in the Astoria embayment are included in the theses of Smith (1975) and Neel (1976).

Both major element geochemical and petrographic analyses indicate the each subtype of Grande Ronde Basalt in the Tillamook embayment is tholeiitic basalt to basaltic andesite, and are quite geochemically distinct from the nearby Tillamook, Siletz River, Nestucca, Cascade Head, and Yachats volcanics (Snavely et al., 1980; Barnes, 1981, Rarey, 1986; Mumford, 1989). Grande Ronde samples from the study area are characterized by an average silica content of 56 weight percent (Appendix IX), a lack of olivine both within the groundmass or as phenocrysts, common glassy groundmass, and an An content of plagioclase that ranges from An_{48} to An_{55} (andesine to labradorite).

Age and Correlation

The age of Grande Ronde Basalt flows and dikes in the present study area is based on stratigraphic position above the lower to middle Miocene Astoria Formation, radiometric K-Ar age dates obtained at Cape Meares by Turner (1970), and K-Ar dates obtained from correlative Grande Ronde flows along the coast of Oregon and on the Columbia Plateau. The results of K/Ar dating of basalt flows at Cape Meares (high Mg N_2 Sentinel Bluff unit of this study) by Turner (1970) yielded ages of 14 +/-1 my and 15.2 +/-0.6 my. Correlative flows on the Columbia Plateau range from 16.5 to 14.5 Ma (Swanson et al., 1979; Snavely et al., 1973;

Mangan et al., 1986; Niem and Cressy, 1973; Beeson and Tolan, 1989; Figure 83).

A supplementary constraint to the maximum age for the Grande Ronde Basalt is provided by the cross-cutting relationship between the N_2 low magnesium-low titanium Winterwater basalt dike at Cape Kiwanda and the Angora Peak member sandstones it cuts (Figure 92). Because the Angora Peak member is Newportian age (early to middle Miocene) at Cape Kiwanda (Snavely and Vokes, 1949; Moore and Addicott, 1987), the dike can be no older than the base of the Newportian stage, which is approximately 18 Ma (Moore and Addicott, 1987; Figure 10).

Correlatives to the Grande Ronde Basalt in northwest Oregon include the Depoe Bay Basalt, exposed approximately 50 kilometers to the south of the present study area at Depoe Bay, Oregon (Snavely et al., 1973). Grande Ronde pillowed and subaerial flows, sills, and dikes (including high and low mg N_2 and R_2 units) are also abundant in the Astoria embayment 50 km to the north in northwest Oregon and southwest Washington (Murphy, 1981; Goalen, 1988; Rarey, 1986; Mumford, 1989; Niem and Niem, 1985; Olbinski, 1983; Peterson, 1984).

SANDSTONE OF WHALE COVE

Nomenclature

The informal name "Sandstone of Whale Cove" was first proposed by Snavely et al. (1973) for a sequence of sandstones and siltstones between the Depoe Bay and Cape Foulweather basalts. Although this sedimentary unit was originally mapped and described by Snavely and Vokes (1949) as Astoria Formation, they noted in their report that these "upper Astoria" strata (Sandstone of Whale Cove of Snavely et al., 1973) were dissimilar to Astoria Formation mapped elsewhere because "upper Astoria" strata were slightly younger (Relizian), interbedded within middle Miocene basalt, and impoverished in fossils.

In Snavely et al.'s (1973) article on the Miocene tholeiitic basalts of coastal Oregon and Washington, the newly introduced informal Sandstone of Whale Cove was briefly described as "a sparsely fossiliferous massive marine sandstone and thin-bedded siltstone of middle Miocene age..." between the Depoe Bay and Cape Foulweather basalts at Depoe Bay. An accompanying geologic map showed the sedimentary unit as a discontinuous series of exposures from Boiler Bay southward to Whale Cove in the Newport embayment.

Snavely and Wagner (1976) illustrated the outcrop pattern of the Sandstone of Whale Cove again on their geologic map of the Cape Foulweather and Euchre Mountain quadrangles, Lincoln County, Oregon. The unit is described in greater detail on the legend of this map, and was reported to be fine- to coarse-grained massive to thick-bedded, concretionary, arkosic sandstone and thin-bedded micaceous carbonaceous siltstone. The sandstone commonly displays cross-bedding, large-scale

load casts, convolute bedding and slump structures. The geologic cross section that accompanied Snavely et al.'s (1976) map depicts the Sandstone of Whale Cove as approximately 100 m of seaward-dipping sandstone, interstratified between pillowed Depoe Bay Basalt and brecciated subaerial Cape Foulweather Basalt. The contact relationships between these basalts and the Sandstone of Whale Cove are also discussed in a field trip guide to the geology of the west-central part of the Oregon Coast Range by Snavely et al. (1980).

Two students working under the direction of Dr. Alan Niem of Oregon State University have also noted the Sandstone of Whale Cove. Goodwin (1973) mapped the unit during his Masters project on the stratigraphy and sedimentation of the Yaquina Formation. Cooper (1981), during his regional reconnaissance of the Astoria Formation, also reported and briefly described these same exposures as Sandstone of Whale Cove.

Strata assigned to the Sandstone of Whale Cove in the Tillamook embayment (this study) have been previously mapped and described by other workers. In 1967, Mangum mapped sandstone outcrops on top of "Columbia River Basalt" (Tcr on her map) southeast of Netarts Bay and assigned them to the Astoria Formation. Later, Schlicker et al. (1972) reassigned these same sandstone exposures to Quaternary unconsolidated surficial deposits of silty sand (SS on their map) overlying "Miocene volcanic rocks". Cooper (1981), in his reconnaissance investigation of the Astoria Formation in Oregon, did not include these sandstones within his Astoria strata in the Tillamook embayment, nor did he delineate their outcrop pattern on his map. The most recent published geologic map covering the thesis area depicts this sandstone between Depoe Bay Basalt and Cape Foulweather Basalt and is designated as marine sandstone (Tms

in Figure 4) equivalent to the Sandstone of Whale Cove of Snavely et al. (1973) (Wells et al., 1983).

In this study the Sandstone of Whale Cove has been extended into the present study area from its nearest exposures at Boiler Bay 56 km to the south primarily on the basis of its similar lithology, depositional environment, and stratigraphic position between the Depoe Bay and Cape Foulweather basalts. However, the Sandstone of Whale Cove is mapped in this investigation between two formations of the Columbia River Basalt Group, the Grande Ronde Basalt and Frenchman Springs Basalt, geochemical equivalents to the Depoe Bay and Cape Foulweather basalts, respectively (Snavely et al., 1973).

Distribution

The Sandstone of Whale Cove (Twc on Plate I) covers approximately 8 square kilometers of the study area and is exposed in a discontinuous series of erosional remnants perched high atop the erosionally resistant Grande Ronde Basalt. Northeast of Oceanside, the Sandstone of Whale Cove is mapped on two ridge tops, separated by the deeply incised Short Creek. A northwest-trending Short Creek fault is projected down the Short Creek drainage, bringing the Sandstone of Whale Cove up on the north side of the fault. East and south of the campground within Cape Lookout State Park, the unit is exposed on separate ridgetops isolated from one another by stream canyons that include Austin and Jackson Creeks.

Northern exposures of the Sandstone of Whale Cove in the vicinity of Cape Meares dip northward from 9 to 22 degrees; southern exposures in the vicinity of Cape Lookout dip westward from 8 to 35 degrees. These

attitudes are generally concordant with those of the underlying Grande Ronde Basalt (Plate I). The Sandstone of Whale Cove forms a part of the dip slope that characterizes the top of the Grande Ronde Basalt.

Exposures of the Sandstone of Whale Cove are rare because the nearly unconsolidated unit is easily eroded and is almost universally obscured by thick scrubby coastal vegetation. However, an excellent exposure of the Sandstone of Whale Cove and its upper contact with the Frenchman Springs Basalt, occurs at locality O-109 (southeast quarter sec. 19, T. 1 S., R. 10 W.). Additional exposures showing sedimentary structures and representative lithologies of the Sandstone of Whale Cove include locality O-108 (northeast quarter sec. 30, T. 1 S., R. 10 W.) and locality CL-85 (northeast quarter sec. 31, T. 2 S., R. 10 W.).

Lithology and Sedimentary Structures

The Sandstone of Whale Cove is moderately indurated to friable. It is poorly indurated, loosely packed, and unconsolidated near its upper contact with the Frenchman Springs Basalt. Minor iron oxide cements are common and typically concentrated along weathered micaceous (oxidized biotite) bedding planes. Rare leisegang banding and common iron-staining are also present in most exposures. Weathered exposures of the Sandstone of Whale Cove typically are dark yellowish orange (10 YR 6/6) to very pale orange (10 YR 8/2) in color. However, fresh exposures free of iron stain range from light gray (N 8) to white (N 9). At its upper baked contact with the Frenchman Springs Basalt, the sandstone is medium gray (N 4) (locality O-109; southeast quarter sec. 19, T. 1 S., R. 10 W.).

Primary sedimentary structures in the Sandstone of Whale Cove are predominately micaceous parallel laminations (3 mm to 1 cm) in sandy

siltstones near the lower contact (Figure 95). These laminations grade to low angle (< 15 degrees) thin-bedded sets of trough cross-bedded (1 cm to 3 cm) micaceous fine-grained sandstone. The cross beds are approximately 50 cm in amplitude, 1 m to 2 m in cross section, and are cut by low angle truncation surfaces (e.g., locality O-108, northeast quarter sec. 30, T. 1 S., R. 10 W.; Figure 96). The cross-bedded intervals have well developed synforms and rare antiformal hummocks. Individual laminae thicken and thin laterally, and flatten upward within each set of cross-strata. Convoluted laminae are also present and truncated by overlying cross-bedded sandstone (e.g. locality CL-85, northeast quarter sec. 31, T. 2 S., R. 10 W.; Figures 95 and 97). These sedimentological characteristics suggest that the parallel laminated and trough cross-stratified sandstones of the Sandstone of Whale Cove may comprise an amalgamated hummocky cross stratified sequence similar to that described by Dott and Bourgeois (1982). Figure 22, from Dott and Bourgeois' (1982) paper, shows various types of hummocky cross stratified sequences. The amalgamated sequence of "truncated contortions" in this figure lacking shell and pebble lags and mudstone interbeds, most closely characterizes the sequence observed in the Sandstone of Whale Cove in the thesis area.

Petrography

Classification and Mineralogy

Four thin sections of the Sandstone of Whale Cove were examined under the petrographic microscope, and two of these underwent a 400 point modal analyses (Appendix V). The results were plotted on Folk's (1968) ternary diagram for sandstone classification (Figure 98). This

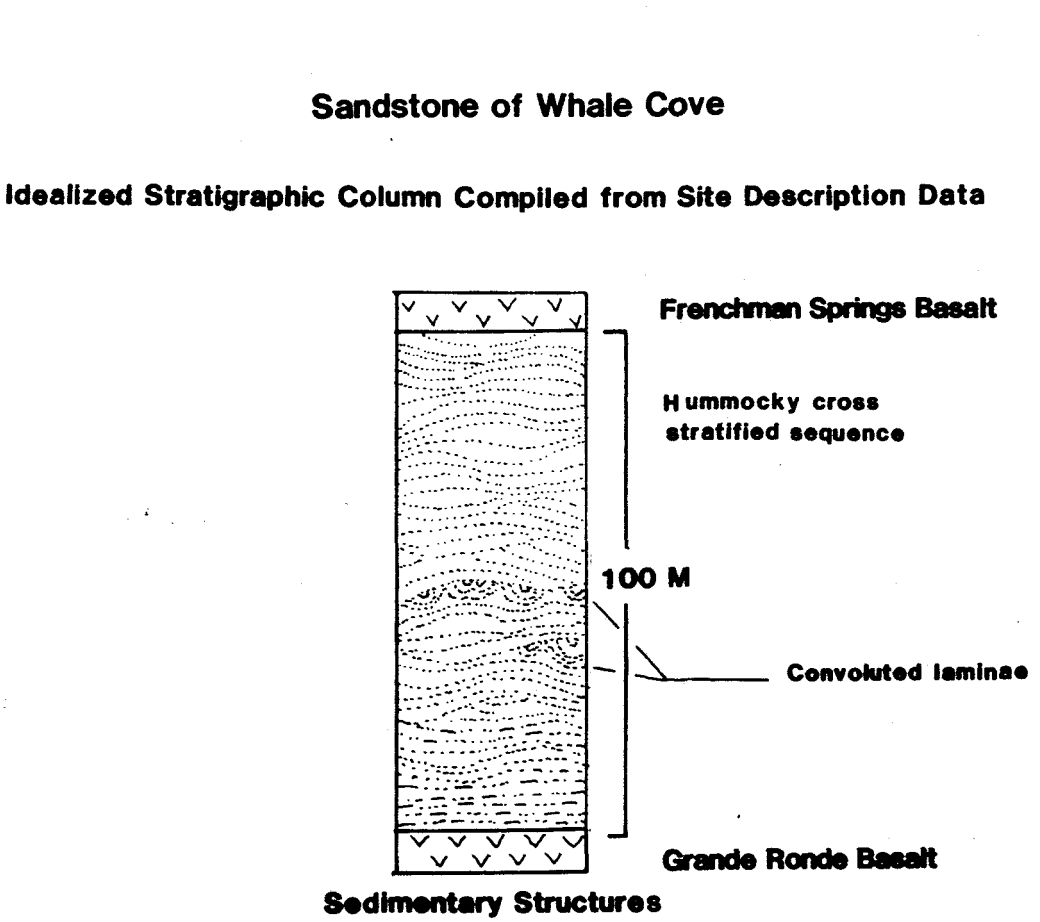

Figure 95. Stratigraphic section of the Sandstone of Whale Cove showing major lithologies and facies. Compiled from site description data.

Figure 96. Hummocky cross-stratified fine-grained sandstone of the Sandstone of Whale Cove (locality CL-88). Preserved antiformal hummock is pictured to left of notebook.

Figure 97. Close-up view of truncated convolute laminae in hummocky cross-stratified fine-grained sandstone of the Sandstone of Whale Cove (locality CL-88).

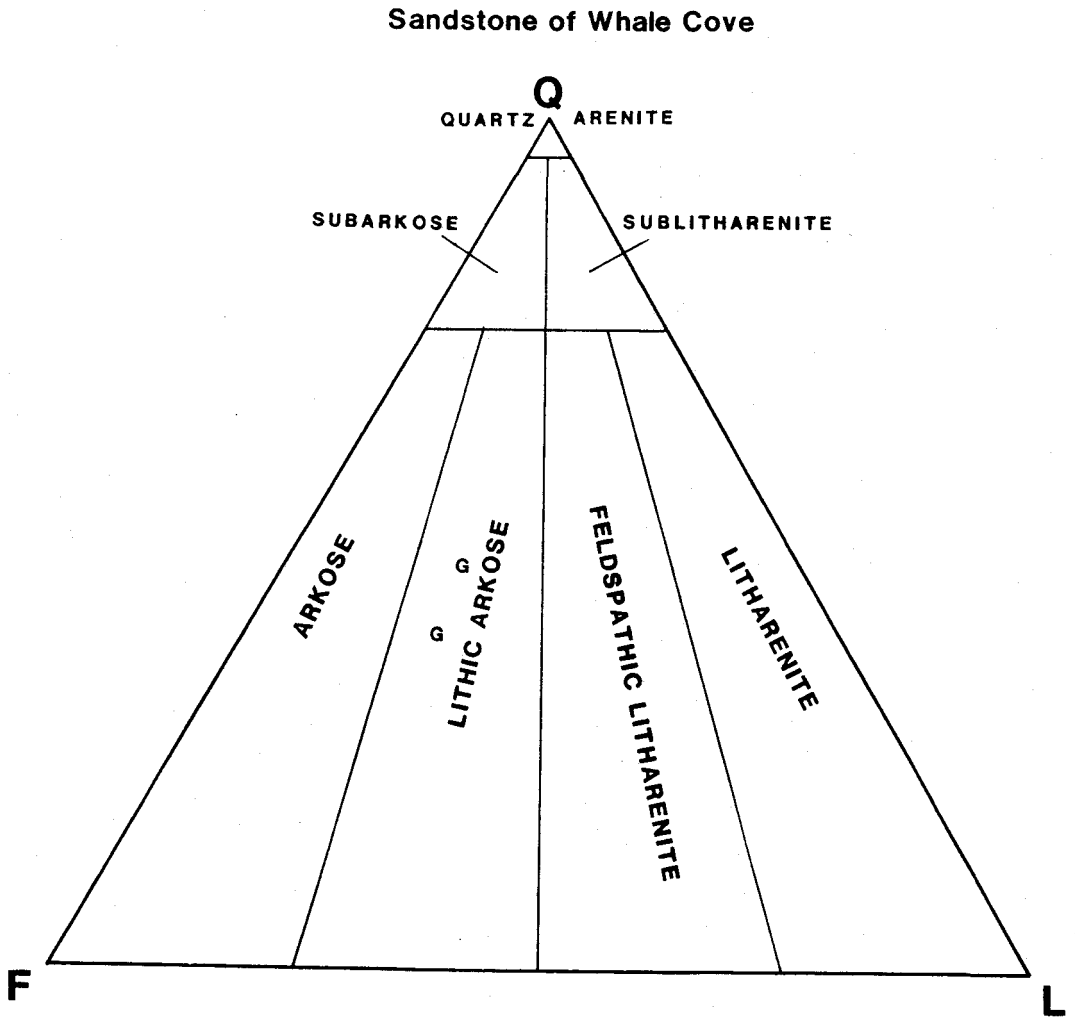

Figure 98. Sandstone classification ternary diagram showing the position of two samples of Sandstone of Whale Cove (G; 400-point modal analysis). End member corners are quartz (Q), feldspar (F), and lithic fragments (L). Modified after Folk (1968).

analysis indicates that the unit is a lithic arkose composed primarily of fresh to slightly altered siliciclastic framework grains dominated by quartz (32-40 percent), feldspar (30-34 percent), and mica (8-11 percent). Lithic fragments account for 16 percent of framework grains (Appendix V; Figure 99).

Modal analyses reveal that strained monocrystalline quartz is more abundant than polycrystalline quartz (20 percent vs. 12 percent respectively), and biotite is slightly more abundant than muscovite (10 percent vs. 7 percent). Orthoclase is the most abundant feldspar, averaging 17 percent of all framework grains, followed by altered untwinned plagioclase (9 percent) and albite-twinned plagioclase feldspar (5 percent), and unaltered microcline (2 percent). Albite twinned plagioclase grains are generally too fine-grained and altered to determine reliable An compositions. Trace amounts of myrmekite were found in sample O-108. Altered "basaltic" rock fragments are the most abundant type of lithic fragment comprising eight percent of the total framework grains, followed by metamorphic rock fragments (phyllite, schist, and quartzite, six percent), granitic rock fragments (two percent), and sedimentary rock fragments (one percent).

Heavy Minerals

Minor framework constituents include heavy minerals (3-8 percent) and glauconite (0-2 percent). A detailed heavy mineral analysis was performed on four samples of the Sandstone of Whale Cove (appendix VII) with minerals > 2.94 s.g. separated from lighter minerals using 1,1-2,2 tetrabromoethane (Figure 100). The heavy mineral populations are dominated by subequal amounts of amphibole and epidote-group minerals,

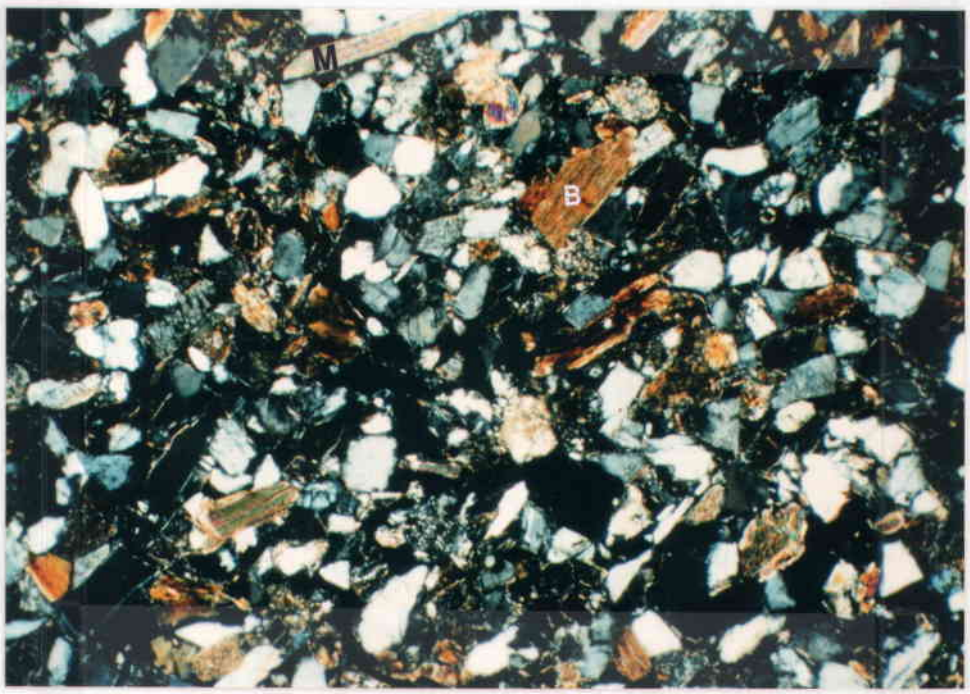

Figure 99. Photomicrograph of sandstone from the Sandstone of Whale Cove. Sandstone is very fine- to fine-grained, well-sorted, and composed of subangular abundant monocrystalline quartz, abundant muscovite (M) and biotite (B) mica, and subordinate plagioclase and orthoclase (unstained) feldspar. Note the thin birefringent clay-rim cement that lines many grain boundaries and the deformed biotite plate in center of photo. Field of view 3.3 mm. Crossed nicols; sample O-108.

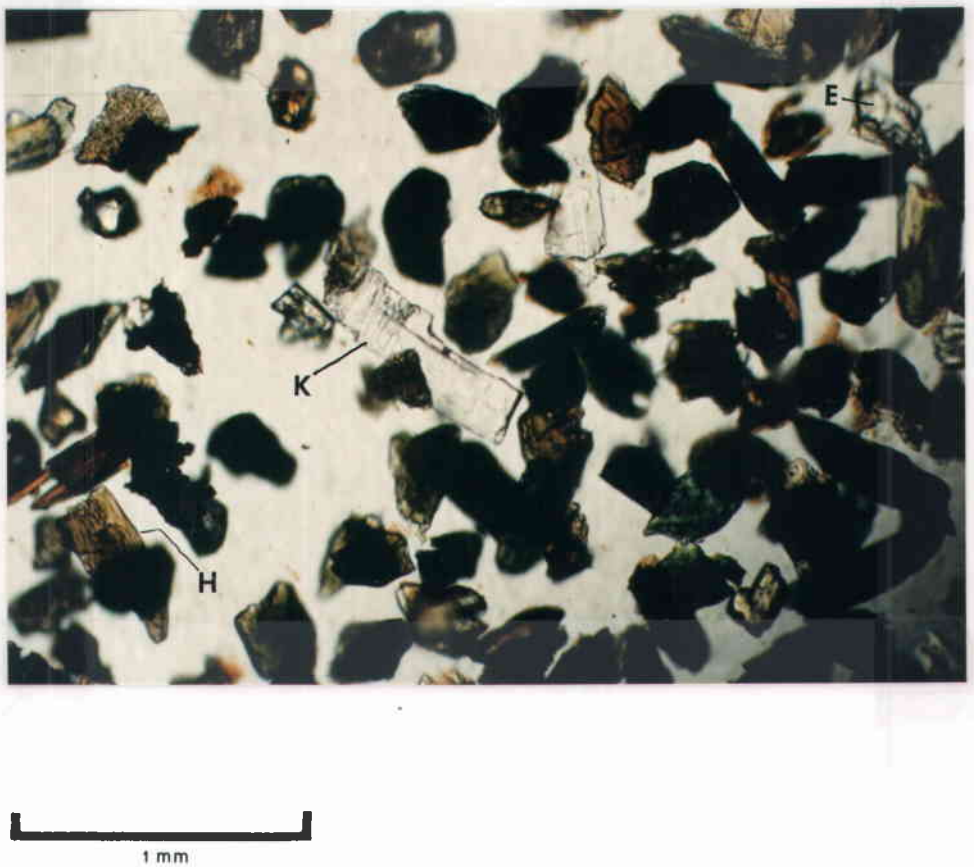

Figure 100. Heavy minerals from sandstones of the Sandstone of Whale Cove with abundant hornblende (H), epidote (E), and rare kyanite (K). Field of view 3.3 mm.

(which account for 77 percent of all non-opaque heavy minerals), followed by brown biotite (seven percent), zircon (four percent), enstatite and augite (three percent and one percent respectively), schorlite (black tourmaline; three percent), kyanite (two percent), and clear garnet (one percent). The provenance significance of both heavy and light framework minerals of all sedimentary rock units is discussed in depth in the provenance section of this thesis.

Compositional and Textural Maturity

Thin section examination and textural analyses reveal that the Sandstone of Whale Cove is a moderately to very well-sorted, silty sandstone and fine- to medium-grained sandstone with angular to subrounded grains and little or no detrital clay matrix. These characteristics indicate that the unit is texturally submature to mature (Folk, 1951). A textural fabric is imparted to the rock by aligned mica and other elongate detrital grains.

The Sandstone of Whale Cove is compositionally immature (Folk, 1951) based primarily on the presence of unstable volcanic rock fragments, which form 11 percent of the framework grains. The compositional immaturity of the unit suggests that chemically unstable rock fragments were rapidly eroded from mountainous provenances and quickly deposited (Folk, 1951). The survival of chemically unstable rock fragments from the source terrain to the basin of deposition indicates that physical weathering processes were more significant than chemical weathering processes (Folk, 1951).

Diagenesis and Diagenetic History

Point counted porosity in the Sandstone of Whale Cove averages approximately 12 percent and includes both reduced primary interparticle porosity and rare secondary porosity created by dissolution of select plagioclase feldspar grains. Smectite (?) clay rim cement accounts for most of the reduction of pore space, ranging from six to 20 percent. Chlorite cement is present as well, but only in trace amounts. Hematite cement is also common ranging from five to 16 percent and is precipitated on top of earlier cements, representing the final stage of cementation during diagenesis or surficial weathering. These cements were probably created during alteration of iron- and magnesium-rich mafic volcanic rock fragments and unstable minerals (e.g. hornblende) during diagenesis.

The diagenetic history of the Sandstone of Whale Cove probably proceeded as follows. Alteration of mafic rock fragments began early in the diagenetic history and contributed ions to pore fluids. These ions reprecipitated in the form of early smectite (?) and chlorite clay-rim cements which reduced primary interparticle porosity. As compaction continued, earlier-formed clay rims were broken. Later, the chemistry of pore fluids changed, and dissolution of some calcic plagioclase grain cores created a small amount of intraparticle secondary porosity. The final stage of diagenesis was precipitation of telogenetic hematite cement over other cements; this stage may have occurred after uplift of the unit into the vadose weathering zone where iron, liberated by continuing alteration of mafic volcanic rock fragments and unstable iron-bearing minerals, was oxidized to form the iron oxide cement.

The presence of clay rim cements and evidence of mechanical crushing indicate that the Sandstone of Whale Cove may have been buried as shallow as 300 meters, or as deep as 1300 meters (Galloway, 1979; Figure 28).

Age and Correlation

Although no fossils were collected from the Sandstone of Whale Cove, the age of the unit is well constrained by the radiometric ages of the Grande Ronde Basalt and Frenchman Springs Basalt, which bound the Sandstone of Whale Cove on the bottom and top, respectively. Because the upper contact of the Sandstone of Whale Cove is baked by the overlying Frenchman Springs Basalt, the minimum age of the sedimentary unit must match that of the basalt, which is dated as 13.6 to 14.5 my (Swanson et al., 1979; Mangan et al., 1986).

The maximum age of the Sandstone of Whale Cove is not as well constrained as the minimum age. However, because the unit overlies N2 high Mg flows of the Grande Ronde Basalt (Plate I), the Sandstone of Whale Cove can be no older than 16.5 my (Swanson et al., 1979; Mangan et al., 1986). Thus, the Sandstone of Whale Cove is a middle Miocene unit (Figure 10). A time correlative unit of the Sandstone of Whale Cove is the Vantage Sandstone of eastern Oregon and Washington (Armentrout et al., 1983).

Depositional Environment

Heavy mineral, textural, petrographic, and provenance analyses indicate that the Sandstone of Whale Cove was deposited as a coarsening-upward sequence in a storm-wave-dominated open middle to

inner shelf environment. Sediment was supplied, in part, by an ancestral Columbia River that delivered abundant arkosic micaceous sand to the nearshore environment, which was subsequently reworked and redistributed by ocean currents. The Sandstone of Whale Cove marks a time of strand progradation, possibly associated with regional uplift or shelf aggradation. This shallowing upward sequence is characterized by a transition from parallel laminated micaceous siltstone deposited below storm wave-base under relatively quiet fair-weather conditions to thick-bedded amalgamated hummocky cross stratified fine- and medium-grained sandstones representative of a storm- wave-dominated lower shoreface environment (Dott and Bourgeois, 1982; Walker, 1984). Because no fossils were found in the Sandstone of Whale Cove, this interpretation is based primarily on sedimentary structures, as well as lithology and textural characteristics. A full discussion of provenance and textural analyses of all sedimentary units including the Sandstone of Whale Cove is provided under the headings of "provenance" and "textural analyses" within this thesis.

The characteristics of fine grain size, abundant carbonaceous plant matter, parallel laminations, and high mica content of sandy siltstone typical of the lower part of the Sandstone of Whale Cove are compatible with relatively fair-weather conditions below storm wave-base, in an environment similar to the prodelta seaward of a wave-dominated delta described by Balsley (1982; Figure 57). Sediments deposited in this environment consist of extensive blankets of parallel laminated siltstone and abundant carbonaceous detritus deposited from suspension, which, presumably would also be enriched in mica flakes, as these minerals are hydrodynamicly unstable in the foreshore or upper shoreface

environment (Dott and Bourgeois, 1982). Sediment was supplied by either the ancestral Columbia River which carried suspended material to the sea, or from remobilized fine-grained sediment initially deposited above storm wave base during fair weather and resuspended during subsequent storm wave activity (Balsley, 1982) and subsequently deposited below storm wave-base.

Although the prodelta deposits associated with wave dominated deltas tend to be extensively bioturbated (Tankard and Barwis, 1982; Hubert et al., 1972; Heward, 1981), Balsley (1982) suggested that bioturbation in these environments can range from weak to intense depending on the rate of sedimentation. If this is the case, a high rate of sedimentation is indicated within the lower Sandstone of Whale Cove by a complete lack of bioturbation.

The upper two thirds of the Sandstone of Whale Cove is dominated by a thick package of amalgamated hummocky cross stratified fine- to medium-grained sandstones (Figures 95 and 96) characteristic of deposition in a storm wave-dominated lower shoreface environment (Dott and Bougeois, 1982). The sequence of hummocky cross-stratification in the Sandstone of Whale Cove lacks fairweather mudstone interbeds and bioturbated or ripple-laminated zones, and is characterized by truncated convolute laminae and common synformal and rare antiformal structures (Figure 95). Similar sequences from the Cape Sebastian Sandstone of southwestern Cape Sebastian, Oregon and the Sandstone of Floras Lake, Cape Blanco, Oregon, were interpreted by Dott and Bourgeois (1982) to indicate deposition on a continental shelf environment subjected to frequent vigorous storm wave activity and high sedimentation rates (Figure 22, "truncated contortions"; Figure 58). Presumably, frequent

large storm waves caused enough agitation of the bottom sediment to eliminate any traces of fairweather sedimentation or bioturbation in the Sandstone of Whale Cove, creating a thick uniform sequence devoid of all but storm weather deposits.

Hummocky cross-stratified sands were probably introduced into the relatively deep, lower energy environment of the lower shoreface by storm-dominated surges or tsunamis (Walker, 1984; Dott and Bourgeois, 1982). Walker (1984) and Dott and Bourgeois (1982) suggest that sand can be transported to the shelf in several ways which include: relaxation return flow from storm surges (described in detail in the Smuggler Cove depositional environment section, Figure 13); storm rip-currents; tsunamis; wind drift currents; density currents; river floods. Ebb tidal deltas may be an additional mechanism for delivering sand outside the "littoral energy fence". These mechanisms may generate shelf turbidites which are reworked above storm wave base to the extent that their Bouma structures have been overprinted by storm wave-induced sedimentary structures (Walker, 1984). Sand may have been supplied to the lower shoreface from either a flooding river or from scour of nearshore sand deposits. This sand was delivered to the shelf by one of the aforementioned processes and deposited from suspension under oscillatory flow conditions during storm wave activity, which created the hummocks and swales that typify the hummocky cross-stratification bedform (Dott and Bourgeois; 1982).

Because modern storm wave activity off the coast of Oregon is capable of stirring sediment to a water depth of up to 200 m (Kulm et al., 1975), the hummocky cross-stratified deposits of the Sandstone of

Whale Cove may represent depths of sedimentation as great as 200 m or as shallow as only a few meters (Dott and Bourgeois, 1982).

Contact Relationships

The lower contact between the Sandstone of Whale Cove and the Grande Ronde Basalt is nonconformable and well exposed in only two locations. Both are inaccessible cliff exposures adjacent to basalt gravel quarries (locality SNB 151, southeast quarter sec. 29, T. 2 S., R. 10 W.; quarry in southwest corner section 20, T. 2 S., R. 10 W.).

The upper contact between the Sandstone of Whale Cove and the Frenchman Springs Basalt is nonconformable and exposed at only one location (locality O-109, southeast quarter sec. 19, T. 1 S., R. 10 W.). Basalt at the contact is brecciated and a 10 cm thick light gray baked sandstone directly underlies the subaerial (?) basalt.

Frenchman Springs Member of the Wanapum Basalt

Frenchman Springs Basalt Chemistry

Outcrops of the plagioclase-phyric Frenchman Springs member of the Wanapum Basalt (Tfs on Plate I) are rare in the Tillamook embayment, and the unit was found in place at only one location northeast of the town of Oceanside (locality CFW on Plate I, southeast quarter sec. 19, T. 1 S., R. 10 W.). The two other small outliers of this unit located atop the basalts that flank southern Netarts Bay (northwest quarter sec. 29, T. 2 S., R. 10 W.; northeast quarter sec. 6, T. 3 S., R. 10 W., Plate I), were mapped solely on the presence of diagnostic plagioclase-phyric basalt float (Snavely, written communication, 1989; Wells, personal communication, 1988; this study). As a result of the relative rarity and lack of exposure of Frenchman Springs Basalt, only two samples of this unit were collected from the thesis area, and both were submitted for geochemical analysis to verify the assignment of this basalt to the Frenchman Springs member (sample localities: CFW, southeast quarter sec. 19, T. 1 S., R. 10 W.; SNB-162, northwest quarter sec. 29, T. 2 S., R. 10 W.).

Major and trace element geochemical analyses of samples CFW and SNB-162 were performed at Dr. Peter Hooper's XRF lab at Washington State University, Pullman, on the Rugaku X-ray fluorescence machine (Appendix IX). The results were subsequently subjected to the same normalization factors as Grande Ronde Basalt analyses of this study in order to bring all geochemical data run on the Rugaku XRF machine into parity with the older results of previous Columbia River Basalt studies run on Peter Hooper's Phillips XRF machine. A complete discussion of the purpose for

these normalization factors, as well as their implementation, is in the Grande Ronde Basalt section.

Geochemistry of Frenchman Springs Basalt Flows of the Tillamook Embayment

The normalized geochemical data of this study was plotted on the silica variation diagrams of Snavely et al. (1973) to determine which flows of the CRBs occur in the Tillamook embayment (Figure 87). The results reveal that samples CFW and SNB-162 plot within or near the fields designated for the Frenchman Springs Basalt, indicating that the uppermost flows of basalt in the study area represent the Frenchman Springs member of the Wanapum Basalt. The geochemistry of Frenchman Springs basalts is generally distinguished from Grande Ronde Basalt by a lower SiO_2 content, and higher TiO_2 and P_2O_5 contents (Swanson et al., 1979).

Recently, Beeson et al. (1985) proposed a six-fold flow unit nomenclature for the Frenchman Springs member on the basis of stratigraphic position, petrographic characteristics, lithology, and each unit's varying P_2O_5, TiO_2, MgO, and chromium contents (Table 2). In order to determine which unit of the Frenchman Springs member occurs in the Tillamook embayment, vertical lines representing the chemistries of samples CFW and SNB-162 have been superimposed upon Table 2 for comparison with select major and minor elements of each unit. The results show that the Frenchman Springs Basalt flows of the Tillamook embayment are most similar to Ginkgo, Silver Falls, and Sentinal Gap flow units, and distinctly different from the Sand Hollow, Palouse Falls, and the Lyons Ferry units. However, because the Sentinal Gap and

Table 2.

Table showing selected compositional variations among units of the Frenchman Springs Member. Bold vertical lines represent samples CFW (solid line) and SNB-162 (dashed). Unit most closely matching the chemical composition of these two samples is stippled. Table modified after Beeson and Tolan (1985).

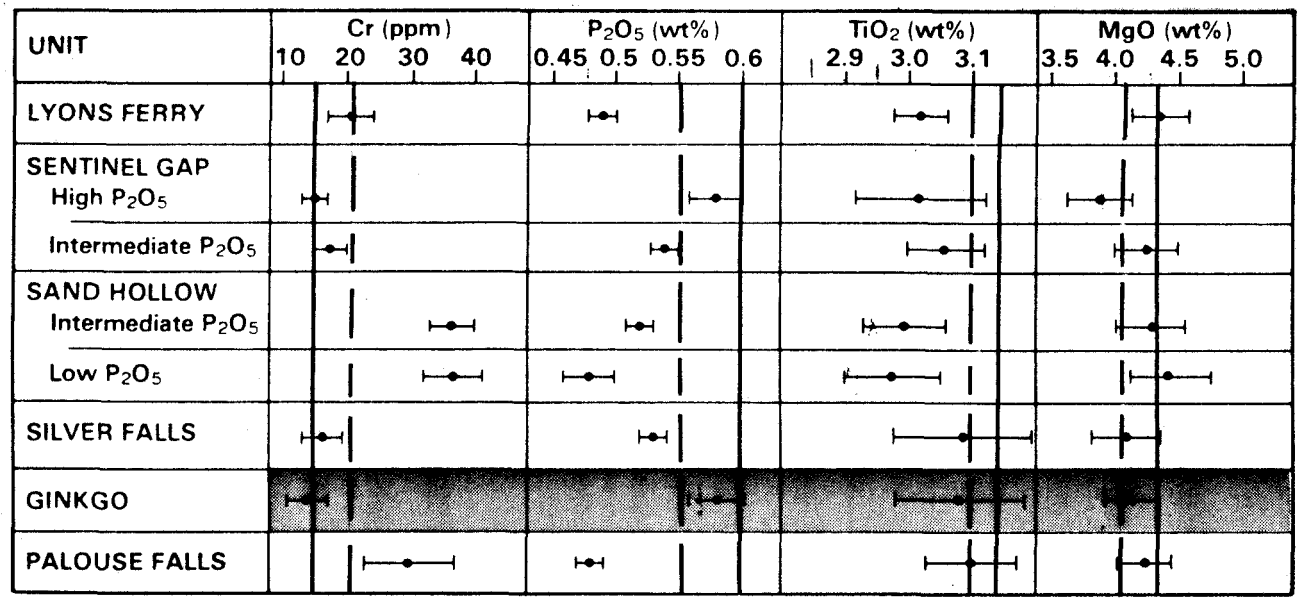

Silver Falls Units are relatively aerially restricted (e.g. eastern Oregon and Portland Oregon area), and only the Sand Hollow and Ginkgo units have been found west of the Oregon Coast Range (Figure 101; Beeson et al., 1985; Niem and Niem, 1985; Goalen, 1988; Murphy, 1981), the Frenchman Springs Basalt flows in the thesis area probably represent Ginkgo Unit basalt. In addition, the moderately plagioclase-phyric Frenchman Springs basalt samples of the study area are similar to the Ginkgo Unit which is reported by Beeson et al. (1985) to be phyric to abundantly phyric, and contrast with the rarely to sparsely plagioclase-phyric Sentinel Gap Unit (Beeson et al., 1985).

Magnetostratigraphy

The magnetic polarity of one oriented basalt sample (sample CFW) was analyzed in the lab with a fluxgate magnetometer, and was positive (Appendix X). This agrees with the polarity of the Frenchman Springs Basalt mapped on the Columbia Plateau, which is normal to excursionary (Figure 83; Swanson et al., 1979), and supports assignment of the uppermost basalt flows in the Tillamook embayment to this rock unit.

Distribution

The Ginkgo Unit of the Frenchman Springs member of the Wanpum Basalt is mapped in three widely separated locations atop the basalt-capped mountains that flank Netarts Bay, east of Cape Meares and Cape Lookout (Plate I). The unit covers only approximately 0.3 km^2 of the Tillamook embayment, and exposures of the Frenchman Springs Basalt are extremely rare due to its restricted aerial extent and thick vegetative cover. However, the unit was found well exposed in a roadcut

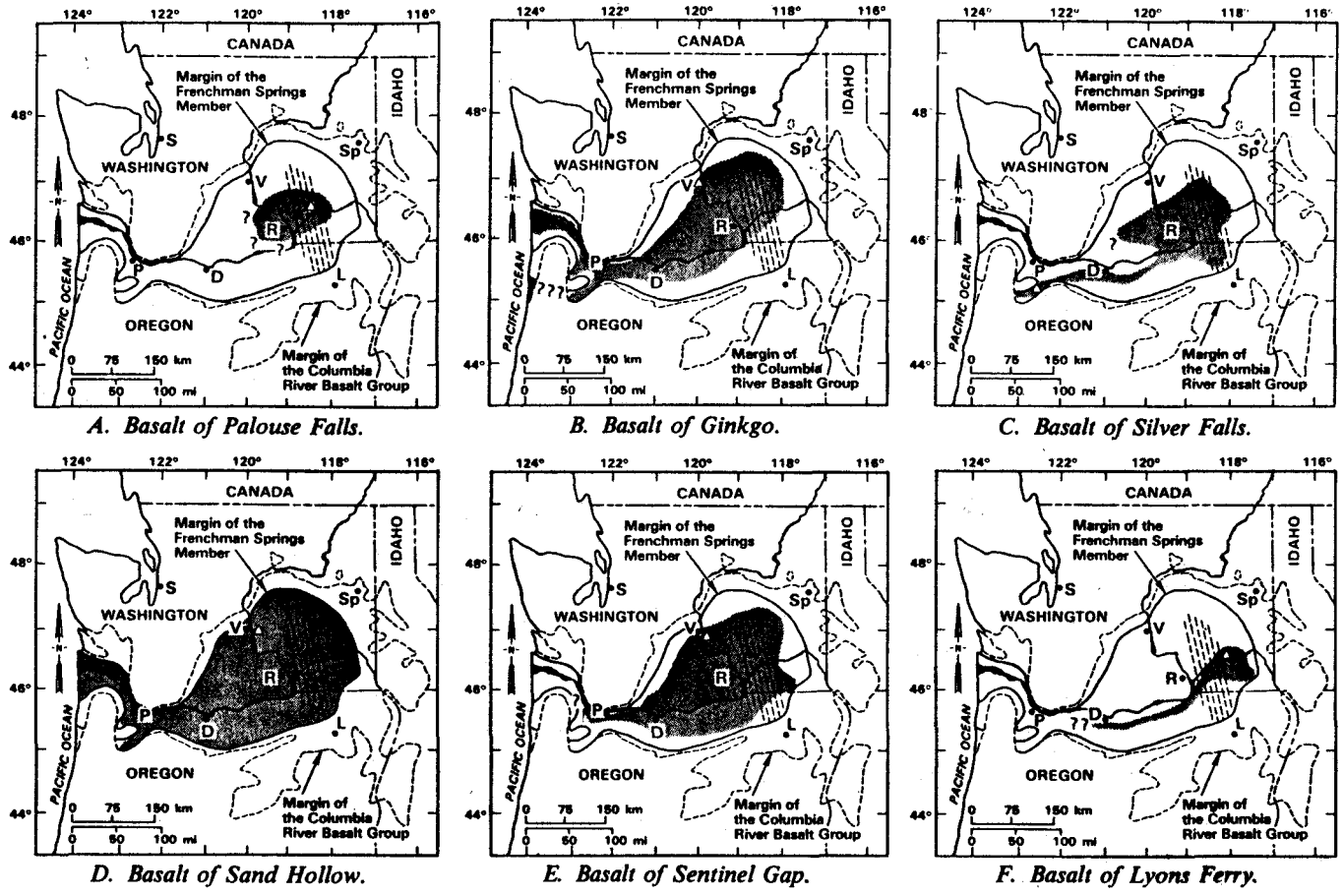

Figure 101. Maps showing the inferred original extent (shaded areas) of units of the Frenchman Springs member of the Wanapum Basalt. After Beeson and Tolan (1985).

at one locality (locality CFW, southeast quarter sec. 18, T. 1 S., R. 10 W.), and is also reported to crop out in the northeast quarter of section 6, T. 3 S., R. 10 W. (Snavely, written communication, 1989; Wells, written communication, 1989). The Frenchman Springs Basalt is also inferred to crop out in the northwest quarter of section 29, T. 2 S., R. 10 W., above the locality where diagnostic plagioclase-phyric basalt float of sample SNB-162 was collected.

Lithology

The brief discription of the lithology of the Frenchman Springs Basalt that follows is based on the only exposure of the unit found in the study area at locality CFW (O-109; Plate I).

At locality CFW and O-109 (same location) the contact between the Sandstone of Whale Cove and overlying Frenchman Springs Basalt is well exposed (Figure 102). The basalt is brecciated at the contact and overlies a one meter-thick bleached and baked zone of the Sandstone of Whale Cove. The brecciated zone grades upward over approximately 30 to 50 cm to a nonvesicular, horizontally and vertically jointed, plagioclase-phyric basalt, which is probably subaerial in origin. The thickness of Frenchman Springs Basalt exposed at locality CFW is only 2 meters. These basalts range from medium light gray (N6) to medium dark gray (N4) where fresh, and are light gray (N8) near the basalt breccia zone.

Petrography

Two thin sections of the Ginkgo Unit of the Frenchman Springs member were cut from samples SNB-162 and CFW. They are hypocrystalline,

Figure 102. Contact between the Sandstone of Whale Cove (W) and horizontally and vertically-jointed flow of the Frenchman Springs Basalt (F). Thin baked zone in sandstone is marked by light brown horizon at contact. Locality O-109.

mineralogically similar, and characterized by several igneous textures. The predominate texture is subophitic, but may be locally ophitic, intergranular, and intersertal within the same slide.

Plagioclase is the most abundant mineral in the Frenchman Springs Basalt (Figure 103), accounting for approximately 55 percent of the total mineralogy of the unit. Plagioclase microlites are both albite and carlsbad-twinned, and fairly medium-grained, ranging from 1.0 to 2.0 mm in length. The An content of select albite-twinned plagiocase crystals estimated using the Michel-Levy method (Kerr, 1979) ranges from AN_{53} to An_{59} (labradorite). Carlsbad-twinned crystals within the groundmass are occasionally continuously zoned, and some occur as rare glomerocrysts intergrown with both plagioclase and pyroxene. Plagioclase laths commonly have skeletal or ragged terminations. Plagioclase crystals also occur as large (>1 cm) phenocrysts visible in hand sample. The one observed in thin section SNB-162 is carlsbad-twinned, subhedral, and zoned, with a partially resorbed anhedral core surrounded by compositionally distinct subhedral rind (Figure 103). Relatively large plagioclase phenocrysts are a diagnostic characteristic used to distinguish Frenchman Springs Basalt from other units of the CRB group (Beeson et al., 1985; Beeson, personal communication, 1989).

Augite microlites in the groundmass compose approximately 30 percent of the Ginkgo Unit basalt (Figure 103), and range in size from 0.5 to 1.5mm. They are typically anhedral, but also occur as rare subhedral crystals. Although the augite in the groundmass frequently partially enclose plagioclase microlites, accounting for the common subophitic texture, augite may also completely enclose small laths, or occur only within the interstitial areas between plagioclase crystals.

Figure 103. Photomicrograph of Frenchman Springs Basalt showing diagnostic large (5 mm) subhedral plagioclase phenocryst in ophitic to subophitic textured groundmass composed of plagioclase microlites, green augite, and opaque magnetite/ ilmenite. Field of view is 6.7 mm. Crossed nicols; sample CFW.

Volcanic glass is also fairly common in the groundmass of samples SNB-162 and CFW. It ranges from 10 to 13 percent of the thin section, and commonly occurs as light brown sideromelane glass.

The opaques in the Ginkgo Unit groundmass are composed of magnetite and ilmenite. These minerals predominately occur as opaque amorphous blebs, but magnetite also occurs as octahedrons.

Age and Correlation

The age of the Frenchman Springs Basalt in the present study area is based on the age of correlative Frenchman Springs flows in western Oregon that yield an average radiometric K-Ar age of 15.5 m.y. (Beeson et al., 1985). Although this overlaps the range of radiometric ages for Grande Ronde Basalts, Beeson et al. (1985) do not think the two units are contemporaneous or interfingered. Instead, they consider all units of the Frenchman Springs to be younger than the Grande Ronde Basalt on the basis of field relationships, which show that the Frenchman Springs overlies, or is channeled into Grande Ronde Basalt.

A northwest Oregon correlative to the Frenchman Springs Basalt of the Tillamook embayment is the Cape Foulweather Basalt of Snavely et al. (1973), which crops out in the Newport and Lincoln City areas of western Oregon and overlies the Sandstone of Whale Cove and Depoe Bay Basalt. However, similar age and geochemistry suggest that the Cape Foulweather Basalt of Snavely et al. (1973) may also be a Frenchman Springs flow (Beeson and Tolan, in press).

Depositional Environment, Origins, and Emplacement Scenarios for Flows and Intrusions of Columbia River Basalt and Sedimentary Interbeds in the Tillamook Embayment

After deposition of the upper Cannon Beach member of the Astoria Formation, the Tillamook embayment experienced a major marine regression which may have been caused by local or regional tectonic uplift during the middle Miocene (Snavely et al., 1980; this study). This resulted in severe dissection of the lower to middle Miocene marine strata in the study area with partial removal of the Angora Peak, Netarts Bay, and Cannon Beach members of the Astoria Formation (Plate I), and establishment of an irregular topography prior to the arrival of the Columbia River Basalt flows. The section that follows describes the emplacement sequences, flow patterns, and depositional setting for each unit of the Grande Ronde and Frenchman Springs Basalts based on a synthesis of data gathered from these CRB units and their respective sedimentary interbeds in the study area.

R_2 Low Magnesium-Low Titanium Grande Ronde Basalt (Grouse Creek Unit)

The (informal) Grouse Creek Unit (R_2 low magnesium-low titanium Grande Ronde Basalt; Tgr_1 on Plate I) is one of a small group of widespread Columbia River Basalt Group flows erupted from the fissure swarms of eastern Oregon and Washington that escaped the Columbia Plateau and ancestral Willamette Valley, and flowed all the way to the middle Miocene coast (Anderson et al., 1987). Amply supplied basalt lava during eruption, this unit, and a few other Miocene coastal basalt flows were capable of reaching to the sea along the pre-existing drainage of the ancestral Columbia River, or through low points in the poorly

developed ancestral coast range of Oregon (Beeson et al., 1979; Beeson et al., 1985; Tolan, personal communication, 1989).

Figure 104 shows the distribution of upper R_2 flows of the Grande Ronde Basalt, which includes the Grouse Creek Unit (Tolan, personal communication, 1989). These flows are present in the Astoria embayment (Goalen, 1988; Murphy, 1981; Niem and Niem, 1985) and extend approximately 75 kilometers up the ancestral Willamette Valley drainage. In the emplacement scenario envisioned for the Grouse Creek and younger CRB flows in the study area, rising lava impounded in the ancestral Willamette Valley overtopped a developing low saddle in the ancestral Oregon coast range and poured westward through this gap into the Astoria and Tillamook embayments (Figure 104). This scenario is supported by the orientation of inclined pillow foresets and breccias in the Grouse Creek Unit, which indicate that these basalts were emplaced by northwestward-flowing lava deltas (Figure 105). The restriction of the Grouse Creek Unit to the northern part of the study area (Figure 105) may indicate that this region offered the path of least resistance for lava flows during this time. Alternatively, the Grouse Creek basalt may have been more widely distributed, but was subsequently eroded in the south (Cape Lookout area) prior to the arrival of the overlying Winterwater Unit (N_2 low magnesium-low titanium Grande Ronde flows).

Figure 105 contains a generalized block diagram that depicts the distribution of submarine and subaerial flows of the Grouse Creek Unit in the Tillamook embayment. The flows are generally subaerial in character in the eastern part of their outcrop area (e.g. locality 4-88, northwest quarter sec. 28, T. 1 S, R.), and foreset-bedded to closely packed pillow lava with a subaerial vesicular upper couplet in the

Distribution of the Upper R_2 Flows of the Grande Ronde Basalt

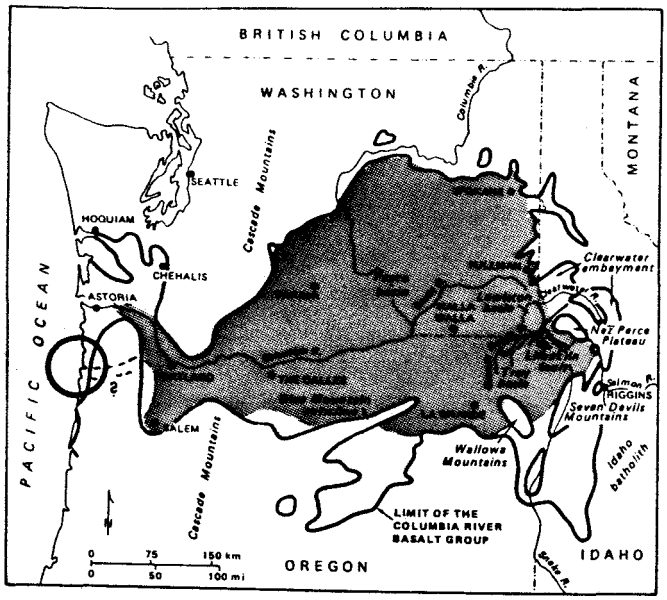

-Tillamook Embayment

Figure 104. Distribution map of the reversed flows (R_2) of the Grouse Creek and Wapshilla Ridge units of the Grande Ronde Basalt. Modified from Anderson et al. (1987).

Grouse Creek Unit

Outcrop and Dispersal Pattern for R_2 Low Mg Low TiO_2 Grande Ronde Basalt

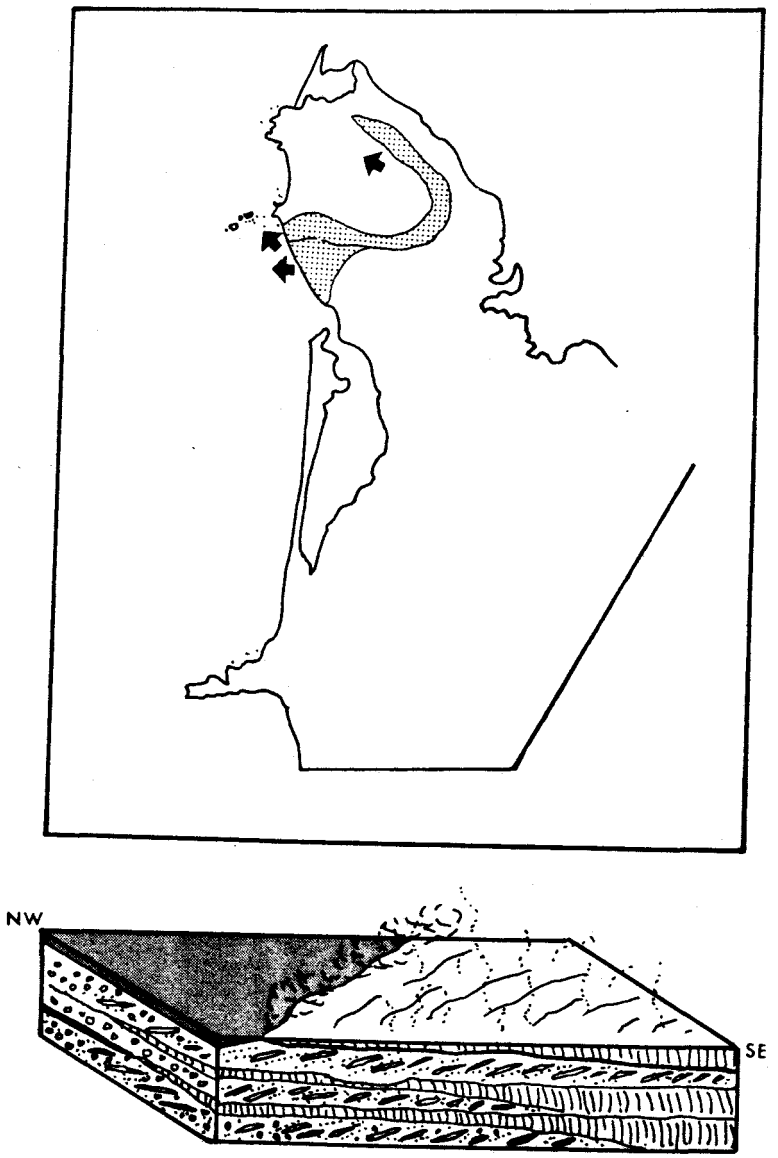

Figure 105. Outcrop and dispersal pattern for the Grouse Creek Unit of the Grande Ronde Basalt with schematic block diagram showing sequence of pillowed and subaerial flows in the thesis area. Arrows indicate direction of flow.

western coastal exposures of Grouse Creek Unit at Maxwell Point (Figure 106). Field evidence (e.g. sedimentary interbeds, lava delta couplets) suggests that one to three flows of this unit entered the study area (Figure 107) and encountered a shallow marine environment to the west. The possibilty that three flows of the Grouse Creek Unit occur in the Tillamook embayment is supported by presence of three to four flows of this unit in the northern Willamette Valley (Tolan, personal communication, 1989).

The best exposures of the Grouse Creek Unit near the village of Oceanside indicate that these flows entered the middle Miocene ocean, built a lava delta complex up to the water surface, then prograded seaward over lava tubes and inclined foreset-bedded pillow palagonite and breccia complexes (Figures 106 and 107). The shallow marine interpretation for western flows of the Grouse Creek Unit is supported by a collection of fossil gastropods (cerathid?) and oysters (Moore, written communication, 1989) taken from a sedimentary interbed between two pillowed basalt flows (locality 13-88, northwest quarter sec. 24, T. 1 S., R. 11 W.; Appendix IV). Identification and environmental interpretation of the fossils by E. Moore (personal communication, 1989) indicate that these articulated mollusks thrived in a protected very shallow marine or intertidal environment (Moore, personal communication, 1989). The fine grain size of the sediment from which the fossils were collected suggests that this carbonaceous mudstone was deposited in a marine environment sheltered from high-energy wave conditions, possibly within a cove or embayment between pillowed flow lobes of the lower Grouse Creek flow.

Figure 106. Grouse Creek Unit (R_2 low MgO-low TiO_2) of the Grande Ronde Basalt at Maxwell Point composed of closely packed pillow basalt with large radially-jointed filled lava tube (A) overlain by subaerial columnar-jointed flow couplet (B). Sequence is overlain by another pillowed flow near the top of the cliff (C).

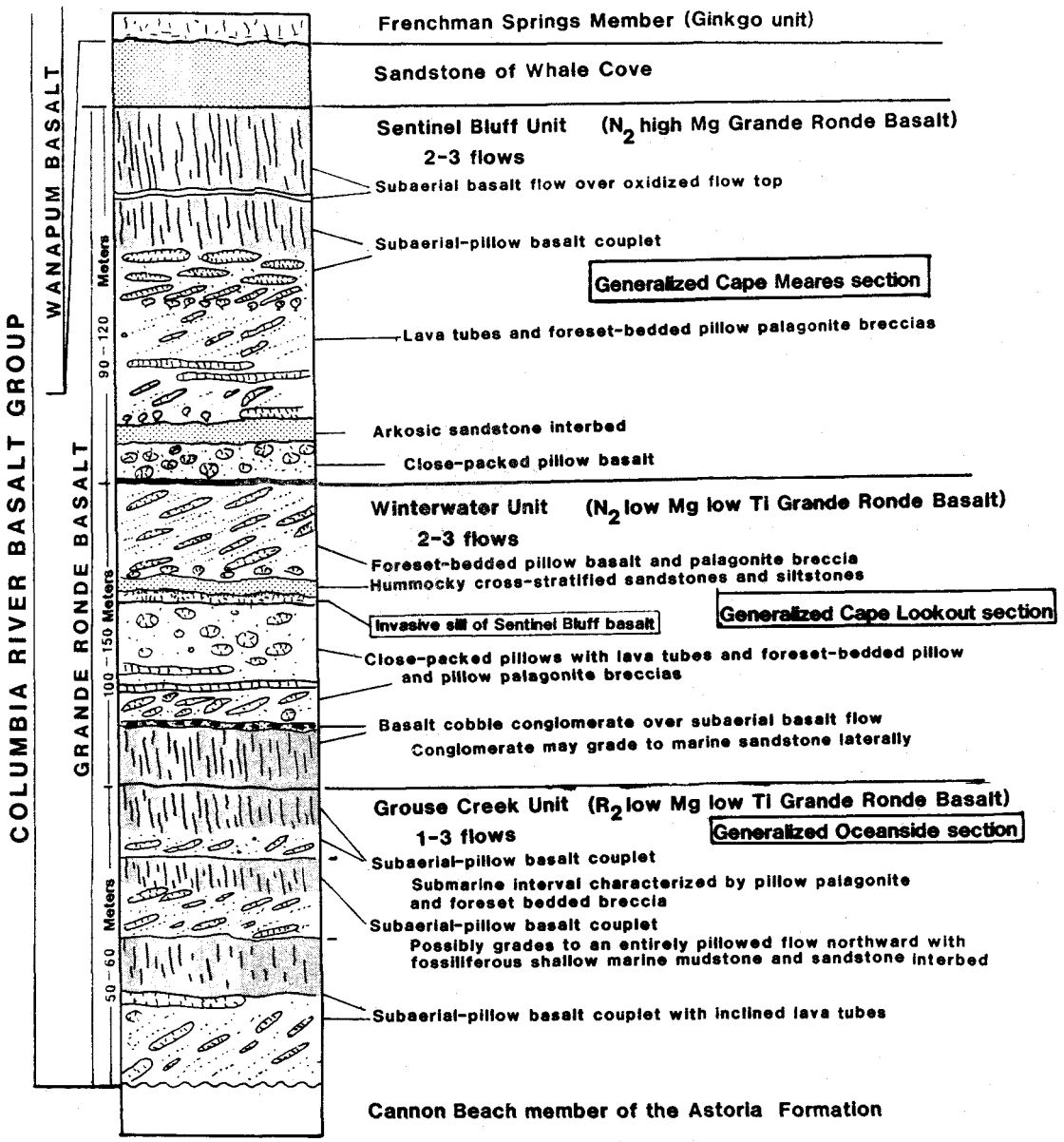

Figure 107. Composite stratigraphic section of the Columbia River Basalt flows in the thesis area compiled from coastal exposures at Cape Meares (Sentinel Bluff Unit), Oceanside Beach State Wayside (Grouse Creek Unit), Cape Lookout (Winterwater Unit), and site CFW (Frenchman Springs member).

N_2 Low Magnesium-Low Titanium Grande Ronde Basalt (Winterwater Unit)

The Winterwater Unit basalts (N_2 low magnesium-low titanium Grande Ronde Basalt; Tgr_2 on Plate I) were erupted on the Columbia Plateau after the Grouse Creek volcanic episode, but may have followed a similar path into the Tillamook embayment (Figure 108). The distribution and dispersal pattern for this rock unit (Figure 109; based on foreset breccia and inclined basalt pillows) shows that the Winterwater basalt was emplaced by 2-3 westward and northwestward-flowing lava flows which streamed into the Cape Lookout and Cape Meares areas. This field evidence supports derivation from an easterly Columbia River Plateau source rather than eruption from local coastal fissures.

At least two and possibly three individual flows of the Winterwater Unit have been identified in the Tillamook embayment (Figure 107). However, because only two flows of the Winterwater Unit have been mapped in the northern Willamette Valley (Tolan, personal communication, 1989), it is likely that the apparent third flow in the Tillamook embayment may represent a lobe of either the first or second flow as no sedimentary interbed occurs between them.

The first of these flows encountered a subaerial environment in the east (e.g. columnar jointed flows at locality CL-71, center sec. 1, T.3 S., R. 10 W.), and were probably following steep-walled channels cut into Astoria strata in the vicinity of Cape Lookout. The lower contact of the Winterwater Unit with Angora Peak member sandstones along Cape Lookout highway (locality CL-72, southwest quarter sec. 6, T. 3 S., R. 10 W.) is characterized by large, chaotically oriented blocks (up to 2-5m long) of arkosic sandstone in contact with platey and columnar-jointed basalt. These large blocks of sandstone may represent

Distribution of the N_2 flows of the Grande Ronde Basalt

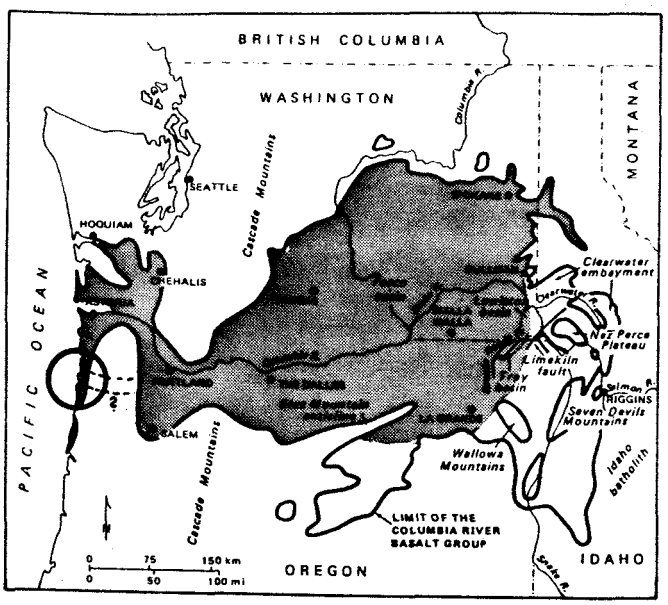

◯-Tillamook Embayment

Figure 108. Distribution map of the N_2 flows of the Grande Ronde Basalt, which include the Winterwater and Sentinel Bluff units. Modified after Anderson et al. (1987).

Winterwater Unit

Outcrop and Dispersal Pattern for N_2 Low Mg Low TiO_2 Grande Ronde Basalt

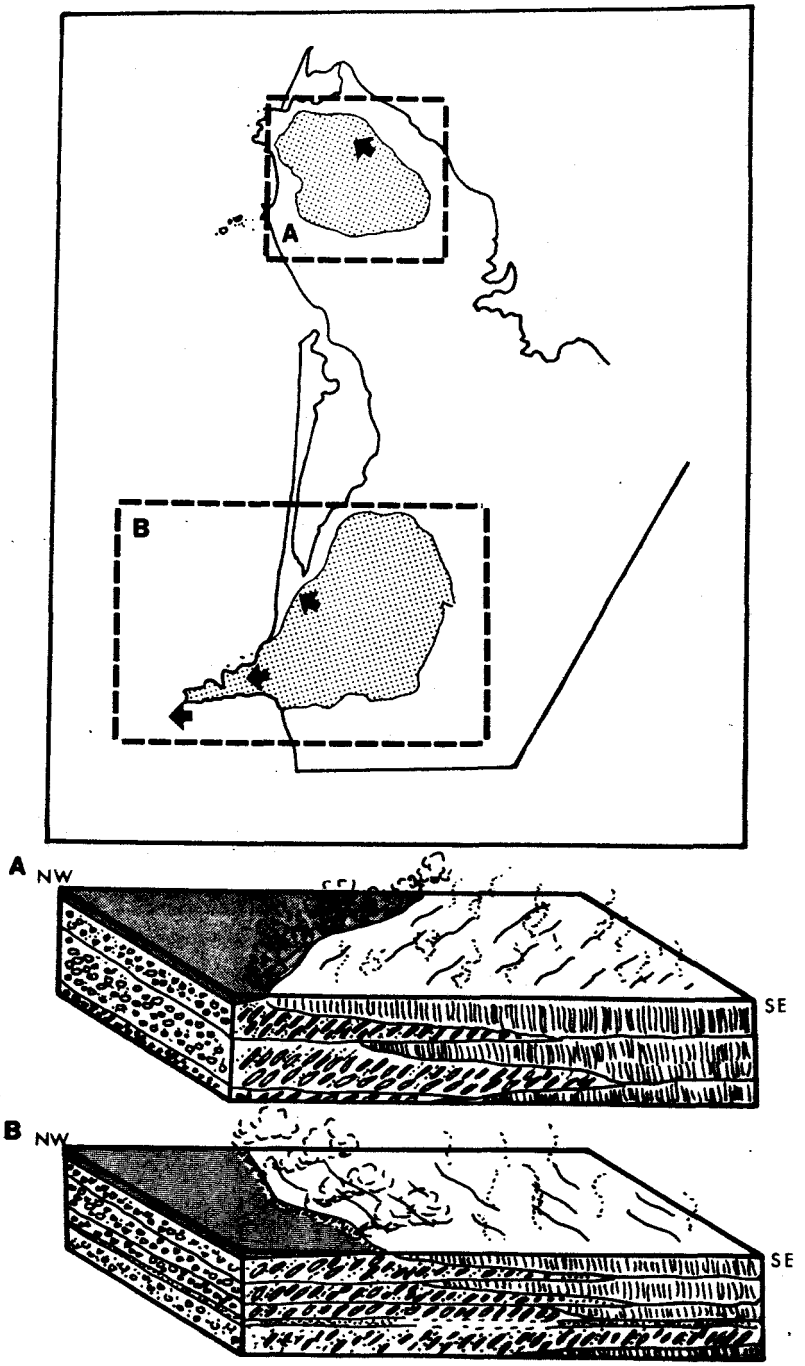

Figure 109. Outcrop and dispersal pattern for the Winterwater Unit of the Grande Ronde Basalt with schematic block diagrams showing sequence of pillowed and subaerial flows, and general flow directions in the thesis area. Arrows indicate direction of flow.

canyon wall failure blocks that formed an erosion-prone talus, preserved by basalt lava which streamed down the canyon and solidified. Alternatively, this chaotic sedimentary breccia may have been produced as a lower Winterwater basalt invasive sill intruded and steam blasted into the semi-consolidated Angora Peak strata (Niem, personal communication, 1989). Similarly steam-blasted chaotic sedimentary breccias associated with thick invasive Grande Ronde sills and dikes occur at Humbug Point, northwest Oregon (Niem, 1976; Smith, 1975). Overlying the vesicular top of the lower subaerial Winterwater flow is a thin (<50 cm) basalt cobble conglomerate (locality 70-88, center sec. 1, T. 3 S., R. 11 W.). This subrounded poorly sorted conglomerate may represent a coastal stream deposit of reworked CRB, or a winter beach lag deposit of CRB cobbles rounded by wave action. It is overlain by closely packed pillow basalt of a second Winterwater basalt flow (Wells et al., in press; Wells, personal communication; Wells, unpublished data).

After the arrival of the first flow of the Winterwater Unit, the southern part of the thesis area near Cape Lookout subsided and the strandline shifted to the east of the present location of the southern basalt pile. This is indicated by the presence of both pillowed basalt flows (e.g. locality CL-138, northeast quarter sec. 1, T. 3 S., R. 10 W.) and an overlying thick (>5 m) fossiliferous arkosic marine sandstone interbed at locality 26-88 (northeast quarter sec. 32, T. 2 S., R. 10 W.). Molluscan fossils were collected atop a pillowed basalt flow at the base of the sandstone bed and include the bivalve Spisula (Mactromeris) sp. which thrived in the marine environment in depths ranging from intertidal and 110 m (Moore, written communication, 1989). A possible

correlative sandstone interbed is also present at the tip of Cape Lookout (locality 72-89; Plate I; Figure 93). This sandstone occurs below a pillowed Winterwater basalt flow (sample 72-89B, Appendix IX and X), and is probably marine based on the presence of storm-wave produced hummocky cross-stratification (Dott and Bourgeois, 1982) and thin mudstone interbeds.

The uppermost Winterwater basalt flows in the eastern and central parts of the study area are columnar jointed and subaerial (e.g. locality SNB-156, northwest quater sec. 32, T. 3 S., R. 10 W.; 5-88, southwest quarter sec. 21, T. 1 S., R. 10 W.), while those to the west composing the upper part of Cape Lookout are pillowed. The block diagrams in Figure 109 illustrate the general distribution of pillowed and subaerial flows for the Winterwater Unit of the Grande Ronde Basalt through time and space. Figure 109-A shows that the Winterwater flows of the northern basalt pile general spread into the marine environment from the southeast, moving into deeper water to the west. Figure 109-B shows that these basalts moved generally west- and northward, encountering a marine-dominated environment to the west, with general progradation of subaerial lava deltas over thier submarine couplets.

Evidence for subsidence within the Tillamook embayment during the eruption of the Grande Ronde Basalts is plentiful, and typically comes in the form of pillowed flows over subaerial flows (Figure 107). The causes of these subsidence or transgression events may have been a response to loading and dewatering of underlying water-saturated sediment by thick overlying flows, local tectonic downwarping, middle Miocene (15.8-13.5 my) eustatic sea level rise (Haq et al., 1987), or a combination of these factors.

It should be noted, however, that each lava delta couplet does not neccessarily indicate subsidence below sea level or even a different flow event. Instead, some of these pillow or foreset breccia flow sequences may be the product of marginal-marine lakes, formed when the previous flow lobes blocked coast range streams. The lakes may have filled quickly enough such that a later lobe could move into a lake dammed by an earlier flow lobe, thus forming a foreset pillowed sequence over the subaerial flow lava delta couplet with no intervening period of subsidence. Although their existence is unlikely in the Tillamook embayment, rapidly formed marginal-marine lakes may also help to explain the rarity of sedimentary interbeds between subaerial and pillowed flows in the Tillamook embayment, as these lakes would not have the time to accumulate sediment. The lava lobe-formed marginal-marine lake hypothesis of this study is modelled after the similar hypothesis of Beeson et al. who suggested an analogous mechanism to form foreset bedded CRB flows in the Columbia River Gorge at Crown Point (Niem, personal communication, 1990).

Origin of Cape Lookout

Cape Lookout is an extremely impressive geomorphic feature that forms a finger-like projection perpendicular to the coast (Figure 110), extending approximately three kilometers into the Pacific Ocean. It is almost completely composed of 2 to 3 Winterwater Unit flows, with the exception of an invasive sill or dike of high magnesium Sentinel Bluff Unit basalt which underlies the sandstone interbed at the tip of the cape (Figure 93). It has been proposed by Macleod (personal communication to Niem, 1980) that Cape Lookout represents inverted

Figure 110. Aerial photograph of Cape Lookout, which extends nearly three kilometers out to sea. Basalt flows at the end of the cape dip to the north.

topography, with the elongate form of the cape reflecting the pre-existing channel these basalts flowed down. This hypothesis is supported by the orientation of pillow foresets which indicate a westward flow direction for the Winterwater Basalt along Cape Lookout (Figure 109) and evidence of channelization in a talus of canyon wall blocks of adjacent Angora Peak member sandstones to the east at locality CL-72 (previously discussed in this section). Alternatively, Cape lookout may simply be a strike ridge that owes its anomalously straight southern flank to the periodic failures of tabular basalt sheets that spall parallel to the columnar joints of lava tubes (Figure 111). A third hypothesis is that the southern flank of Cape Lookout owes its scarp-like southern face to an east-west trending fault. If it is an uplifted fault block, then the south side of the cape represents a steep fault-controlled anti-dip slope opposite a gentler wave-eroded dip slope on the north (Plate I). However, exposures are poor and the southern steep "fault" faces may have eroded northward by wave erosion from its original position, which may now be buried by Quaternary sand dunes, or obscured by thick vegetation. Seismic, gravity, and magnetic data indicate that basalt composing Cape Lookout does not extend much further west than the present snub end of the Cape (Plate I; Snavely, personal communication to Niem).

N_2 High Magnesium Grande Ronde Basalt (Sentinel Bluff Unit)

Field evidence of sedimentary interbeds and oxidized flow tops indicates that at least two, and possibly three flows of the Sentinel Bluff Unit (N_2 high magnesium Grande Ronde Basalt) entered the Tillamook embayment after emplacement of the Winterwater flows (Figure 107). The

Figure 111. South side of Cape Lookout. Vertical cliffs may be maintained by large wall-failure slabs (foreground) that break off parallel to vertical joint sets in the basalt. Note the Angora Peak member sandstones that underlie the large basalt slabs.

possibility that three flows of Sentinel Bluff Unit basalt occur in the thesis area is supported by the presence of three subaerial Sentinel Bluff flows in the northern Willamette Valley (Tolan, personal communication, 1989). The field relationships between the Winterwater and Sentinel Bluff units of Grande Ronde Basalt suggest that the northern part of the study area had undergone a period of uplift, dissection, channelization, and subsidence prior to arrival of the Sentinel Bluff basalt flows. This is supported by the distribution of these high magnesium basalts which appear to be entrenched into older Winterwater and Grouse Creek flows (Plate I). For example, there are horizontal cooling columns of a subaerial Sentinel Bluff flow against a Grouse Creek (?) flow in a seacliff 50 m north of the outfall of Short Creek (northeast quarter sec. 24, T. 1 S., R. 11 W.). These horizontal columns are typical of intracanyon basalt flows (Niem, personal communication, 1989).

Figure 108 shows the wide distribution of N_2 Grande Ronde flows in Oregon and Washington, which flowed to the coast in the Grays Harbor, Willipa Bay, and Astoria embayment areas (Anderson et al., 1987). Although this distribution pattern suggests that Sentinel Bluff basalt also flowed into the Tillamook embayment from the Astoria embayment to the north, the bent columns, inclined pillow forsets, forset palagonite breccias (Figure 90) and associated subaerial flows of these lava deltas indicate westward or northwestward lava dispersal toward the Cape Meares and Cape Lookout areas (Figure 112). Because this suggests derivation from the east, the Sentinel Bluff Unit probably followed the same path into the Tillamook embayment as that taken by older Grande Ronde basalt units.

Sentinel Bluff Unit

Outcrop and Dispersal Pattern for N_2 High Mg Grande Ronde Basalt

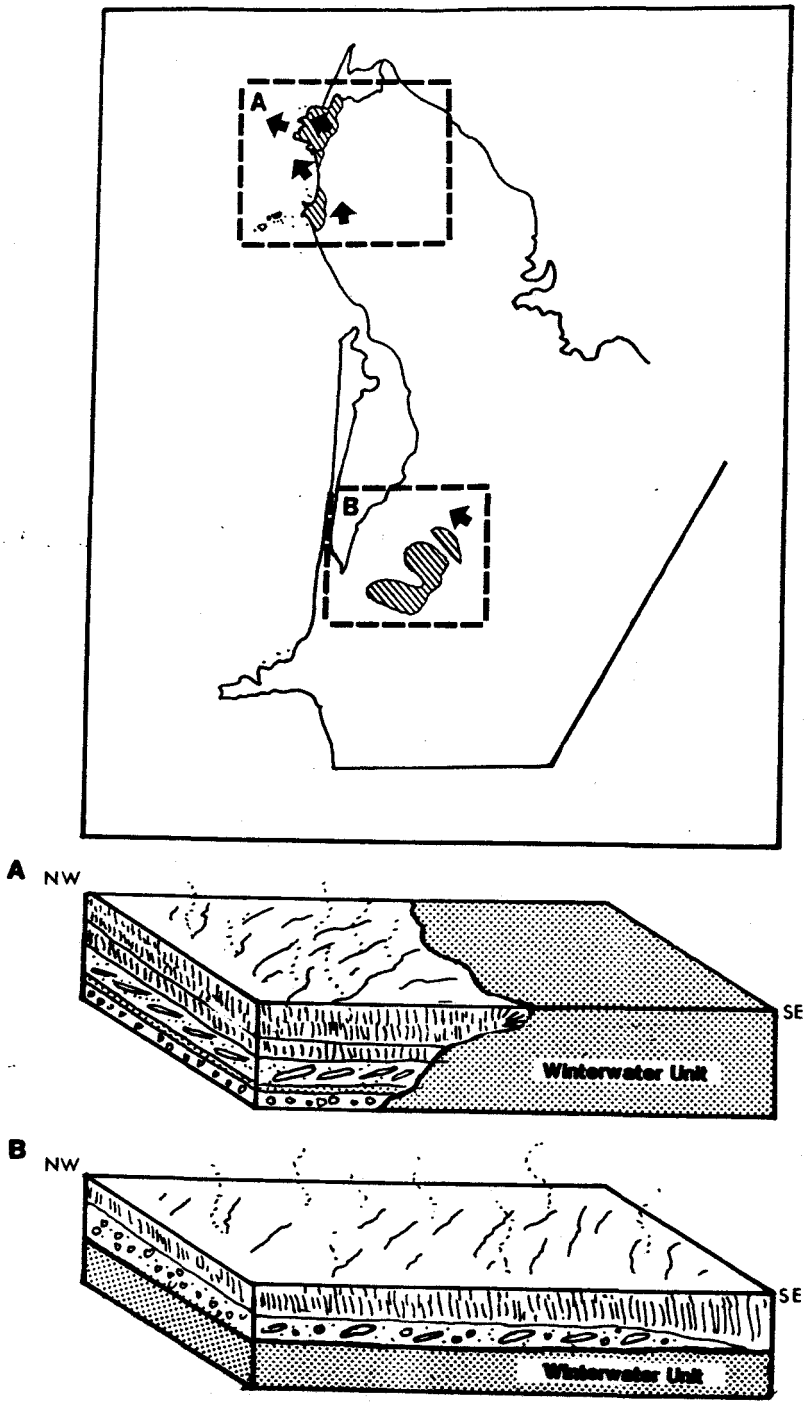

Figure 112. Outcrop and dispersal pattern for the Sentinel Bluff flows of the Grande Ronde Basalt with schematic block diagrams showing the sequence of pillowed and subaerial flows, flow directions, and intracanyon relationship to older Winterwater basalt flows at Cape Meares (112-A). Arrows indicate direction of flow.

The first closely pillowed flows of the Sentinel Bluff Unit encountered a marine environment in the Tillamook embayment which was probably fairly shallow in the southern part of the thesis area, and deepened to the north (Figures 107 and 112 A-B). The basalts streamed down deep drowned valleys and channels carved along the west side of the Grouse Creek and Winterwater flows in the northern part of the thesis area, and pooled in the present location of the Cape Meares headland, where the thickest acculmulations (90-120 m) of Sentinel Bluff basalt occur (Figure 90). In the southern CRB outcrop (Cape Lookout area) the Sentinel Bluff flow appears to be thinner (approximately 50 m), and may represent a periferal lobe of this basalt which caps the Winterwater unit basalts in this vicinity. However, more intensive sampling and new quarry exposures may reveal that Sentinel Bluff flows are also fairly thick and channelized into the southern basalt outcrop as well. Similarly, although present mapping indicates that the Sentinel Bluff Unit in the northern basalt pile (Figure 112-A) is restricted to the west side making up the headlands at Cape Meares, future study may also reveal the presence of Sentinel Bluff basalt on top of the Winterwater Unit to the east as well.

A down-faulted thick (10 m) arkosic sandstone interbed occurs between two high MgO pillowed flows of the Sentinel Bluff Unit at locality 17-88 (southeast quarter sec. 13, T. 1 S., R. 11 W.; Figure 91), supporting the existence of at least two high magnesium flows of the Grande Ronde Basalt in the Tillamook embayment (Figure 107; Plate I). A storm wave-dominated marine depositional environment for the pillowed basalts above and below the interbed is supported by the

presence of amalgamated hummocky cross-stratification within the sandstone (Dott and Bourgeois, 1982).

The thick (>20 m) pillow and pillow palagonite breccias of the Sentinel Bluff Unit at Cape Meares (generalized Cape Meares section, Figure 107) ultimately built up above sea level in its uppermost part, as indicated by the transition of closely packed pillow basalt to subaerial columnar-jointed basalt (lava delta couplet) exposed on the 50 m tall inaccessable south-facing seacliff at Cape Meares. The thickness of the underlying pillowed and palagonite breccia suggest that the Sentinel Bluff basalt flowed into water at least 20 m in depth. A 1 m thick reddish oxidized zone developed on top of the associated subaerial portion of the lava delta couplet (Snavely et al., 1973), and another younger subaerial basalt of the Sentinel Bluff Unit flowed over the top. Similarly, the uppermost part of the Sentinel Bluff Unit in the southern basalt pile (Cape Lookout area) also grades from pillowed to subaerial basalt just below the contact with the Sandstone of Whale Cove. These data suggest that most of the Tillamook embayment was subaerially exposed when the last Sentinel Bluff flow entered the study area (Figure 112).

The sandstone interbed separating two pillowed Sentinel Bluff flows at locality 17-88 (previously described) and the oxidized flow top between two subaerial Sentinel Bluff flows (Figure 107), indicate that two and possibly three flows of this unit flowed into the Tillamook embayment.

Frenchman Springs member of the Wanapum Basalt (Gingko Unit)

The final Columbia River Basalt flow to reach the Tillamook embayment was that of the Gingko Unit of the Frenchman Springs Basalt, which rests on top of the Sandstone of Whale Cove in three locations in the Tillamook embayment (Figure 102; Figure 113; Plate I). Unfortunately, only one small logging road exposure of this unit is available for evaluation (locality O-108, southeast quarter sec. 19, T. 1 S., R. 10 W.), and it yields no definitive information regarding paleocurrent dispersal patterns for Frenchman Springs lavas.

Figure 114 shows the distribution of the Frenchman Springs member basalts which flowed to the coast in the Astoria, Tillamook, and Newport embayments during the middle Miocene. Beeson et al. (1979) hypothesized the existence of a trans coast range pathway for Frenchman Springs flows south of the Tillamook embayment to explain the occurrence of the pillow flows, palagonite breccias, ring and radial dikes, and sills of this unit at Cape Foulweather in the Newport area (Figure 101-B). Using the flow patterns of older CRB flows in the study area as an analog, it is hypothesized that the Gingko Unit flowed westward through a different, more northerly path across the coast range (Figure 114).

During the period following emplacement of the last subaerial flow of the Sentinel Bluff Unit in the Tillamook embayment but preceding emplacement of the Ginkgo flow, the area subsided, was transgressed by the sea, and received approximately 100 m of arkosic-micaceous inner to middle shoreface sandstone deposits of the Sandstone of Whale Cove (described in the Sandstone of Whale Cove section). However, based on the lack of pillowed basalt at the base of the Gingko Unit at the contact with the Sandstone of Whale Cove (locality O-108, southeast

Outcrop and Possible Dispersal Pattern for Ginkgo Unit Flows of the Frenchman Springs Member Basalt

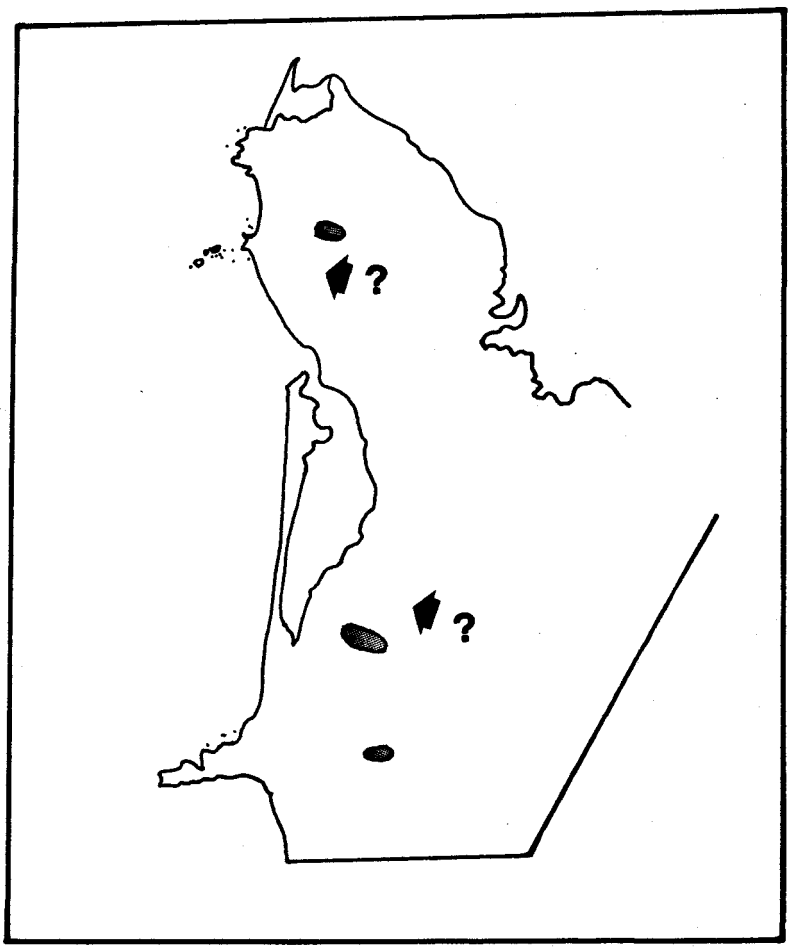

Figure 113. Outcrop map of the Ginkgo Unit of the Frenchman Springs Basalt in the thesis area. Flow directions (arrows) are inferred from the dominant flow pattern of older Columbia River Basalt Group units in the study area, and the existence of Ginkgo flows to the east in the Salem area.

Distribution of the Frenchman Springs Member of the Wanapum Basalt

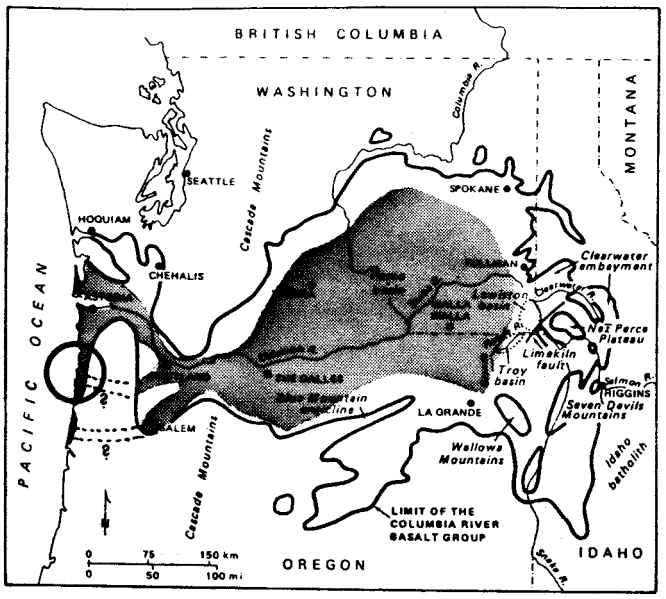

-Tillamook Embayment

Figure 114. Distribution map of Frenchman Springs Basalt flows. Modified from Anderson et al. (1987).

quarter sec. 19, T. 1 S., R. 10 W.), a marine regression may have occurred following deposition of this sandstone unit prior to the arrival of the plateau-derived Gingko flows.

Evidence for the existence of the Gingko Unit occurs in both the northern and southern parts of the study area (Plate I). This suggests that at the time of Gingko flow emplacement, this basalt was laterally extensive, possibly following subaerial river channel systems established within the Sandstone of Whale Cove following uplift. However, subsequent uplift and erosion in the study area has left only three isolated patches of the Gingko Unit basalt capping the Cape Meares and Cape Lookout area basalt piles (Plate I).

Invasive Miocene Dikes and Sills of Columbia River Basalt in the Tillamook Embayment

The results of geochemical and magnetostratigraphic analyses of three samples (K-1, 72-89, CL-75; discussed in Grande Ronde section; Appendix IX and X) collected from two invasive dikes and one sill in the Tillamook embayment reveal that they are composed of Columbia River Basalt (Plate I). The two dikes both cut through early to middle Miocene sandstones of the Angora Peak member of the Astoria Formation but represent two different flow units of the Grande Ronde Basalt, with the dike exposed at Cape Kiwanda (Figure 92) composed of the N_2 low magnesium Winterwater Unit, and the dike at locality CL-75 on Cape Lookout Road composed of the N_2 high magnesium Sentinel Bluff Unit. The basalt sill exposed on the nose of Cape Lookout (Figure 93) is composed of Sentinel Bluff Unit basalt, and was injected parallel to a sandstone interbed within the Winterwater group of flows.

In the preceding sections, a case was made for derivation of the basalt flows in the Tillamook embayment from westward-flowing Columbia Plateau-derived Grande Ronde and Frenchman Springs basalt flows based on similar geochemical, magnetostratigraphic, petrographic, and paleocurrent evidence. However, the presence of a few dikes and sills of similar chemistry in same area would seem to suggest that the thick package of basalts in the Tillamook embayment were actually locally derived. In spite of evidence that would suggest the contrary, the emplacement scenario interpreted for these sills and dikes is that they represent invasive extensions of subaerial and submarine basalt flows fed by Miocene fissure eruptions on the Columbia Plateau, which flowed overland into the Tillamook embayment. The mechanism of invasion used to explain the presence of dikes and sills in the thesis area is based on the controversial invasive hypothesis of Beeson et al. (1979).

Beeson et al. (1979) published a startling new hypothesis regarding the origin of Miocene coastal basalts in Oregon and Washington. They suggested that these coastal basalts in western Oregon and Washington were extensions of basalt flows erupted from fissure swarms on the Columbia Plateau that swept westward to the sea and locally invaded soft, wet, unlithified Miocene coastal sediment to form invasive sills and dikes. The invasive hypothesis was compelling to some because it effectively dealt with the problem of matching middle Miocene basalt geochemistries, petrographies, and ages between coastal and Columbia Plateau flows, divided from one another by the calc-alkaline Western Cascade volcanic chain. Perhaps most importantly, the invasive hypothesis provided a mechanism for emplacement of the sills and dikes that previous workers in western Oregon used as evidence for local vents

(Snaveley et al., 1973; Rarey, 1986; Niem and Niem, 1985; Cressy, 1974; Smith, 1975).

Beeson et al.'s (1979) invasive hypothesis was not without its problems, however. In the Astoria embayment some Miocene coastal basalt sills and dikes intrude late Eocene strata which were probably deep (>1000 m) and well lithified at the time of basalt emplacement (Rarey, 1986; Niem and Niem, 1985; Goalen, 1988; Nelson, 1985; Olbinski, 1983; Wells, 1981). Because Beeson et al.'s (1979) model provided no mechanism for the deep basalt lava invasion of lithified sediment, many workers viewed both hypotheses of a Columbia Plateau origin for coastal Miocene basalt and basalt invasion of coastal sediment with skepticism. However, mounting field, petrographic, geochemical and paleomagnetic evidence in the Astoria embayment is strongly suggesting the invasive process is the correct one for the origin of Miocene basalt sills and dikes in western Oregon and Washington (Wells and Niem, 1987; Beeson et al., 1979; Goalen, 1988; Murphy, 1981; Nelson, 1985; Peterson, 1984; Rarey, 1986; Mumford, 1989).

There may have been additional processes related to basalt invasion that might help to explain how shallow and deep basalt invasion of both unlithified and lithified Eocene, Oligocene, and Miocene sediment is possible. The following is a modification of the model of Beeson et al. (1979) for basalt invasion that includes a hypothesis regarding the role pneumatic and hydraulic processes could have played during Columbia River Basalt lava invasion of sedimentary strata. It should be noted that no effort has been made to verify the model with quantitative analyses, and it is submitted here in the hope that subsequent workers

who understand the interactions of hydraulic, pneumatic, and rheological behavior of lavas and sedimentary rocks can test its validity.

A Modified Model for Basalt Invasion

Figure 115 is a schematic illustration of the modified model for basalt invasion. In the scenario envisioned for invasion, a Columbia River Basalt flow passes over water-saturated, loose, semi-consolidated, yielding sediment (1 and 2 in Figure 115). The base of the denser flow loads into the soft substrate, and in places forms shallow-rooted sills and dikes in the manner originally described by Beeson et al. (1979). At some critical depth, however, the pressure head of dense basalt lava (approximately 2.75 g/cm^3; Murase and McBirney, 1973) becomes high enough to fracture formation in a process similar to that exhibited when the hydraulic pressure of a column of heavy drilling mud in a well bore exceeds the fracture pressure of a formation (Adams, 1985; Anderson et al., 1973). Augmented by the pneumatic pressures associated with the superheated steam of flashing intrastratal waters (as evidenced by the peperite dikes in the study area and in the Astoria embayment), the basalt literally blasts and pushes its way downward into increasingly lithified strata through processes of hydro-fracing (fracturing with high fluid pressure) and pneumo-fracing (fracturing with high pneumatic pressure). The avenue of deep invasion may also follow some pre-existing structure such as a fault or joint as Nelson (1985), Goalen (1988), and Niem and Niem (1985) suggested for the 20 km invasive Beneke Dike in northwest Oregon.

With greater depth of invasion, lithostatic pressures eventually become high enough that intraformational waters no longer flash to

Figure 115. Schematic diagram showing the process by which basalt lava may invade deep lithified Eocene through Miocene strata.

Modified Invasive Basalt Hypothesis

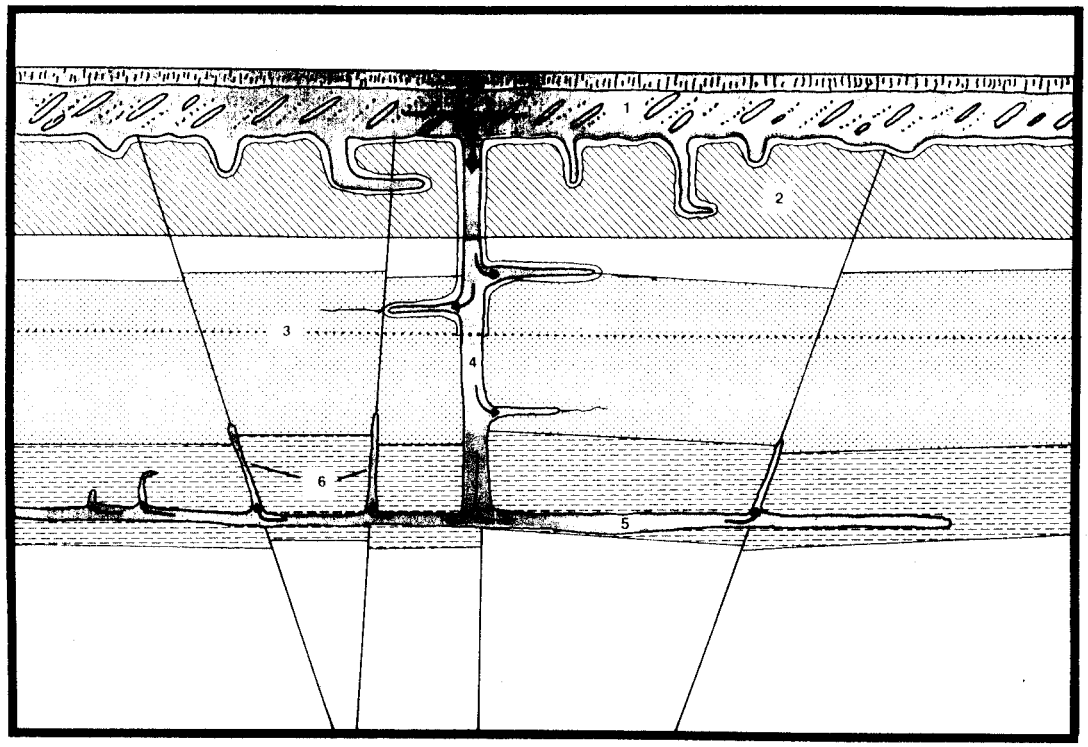

1. Columbia River Basalt lava flowing over and invading coastal Oregon and Washington strata
2. Zone of uncompacted, water-saturated, yielding sediment cut by shallow-seated sills and dikes emplaced through the process of invasion, driven by the large density contrast between basalt lava and water-saturated uncompacted sediment
3. (Dotted line) Depth below which pepperites and other steam-blasting features no longer occur due to building lithostatic pressure with depth
4. Deep invasive dike emplaced along zone of weakness in consolidated strata. Pressure head of basalt column was sufficient to fracture formation or widen pre-existing fracture to allow downward propagation of dike
5. Deep basalt sill formed when dike encountered horizon where resistance to lateral injection was less than the resistance to vertical injection
6. Apophyses injected upward along pre-existing faults or joints under the force of the basalt column pressure head of the main feeder dike

Figure 115.

steam. Below this depth (3 in Figure 115), features associated with steam blasting and sediment fluidization such as dike-wall breccias or pepperites (Kokelaar, 1982), no longer occur, and chill margins are relatively undisturbed. This may also occur in more consolidated sedimentary strata that lack abundant water (e.g. compacted mudstone). Because higher lithostatic pressures inhibit or prevent steam flash, invading basalt continues to inject downward along a pre-existing fault or joint, primarily under the force of its own high pressure head, which may be supplimented by high pneumatic pressures higher within the column of basalt lava.

At certain key horizons (e.g. bedding planes or horizontal joints) where lithostatic pressure of overlying strata is less than the pressure head of the basalt column, lateral extensions of the main feeder dike may develop, injected parallel to bedding under the combined pneumatic and "hydraulic" pressures generated in the associated main basalt lava column. The invasive dike (4 in Figure 115) finally terminates at a depth where it becomes easier to inject laterally than to propagate to greater depth, thus forming a deep sill (5 in Figure 115). Provided the head pressures are still high, apophyses (6 in Figure 115) may inject back upward from the sill along small fractures or other additional zones of weakness. These apophyses form dikes that appear to have been sourced from deep-seated magma chambers, but were actually fed by invasive basalt lava derived from the surface.

Although points of invasion are difficult to identify in the Tillamook embayment, a site of shallow basalt invasion is exposed 100 m north of Happy Camp (locality 85-80, northwest quarter sec. 32, T. 1 S., R. 10 W.). Here, invading R_2 Grouse Creek basalt has shoved aside

strongly disturbed Astoria Formation strata that include peperite dikes of fluidized sediment and basalt. A closely packed pillow is enclosed in disturbed Astoria sediment, and appears to have sunk into unlithified fine-grained sand. Other sites of invasion may underlie thick accumulations of pillowed mega-tube bearing basalt lava delta complexes in the Tillamook embayment (e.g. Cape Lookout or Cape Meares).

PROVENANCE

Introduction

Lithic-rich sandstones within the thesis area reflect a provenance that was both diverse and dynamic. Erosion of widespread Tertiary volcanic terrains and active volcanism in the provenance resulted in deposition of volcaniclastic-rich strata in the Tillamook embayment (Appendix V). However, extensive exposures of pre-Tertiary granitic, metamorphic, and sedimentary rocks also contributed lithic fragments and abundant micaceous quartzo-feldspathic sediment. This resulted in formation of a broad spectrum of sandstone compositions observed in the study area, ranging from volcanic litharenite to micaceous arkose. Paleocurrent dispersal patterns and thin section and heavy mineral analyses indicate that these sediments were primarily transported into the Tillamook embayment via the ancestral Columbia River drainage system, with subordinate amounts of sediment derived from provenances within the smaller drainage basins of the ancestral Oregon Coast Range, Cascade volcanic arc, and possibly the Smith and Klamath Rivers of southwestern Oregon and northwestern California.

The sections that follow discuss in detail the granitic, volcanic, metamorphic, and sedimentary provenances that may have contributed to the Oligocene to middle Miocene strata of the Tillamook embayment. Evidence used to determine provenances was gathered through petrographic, hand sample, and heavy mineral analyses, and evaluated through a literature search of Pacific Northwest geological provinces. Owing to the general uniformity of the lithic fragment and mineral

content of rock units in the thesis area, the following discussion pertains to the entire Oligocene-Miocene sedimentary sequence.

Volcanic Sources

Volcanic rock fragments dominate the lithic suite of sandstones in the thesis area and include abundant basaltic rock fragments and some andesitic and rhyodacitic rock fragments, as well as minor pumice and rare ignimbrite clasts (Appendix V). These volcaniclastic fragments, as well as tuffs, tuffaceous mudstones, abundant green hornblende, lamprobolite, clinopyroxene, orthopyroxene, oscillatory zoned plagioclase, magnetite, and ilmenite (Appendices V and VII), suggest both contemporaneous and older calcalkaline volcanism in the provenance.

The primary source of volcaniclastic detritus shed into the Tillamook embayment was probably basalts and basaltic andesites of the middle to upper Eocene Tillamook, lower to middle Eocene Siletz River, and upper Eocene Grays River volcanics of the ancestral northern Oregon and southern Washington Coast Ranges (Wells, et al., 1984; Niem and Niem, 1984; Duncan, 1982). Fragments of pilotaxitic flow-textured basalt (i.e. aligned plagioclase microlites with ilmenite opaques) are common in thin sections, and probably were derived from similarly flow-textured Tillamook Volcanics (Niem, personal communication). Snavely and Wagner (1963) suggested the Tillamooks were uplifted during the Oligocene and early Miocene and exposed in a structural high east of the town of Tillamook, Oregon. Much of the augite and ilmenite present in heavy mineral suites (Appendix VII) of the Bewley Creek formation, Angora Peak member, and the Sandstone of Whale Cove may have also been derived from Tillamook sources. Sediments in modern streams draining the augite- and

plagioclase-phyric Tillamook Volcanics are extremely enriched in these minerals (Niem and Glenn, 1980; Clemens and Komar, 1988; Mumford, 1989).

Large cobbles of vesicular basalt up to 15 cm in diameter collected from inner neritic sandstones of the Angora Peak member of the Astoria Formation at Cape Kiwanda are dissimilar to Tillamook basalt, lacking characteristic pilotaxitic flow texture and both augite and plagioclase phenocrysts. However, they do resemble late Eocene Cascade Head Basalt in thin section (Snavely, personal communication). Because basalt cobbles would not survive long transport or travel far in the swash zone, they were probably derived from nearby highlands composed of Casacade Head Basalt to the south. The upper Eocene Goble Volcanics and Cole Mountain basalts of northwestern Oregon and southwestern Washington, which are associated with early Western Cascade volcanism (Wells et al., 1984; Niem and Niem, 1984; Rarey, 1986; Mumford, 1989), may have also contributed additional basaltic material to the Tillamook embayment.

In addition to the previously described basalt provenances, some of the glassy or palagonitic basaltic rock fragments with intersertal texture in sandstone interbeds of the Grande Ronde Basalt (site 17-88) and the Sandstone of Whale Cove may have been derived from the Grande Ronde Basalt and older flows of the Columbia River Basalt Group. A Columbia River Basalt provenance is also considered for a basaltic grit collected in the Angora Peak member at site CL-74 (southwest quarter sec. 6, T. 3 S., R. 10 W.). The origin and possible provenance significance of this deposit is discussed in the Angora Peak section.

The primary source of intermediate to felsic volcanic rock fragments, zoned plagioclase, orthopyroxene, and ignimbrite fragments

found within the Oligocene-Miocene sandstones of the Tillamook embayment was probably the active late Eocene to middle Miocene western Cascade arc of Oregon and Washington (Priest, 1989; Wells et al., 1984; Priest et al., 1982; Hammond, 1979). Volcanic detritus may have been shed into the ancestral Columbia River drainage system from Western Cascade andesites, dacites, rhyolites, tuffs, pyroclastic flows and subordinate basalts of the Ohanapecosh, Fifes Peak, and Stevens Ridge volcanics of Washington (Priest et al., 1982), and the Colestin, Fisher, and Little Butte volcanics of Oregon.

The tuffaceous nature of the Smuggler Cove formation and Sutton Creek member of the Nye Mudstone, and the abundant pumice, ignimbrite, and felsic volcanic fragments within the Bewley Creek formation, suggest pulses of contemporaneous explosive volcanism in the western Cascades. However, because younger strata in the study area (e.g. Angora Peak, Netarts Bay, Cannon Beach members and Sandstone of Whale Cove) are relatively impoverished in these volcaniclastic rock fragments, deposition of Tillamook embayment strata may correlate with the waning stages of vigorous volcanic activity reported in the arc from the Oligocene through the early Miocene (Wells et al., 1984; Niem and Niem, 1984).

An additional source of intermediate to felsic volcanic rock fragments and green hornblende, may have been the upper Eocene hornblende-andesites of the Clarno Formation of central Oregon (Wells et al., 1984; Oles and Enlows, 1971). In addition, other volcanic sources of brown hornblende, lamprobolite, sanidine, and orthopyroxene include the clinopyroxene-bearing andesites, dacites, and rhyolites of the Eocene Challis Volcanics of northeastern Washington, central Idaho, and

southern British Columbia (Link and Hackett, 1988; Lewis et al. 1987, Moye et al., 1988; Wells et al. 1984; Lewis, Personal communication, 1989) and the Oligocene intermediate to rhyolitic ashflows and tuffs of the John Day Formation of east-central Oregon (Niem and Niem, 1984).

Metamorphic Sources

Untwinned plagioclase, coarse muscovite and biotite, phyllite, schist, and minor metamorphic quartzite rock fragments and pebbles in sandstones of the thesis area (Appendix V and VII) indicate that regionally metamorphosed rocks provided a significant quantity of extrabasinal sediment to the Tillamook embayment via an ancestral Columbia River drainage system. The strong influence of low to high rank metamorphic provenances is also indicated by the presence of minor blue-green hornblende, rare blue amphibole, sillimanite-actinolite, chlorite, epidote, clinozoisite, zoisite, garnet, staurolite, and kyanite in heavy mineral grain mounts (Appendix VII).

The principal source of metamorphic detritus was possibly the muscovite, kyanite, staurolite, sillimanite, chlorite, and garnet-bearing phyllites, schists, and gneisses of the Precambrian Shuswap metamorphic complex of southern British Columbia and the Precambrian Belt Supergroup and older metamorphics of western Montana, northern Idaho, and southern British Columbia, which are also epidote-bearing (McMullin and Greenwood, 1988; Lewis, personal communication, 1989). Additional contributions of schist, phyllite, epidote, blue amphibole, chlorite, kyanite, and muscovite may have been derived from North Cascades greenschists and blueschists of the Shuksan Metamorphic Suite, as well as the greenschists and phyllites of the Darrington Phyllite, Precambrian Okanogan Highlands of northwestern

Washington (Misch, 1977), and the Burnt River Schist and amphibolites of the Canyon Mountain Complex of central and northeast Oregon. Kyanite in particular, may have also been derived from the Chiwaukum Schist (Vance, 1989). Subordinate contributions of metamorphic sediment may also have been made from the greenschists, blueschists, amphibolites, gneisses and greenstones of the late Triassic Martin Bridge Formation that flanks the Wallowa Batholith of eastern Oregon (Link and Hackett, 1988; Onasch, 1987; Aliberti and Manduca, 1988). Other less likely or minor sources include the hornblende schists and phyllites of the Paleozoic Central Metamorphic Belt and glaucophane-bearing blueschists of the Jurrasic-Cretaceous Franciscan Formation of the Klamath terrane of southern Oregon and northern California (Irwin, 1974; Hotz, 1974). The geographic position of these provenances, however, requires northward littoral or longshore transport of sediment into the Tillamook embayment.

Granitic Sources

Although granitic rock fragments are relatively minor lithic constituents in the sandstones of the thesis area, granitic provenances are strongly reflected in the composition of monomineralic framework grains. Minerals present in thin section and heavy mineral grain mounts that suggest a granitic provenance include microcline, albite and oligoclase feldspar, polycrystalline quartz, myrmekite, perthite, green and blue-green hornblende, sphene, schorlite, rutile, orthopyroxene, zircon, ilmenite, magnetite, biotite, and muscovite (Appendix V and VII). The existence of granitic rocks in the provenance is also confirmed by the presence of a hornblende gabbro cobble and a two-mica granite boulder (17 cm and 26 cm diameters, respectively within the

Angora Peak member of the Astoria Formation at Cape Kiwanda (petrographies and scenarios for emplacement described in the Angora Peak section).

Most of the granitic detritus delivered to the Tillamook embayment was probably derived within the ancestral Columbia River basin from the extensive exposures of the Cretaceous to Eocene green and blue-green hornblende, biotite, muscovite, epidote, and zircon-bearing granites, granodiorites, and tonalites of the Idaho Batholith (Lewis et al., 1987; Lewis, personal communication, 1989), and the Cretaceous Spirit Pluton and Eocene granitic intrusions of northeastern Washington, and southern British Columbia (Wells et al., 1984; Scheidegger et al., 1971). Relatively minor contributions may have been shed from silicic granitic rocks of the Wallowa Batholith and Bald Mountain Stock of eastern and northeastern Oregon and western Idaho (Lewis, personal communication, 1989; Vallier and Brooks, 1987). Subordinate to these Columbia River basin sources are the more limited Jurassic-Cretaceous hornblende and biotite-bearing quartz diorites within the Klamath terrain (Irwin, 1974) which may have contributed granitic detritus to the thesis area via northward-moving longshore currents.

The chemical composition and petrographic characteristics of the two-mica granite boulder (sample 80-89A; Appendix IX) collected from the Angora Peak member at Cape Kiwanda roughly match those of the muscovite-biotite (two-mica) granite in the core of the southern lobe of the Idaho Batholith (Lewis, personal communication, 1989; Lewis et al., 1987) making this a likely source. However, the petrographic and geochemical characteristics of a hornblende gabbro (?) or amphibolite (?) cobble (sample 80-89E; Appendix IX) collected at the same locality

do not match typical Idaho Batholith chemistries (Lewis, personal communication, 1989; Lewis et al., 1987) or the average chemical compositions of intrusive rocks within the central Oregon Coast Range (Snavely et al., 1980; Barnes, 1981). Although this cobble may have been derived from one of the other granitic or metamorphic provenances listed previously, the extensive search of available geochemical data required to pinpoint a source was out of the scope of this study. Thus, more work is warranted to establish a provenance for this exotic cobble.

Sedimentary Sources

Although intrabasinal rip-ups are the most common sedimentary lithic fragments, especially in the deep-marine turbidite sandstones of the Cannon Beach and Netarts Bay members of the Astoria Formation, chert, mica, sedimentary quartzite, and the abraded minerals of zircon, tourmaline, garnet, epidote, quartz, and feldspar observed in thin section and heavy mineral grain mounts suggest recycling and previous transport histories. Some of these minerals may have been recycled from nearby older Tertiary strata exposed during Oligocene and early Miocene uplift in the Oregon Coast Range (Snavely and Wagner, 1963; this study). However, many may have been derived from more distant sources including Precambrian Belt Supergroup and pre-Belt sedimentary rocks in western Montana, northern Idaho, and southern British Columbia (Lewis et al., 1987; Whipple et al., 1984), or the chert-rich Western Paleozoic and Triassic Belt of the Klamath terrain (Irwin, 1974). Among other minerals, chert may also have been sourced from the Paleozoic section of the western Blue Mountains (Baldwin, 1981)

A large rounded cross-bedded sedimentary quartzite cobble (> 22 cm diameter; sample 80-88F petrography described in the Angora Peak

section) was collected at Cape Kiwanda in the same stratigraphic horizon as the large granitic clasts described previously. The cobble is an arkosic sandstone consisting of subangular quartz and plagioclase feldspar, with minor amounts of muscovite and phyllite rock fragments. It is completely cemented with a quartz cement, and similarly cemented sandstones are totally unlike older Tertiary strata of the Oregon Coast Range (Niem, personal communication, 1989). This sedimentary quartzite cobble, and other pebbles and sand-sized grains of similar lithology collected from the Angora Peak member of the Astoria Formation in this study are especially diagnostic of provenance because sources for this rock type are extremely limited. Cressy (1974) reported similar pebbles of sedimentary quartzite in the Angora Peak member 50 km to the north and suggested that the only sources for sedimentary quartzite are the Paleozoic sedimentary section of the Belt Series rocks of Montana and Idaho. The distant provenances suggested by the presence of the two-mica granite and the sedimentary quartzite (Idaho Batholith and Belt Series rocks of Montana and Idaho, respectively) are strong evidence supporting the liklihood that the Tillamook embayment was supplied, in large part, by an ancestral Columbia River system.

Point counted sandstones of the thesis area were plotted on the figures of Dickinson and Suczek (1979; Figures 116-A and B) as an aid to determine the plate tectonic setting in which strata of the study area were deposited. Tillamook embayment sandstones generally plot within the magmatic arc provenances field of both Figure 116-A and 116-B in positions Dickinson and Suczek (1979) interpreted to represent a slightly to profoundly dissected magmatic arc source terrane, and deposition within a forearc setting. Although this agrees well with the

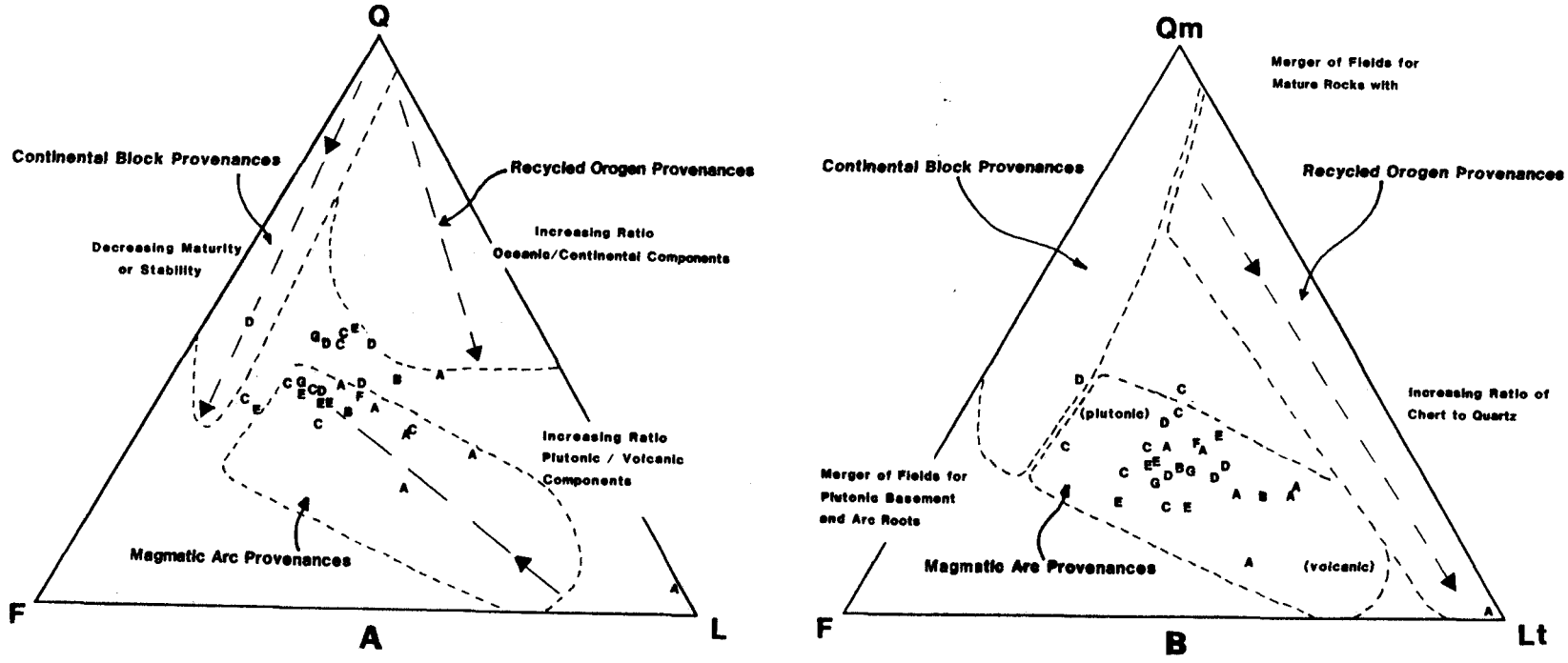

Figure 116. Ternary diagrams showing the composition of point counted sandstones from the study area relative to the provenance fields of Dickinson and Suczek (1979). Figure 116-A end members are Q - mono and polycrystalline quartz, F - total feldspar, L - total lithic fragments. Figure 116-B end members are Qm - monocrystalline quartz, F - total feldspar, Lt - total lithic fragments including polycrystalline. Modified after Dickinson and Suczek (1979).

provenances previously described for sedimentary rocks of the thesis area, the composition of Tillamook embayment sandstones has probably been most strongly influenced by the end members of a completely undissected Western Cascade volcanic chain and Eocene coast range basalts, and the deeply dissected older arc terrane of the Idaho Batholith.

TEXTURAL ANALYSIS

In order to show textural similarities and differences, quantify grain size characteristics, and provide a line of evidence for the interpretation of depositional environment, 35 samples of sandstones were subjected to grain size analyses. These sandstones were collected from the Bewley Creek formation, Sutton Creek member of the Nye Mudstone, Sandstone of Whale Cove, and a sandstone interbed within the Grande Ronde Basalt, as well as from the Angora Peak, Netarts Bay, and Cannon Beach members of the Astoria Formation. Grain size data obtained from sieving was reduced to the statistical parameters of skewness, median, mean, standard deviation, and kurtosis using the statistical formulae of Folk and Ward (1957). All statistics showing grain size distributions of different samples are listed in Appendix VI. Table 3 summarizes the statistical parameters which have also been plotted on the bivariant diagrams of Passega (1957) and Kulm et al. (1975) for comparison and environmental analysis.

Statement on the Exclusion of Friedman Diagrams

Previous doctoral and master's students have made extensive use of Friedman's (1962) bivariant diagrams in the attempt to further define the depositional environments of northwestern Oregon Tertiary rock units on the basis of sandstone grain size distributions (e.g. Rarey, 1985; Cressy, 1974; Murphy, 1981; Mumford, 1989; Cooper 1981). Friedman sampled the modern sediments of rivers, beaches, and inland and offshore dunes, and through sieve analyses graphed their environmentally sensitive statistical parameters of standard deviation, skewness, and mean grain size against one another on bivariant plots. Through

Table 3.

Average of Grain Size Distributions of Sandstones of the Thesis Area

UNIT	Statistics Calculated Using the formulae of Folk and Ward										
	MEAN (PHI)		STD. DEV. (PHI)		SKEWNESS		COARSEST 1% (MICRONS)		MEDIAN (MICRONS)		# OF SAMPLES
	Average	Range	Average	Range	Average	Range	Average	Range	Average	Range	
Bewley Creek formation	2.27	1.00-3.32	0.97	0.67-1.47	0.35	0.19-0.50	738	268-2150	281	117-575	13
Sutton Creek member of the Nye Mudstone	1.75	1.70-1.80	0.77	0.63-0.91	0.28	0.25-0.31	722	575-870	298	287-309	2
Astoria Formation											
Angora Peak member	2.88	1.95-3.18	0.60	0.51-0.78	0.22	0.17-0.48	307	202-408	150	117-278	6
Netarts Bay member	1.76	1.65-1.90	1.14	0.96-1.35	0.25	0.00-0.54	1679	468-2820	295	268-317	3
Cannon Beach member	2.05	1.51-2.70	0.88	0.70-1.03	0.28	0.02-0.52	698	380-1300	253	154-340	6
Columbia River Basalt Sedimentary Interbeds											
Grande Ronde Basalt Sandstone Interbed	3.18	---------	0.47	--------	0.19	--------	265	--------	110	--------	1
Sandstone of Whale Cove	2.90	2.27-3.71	0.76	0.73-0.79	0.18	0.61-0.20	372	250-485	155	80-235	4

VERBAL TERMS DESCRIBING GRAINSIZE STATISTICS (Folk, 1957)

	MEAN GRAINSIZE	SORTING	SKEWNESS	Percent Lithic Fragments (from modal analyses)	Coarsest 1% (range)
Bewley Creek formation	Fine grained	Mod. to P. Sorted	V. Pos. to Pos. Skew	45	Medium gr. sd. to v.f. gravel
Sutton Creek member of the Nye Mudstone	Medium grained	Mod. Sorted	Pos. Skew	29	Coarse
Astoria Formation					
Angora Peak member	Fine grained	Mod. to Well Sorted	Pos. Skew	22	fine to medium
Netarts Bay member	Medium grained	P. Sorted	Pos. Skew	19	medium to v. fine gravel
Cannon Beach member	Fine grained	Mod. Sorted	Pos. Skew	21	Medium to v. coarse
Columbia River Basalt Sedimentary Interbeds					
Grande Ronde Basalt Sandstone Interbed	V. fine grained	Well Sorted	Pos. Skew	28	Medium
Sandstone of Whale Cove	Fine grained	Mod. Sorted	Pos. Skew	16	Medium

empirical study, he found that sands from these different depositional environments tended to plot in certain fields, which he defined on his diagrams. However, because marine sandstone samples from this and previous studies of northwestern Oregon Tertiary rock units frequently plot in the "river" and "inland dune" fields on his diagrams, the appropriateness of the use of Friedman diagrams as a determinant of depositional environment has been called into question.

Friedman diagrams may be inappropriate for use in this study because the boundaries of the depositional environment-fields they contain were defined through extensive sampling of quartzo-feldspathic sands from modern environments on the east coast of the United States. The lithic-rich sediments analyzed in this study contrast with the sands Friedman used and sedimentological and petrographic data indicate Tillamook embayment strata were deposited within an energetic storm-wave dominated marine setting along a tectonically active convergent margin off the west coast of the United States. Furthermore, Friedman's diagrams do not provide fields for sediment deposited in either a continental shelf or deeper marine environment. In addition, because Friedman's depositional environment fields were defined using modern sediment, they are not compensated for the effect diagenesis and disaggregation techniques may have on the grain size distributions of ancient, moderately to strongly cemented lithic-rich sandstones. For these reasons, statistical parameters from this study are not displayed in Friedman diagrams, but are illustrated using bivariant diagrams from Passega (1957) and Kulm et al. (1975).

Kulm et al.'s (1975) bivariant diagrams are especially well suited to the analyses of shallow marine sandstones of the thesis area because

their graphs provide both beach and offshore sand fields defined using beach and shelf sand from the modern Oregon coast. Although these diagrams are also unadjusted for the effect diagenesis may have on the grain size distribution of ancient lithic-rich sandstones, they are advantageous because the composition of sand being deposited on the modern Oregon beach and shelf, as well as the storm wave-dominated conditions operating there, may be analogous to depositional conditions and sandstone compositions of the past. As a result, the fields on Kulm et al.'s (1975) diagrams may be more suitable than those defined on Friedman's diagrams for evaluating the depositional environments of Tillamook embayment shallow-marine Miocene sandstones. Passega's (1957) diagram, though similar to Friedman's diagrams because it was also constructed using sediment from modern environments, is superior because it contains diverse fields that describe transport processes as well as depositional environments, thus making the Passega diagram more flexible.

Shelf Sandstones

On the basis of paleoecological information provided by molluscan fossils, and evidence supplied by sedimentary structures (e.g. hummocky cross-stratification) and thin-section petrography, the Bewley Creek formation, Angora Peak member of the Astoria Formation, Sandstone of Whale Cove, and the sandstone interbed within the pillowed Grande Ronde Basalt (locality 17-88; Figure 91) all appear to be predominately shallow-marine inner to middle shelf deposits. They have been grouped together in this section so their textural characteristics may be compared to one another, and to the characteristics of the modern shelf sands off Oregon described by Kulm et al., 1975.

Among these sandstone units, the Bewley Creek formation is the most coarse-grained, ranging from very fine- to coarse-grained, with a mean grain size of 2.27 phi (Table 3). It is followed by the very fine- to medium-grained Angora Peak member, with a mean grain size of 2.88 phi; the very fine- to fine-grained Sandstone of Whale Cove, with mean grain size of 2.9 phi; and the very fine-grained Grande Ronde Basalt sandstone interbed, with its mean grain size of 3.18 phi (Table 3). The wide range of grain sizes and overall coarseness of the Bewley Creek formation suggests that this unit was deposited under a variety of energy conditions that tended to be higher than those under which the Angora Peak member, the Sandstone of Whale Cove, and the Grande Ronde Basalt sandstone interbed were deposited. This is consistent with sedimentary structures and grain sizes observed in the Bewley Creek formation in the field, which range from medium to coarse-grained sandstone with abundant trough cross-beds representative high-energy inner shelf conditions, to hummocky cross-stratified and subhorizontally laminated micaceous fine-grained storm-dominated lower shoreface sands (Walker, 1984, Dott and Bourgeois, 1982). The other three shelf sandstone units are predominately hummocky cross-stratified to subhorizontally laminated micaceous fine-grained lower shoreface sandstones (Dott and Bourgeois, 1982).

Standard deviation values listed in Table 3 show that the Bewley Creek formation is distinguished from the other units because it is only moderately to poorly sorted (0.67-1.47 phi), as compared to the Angora Peak member of the Astoria Formation and the Sandstone of Whale Cove which are moderately sorted (0.51-0.78 phi and 0.73-0.79 phi respectively), and the Grande Ronde Basalt sandstone interbed which is

well sorted (0.47 phi; Table 3). The Bewley Creek formation also differs from the other sandstone units because its grain size distributions tend to be very positively skewed (0.35 in Table 3), whereas all other sandstone samples are only positively skewed, ranging from 0.17 to 0.28 (Table 3).

The tail of fines indicated by the positive skewness of all samples analyzed, and the moderate to poor sorting of Bewley Creek formation sandstones, may seem inconsistent with fossil evidence and sedimentary structures that suggest these sandstones were deposited on a high-energy storm-dominated inner to middle shelf. However, thin section analyses and scanning electron microscopy reveal that many shelf sandstones in the thesis area are enriched in moderately to extensively altered mafic to intermediate volcaniclastic fragments, moderately to extensively cemented with diagenetic clay. These soft altered rock fragments and diagenetic clay-rim cements may be more suseptible to crushing than quartz and feldspsar during sample preparation prior to sieving, which would artificially increase dispersion of the grain size distribution and bias it toward the finer clay and silt grain sizes. This could account for positive skewness and high standard deviation values of volcaniclastic sandstone units observed in the thesis area. Because the Bewley Creek formation sandstones contain an average of 37% volcaniclastic fragments (Appendix V), these sandstones would be quite prone to diagenetic alteration, which may help explain why this is the only unit that is moderately to poorly sorted and very positively skewed. However, because the volcanclastic lithic content of the Angora Peak member, Grande Ronde Basalt sandstone interbed and Sandstone of Whale Cove is also high, averaging 23%, the grain size distributions of

these sands may have been similarly biased. Although bioturbation must also be considered as a causitive factor for increasing dispersion (standard deviation) within grain size populations, the current-formed sedimentary structures (e.g. lamination, cross bedding) from most collection sites were well preserved, indicating that the influence of bioturbation on these grain size distributions was probably minor.

Figure 117 is a graph of standard deviation vs. skewness that includes three fields that represent where sand, mixed sand and mud, and mud from the modern Oregon continental shelf plot (Kulm, et al., 1975). Nearly all samples from the Sandstone of Whale Cove, Grande Ronde Basalt sandstone interbed, Bewley Creek and Angora Peak member sandstones plot within the field that typifies sand from the modern inner to middle shelf of Oregon (Figure 117). This agrees well with fossil, petrographic and sedimentary structures which support this environmental interpretation for these units.

In figures 118-A and 118-B, which are graphs of mean diameter vs. skewness and mean diameter vs. standard deviation, Kulm et al. (1975) have defined two fields where modern Oregon beach sand and offshore sand plot. The Sandstone of Whale Cove and Grande Ronde Basalt sandstone interbed plot within or near the offshore sand field, while the Bewley Creek and Angora Peak members of the Astoria Formation show greater dispersion (standard deviation) toward larger grain sizes. This dispersion is expected as sedimentary structures and grain sizes of both the Bewley Creek and Angora Peak sandstones suggest inner and middle shelf depositional environments. Points that plot between the beach sand and offshore sand fields probably reflect the continuum of energies that exist between the beach and offshore environment. The displacement of

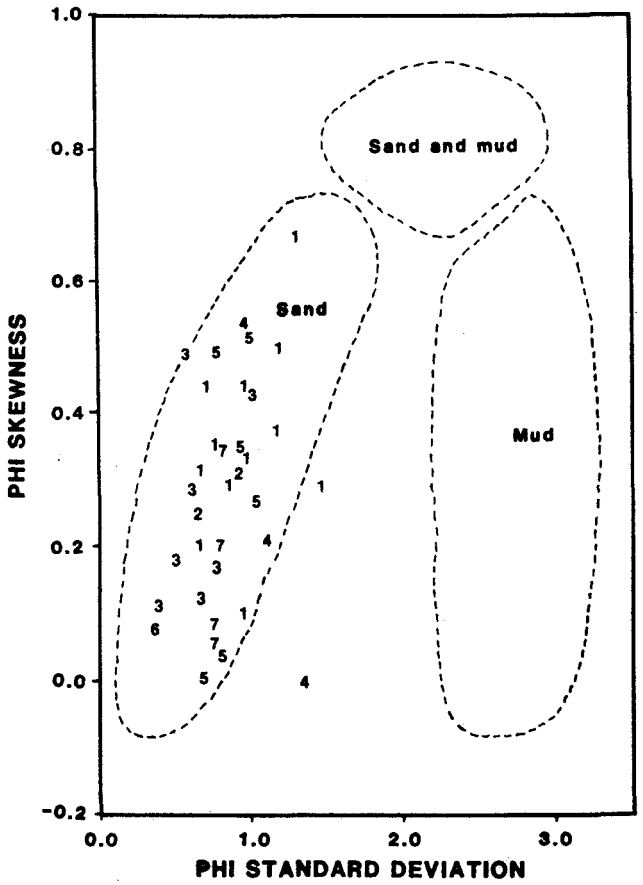

1. Bewley Creek formation
2. Sutton Creek member, Nye Mudstone
3. Angora Peak member, Ast. Fm.
4. Netarts Bay member, Ast. Fm.
5. Cannon Beach member, Ast. Fm.
6. Grande Ronde sandstone interbed
7. Sandstone of Whale Cove

Figure 117. Diagram showing where statistical parameters of standard deviation and skewness for thesis area Oligocene and Miocene sandstones plot relative to fields defined by Kulm et al. (1975) for sediment analyzed from samples cored from the modern continental shelf off Oregon. Modified after Kulm et. al. (1975).

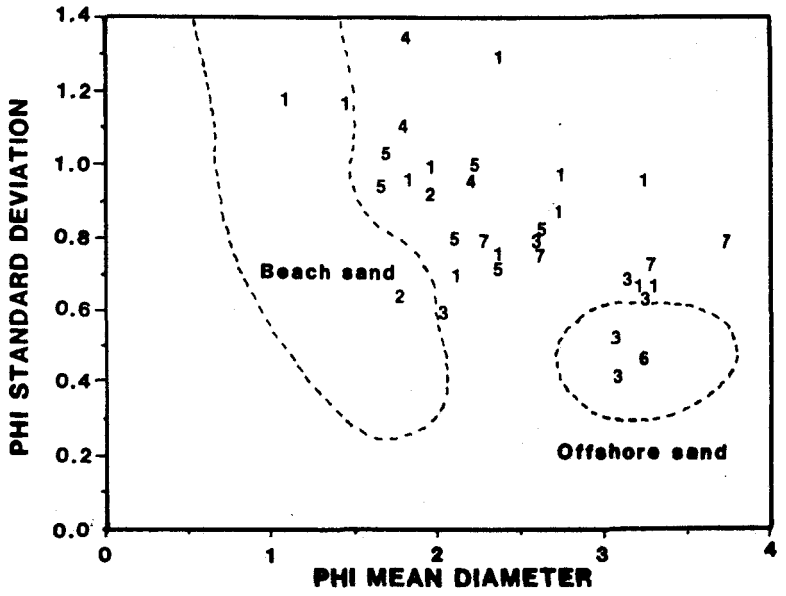

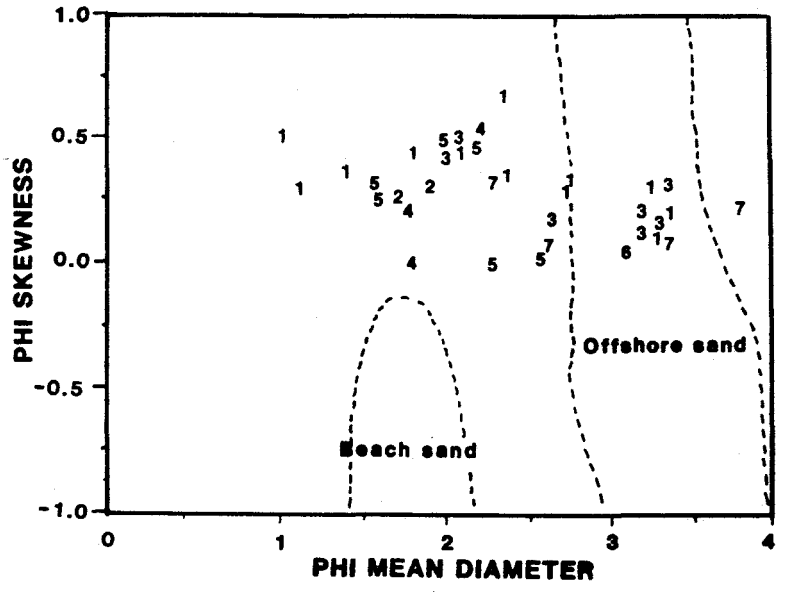

Figure 118. A) Phi mean diameter vs. phi standard deviation of thesis area sandstones plotted against fields defining typical modern Oregon continental shelf sediment. B) Phi mean diameter vs. skewness for thesis area sandstones plotted against fields defining typical modern Oregon shelf sediment. Rock unit number assignments as in Figure 117. Modified after Kulm et al. (1975).

points above the beach field in figure 118-B may reflect the effects of diagenesis, disaggregation, or bioturbation on grain size distributions, skewing the population in the positive, or fine-grained direction.

Figure 119 is a bivariant diagram constructed by Passega (1957) which graphs median grain size vs. the coarsest one percent from each sample sieved. The coarsest one percent of each grain size distribution is thought to represent the competence of the transporting medium, and the median is representative of the total population of grains undergoing transport (Royse, 1970). All samples plot within or near the rivers-tractive current field, and most are contained within the beaches field on the Passega diagram. Because fossil and petrographic evidence and sedimentary structures suggest an offshore marine environment for these strata, the tractive currents interpretation is favored, which would be compatible with deposition on a storm wave-dominated shelf swept by longshore currents.

Submarine Channel-fill and Turbidite Sandstones

Sedimentary structures, lithologies, and fossil evidence indicate that the sandstones of the Sutton Creek member of the Nye Mudstone, and Netarts Bay and Cannon Beach members of the Astoria Formation were deposited as deep marine submarine channel fill deposits or slope turbidites (see depositonal environment sections). Because these units have depositional environmental affinities to one another, their textural characteristics are compared to the modern depositional environments defined in the Passega (1957) diagram, to the shelf sands previously discussed on the Kulm (1975) bivariant diagrams, and to each other.

Figure 119. Passega (1957) diagram of median diameter vs. diameter of the coarsest 1% (both in microns) for shallow-marine sandstones of the thesis area. Modified after Passega (1957).

Sandstone of Whale Cove ( )
Grande Ronde Basalt sandstone interbed (#)

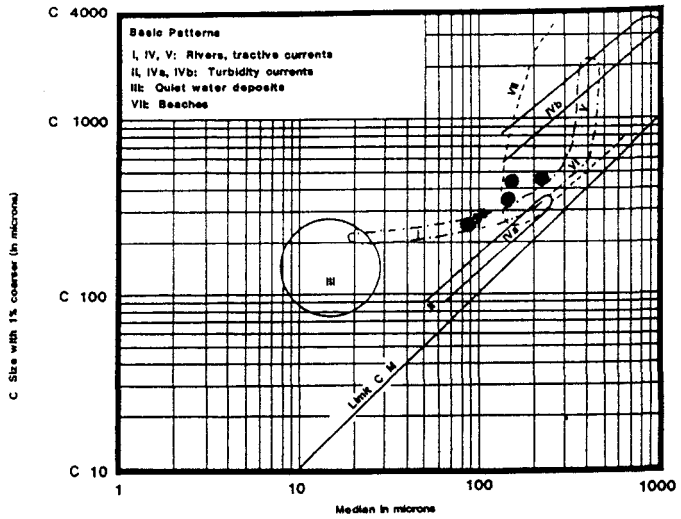

Angora Peak member
Astoria Formation

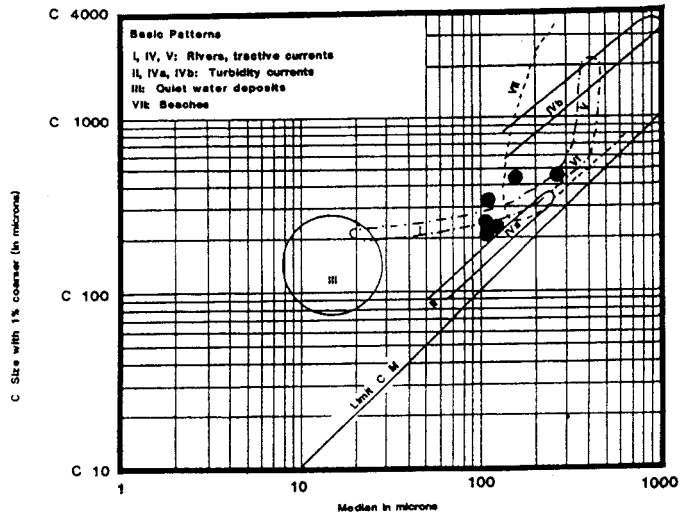

Bewley Creek formation

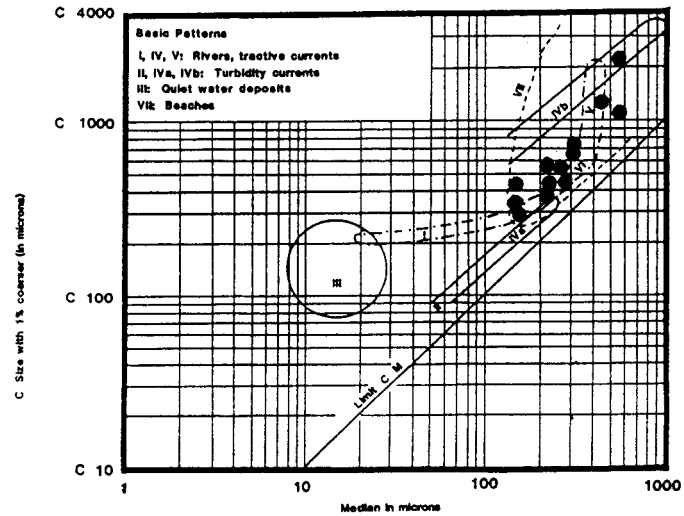

Figure 119.

The grain sizes tabulated in Table 3 show that the Netarts Bay member of the Astoria Formation and Sutton Creek member of the Nye Mudstone members tend to be medium-grained, with a mean value of 1.76 phi and 1.75 phi, respectively. The Cannon Beach member tends to be finer, from medium to very fine-grained, with a mean grain size of 2.05 phi (Table 3). The larger mean grain sizes of the Netarts Bay and Sutton Creek sandstones may reflect higher energies of deposition associated with high-density grain flows and turbidity currents. This interpretation is supported by bedding characteristics (e.g. Bouma sequence, graded bedding), internal sedimentary structures, deep marine bathyal forams, and stratigraphic context which suggest deposition in a relatively high-gradient submarine channel or canyon head incised into the continental slope or outer continental shelf (see respective depositional environments). The smaller average grain size and thin-bedded nature of most Cannon Beach member sandstones may indicate deposition from more dilute, finer-grained, and less energetic overbank turbidites (Walker and Mutti, 1973) associated with activity within a nearby channel.

The sandstones of all three units tend to be positively skewed, with skewness values ranging from 0.25-0.28 (Table 3). This positive skewness is the result of a bias toward the fine end of the grain size distribution. Although some detrital silt and clay was probably deposited along with the sand during rapid deposition by the turbulent density current, perhaps within the Bouma T_d and T_e layers of turbidite beds, some of the fines may have been created from the crushing of small siltstone rip-ups observed in thin sections of sandstones from each of these three members. Furthermore, diagenetic alteration processes that

make pore-fill cements and altered unstable lithic fragments more suseptible to crushing during sample preparation, may also account for some post-depositional generation of fines (silt and clay) creating an artificial positive skewness not present during deposition.

Table 3 shows that the Cannon Beach member, though predominately moderately sorted, ranges from moderately sorted to poorly sorted (0.70-1.03). The Sutton Creek member of the Nye Mudstone is moderately sorted (0.63-0.91 phi), and the Netarts Bay member is predominately poorly sorted with a standard deviation value ranging from 0.96-1.35 (Table 3). The poor sorting of the submarine channel-fill and turbidite facies of the Netarts Bay and Cannon Beach members may be the result of several factors. Sedimentary structures within the Netarts Bay member indicate that it is partially composed of grainflow and fluidized flow deposits resulting from rapid deposition and loading by hyperconcentrated density flows (Walker, 1984; Reinech and Singh, 1980). Grainflow deposits are typically ungraded to poorly graded (Reinech and Singh, 1980), consistent with high standard deviation values of Netarts Bay member sandstones which indicate poor sorting. Furthermore, laboratory disaggregation and homogenization of originally well-graded turbidite sands of both the Cannon Beach and Netarts Bay members, may have resulted in a poorer sorting value than existed within sands just after deposition. As only two samples of the Sutton Creek member of the Nye Mudstone were sampled for textural analysis, more detailed sampling may show that this unit is also subject to the aforementioned effects on sorting.

The Passega diagram in Figure 120 shows that most samples from each of the deep marine sands plot within the beaches field VII near

Figure 120. Passega (1957) diagram of median diameter vs. diameter of the coarsest 1% (both in microns) for submarine channel, canyon head, and slope turbidite sandstones of the thesis area. Modified after Passega (1957).

Sutton Creek member
Nye Mudstone

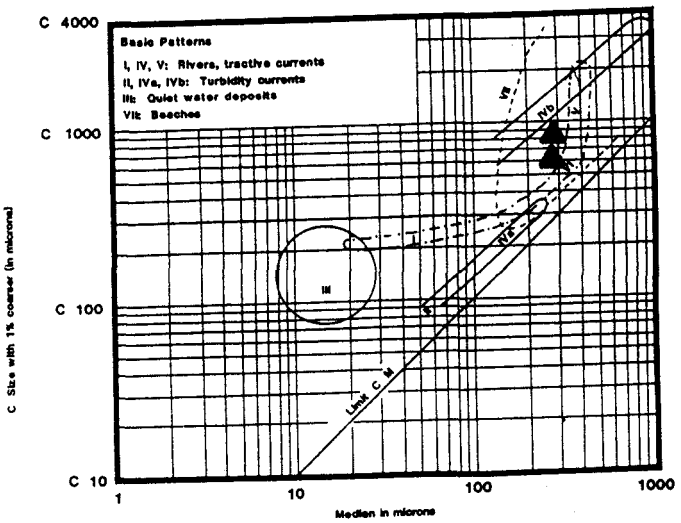

Netarts Bay member
Astoria Formation

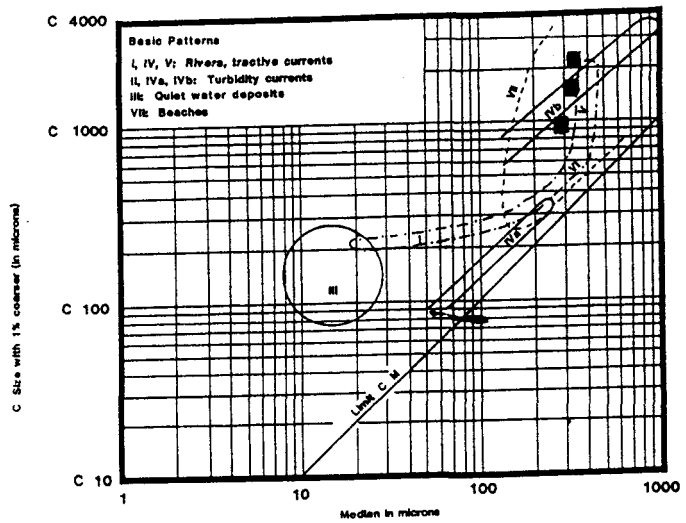

Cannon Beach member
Astoria Formation

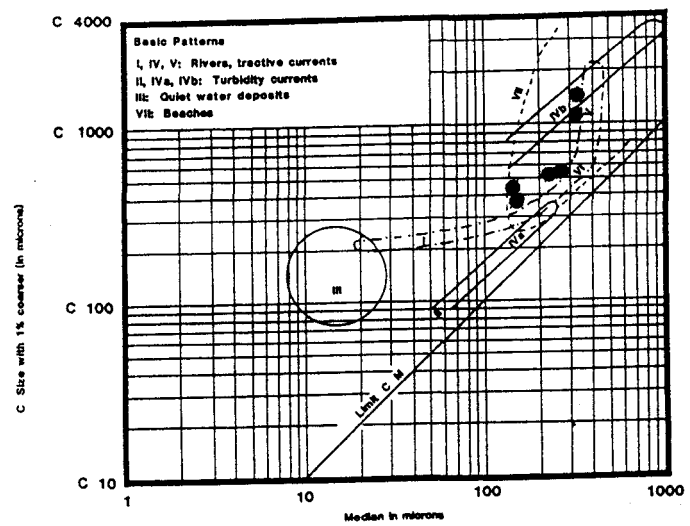

Figure 120.

sub-field IVb, which is appropriate for turbidites, or near sub-field IV, which is typical for rivers and tractive currents. The dispersion of Cannon Beach member data points outside of the turbidite fields is interesting because most samples from this unit were taken from deep-marine thin-bedded sandstones displaying classic Bouma structures. Errors in sampling and sample preparation may have caused some artificial biasing of grain size populations resulting in the dispersion of these data points outside of the turbidite fields. Dispersion of the points from each of these sandstone units toward the "rivers-tractive currents" field may also be the result of turbidite amalgamation. The grain size distributions of samples from Bouma B and B-C amalgamated turbidite sands may be biased toward the tractive currents field, as these Bouma intervals reflect tractive depositional processes, the Bouma D and E layers deposited from suspension having been stripped by successive turbidity currents. Samples from grain flow deposits common in the Netarts Bay member also plot outside the "turbidite" field. However, because the Passega diagram has no corresponding field for this type of transport medium, it may be inadequate for evaluating these types of deposits. The diagenetic and sampling effects on grain size populations may also account for some displacement of these points away from the turbidity current and tractive current fields. In general, the deep marine sandstones plot on the Passega diagram with larger coarsest 1% values than do the shelf sands discussed earlier in this section, which may reflect the greater competency of the transport media that deposited these deep-marine sandstones.

The bivariant diagrams of Kulm et al. (1975), though not suited to evaluate the depositional environment of deep marine channel fill and

turbidite sandstones, are useful for comparing these units to one another, and may also provide clues as to the source of these sands. In each of the three diagrams (Figures 117 and 118-A and B), deep water sandstones tend to group among the shelf sand data points, which may indicate that some of the textural characteristics of the deep marine sandstones, such as grain size, were inherited from the sands on the continental shelf. Channels feeding these deeper water deposits may have cut into the shelf and slope, and supplied shelf sand that was swept into the submarine channels by storm wave action, and contour, turbidity, and longshore currents.

Figures 118-A and B show that the Sutton Creek member of the Nye Mudstone, Netarts Bay, and Cannon Beach members tend to plot among the coarsest-grained shelf sandstones of the Bewley Creek formation, Angora Peak member of the Astoria Formation, Sandstone of Whale Cove, and the sandstone interbed within the Grande Ronde Basalt. This may reflect the relatively high competency of the transport media that deposited these strata, or that some sand that fed these deep water deposits was sourced from the inner shelf, or a combination of these two factors.

STRUCTURAL GEOLOGY

Regional Structural Geology of the Northwest Oregon Coast Range

The Tertiary strata within the Tillamook embayment occur on the western flank of the Northern Coast Range uplift, a broad arch cored by a 5000 to 7000 m thick basement of lower to middle Eocene Siletz River Volcanics and the middle Eocene Tillamook Volcanics (Snavely and Wagner, 1964). Although this uplift was originally described by Snavely and Wagner (1964) as a northward-plunging anticlinorium, subsequent study conducted by Wells et al. (1983), several graduate students at Oregon State University (e.g. Mumford, Safely, Rarey, Murphy, Cooper), Niem and Van Atta (1973), and Niem and Niem (1985) revealed little evidence to substantiate the existence of subsidiary folds over the arch. Instead, geological study of Clatsop county, Oregon, shows that the style of deformation in both the Eocene basement volcanic rocks and thick overlying Tertiary sedimentary and volcanic strata is dominated by a complex network of northwest-trending right-lateral, northeast-trending left-lateral, and older east-trending oblique-slip faults (Niem and Niem, 1985; Wells et al., 1983, Snavely and Wagner, 1964).

Several plate tectonic scenarios have been formulated to describe the timing and style of uplift and deformation in the northern Oregon Coast Range, and many of these are still being debated. One of the most widely accepted hypotheses is that western Oregon has undergone a long history of deformation resulting from the oblique subduction of the northward-moving Farallon and Juan de Fuca plates under the North American Plate (Wells and Heller, 1988; Wells et al., 1984; Wells and

Coe; 1985; Magill et al., 1981; Snavely, 1987; Niem and Niem, 1984). In response to the relative motion between these plates, some of the fault patterns on the leading edge of the North American Plate may have been the result of distributed dextral shear (Wells and Heller, 1988; Niem and Niem, 1985) which could account for increasing amounts of observed clockwise crustal rotation in volcanic rocks with decreasing distance from the western edge of the North American Plate (Wells and Heller, 1988).

Uplift and faulting of Tertiary strata in western Oregon may have occurred during discrete episodes corresponding to periodic high rates of convergence between the subducting Farallon (and later the Juan de Fuca Plate) and the North American Plate (Snavely, 1987; Niem and Niem, 1984). According to Snavely et al. (1980) these periods occurred during the late-early Eocene, middle-late Eocene, late-middle Miocene, Pleistocene and Holocene. Fault patterns and types within Clatsop and northernmost Tillamook Counties, Oregon, also provide clues regarding the tectonic history of western Oregon. Field evidence in this region suggests that the first episode of faulting occurred during the late Eocene, and was characterized by block-faulting created under an extensional stress regime (Niem and Niem, 1985; Snavely, 1987; Nelson, 1985). This was followed in post middle Miocene time by the creation of northwest and northeast-trending oblique-slip faults, and subordinate southward-verging thrust faults reflecting both north-south compression and wrench fault tectonics (Niem and Niem, 1985; Nelson, 1985).

In any structural interpretation of northwest Oregon it should be noted that the long history of Tertiary crustal rotation (up to 80° in accreted middle Eocene seafloor; Wells and Heller, 1988), coupled with a

similarly long history of faulting, may have resulted in deformation of crustal blocks along faults inherited from previous tectonic episodes (Wells and Heller, 1988). This added complexity makes it difficult to unravel the regional tectonic/folding-faulting history of the northwest Oregon.

Folding in the Thesis Area

Oligocene and Miocene strata in the Tillamook embayment generally dip westward from 10 to 25°, and are broadly deformed as a gently westward-plunging syncline that spans from Cape Meares to Cape Lookout (Cooper, 1981; this study; Plates I and II). The northern limb of this fold is defined by the northwest-striking, southwest-dipping Angora Peak and Cannon Beach strata that crop out adjacent to Tillamook Bay from Pitcher Point to Memaloose Point. The southern limb is defined by the northeast to east-striking, northwest and northward-dipping strata within Cape Lookout State Park (Plate I). The synclinal axis is difficult to locate precisely due to local structural perturbations near faults, however it generally trends through Netarts Bay where Cooper (1981) originally mapped it.

Faulting in the Thesis Area

Faults in the Pacific Northwest are notoriously difficult to locate or trace over a long distance because they are typically obscured by thick vegetation. As a result, several faults in the study area have been defined (Plate I) through means other than direct observation of offset, gouge zones, and slickensides. These methods include the apparent offset of rock unit contacts, juxtaposition of differing rock

types based on general outcrop patterns, and aligned rock attitudes discordant with regional trends. The latter criteria was used with extreme caution because slumps, slides, and folds may also be the cause of local changes in attitude.

In order to facilitate the process of locating faults in the thesis area, a lineament map (Figure 121) was constructed using low altitude aerial photographs, USGS topographic maps, and satellite (ERTS) images. Figure 121 shows that the study area is crossed by numerous northwest- and northeast-trending lineaments, most of which correspond with the axes of stream drainages incised onto the dip or antidip slope of strata in the Tillamook embayment (Plate I). However, comparison of Figure 121 with the thesis area fault pattern illustrated on Figure 122 shows that some of these lineaments and drainages are also fault controlled. Given the extent to which the area is vegetated, it is probable that many other lineaments illustrated in Figure 121 may correspond to faults that were undetected in this study.

Figure 122 is a compilation of faults discovered during the course of both this study and that of R. Wells, P. Snavely Jr., and N. Macleod of the USGS who are presently mapping a large region which includes the Tillamook area. Of these faults, all were observed directly with the exception of the Sand Creek, Tillamook River, Beaver Creek, Short Creek, and Netarts Bay faults, which were delineated on the basis of apparent stratigraphic offset and anomalous rock attitudes alone.

The study area is dominated by many northwest- and northeast-trending faults, and a subordinate number of east-trending faults (Figure 122). Most were mapped within the well exposed seacliffs of Columbia River Basalt units south of the Cape Meares headland and in

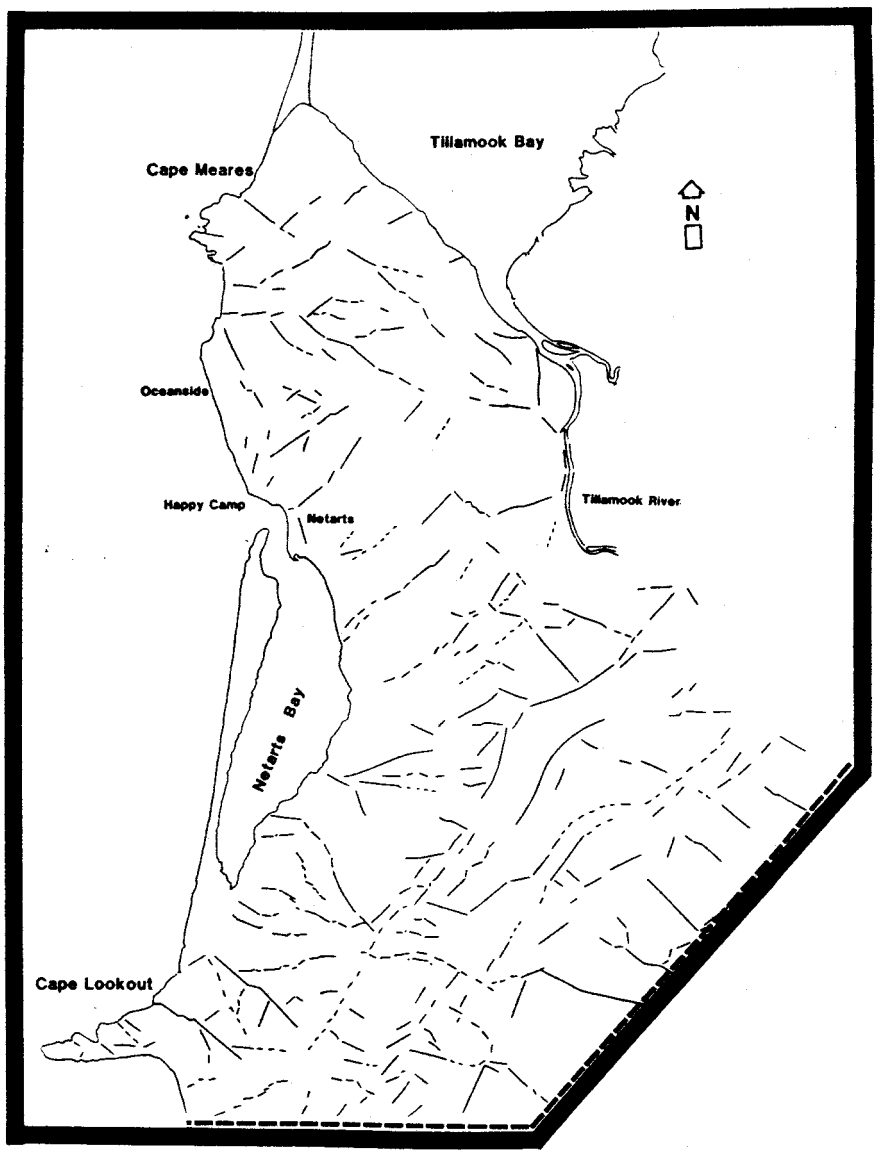

Figure 121. Lineament map of the study area

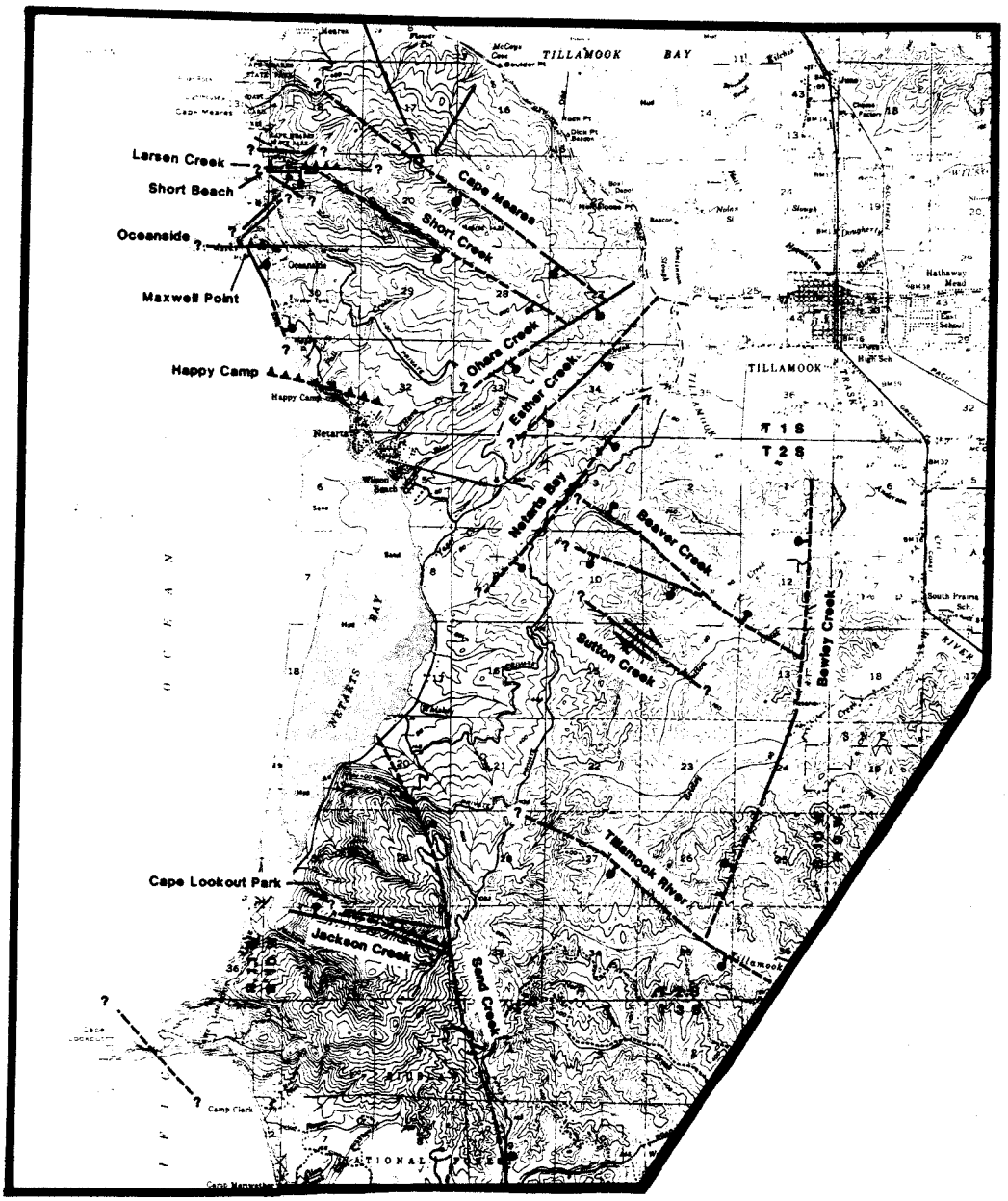

Figure 122. Fault map of the study area.

basalt rock quarries. However, a few faults were also observed within fresh logging road cuts. Unfortunately, the cross-cutting relationships and relative ages of most of these faults is difficult to determine because offset is typically relatively minor, fault traces are hard to follow, piercing points are not well defined, and fault intersections are almost universally hidden beneath thick coastal vegetation.

Northwest-Trending Faults

The Maxwell Point fault is located at Maxwell Point just north of the Oceanside Beach State Wayside in a seacliff composed of Columbia River Basalt (northeast quarter sec. 25, T. 1 S., R. 11 W.). It is very well exposed (Figure 123) and characterized by an eastward-dipping high angle fault plane (80°) that strikes N 35° W. The dip of the basalt pillow breccia complex on the east side of the fault appears to have been dragged upward into the fault plane, suggesting this is a normal or oblique-slip fault. The amount of throw is difficult to determine because the relative stratigraphic position of these juxtaposed volcanic horizons is not known.

The Cape Meares fault cuts through the northern part of the study area (Plate I; Figure 122) and is exposed at locality 7-88 (northeast quarter sec. 28, T. 1 S., R. 10 W.). It offsets pillow basalts of the Columbia River Basalt, trends N 45° W, and dips to the west at 73°. Deformation of pillows suggests that the fault is downthrown on the south side and subhorizontal slickensides within the fault plane indicate that the last motion along the fault was oblique strike-slip. The Cape Meares fault is dashed all the way to the north side of Cape Meares where it is obscured by Quaternary landslide deposits. This fault

Figure 123. High angle oblique-slip fault at Maxwell Point. Note how elongate pillows within the seacliff of Grande Ronde pillow palagonite breccia in downthrown block (right half of photo) are dragged upward into the fault plane. Motel suite at top of landsliding cliff for scale.

may be responsible for the northwest-trending cliff face on the north side of Cape Meares.

The Sutton Creek fault (Figure 122) was mapped by R. Wells of the U.S. Geological Survey who found subhorizontal slickensides suggesting oblique strike-slip as the latest motion along this fault. It strikes N 45° W and may account for right-lateral separation of Netarts Bay member strata and anomalous attitudes in the Cannon Beach member in the northeast quarter of section 15, T. 2 S., R. 10 W. (Plate I).

The Happy Camp fault is located 100 m north of Happy Camp in a sea cliff on the north side of Fall Creek (center sec. 31, T. 1 S., R. 10 W.), and strikes approximately N 28° W and dips 10° to the north. This fault is quite interesting and potentially important because it appears to be a thrust which offsets Columbia River Basalt approximately 1 meter and dies in unconsolidated Quaternary beach basalt gravel which has no shear strength. It should be pointed out, however, that the fault exposure is rather poor near the unconsolidated gravel, and it remains ambiguous whether the Quaternary deposits are actually involved in the thrust faulting.

Northeast-Trending Faults

The Bewley Creek fault in the eastern part of the study area (Figure 122) is exposed at locality SNB-100 (center sec. 24, T. 2 S., R. 10 W.), and juxtaposes Smuggler Cove formation siltstones with Bewley Creek sandstones along most of its length (Plate I). The fault is characterized by a 1 meter wide subvertical zone of sheared siltstone which strikes N 25° E. Sandstone beds on the west side of the fault are dragged up into the gouge zone. Northeast of locality SNB-100 the fault strikes in a more northerly direction and is obscured by Quaternary

alluvium in section 1, T. 2 S., R. 10 W. The northward deflection of the fault is based on the anomalous opposing rock attitudes in section 13, T. 2 S., R. 10 W., and juxtaposed Smuggler Cove formation siltstones opposite Bewley Creek formation sandstones. Approximately 2 km of left-lateral separation is indicated by the displacement of the lower contact of the Bewley Creek Formation.

Ray Wells of the U.S. Geological Survey also mapped both the Ohara and Esther Creek faults. The Ohara Creek fault strikes approximately N 45° E, dips to the south at 50°, and is downthrown on the south side. Similarly, the Esther Creek fault strikes approximately N 45° E, and may also be downthrown to the south.

The Netarts Bay fault parallels the Esther Creek fault and is downthrown on the south side. Although no direct evidence for this fault was found in the field, the wide stratigraphic separation of Angora Peak strata between section 1, T. 2 S., R. 10 W., and section 35, T. 1 S., R. 10 W., suggests either left-lateral or normal (down on the south) motion along an intervening fault. The fault was mapped to correspond with the topographic depressions along Yager and Fagan Creeks.

East-Trending Faults

The Jackson Creek fault (Figure 122) is exposed in the southern part of the study area at two locations in Grande Ronde Basalt: CL-84 (northeast quarter sec. 32, T. 2 S., R. 10 W.) and CL-85 (northeast quarter sec. 31, T. 2 S., R. 10 W.). At CL-84 the fault strikes N 65° W, dips to the south at approximately 70°, and is characterized by a 1.5 m wide gouge zone. Columbia River Basalt composes the hanging wall, and an interflow sandstone interbed composes the footwall. Sandstone beds are dragged upward into the fault gouge zone suggesting this is a high angle

reverse fault. At locality CL-85 to the west, the Jackson Creek fault strikes N 70° W and dips to the south at 47°. Columbia River Basalt occupies the hanging wall, and the Sandstone of Whale Cove occupies the footwall. The fault plane is very sharp and well defined, however no evidence of drag is present in either the basalt or sandstone interbed. Because the basalt at CL-85 does not resemble the plagioclase-phyric Frenchman Springs Basalt which overlies the Sandstone of Whale Cove, it probably represents Grande Ronde Basalt which underlies this sedimentary unit, thus indicating that the Jackson Creek fault is is a high angle reverse fault. Approximately 50 m of throw is estimated for the Jackson Creek fault.

Twenty meters to the north of the Jackson Creek fault at locality CL-84 is the Cape Lookout Park fault (Figure 124), which strikes N 75° W and dips 35° to the north. This fault is very well exposed, is up on the north side, and appears to be a thrust along which three meters of displacement (measured in the plane of the fault) has occurred. Thrust motion along this fault is further indicated by drag folding within sandstone strata which sweep upward into the underside of the fault plane from the south side. The hanging wall is composed of a Grande Ronde Basalt flow and overlying sandstone interbed, and the footwall is composed of the adjacent sandstone interbed. Vertical separation of strata on either side of the Cape Lookout Park fault is approximately one meter.

The Larsen Creek fault is located at locality M-114 (northeast quarter sec. 19, T. 1 S., R. 10 W.), strikes due east, and dips to the north at 25°. The fault occurs within altered basalt pillows of the Grande Ronde Basalt, and similarity of lithological characteristics

Figure 124. Thrust fault with small offset of basalt flow and sandstone interbed within Winterwater Unit of the Grande Ronde Basalt (locality CL-84). Notebook for scale.

above and below the fault suggest that the amount of throw along the Larsen Creek fault is fairly small. One of the basalt pillows appears to have been cut by the fault, with the upper half moved approximately two meters to the south along the fault plane. If this is a reliable piercing point, the Larsen Creek fault is a thrust fault with approximately two meters of offset.

Possible Stress Regimes Accounting for the Pattern of Faulting Mapped in the Tillamook Embayment

North-South Compressional Stress Regime

The apparent and observed sense of motion along many faults in the Tillamook embayment suggest that they may have been created during a post middle Miocene compressional stress regime that was oriented north-south. The theoretical pattern of faulting established under these conditions is northwest-trending right-lateral, northeast-trending left lateral, and east-west trending thrust and reverse faults (Davis, 1984). Strata cut by the northeast-oriented Ohara Creek, Esther Creek, Netarts Bay, and Bewley Creek faults all have an apparent left-lateral separation, and strata cut by the northwest-oriented Beaver Creek, Sutton Creek, and Sand Creek faults have an apparent right-lateral separation. East-west striking faults in the Tillamook embayment including the Cape Lookout Park, Oceanside, and Larsen Creek faults, are all low angle thrust faults, and the east-trending Jackson Creek fault is a high angle reverse fault. The pattern of observed offset and stratigraphic separation support a north-south compressional regime, and agrees with the studies of Niem and Niem (1985) and Nelson (1985), who also interpreted many of the faults of Clatsop and Northernmost

Tillamook Counties to be the product of post middle Miocene north-south compression.

It should be noted that many of the faults directly observed in the thesis area show characteristics of normal motion (e.g. drag folding along the Maxwell Point, Cape Meares, and Bewley Creek faults). This may have been caused by oblique-slip motion along these faults, possibly related to a wrench fault tectonic regime (discussed below), or may represent a later period of extension which occurred on pre-existing strike-slip faults. Alternatively, the faults that appear to have a normal component may have been created under an exclusively extensional stress regime.

Dextral Shear-Couple Stress Regime

Paleomagnetic data collected from western Oregon indicate that the region has undergone substantial cumulative clockwise rotation since the middle Eocene (Wells et al., 1984; Wells and Heller, 1988). Wells et al. (1984) and Wells and Heller (1988) suggested that this rotation could be explained, in part, by small block rotations within a dextral shear couple, and noted that the pattern of faulting in northwest Oregon is largely consistent with Riedel shear rotation (Wells and Coe, 1985). In their description of fault patterns in the Astoria Basin, Niem and Niem (1985) suggest that at least part of the pattern may be attributed to a regime of wrench fault tectonics. The pattern of faulting theorized to occur under a dextral wrench fault tectonic regime are north and northwest-trending oblique-slip dextral faults and east-west trending sinistral faults (Wilcox et al., 1973). Pull apart basins and high angle normal faults also may develop where oblique-slip faults diverge (Wilcox et al., 1973).

In the study area, strata cut by the northwest-trending Sand Creek, Beaver Creek, and Sutton Creek faults display right-lateral separation. These may correspond to the right-lateral northwest-trending faults predicted in a wrench fault tectonic regime. Strata cut by the northwest-trending Cape Meares and Short Creek faults show left-lateral separation, may have originally developed as east-west trending sinistral faults, but later rotated clockwise to their present northwesterly position during subsequent dextral shearing of the area in the late middle Miocene.

GEOLOGIC HISTORY OF THE TILLAMOOK EMBAYMENT

Strata within the Tillamook embayment were deposited after a time of profound tectonic reorganization within the Pacific Northwest which was initiated by the accretion of a portion of the Farallon Plate to the North American Plate during the middle Eocene (Snavely et al., 1973; Wells et al., 1984). This caused substantial changes in the configuration of the ancestral North American Plate margin as the pre-accretion subduction zone shifted from its old position beneath the present Cascade arc, westward to its current location (Snavely et al., 1980). Upon docking with the North American Plate, this accreted basement of seafloor and seamount basalt (Siletz River Volcanics) began receiving terrigenous siliciclastic sediment from prograding depositional systems (e.g. Yamhill, Hamlet and Cowlitz fm.). Contemporaneous with middle to late Eocene sedimentation, shield volcanoes of the Tillamook Volcanics were erupted on the accreted plate as seamounts (Wells et al., 1984).

The accreted section of the Farallon plate began to function as a forarc basin in western Oregon upon establishment of the Western Cascade volcanic arc in the late Eocene and early Oligocene (Niem and Niem, 1984). From the time of the onset of Western Cascade volcanism, a depo-tectonic configuration was achieved that has strongly influenced sedimentation patterns in northwestern Oregon through Neogene and Holocene time. This configuration was characterized by oblique subduction of the Juan de Fuca Plate to the west of the forearc basin (Wells and Heller, 1988), Western Cascade arc volcanism to the east, and an uplifted granitic and metamorphic provenance in eastern Oregon,

western Montana, Idaho, and northeastern Washington drained by a westward-flowing ancestral Columbia River. This dynamic depo-tectonic framework existed during deposition of the upper Oligocene to middle Miocene strata of the Tillamook embayment.

The geologic history of the study area opened during a significant period of shallowing within the forearc basin, possibly initiated by broad uplift of the ancestral Oregon Coast Range through the late Oligocene and early Miocene (Snavely and Wagner, 1963). During this time marine sedimentation was restricted to four embayments on the west side of the Oregon and Washington Coast Ranges: the Tillamook, Newport, Astoria, and Grays River embayments (Snavely and Wagner, 1963). This marine regression is recorded in the Tillamook embayment within strata of the Zemorrian to lower Saucesian Smuggler Cove formation.

Smuggler Cove formation strata were deposited in a pro-delta slope setting seaward of an ancestral Columbia River-fed westward-prograding shallow-marine wave-dominated Bewley Creek formation depositional system. Increasing proximity to this system with time is marked by a transition from lower to middle bathyal tuffaceous continental slope mudstones, through thin turbidite sandstone-bearing upper bathyal slope mudstones, to outer shelf turbidite sandstones, siltstones, and bioturbated fossiliferous silty sandstones. The shallowing-upward sequence within the Smuggler Cove formation, and tuffaceous nature of mudstones within this unit suggest that these late Zemorrian to early Saucesian strata were deposited during a marine regressive phase that corresponded with a period of explosive silicic volcanism in the Western Cascade arc.

Regional uplift or a pulse of rapid sedimentation during the lower Miocene (Pillarian-stage) caused storm wave-dominated hummocky cross-stratified fine-grained lower shoreface deposits and superjacent shallow marine coarse-grained cross-bedded and channelized sandstones of the Bewley Creek formation to prograde westward into the Tillamook embayment. Conformably overlying the Smuggler Cove formation, these strata represent either a wave-dominated delta-inner shelf complex or a wave-dominated shelf and ebb-tidal delta system. Abundant micaceous quartzo-feldspathic sediment was supplied to this depositional system by an ancestral Columbia River drainage system, which primarily sourced siliciclastic sediment from distant Idaho batholith sources. Proximal sources have also influenced the composition of Bewley Creek arkosic-lithic sandstones, however, with minor contribution of mafic volcaniclastic detritus from the Tillamook Volcanics. Although some of the silicic volcanic detritus present in Bewley Creek formation sandstones may have been eroded from from older rhyodacitic and dacitic flows of the ancestral Western Cascade arc, abundant cross-bedded pumiceous coarse-grained sandstones and tuffaceous mudstones attest to contemporaneous vigorous Western Cascade arc volcanism. Voluminous volcaniclastic detritus shed into the ancestral Columbia River during these catastrophic eruptive events may have been partly responsible for the rapid initial progradation of this unit into the Tillamook embayment. Bewley Creek formation shallow marine sedimentation finally ceased during a marine transgression that caused a rapid transition from shoreface conditions to outer shelf and slope conditions in the Tillamook embayment. This may have resulted from a reduction in volcanic activity-related sedimentation from the Western Cascade arc, increased

rate of subsidence in the forearc, migration of the debouchment point of the Columbia River away from the Tillamook embayment, or a combination of these factors.

Marine transgression in the Tillamook embayment caused a rapid facies shift which culminated in the deposition of early Miocene (Pillarian-stage) upper bathyal slope mudstones of the Sutton Creek member of the Nye Mudstone. These fine-grained strata were deposited in a low energy environment characterized by hemipelagic and rare turbidite sandstone sedimentation. Although rare thin tuff beds present in the Sutton Creek member attest to continuing silicic volcanism in the Western Cascade arc, the unit is much less tuffaceous than Smuggler Cove formation mudstones, suggesting that explosive silicic volcanic activity was substantially reduced during Sutton Creek time. Late in the geological history of this unit a marine regression occurred, signifying westward progradation of the wave-dominated shallow marine Angora Peak of the Astoria Formation depositional system. Shallowing of the Tillamook embayment is marked by a coarsening-upward transition from laminated mudstones to turbidite sandstone- and mudstone-filled nested submarine channels within the upper part of the unit. These channels, or sea gullys, were cut into the upper slope and outer shelf, and acted as conduits that allowed surplus sediment to bypass the Angora Peak member depositional system on the shelf for delivery to the slope.

During the second marine regression of the lower Miocene (Pillarian-stage), the wave-dominated delta complex or wave-dominated shelf and ebb tidal delta system of the Angora Peak member prograded westward into the northern part of the Tillamook embayment Cape Meares area). Abundant arkosic-micaceous sediment was transported to a shallow

marine environment by the ancestral Columbia River, and subsequently reworked by strong storm waves into thick amalgamated hummocky cross-stratified lower shoreface sandstone deposits. At the time of maximum progradation or regression, the northern part of the study area was cut by shallow marine channels representing nearshore submarine delta distributary or ebb tidal channels. These were subsequently filled by coarse-grained quartzo-feldspathic and volcaniclastic detritus. Although the same provenances that contributed to the Bewley Creek formation also supplied sediment to the Angora Peak member, Angora Peak member sandstones in the Tillamook area are generally less enriched in volcaniclastics, and lack both pumice or tuff interbeds. This may indicate that progradation of the Angora Peak member depositional system proceeded during a period of relative quiesence in the Western Cascade arc. Subsidence in the Tillamook embayment followed, and deeper marine facies of the Cannon Beach and Netarts Bay members succeeded Angora Peak sedimentation in the northern part of the Tillamook embayment. In the southern part of the Tillamook embayment at Cape Kiwanda, sedimentary strata had been subaerially exposed and extensively eroded during the late Pillarian-stage. However, while the subsidence in the Tillamook embayment to the north was causing a shift from middle shelf to outer shelf and slope conditions, Newportian-stage lower and upper shoreface Angora Peak strata were being deposited in the Cape Kiwanda area.

Although sedimentation could not keep pace with the rate of subsidence at the end of Angora Peak time, the ancestral Columbia River was still delivering abundant arkosic-micaceous sediment to the shelf east of the Tillamook embayment. Some fine to medium-grained arkosic-micaceous sandstones of the overlying Netarts Bay member were

deposited within a submarine canyon head and smaller channels incised into the outer shelf and slope by turbidity currents and other tractive currents carrying surplus sand to the slope. Deposition of Netarts Bay member massive grainflow and high-concentration turbidite sandstones was abruptly terminated when channels were abandoned as coarse clastic detritus became increasingly trapped on the shelf and in estauries during transgression.

The lower to middle Miocene (Saucesian) Cannon Beach member of the Astoria Formation was deposited both contemporaneously with and following Netarts Bay member channel-fill sandstones and bathyal mudstones. Characterized by a thick sequence of middle to upper bathyal mudstones and some thin-bedded turbidite sandstones, most of the Cannon Beach member reflects a continental slope environment that was increasingly starved of coarse clastic material as transgression continued. However, regression late in Cannon Beach time within the Tillamook embayment is chronicled by a thickening and coarsening upward transition from laminated bathyal slope mudstones, through an upper slope-outer shelf interbedded and amalgamated turbidite sandstone-rich nested-channel facies, to outer and middle shelf bioturbated sandstones. Similar to the Sutton Creek member of the Nye Mudstone, Cannon Beach member mudstones are not very tuffaceous, indicating a continuing moderate level of Western Cascade volcanism through Cannon Beach time.

After deposition of the Cannon Beach member, the Tillamook embayment experienced a major marine regression that may have been initiated by local or regional uplift of the northern Oregon Coast Range during the middle Miocene. This culminated in substantial erosion of lower to middle Miocene Cannon Beach and Netarts Bay member strata in

the Cape Lookout area, and was followed by a small amount subsidence or transgression prior to the arrival of the first flows of the Columbia River Basalt in the Tillamook embayment. These Columbia Plateau-derived basalts were erupted from fissure swarms in eastern Oregon and Washington and flowed down the ancestral Columbia River drainage system (Snavely and Wagner, 1963) to the coast of Oregon and Washington (Beeson et al., 1979). They accessed the Tillamook embayment by flowing westward through a saddle or gap in the ancestral northern Oregon Coast Range that existed to the east.

The R_2 low MgO Grouse Creek unit flows of the Grande Ronde Basalt were the first to reach the Tillamook embayment. These basalts flowed into the northern part of the study area where they encountered a shallow marine environment and formed closely packed pillows. The N_2 low MgO Winterwater unit of the Grande Ronde Basalt followed, and flowed into both the Cape Meares and Cape Lookout areas. The first flow of this unit formed a submarine lava delta with an overlying subaerial couplet. Subsequent flows are entirely composed of foreset bedded pillow basalts and pillow palagonite breccias. The N_2 high MgO Sentinel Bluff Unit, last of the Grande Ronde Basalt flows to reach the Tillamook embayment, also moved into the Cape Meares and Cape Lookout areas. However, these flows built upward from pillow palagonite foreset breccias to columnar-jointed flows, indicating substantial aggradation of the basalt pile from submarine to subaerial conditions. Several marine sedimentary interbeds occur between Grande Ronde flows and are predominantly composed of arkosic-micaceous sandstone. The Sentinel Bluff and Winterwater basalts compose local invasive peperitic sills and dikes in the study area. These may have been injected into Miocene strata along

zones of weakness, possibly joints or faults, under the a combination of pressure head and pneumatic pressure generated from the flash of superheated formation water.

Emplacement of the last Grande Ronde Basalt Unit in the Tillamook embayment was followed by rapid subsidence during which hummocky cross-stratified lower shoreface deposits of the middle Miocene Sandstone of Whale Cove were deposited over both Sentinel Bluff and Winterwater basalt flows. Compositionally similar to sandstones of the Angora Peak member of the Astoria Formation, the Sandstone of Whale Cove is predominately arkosic-micaceous, and was deposited on a storm wave-dominated shelf that was richly-supplied sediment from an ancestral Columbia River or reworked Astoria Formation sandstone.

Responding to local or regional uplift during the middle Miocene, the Tillamook embayment experienced another period of subaerial exposure. During this time the plateau-derived plagioclase-phyric Ginkgo Unit of the Frenchman Springs Basalt flowed into both the Cape Meares and Cape Lookout areas, possibly following the same pathways as the preceding Grande Ronde Basalt units took into the Tillamook embayment.

Emplacement of the Ginkgo Unit in the study area has been followed by broad post middle Miocene uplift (Snavely and Wagner, 1963), which ulimately culminated in the incorporation of the Tillamook embayment section into the uplifted northern Oregon Coast Range. Considerable deformation of these strata has occurred since the late middle Miocene, and some faulting and minor folding may also have been taking place contemporaneously with deposition of rock units in the Tillamook embayment. Paleomagnetic data indicate that the Columbia River Basalts in the Tillamook embayment have rotated clockwise approximately 25°,

which may be related to a Neogene dextral shear couple associated with oblique subduction of the Juan de Fuca Plate under the North American Plate (Wells et al., 1984; Wells and Heller, 1988). The high angle northwest, northeast, and east-trending faults in the Tillamook embayment may have been created, in part under this stress regime. However, low angle east-trending thrust faults, and separation along several northwest and northeast-trending faults also suggest a period of post middle Miocene north-south compression. North-south compression is further indicated by the broad westward-plunging syncline which folds all mid-Tertiary Oligocene and Miocene strata in the Tillamook embayment.

SOURCE ROCK POTENTIAL

Introduction

Since the discovery of commercial quantities of natural gas in northwest Oregon at the Mist Gas Field in 1979 several oil companies have been re-evaluating the petroleum potential of the Pacific Northwest, and now view the region as a frontier of moderate to high potential. As a part of this renewed optimism, this study has been supported, in part, by the Unocal and Exxon Corporations who are seeking to increase their knowledge of northwest Oregon stratigraphy and structure through the funding of basic geological research.

Given the current interest in the hydrocarbon potential of northwest Oregon, one of the primary goals of this thesis project was to evaluate both the reservoir and source rock potential of rocks within the Tillamook embayment. Reservoir rock quality was evaluated through thin section petrography and scanning electron microscopy, and is discussed in the petrography section of each sandstone-bearing unit. The source rock potential of fine-grained strata in the Tillamook embayment was evaluated through a three step process which included: 1) collection of a total of ten source rock samples from the Cannon Beach member of the Astoria Formation, Sutton Creek member of the Nye Mudstone, and the Smuggler Cove formation within the study area; 2) processing of these samples by Exxon laboratories to determine vitrinite reflectance-thermal maturation values and rock-eval pyrolysis factors; 3) interpretation of source rock data upon return from Exxon.

Pyrolysis

Table 4 summarizes the results of pyrolysis and vitrinite reflectance analyses perfomed by Exxon. The values of S1, S2, S3 (expressed in kilograms per ton), TOC (total organic carbon; expressed in percent of sample), and T max (expressed in ^{o}C) were determined through the process of pyrolysis during which samples are heated to release volatile matter (Tissot and Welte, 1978). The value of S1 corresponds to free or adsorbed hydrocarbons that are liberated first during the heating process (Tissot and Welte, 1978). The value of S2 corresponds to hydrocarbons and hydrocarbon-like compounds within kerogen that volatilize at higher temperatures (Tissot and Welte, 1978). The S3 values indicate the amount of CO_2 and water released during the final high temperature stages of pyrolysis (Tissot and Welte, 1978). The TOC values are a measure of the total amount of organic carbon present in the sample, expressed as a percentage of the sample weight (Law et al., 1984), and the value of T max corresponds to the temperature that existed during the peak of S2 hydrocarbon liberation (Tissot and Welte, 1978). Individually and in combination, these values are useful indices for determining source rock quality and stage of maturation.

The amount of total organic carbon (TOC) in a rock is a general guide to source rock quality, and rocks containing TOC values exceeding 0.5% are generally considered to be effective hydrocarbon source rocks (Law et al., 1984). Samples collected from the Tillamook embayment have TOC values that range from 0.44 to 1.35% (Table 4). Cannon Beach member mudstones tend to be the most enriched, averaging 1.29% TOC, followed by the Sutton Creek member (1.12%), and the Smuggler Cove formation (0.76%). These TOC values probably reflect the disseminated terrigenous

organic matter observed within the mudstones of each of these rock units. It is important to point out that TOC of a rock can be greatly depleted by epigenetic surface weathering (Law et al., 1984), which can penetrate to significant depths within rocks of the Pacific Northwest. Although care was taken to collect the freshest samples possible, the TOC values of these samples may still have been depressed during deep weathering.

Table 4

Source Rock Analysis

Sample #	T Max	S1	S2	S3	S1+S2	S1/S1+S2	Ro	TOC	HI	OI
Cannon Beach member, Astoria Fm.										
NNB-6A	424	0.07	0.84	1.14	0.91	0.07	0.45	1.35	62	84
51-88	424	0.05	0.54	1.01	0.59	0.08	0.45	1.35	40	74
60-88	425	0.04	0.61	1.40	0.65	0.06	0.46	1.18	51	118
M-117	414	0.02	0.35	0.67	0.37	0.05	0.47	1.28	27	52
Sutton Creek member, Nye Mudstone										
CL-144	408	0.04	0.44	0.47	0.48	0.08	0.41	0.97	45	48
CL-145	419	0.02	0.41	0.67	0.43	0.04	0.46	1.27	32	52
Smuggler Cove formation										
36-88	427	0.01	0.36	0.38	0.37	0.02	0.41	0.91	39	41
CL-482	443	0.03	0.11	0.71	0.14	0.21	0.55	0.44	25	161
63-88	424	0.06	0.99	0.67	1.05	0.05	0.38	0.85	116	78
65-88	422	0.02	0.58	0.15	0.60	0.01	0.42	0.85	68	16

Whether a source rock is capable of generating oil or only natural gas is a function of the type of kerogen present. Three main types have been identified through the graphing of two indices: the hydrogen index (HI; S2/organic carbon) and oxygen index (OI; S3/organic carbon) (Figure 125; Tissot and Welte, 1978). Types I and II are the hydrogen-rich kerogens that are capable of generating oil or gas. Type III kerogen, however, is hydrogen difficient and capable of generating only natural

gas. Figure 125 shows that the source rock samples collected from the Tillamook embayment possess type III kerogen. Most of the kerogen within rocks of western Oregon are of this type (Law et al., 1984), and thus are regarded as gas source rocks.

Another valuable parameter for evaluating source rocks is the genetic potential, which is based on the total amount of mature and immature hydrocarbon present in a sample. It is calculated as the sum of S1 and S2 values and expressed in kilograms of hydrocarbon per metric ton of rock (Table 4; Tissot and Welte, 1978). Figure 126 has been sectored into empirically-derived fields defining source rock "quality" based on genetic potential, and shows that most samples collected in the study area are non source rocks, containing less than 2 kg/metric ton of hydrocarbon. Sample 63-88 stands out, however, as the only sample containing hydrocarbons in quantities exceeding 2 kg/metric ton.

The T max value calculated during pyrolysis (Table 4) is an index developed to help determine if a source rock has thermally matured to the point where it can generate oil or natural gas. When the S2 volatiles are driven from a sample at temperatures below 435°C the source rock is generally deemed thermally immature, indicating the rock has not been buried deep enough to "cook" or mature organic material into oil or gas (Law et al., 1984). Figure 127 shows that all samples colllected during this study are immature with the exception of Smuggler Cove sample CL-48Z, which is mature.

Another measure of the thermal maturity of a source rock is the transformation ratio (TR), which is calculated with the equation (S1/S1+S2) (Law et al., 1984). Because mature oil and gas-bearing rocks are enriched in S1 volatiles, the transformation ratio increases with

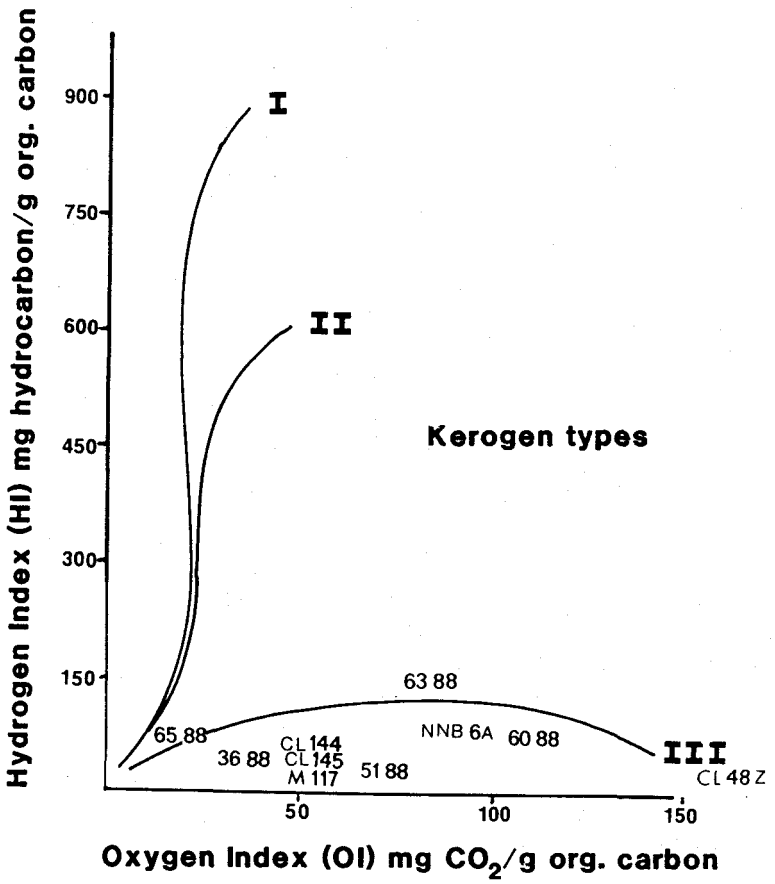

Figure 125. Classification of source rock types for samples collected from the Tillamook embayment by using hydrogen and oxygen indices. Slightly modified from Tissot and Welte (1978).

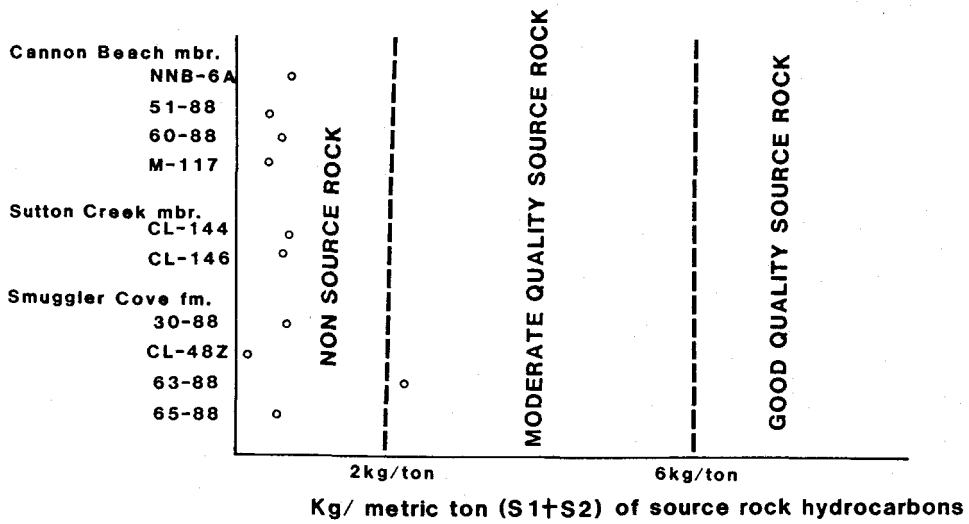

Figure 126. Classification of source rock quality based on Kg/ metric ton (S1 + S2) of source rock hydrocarbons (Tissot and Welte, 1979).

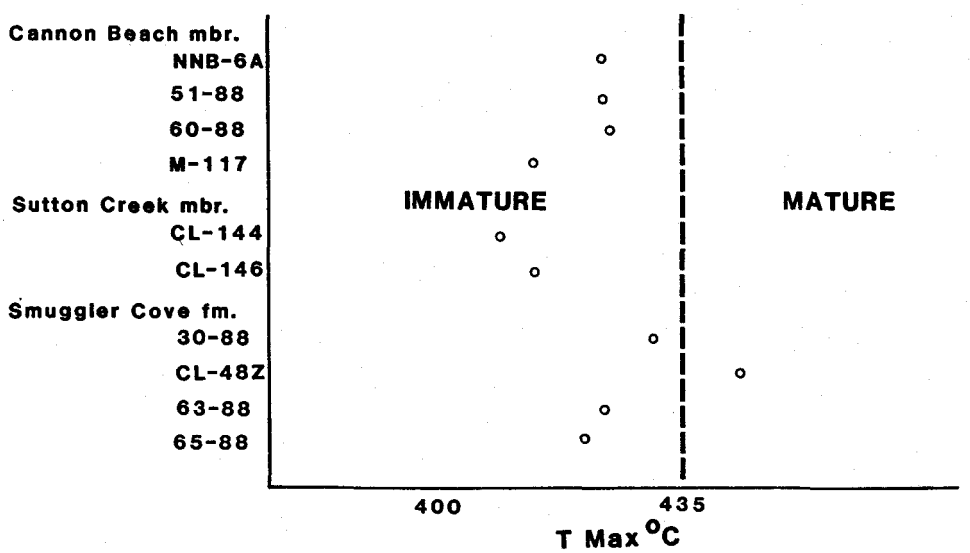

Figure 127. Classification of source rock maturity for thesis area samples based on T Max °C (Tissot and Welte, 1979).

maturity. A ratio of 0.1 represents the boundary between immature source rock and the oil generation window, and Figure 128 shows samples from the study are generally immature, averaging a TR of 0.067.

Vitrinite Reflectance

Vitrinite reflectance is an alternative method for determining the thermal maturity of source rocks that is independent of the pyrolysis technique. In the vitrinite reflectance method, the reflectance of disseminated organic matter (macerals) in fine-grained sedimentary rocks is measured in reflected light (Tissot and Welte, 1978). With increasing levels of thermal maturation, macerals of vitrinite, huminite, and inertinite become more reflective (Tissot and Welte, 1978). The reflectance value used to describe the thermal maturation level of a source rock usually corresponds to the group of macerals that give the lowest reflectance reading (population 1). The lowest reading is favored because macerals with higher reflectance often represent recycled or reworked organic matter from sedimentary units with different burial or thermal histories (Tissot and Welte, 1978). The average vitrinite reflectance values for population 1 macerals of samples collected from the study area are listed as Ro on Table 4 and plotted in Figure 129.

Figure 129 is sectored into fields defined by generally accepted vitrinite reflectance values that represent source rock maturity thresholds. The overlap between the immature and mature stages is the result of dissagreement among workers regarding where the boundary should be placed (Law et al., 1984). With the exception of sample CL-482, all samples are in the immature-diagenesis stage, which agrees with other results presented in this section.

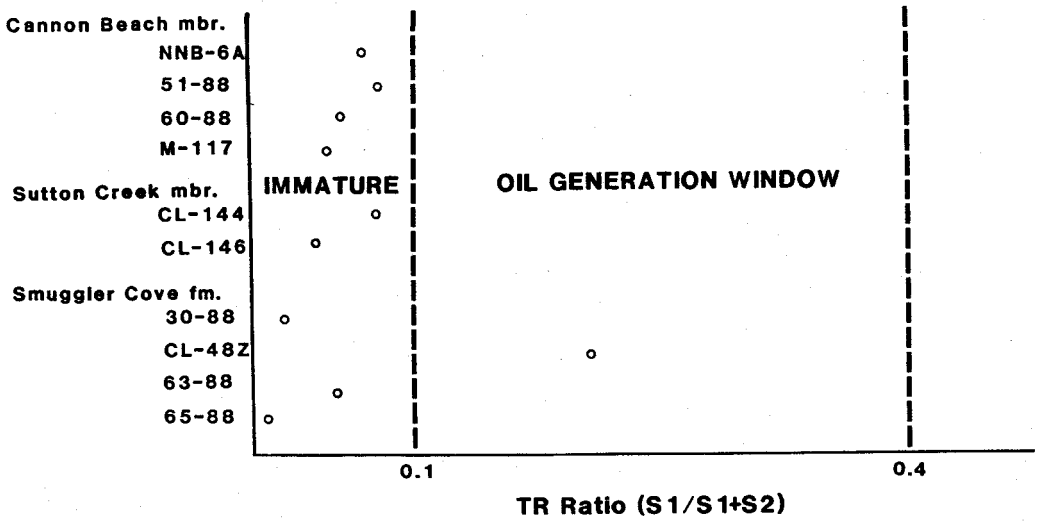

Figure 128. Source rock maturity evaluation diagram based on TR ratio (S1 / S1 + S2) (Tissot and Welte, 1979).

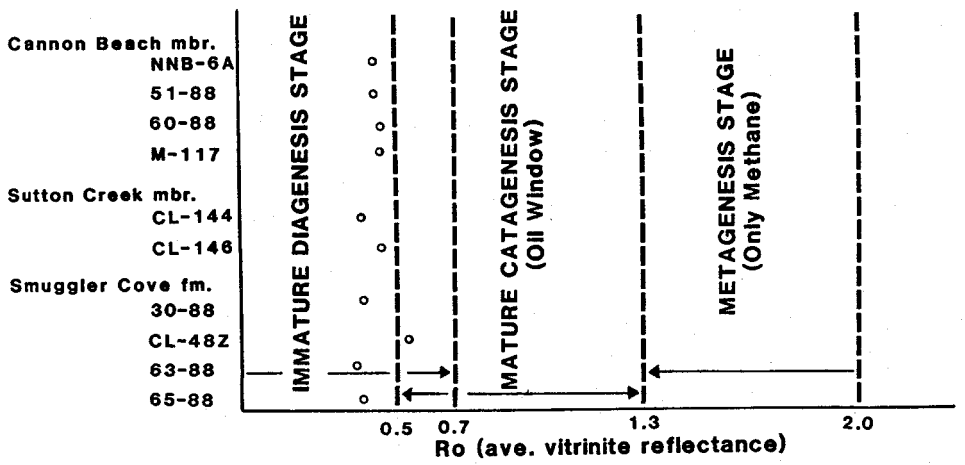

Figure 129. Classification of source rock maturity for thesis area samples based on the average value of vitrinite reflectance (Tissot and Welte, 1979; Law et al., 1984).

Because different types of kerogen have different vitrinite reflectance thresholds at which they mature, Figure 130 shows the position of thesis area sample vitrinite reflectance values with respect to kerogen type III. Again, these samples prove to be immature.

Conclusions

The results of the source rock analysis for mudstones of the Cannon Beach member of the Astoria Formation, Sutton Creek member of the Nye Mudstone, and Smuggler Cove formation are listed below:

1) Kerogen within mudstones inlcude type III kerogen, capable of generating natural gas only.

2) The TOC content of mudstones within the Tillamook embayment is sufficiently high to be considered a potential lean source rock.

3) The vitrinite reflectance, TR ratio, and T max indices all indicate that thesis area mudstones are generally too immature to generate natural gas.

Although these results suggest the Oligocene and Miocene section in the Tillamook embayment have low source rock potential, it should be noted that thermal maturation is the primary criteria that has not been met. Provided these strata could be thermally matured, either through deep burial, or by close proximity to middle Miocene basaltic sills and dikes as Niem and Niem (1985) suggest, these Tertiary strata could function as source rocks for natural gas.

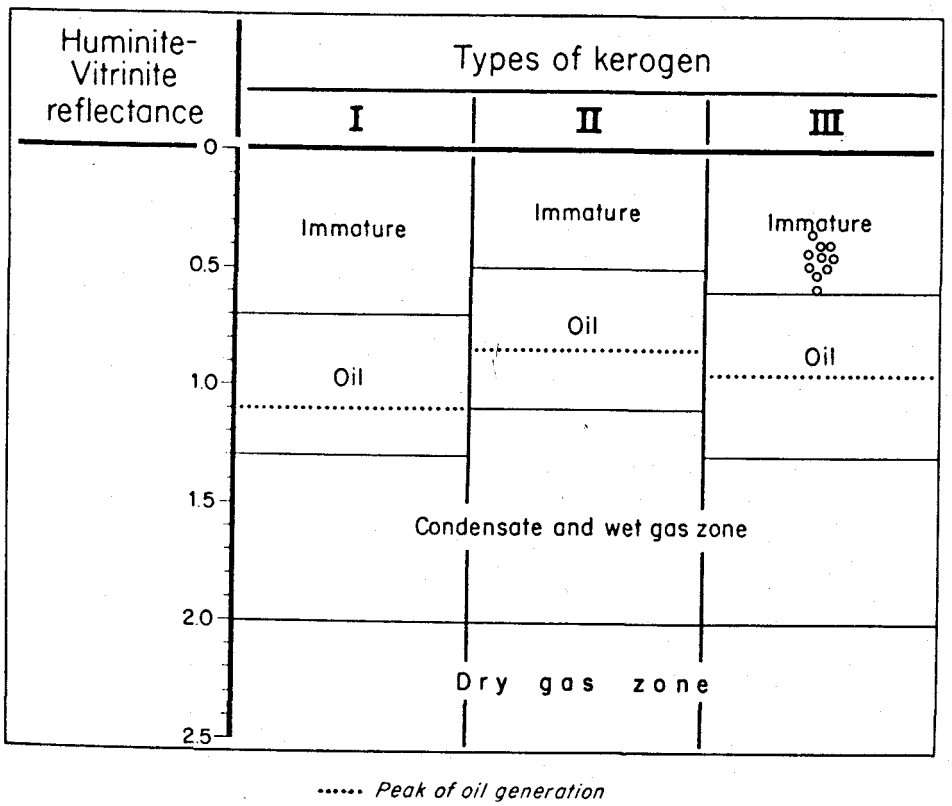

Figure 130. Classification of source rock maturity for thesis area samples based on vitrinite reflectance and kerogen type. After Tissot and Welte (1979).

QUATERNARY DEPOSITS

Quaternary deposits cover approximately 15 km^2 of the study area and include (in decreasing order of abundance): stream and river deposits (Qal); coastal dune deposits (Qd); colluvium (Qc); terrace deposits (Qt); landslide and slump deposits (Qls); and marsh deposits (Qm) (Plate I). Modern stream and river deposits underlie and flank the lower reaches of nearly all streams in the study area. They are most widespread at the base of Beaver, Sutton, Fagan, and Bewley Creeks, where they join the Tillamook River flood plain. These low-lying regions are typically heavily vegetated bogs and fresh-water swamps. A small but potentially important Quaternary stream deposit occurs along a seacliff just north of Happy Camp in section 31, T. 1 S., R. 10 W.. Here, approximately 10 m of unconsolidated basalt stream gravels overlying Columbia River palagonite breccias are offset about 1 meter by a southward-verging thrust fault (Figure 131; Wells, personal communication, 1988). However, this exposure is fairly weathered, and the cross-cutting relationship is difficult to make out. Nearby are invasive palagonite breccia dikes that deform Miocene (?) sandstone. Thus, the southward-verging thrust may be misinterpreted as Quaternary structure, and may actually be related to a period of middle Miocene basalt invasion.

Quaternary dune deposits are present along the coast at Cape Kiwanda, between the villages of Netarts and Oceanside, north of Sand Lake on the southern flank of Cape Lookout, and along Netarts Spit in Cape Lookout State Park. Although most of the sand dunes at Cape Kiwanda are inactive and capped by thick scubby coastal vegetation, a well exposed 15 m thick cross-section of these deposits reveals the

Figure 131. Low-angle southward verging Quaternary (?) thrust fault which offsets unconsolidated basalt pebble and cobble-bearing Quaternary stream deposits at locality 85-89, T. 1 S., R. 10 W., sec. 31, center. Subhorizontal dashed line indicates fault, approximately 2 meters above the author's head. Offset channel wall is to the left of the author.

dynamic history of dune field activity punctuated by periods of stability indicated by at least four stacked soil horizons, each exceeding 1 meter in thickness. The dune field south of Cape Lookout and north of Sand Lake is mostly stabilized by forest, but a large northeast-southwest elongate area remains active. Air photos show northeast-trending sand ridges, and ground reconnaissance revealed a predominance of northwest-trending dune crests in this region, both indicating that the dunes were primarily sculpted by strong southwesterly winds. The dune deposits between Netarts and Oceanside are stabilized by vegetation, however landsliding along the steep slope on the west side of the Netarts-Oceanside coastal highway has been a long-term problem for the Netarts municipal water district, which has routed water mains through this unstable dune sand. Most of the dunes along Netarts Spit are also stablized by thick forest.

The Quaternary colluvium deposits in the study area occur as talus piles or aprons surrounding highlands composed of Columbia River Basalt. They are almost exclusively composed of an unsorted, clast-supported, chaotic assortment of basalt cobbles and boulders which probably came to rest following small rock falls and avalanches off the cliff-forming basalt flows. Although mostly unvegetated, some colluvium deposits in the Tillamook embayment are covered by coastal scrub and forest.

Quaternary terrace deposits bound the east and south sides of Netarts Bay and are also exposed southwest of the Cape Lookout State Park parking lot. They are primarily composed of up-lifted stacked sequences of estuarine and marsh strata (Qte), however subordinate fluvial (Qtf) and colluvium (Qtc) deposits are locally included within these terraces as well. The stacked estuarine and marsh strata within

terraces bordering Netarts Bay have been studied in detail by C. Peterson and M. Darienzo of Oregon State University for signs of co-seismic subsidence to help resolve the neotectonic history of western Oregon (Peterson et al., 1988; Darienzo and Peterson, 1987; Darienzo, 1987). These deposits are characterized by root structure-bearing crudely laminated to bioturbated mudstones and sandstones alternating with buried peat or Spruce tree rooted forest horizons capped by a thin layer of sand (Peterson et al., 1988; this study). These sequences may signify episodic marine incursions or tsunamis caused by local subsidence following a large subduction zone earthquake, with subsequent periods of estuary aggradation and marsh development (Peterson et al., 1988).

Slumps and landslides are common in the study area, and tend to occur on steep slopes or within fine-grained rock units. Most active slumps were mapped anywhere that head wall scarps were discovered. However, the aerial extent of these slides is only estimated on Plate I due to thick obscuring vegetation. The two largest slope failures are mapped within mudstones of the Cannon Beach member of the Astoria Formation in sections 21 and 16, and 7 and 18 of T. 1 S., R. 10 W. (Plate I). The largest slide is well exposed on the north side of Cape Meares, and may actually underlie the town of Cape Meares. It is characterized by hummocky topography with numerous sag ponds, and sparce dead trees standing at high angles from the vertical. The toe of the slide emerges along the beach and is composed of a chaotic mixture of mud, logs, and large boulders. Ocean erosion at the base of the slump is undercutting the slope and causing instability. A cross section of a debris flow, and fluvial and reworked terrace gravels is well exposed on

the north side of Cape Lookout along the beach. Some debris flows include well preserved carbonized pine cones (Niem, Personal communication, 1988).

Marsh deposits occur near sea level in the northernmost part of the study area near Cape Meares Lake (a.k.a. Bayocean Creek Lake), on the east side of Netarts Spit, and on the southern end of Netarts Bay. The marsh deposits on the south side of Netarts Bay have been cored by Curt Peterson and Mark Darienzo for their study of the neotectonic history of northwestern Oregon. The results of their work revealed several Holocene buried peat horizons similar to the sequences exposed in the terraces fringing Netarts Bay. These buried peats may chronicle several recent subsidence events attending subduction zone earthquakes (Peterson et al., 1988).

The cliffs that flank the southwest side of Tillamook Bay include sea caves and a wave-cut notch in Angora Peak member sandstone. These features indicate exposure of the cliff to direct wave attack during either a higher sea level stand, or preceding uplift of the region.

CONCLUSIONS

Each of the objectives listed in the Geologic Problems and Purpose of Investigation section of this thesis have been achieved, and the following section summarizes the conclusions inspired by these objectives.

1. Tuffaceous bathyal mudstones and turbidite sandstones forming the base of the stratigraphic sequence in the study area are Zemorrian to early Saucesian (Oligocene to lower Miocene) in age, and assigned to the Smuggler Cove formation in this study. This unit conformably underlies sandstones of the Bewley Creek formation (informal), and is disconformably overlain by the Angora Peak member of the Astoria Formation.

2. The unnamed sandstone first identified by Snavely, Wells, and MacLeod below the Angora Peak member is broken out as a separate unit informally named the Bewley Creek formation in this study. These pumiceous arkosic volcaniclastic strata are Pillarian stage (lower Miocene) in age, unrelated to a contemporaneous Yaquina formation delta in the Newport embayment, and represent a shallow-marine wave-dominated proto-Astoria Formation depositional system supplied by an ancestral Columbia River during a period of active volcanism in the Western Cascade arc.

3. The unnamed mudstone first recognized by Wells, Snavely, and MacLeod as directly underlying the Angora Peak member was broken out and informally named the Sutton Creek member of the Nye Mudstone in this

study. It is a lower Miocene unit deposited in an upper bathyal slope and channelized outer shelf environment.

4. The micaceous-arkosic sandstones of the Pillarian to Newportian (lower to middle Miocene) Angora Peak member were deposited in a wave-dominated shallow-marine setting adjacent to the debouchment point of an ancestral Columbia River. The fluvial facies mapped by Cooper (1981) within the Angora Peak member in the northern part of the thesis area contain shallow-marine Mollusks and actually represent either subaqeous wave-dominated delta distributary channel deposits or ebb-tidal delta channel-fill deposits. Rounded cobble and boulder deposits in the Angora Peak member at Cape Kiwanda contain exotic two-mica granite and sedimentary quartzite clasts possibly derived from the Idaho Batholith and the Belt Series rocks of Montana and Idaho, respectively. The presence of these exotic clasts are strong evidence supporting the hypothesis that the Tillamook embayment sourced coarse clastic material from an ancestral Columbia River.

5. A submarine canyon and channel facies was identified within the Angora Peak and Cannon Beach members of Cooper (1981), and informally designated in this study as the Saucesian (lower to middle Miocene) Netarts Bay member of the Astoria Formation. This arkosic-micaceous and volcaniclastic-rich sandstone unit contains large canyon or channel-wall slump blocks and clastic dikes. The unit was deposited in a dissected outer shelf to slope environment characterized by channelized high-energy grainflow and turbidity current activity which alternated with periods of low-energy hemipelagic silt and clay deposition.

6. A previously undescribed coarsening and shallowing-upward sequence is present in the Saucesian (lower to middle Miocene) Cannon Beach member (Tcb_2 on Plate I) and may record initial uplift of the Oregon coast range that preceded eruption of the middle Miocene Columbia River Basalts.

7. The basalts previously mapped in the study area as coastal Depoe Bay and Cape Foulweather basalt actually represent distal subaerial and subaqeous lava deltas of the Grande Ronde and Frenchman Springs basalt of the Columbia River Basalt Group (CRB) which flowed to the west into the shallow marine Tillamook embayment through a saddle in the ancestral northern Oregon Coast Range. Three units of the Grande Ronde Basalt were mapped and defined on the basis of geochemical composition and magnetic polarity and include (from oldest to youngest): the Grouse Creek Unit (R_2 low MgO-low TiO_2 subtype), one to three flows; the Winterwater Unit (N_2 low MgO-low TiO_2 subtype), two to three flows; and the Sentinel Bluff Unit (N_2 high MgO subtype), two to three flows. Some peperitic dikes and sills occur where these flows have invaded older semi-lithlfied Miocene strata. The porphyritic Ginkgo Unit of the Frenchman Springs Basalt is the youngest CRB flow in the area and overlies the shallow marine arkosic-micaceous Sandstone of Whale Cove, which was extended into the thesis area from the Newport embayment where it is interbedded between Depoe Bay and Cape Foulweather basalts (age and petrologically equivalent to the Grande Ronde and Frenchman Springs Basalt, respectively).

8. The results of source rock analyses of mudstones from the Cannon Beach and Sutton Creek members, and Smuggler Cove formation indicate

that they contain type III kerogen, which is capable of generating only natural gas. The TOC (total organic carbon) content of these mudstones is sufficiently high for these rocks to be considered potential source rocks, but the vitrinite reflectance, TR ratio, and T max indices all indicate that thesis area rocks are generally too thermally immature to generate natural gas.

REFERENCES

Adams, N.J., 1985, Drilling Engineering, a Complete Well Planning Approach: Pennwell Pub. Co., 440 p.

Aliberti, E.A., and Manduca, C.A., 1988, A transect across an island arc-continent boundary in west-central Idaho; in Link, P.K., and Hackett, W.R., eds., Guidebook to the Geology of Central and Southern Idaho: Idaho Geological Survey, Bull. 27, p. 99-107.

Alger, M.P., 1985, in Olmstead, D.L., Mist Gas Field: exploration and development, 1979-1984: Oregon Dept. of Geol. and Min. Industries Oil and gas Invest. 10, p. 6-9.

Anderson, J.L., Beeson, M.H., Bentley, R.D., Fecht, K.R., Hooper, P.R., Niem, A.R., Reidel, S.P., Swanson, D.A., Tolan, T.L., and Wright, T.L., 1987, Distribution maps of stratigraphic units of the Columbia River Basalt Group: Washington Div. Geol. and Earth Res. Bull. 77, p. 183-195.

Armentrout, J.M., Hull, D.A., Beaulieu, J.D., and Rau, W.W., 1983, Correlation of Cenozoic units of western Oregon and Washington: Oregon Dept. Geol. and Min. Industries, Oil and Gas Invest. 7, 90 p.

Baldwin, E.M., 1981, Geology of Oregon, 3rd edition: Kendall/Hunt Pub. Co., Dubuque, Iowa, 170 p.

Balsley, J.K., 1982, Wave dominated deltas, shelf sands, and submarine fans: Clastic depositional models for hydrocarbon exploration: Amer. Assoc. Pet. Geol., field trip guide notes, 117 p.

Barnes, M.A., 1981, The geology of Cascade Head, an Eocene volcanic center: M.S. thesis, University of Oregon, Eugene, 93 p.

Beeson, M.H., Perttu, R., and Perttu, J., 1979, The origin of the Miocene basalts of coastal Oregon and Washington: Oregon Geology, v. 41, p. 159-166.

Beeson, M.H., Fecht, K.R., Reidel, S.P., and Tolan, T.L., 1985, Regional correlations within the Frenchman Springs Member of the Columbia River Basalt Group: New insights into the middle Miocene tectonics of northwest Oregon: Oregon Geology, v. 47, p. 87-96.

Beeson, M.H., and Tolan, T.L., 1987, Columbia River Basalt Group in western Oregon: Factors controlling flow emplacement [abs.], Geol. Soc. Amer. Abs. with Programs, 83rd Annual Meeting, Hilo, Hawaii, May 20-22, p. 358.

Beeson, M.H., and Tolan, T.L., 1989, The Columbia River Basalt Group in the Cascade Range: a middle Miocene reference datum for structural analysis, in Muffler, L.J., Weaver, C.S., and Blackwell, D.D., Workshop XLIV: Geological, geophysical, and tectonic setting of the Cascade Range: U.S. Geol. Survey Open File Report 89-178, p. 257-290.

Beeson, M.H., 1989, Portland State University, Oregon, personal communication.

Beeson, M.H., Mangan, M.T., Wright, T.L., Wells, R.E., and Bentley, R.D., in press, Correlation of Miocene flows of the Columbia River Basalt Group from the central Columbia River Plateau to the Coast of Oregon and Washington, in Reidel, S.P., and Hooper, P.R., eds., Volcanism and tectonism in the Columbia River flood-basalt province: Boulder Colorado, Geol. Soc. Amer. Spec. Paper 239.

Berkman, T.A., 1989, Oregon State University, personal communication.

Berry, L.G., and Mason, B., 1959, Mineralogy: Concepts, Descriptions, Determinations: W.H. Freeman and Co., San Francisco, 630 p.

Blatt, H., 1979, Diagenetic processes in sandstones, in Scholle, P.A., and Schluger, P.R., eds., Aspects of diagenesis: SEPM Spec. Pub. No. 26, p. 141-157.

Blatt, H., Middleton, G., and Murray, R., 1980, Origin of Sedimentary Rocks, 2nd edition: Prentice-Hall Pub. Co., Englewood Cliffs, New Jersey.

Blatt, H., 1982, Sedimentary Petrology, 1st edition: W.H. Freeman and Pub. Co., San Francisco, 564 p.

Boothroyd, J.C., 1985, Tidal inlets and tidal deltas, in Davis, R.A., ed., Coastal Sedimentary Environments, 2nd ed.: Springer-Verlag Pub. Co., New York, p. 379-438.

Braislin, D.B., Hastings, D.D., and Snavely, P.D., Jr., 1971, Petroleum potential of western Oregon and Washington and adjacent continental margin: Amer. Assoc. Petrol. Geol. Mem. 15, p. 229-238.

Bruer, W.G., Alger, M.P., Deacon, R.J., Meyer, H.J., Portwood, B.B., and Seeling, A.F., 1984, Northwest Oregon correlation section 24: Pacific section: Amer. Assoc. Petrol. Geol., Cross-section Committee, 1 sheet.

Burns, L.K., and Ethridge, F.G., 1979, Petrology and diagenetic effects of lithic sandstones: Paleocene and Eocene Umpqua Formation, southwest Oregon, in Scholle, P.A., and Schluger, P.R., eds., Aspects of diagenesis, SEPM spec. pub. no. 26, p. 307-317.

Byerly, G.R., and Swanson, D.A., 1978, Invasive Columbia River Basalt flows along the northwestern margin of the Columbia Plateau, north-central Washington [abs.]: Geol. Soc. Amer. Abs. with Programs, v. 10, p. 98.

Carlisle, D., 1963, Pillow breccias and their aquagene tuffs, Quadra Island, British Columbia: Jour. Geol., v. 71, p. 48-71.

Carter, J.W., 1976, The environmental and engineering geology of the Astoria Peninsula area, Clatsop County, Oregon: M.S. thesis, Oregon State University, Corvallis, 138 p.

Chamberlain, C.K., 1989, University of Wisconsin, Eau Claire, written communication.

Chan, M.A., and Dott, H., Jr., 1986, Depositional facies and progradational sequences in Eocene wave-dominated deltaic complexes, southwestern Oregon: Amer. Assoc. Pet. Geol., v. 70, p. 415-429.

Clemens, K.E., and Komar, P.D., 1988, Oregon beach sand compositions produced by the mixing of sediments under a transgressing sea: Jour. Sed. Pet., v. 58, p. 519-529.

Conrad, T.A., 1948, Fossil shells from Tertiary deposits on the Columbia River near Astoria: Amer. Jour. Sci., v. 5, p. 432-433.

Cooper, D.M., 1981, Sedimentation, stratigraphy and facies variation of the lower to middle Miocene Astoria Formation in Oregon: Ph.D. thesis, Oregon State University, Corvallis, 546 p.

Coryell, G.F., 1978, Stratigraphy, sedimentation, and petrology of the Tertiary rocks in the Bear Creek-Wickiup Mountain-Big Creek area, Clatsop County, Oregon: M.S. thesis, Oregon State University, Corvallis, 178 p.

Cressy, F.B., 1974, Stratigraphy and sedimentation of the Neahkahnie Mountain-Angora Peak area, Tillamook and Clatsop counties, Oregon: M.S. thesis, Oregon State University, Corvallis, 148 p.

Cushman, J.A., Stewart, R.E., and Stewart, K.C., 1947, five papers on Foraminifera from the Tertiary of western Oregon: Oregon Dept. Geol. and Min. Industries, Bull. 36, p. 1-11.

Dall, W.H., 1909, The Miocene of Astoria and Coos Bay, Oregon: U.S. Geol. Survey Prof. Paper 59, 278 p.

Darienzo, M.E., 1987, Late Holocene geologic history of a Netarts Bay salt marsh, northwest Oregon coast, and its relationship to relative sea level changes: M.S. thesis, University of Oregon, 94 p.

Darienzo, M.E., and Peterson, C.D., 1987, Episodic tectonic subsidence recorded in late Holocene salt marshes, northwest Oregon [abs.]: EOS, v. 68, p. 1469.

Davis, G.H., 1984, Structural Geology of Rocks and Regions: John Wiley and Sons, Inc., New York, 492 p.

Davis, R.A., 1985, Beach and nearshore zone, in Davis, R.A., ed., Coastal Sedimentary Environments, 2nd ed.: Springer-Verlag Pub. Co., New York, p. 379-438.

Dickinson, W.R., 1970, Detrital modes of New Zealand graywackes: Sedimentary Geology, v. 5., p. 37-56.

Dickinson, W.R., 1979, Cenozoic plate tectonic setting of the Cordilleran region in the United States; in Armentrout, J.M., Cole, M.R., and TerBest, H., Jr., eds., Cenozoic paleogeography of the western United States: SEPM, Pacific Coast Paleogeography Symposium 3, p. 1-13.

Dickinson, W.R., and Suczek, C.A., 1979, Plate tectonics and sandstone compositions: Amer. Assoc. Petrol. Geol., v. 63, p. 2164-2182.

Diller, J.S., 1896, Geological reconnaissance in Northwestern Oregon: U.S. Geol. Survey 17th Annual Report, p. 1-80.

Dott, R.H., and Bird, K.J., 1979, Sand transport through channels across an Eocene shelf and slope in southwestern Oregon, U.S.A., in Doyle, L.J., and Pilkey, O.H., eds., Geology of continental slopes: SEPM, Spec. Pub. No. 27, p. 327-342.

Dott, R.H, and Bourgeois, J., 1982, Hummocky stratification: significance of its variable bedding sequences: Geol. Soc. Amer. Bull., v. 93, p. 663-680.

Duncan, R.A., 1982, A captured island chain in the coast range of Oregon and Washington: Jour. Geophys. Res., v. 87, p. 10,827-10,837.

Frye, W.H., 1976, Stratigraphy and petrology of late Quaternary terrace deposits around Tillamook Bay, Oregon: M.S. thesis, University of Oregon, Eugene.

Folk, R.L., 1951, Stages of textural maturity in sedimentary rocks: Jour. Sed. Pet., v. 21, p. 127-130.

Folk, R.L., and Ward, W., 1957, Brazos River bar: a study in the significance of grain size parameters: Jour. Sed. Pet., v. 27, p. 3-26.

Folk, R.L., 1968, Petrology of sedimentary rocks,: Hemphill Pub. Co., Austin Texas.

Folk, R.L., 1974, Petrology of Sedimentary Rocks, 2nd. ed.: Hemphill Pub. Co., Austin, Texas, 179 p.

Fox, D.S., Bell, S., Nehlson, W., and Damron, J., eds., 1984, The Columbia River estuary, atlas of physical and biological characteristics: Columbia River Estuary Data Program, U.S. Army Corp of Engineers.

Friedman, G.M., 1962, On sorting coefficients and lognormality of grain size distributions of sandstones,: Jour. Geol., v. 70, p. 737-753.

Galloway, W.E., 1979, Diagenetic control of reservoir quality in arc-derived sandstones: implications for petroleum exploration, in Scholle, P.A., and Schluger, P.R., eds., Aspects of diagenesis, SEPM Spec. Pub. No. 26, p. 251-262.

Goalen, J.S., 1988, The geology of the Elk Mountain-Porter Ridge area, Clatsop County, northwest Oregon: M.S. thesis, Oregon State University, Corvallis, 356 p.

Goodwin, C.J., 1973, Stratigraphy and sedimentation of the Yaquina Formation, Lincoln County, Oregon: M.S. thesis, Oregon State University, Corvallis, 121 p.

Gregory, M.R., Ballance, P.F., and Gibson, G.W., 1979, On how some rays (Elasmobranchia) excavate feeding depressions by jetting water: Jour. Sed. Pet., v. 49, p. 1125-1130.

Hammond, P.E., 1979, A tectonic model for evolution of the Cascade Range, Pacific Coast Paleogeography Symposium: SEPM Spec. Pub., 3, p. 219-237.

Haq, B.U., Hardendol, J., Vail, P.R., Wright, R.C., Stover, L.E., Baum, G., Loutit, T., Gombos, A., Davies, T., Pflum, C., Romine, K., Posamentier, H., and Jan du Chene, R., 1987, Mesozoic-Cenozoic cycle chart, in Wilgus, C.K., Hastings, B.S., Kendall, C.G., Posamentier, H.W., in Ross, C.A., and Van Wagoner, J.C., eds., Sea-level changes: An integrated approach: SEPM Spec. Pub. No, 42, Plate 1.

Harrison and Eaton (firm), 1920, Report on investigations of oil and gas possibilities of western Oregon: Oregon Bur. Mines and Geology, Mineral Resources of Oregon, v. 3, no. 1, p. 3-31.

Heitman, H.L., 1989, Unocal Corporation, written communication.

Heller, P.L., and Ryberg, P.Y., 1983, Sedimentary record of subduction to forearc transition in the rotated Eocene basin of western Oregon: Geology, v. 11, p. 380-383.

Heller, P.L., and Dickinson, W.R., 1985, Submarine fan facies model for delta-fed, sand-rich turbidite systems: Amer. Assoc. Pet. Geol., v. 69, p. 960-976.

Heward, A.P., 1981, A review of wave-dominated clastic shoreline deposits: Earth Sci. Review, v. 17, p. 223-276.

Hooper, P.R., Reidel, S.P., Brown, J.C., Bush, J.H., Holden, G.S., Kleck, W.D., Robinette, M., Sundstron, C.E., and Taylor, T.L., 1976, Major element analyses of Columbia River Basalt, Part I: Pullman, Basalt Research Group, Washington State University, Open File Report.

Hotz, P.E., 1974, Blueschist metamorphism in the Yreka-Fort Jones area, Klamath Mountains, California, in McGeary, D.F., ed., Geologic guide to the southern Klamath Mountains: Geol. Soc. Sacramento, Sacramento, California, p. 101-109.

Howe, H.V., 1926, Mid-Tertic type of Pacific Coast: Pan American Geologist, v. 45, no. 4, p. 295-306.

Howell, D.G., and Normark, W.R., 1982, Sedimentology of submarine fans, in Scholle, P.A., and Spearing, D.R., eds., Sandstone depositional environments: Amer. Assoc. Pet. Geol. Mem. 31, p. 365-404.

Hubert, J.F., Butera, J.G., and Rice, R.F., 1972, Sedimentology of upper Cretaceous Cody-Parkman delta, southwestern Powder River Basin, Wyoming: Geol. Soc. Amer. Bull., v. 83, p. 1649-1670.

Hyndman, D.W., 1972, Petrology of Igneous and Metamorphic Rocks: McGraw-Hill Pub. Co., New York, 533p.

Irwin, W.P., 1974, Terranes of the western Paleozoic and Triassic Belt in the southern Klamath Mountains province, California, in McGeary, D.F., ed., Geologic field guide to the southern Klamath Mountains: Geol. Soc. of Sacramento, Sacramento, California, p. 17-36.

Jackson, M.K., 1983, Stratigraphic relationships of the Tillamook Volcanics and the Cowlitz Formation in the upper Nehalem River-Wolf Creek area, northwestern Oregon: M.S. thesis, Portland State University, Portland, 118 p.

Kerr, P.F., 1977, Optical Mineralogy, 4th ed.: McGraw Hill Pub. Co., San Francisco, 492 p.

Kokelaar, P.B., 1982, Fluidization of wet sediments during the emplacement and cooling of igneous bodies: Jour. Geol. Soc. London, v. 139, p. 21-33.

Kulm, L.D., Scheidegger, K.F., Byrne, J.V., and Spigai, J.J., 1968, A preliminary investigation of the heavy mineral suites of the coastal rivers and beaches of Oregon and northern California: The Ore Bin, v. 30, p. 165-180.

Kulm, L.D., Roush, R.C., Harlett, J.C., Neudeck, R.H., Chambers, D.M., and Runge, E.J., 1975, Oregon continental shelf sedimentation: interrelationships of facies distribution and sedimentary processes: Jour. Sed. Pet., v. 83, p. 145-175.

Kulm, L.D., and Scheidegger, K.F., 1979, Quaternary sedimentation on the tectonically active Oregon continental slope, in Doyle, L.J., and O.H. Pilkey, Jr.eds., Geology of continental slopes: SEPM Spec. Pub. No. 27, p. 247-264.

Law, B.E., Anders, D.E., Fouch, T.D., Pawlewicz, M.J., Lickus, M.R., and Molnaar, C.M., 1984, Petroleum source rock evaluations of outcrop samples from Oregon and northern California: Oregon Geology, v. 46, p. 77-81.

Lewis, R.S., Kiilsgaard, T.H., Bennett, E.H., and Hall, W.E., 1987, Lithologic and chemical characteristics of the central and southeastern part of the southern lobe of the Idaho Batholith, in Vallier, T.L., and Brooks, H.C., eds., Geology of the Blue Mountains region of Oregon, Idaho, and Washington: The Idaho Batholith and its Border Zone:U.S, Geol. Survey Prof. Paper 1436, p. 171-196.

Lewis, R.S., 1989, Idaho Geological Survey, personal communication.

Lindgren, W., 1901, The gold belt of the Blue Mountains of Oregon: U.S. Geol. Survey 22nd Ann. Report., pt. 11, p. 551-776.

Link, P.K., and Hackett, W.R., 1988, Guidebook to the Geology of Central and Southern Idaho: Idaho Geological Survey, Bull. 27, p. 87-107.

MacLeod, N.S., 1980, U.S. Geol. Survey, personal communication to A.R. Niem, Oregon State University, Corvallis.

Magill, J.R., Cox, A.V., and Duncan, R.A., 1981, Tillamook volcanic series: further evidence for tectonic rotation of the Oregon Coast Range: Jour. Geophy. Res., v. 86, p. 2953-2970.

Magill, J.R., Wells, R.E., Simpson, R.W., and Cox, A.V., 1982, Post 12 m.y. rotation of southwest Washington: J. Geophys. Res., v. 87, p. 3761-3776.

Mangan, M.T., Wright, T.L., Swanson, D.A., and Byerly, D.A., 1986, Regional correlation of Grande Ronde Basalt flows, Columbia River Group, Washington, Oregon, and Idaho: Geol. Soc. Amer. Bull., v. 97, P. 1300-1318.

Mangum, D., 1967, Geology of Cape Lookout State Park, near Tillamook, Oregon: The Ore Bin, v. 29, p. 85-109.

Markert, J.C., and Al-Shaleb, Z., 1985, Diagenesis and evolution of secondary porosity in Upper Minnelusa sandstones, Powder River Basin, Wyoming, in McDonald, D.A., and Surdam, R.C., eds., Clastic Diagenesis, Amer. Assoc. Petrol. Geol. Mem. 37, p. 367-389.

Mason, R., 1980, Petrology of Metamorphic Rocks: George Allen and Unwin Pub. Co., London, 254 p.

May, J.A., Warme, J.F., and Slater, R.A., 1983, Role of submarine canyons on shelfbreak erosion and sedimentation: modern and ancient examples, in Stanley, D.J., and Moore, G.T., eds., The shelfbreak: critical interface on continental margins: SEPM Spec. Pub. No. 33, 467 p.

McMullin, D.W.A. and Greenwood, H.J., 1988, Metamorphism in and near the northern end of the Shuswap Metamorphic Complex, south-central British Columbia, in Current research part E, Cordillera and Pacific Margin: Geol. Survey of Canada, Paper 88-1E, p. 57-64.

Merriam, J.C., 1901, A contribution to the geology of the John Day basin: California University Dept. Geol. Sci. Bull., v. 2, p. 269-314.

Miall, A.D., 1985, Principals of Sedimentary Basin Analysis: Springer-Verlag Pub. Co., 490 p.

Misch, P., 1977, Bedrock geology of the northern Cascades; in Geological Excursions in the Pacific Northwest: Geol. Soc. Amer. Annual Meeting, Seattle, p. 1-12.

Moore, E.J., 1963, Miocene marine mollusks from the Astoria Formation in Oregon: U.S. Geol. Survey Prof. Paper 419, 109 p.

Moore, E.J., 1976, Oligocene marine mollusks from the Pittsburg Bluff Formation in Oregon: U.S. Geol. Survey Prof. Paper 922, 66 p.

Moore, E.J., and Addicott, W.O., 1987, The Miocene Pillarian and Newportian (Molluscan) stages of Washington and Oregon and their usefulness in correlations from Alaska to California, in Shorter contributions to paleontology and stratigraphy: U.S. Geol. Survey Bull. 1664.

Moore, E.J., 1988 and 1989, Oregon State University, personal and written communication.

Moore, J., 1975, written communication to Reichhold Energy Corp.

Moore, J, 1980, written communication to Oregon Nat. Gas. Dev. Corp.

Moye, F.J., Hackett, W.R., Blakley, J.D., and Snider, L.G., 1988, Regional geologic setting and volcanic stratigraphy of the Challis volcanic field, central Idaho; in Link, P.K. and Hackett, W.R., eds., Guidebook to the Geology of Central and Southern Idaho: Idaho Geological Survey, Bull. 27, p. 87-98.

Mumford, D.E., 1989, Geology of the Elsie-lower Nehalem River area, south-central Clatsop and northernmost Tillamook counties, northwestern Oregon: M.S. thesis, Oregon State University, Corvallis, 392 p.

Murase, T. and McBirney, A.R., 1973, Properties of some common igneous rocks and their melts at high temperatures: Geol. Soc. Amer. Bull., v. 84, p. 3563-3592.

Murphy, T.M., and Niem, A.R., 1980, Age, facies relations, and a river mouth/tidal flat depositional model for the Clifton Formation, northwestern Oregon [abs.]: Geol. Soc. Amer. Annual Conference, Cordilleran Section, Corvallis, Oregon.

Murphy, T.M., 1981 Geology of the Nicolai Mountain-Gnat Creek area, Clatsop County, northwest oregon: M.S. thesis, Oregon State University, Corvallis, 355 p.

Neel, R.H., 1976, Geology of the Tillamook Head-Necanicum Junction area, Clatsop County, northwestern Oregon: M.S. thesis, Oregon State University, Corvallis, 190 p.

Nelson, M.P., 1978, Tertiary stratigraphy and sedimentation in the Lewis and Clark River - Young's River area, Clatsop County, northwestern Oregon: M.S. thesis, Oregon State University, Corvallis, 242 p.

Nelson, D.E., 1985, Geology of the Fishhawk Falls - Jewell Area, Clatsop County, Northwest Oregon: M.S. thesis, Oregon State University, Corvallis, 374 p.

Niem, A.R., and Cressy, F.B., Jr., 1973, K-Ar dates for sills from the Neahkahnie Mountain and Tillamook Head areas of the Northwest Oregon coast: Isochron/West, No.7, p. 13-15.

Niem, A.R., and Van Atta, R.O., 1973, Cenozoic stratigraphy of northwestern Oregon and adjacent southwestern Washington, in Beaulieu, J.D., ed., Geologic field trips in northern Oregon and southern Washington: Oregon Dept. Geol. and Min. Industries Bull. 74, p. 75-89.

Niem, A.R., 1975, The geology of Hug Point State Park, northern Oregon Coast: The Ore Bin, v. 37., p. 17-36.

Niem, A.R., 1976, Tertiary volcaniclastic deltas in an arc-trench gap, Oregon Coast Range [abs.]: Geol. Soc. Amer. Abs. with Programs, v. 8, no. 3, p. 400.

Niem, A.R, and Niem, W.A., 1984, Cenozoic geology and geologic history of western Oregon, in Kulm, L.D., ed., Atlas of the ocean margin drilling program, western Oregon-Washington continental margin and adjacent ocean floor, Region V: Ocean Margin Drilling Program Regional Atlas Series, Atlas I: Marine Science International, Woods Hole, Mass., sheets 17 and 18.

Niem, A.R., and Niem, W.A., 1985, Oil and gas investigation of the Astoria Basin, Clatsop and northernmost Tillamook Counties, Northwest Oregon: Oregon Department of Geology and Mineral Industries, Oil and Gas Investigation 14, Plate 1.

Niem, A.R., 1988 and 1989, Oregon State University, personal communication.

Niem, A.R. and Wells, R.E., in prep, Geology of the Columbia River Basalt Group in the Astoria Basin, Oregon and Washington, evidence for invasive flows.

Niem, W.A, and Glenn, J.L., 1980, Results of heavy mineral analyses of surface sediment in Tillamook Bay, Oregon [abs.]: Geol. Soc. Amer. Abs. with Programs, 76th annual meeting, v. 12, p. 144.

Niem, W.A., Niem, A.R., and Snavely, P.D., Jr., in press, Late Cenozoic continental margin of the Pacific Northwest - sedimentary embayments of the Oregon - Washington coast, in Christiansen, R., and Yeats, R.S., eds., Geol. Soc. Amer. Decade of North American Geology.

Nilsen, T.H., 1978, Turbidites of the northern Appennines: Introduction to facies analysis: International Geology Review, v. 20, p. 125-166.

Normark, W.R., 1982, Growth patterns in deep sea fans, in Tillman, R.S., and All, S.A., eds., Deep water canyons, fans and facies: Models for stratigraphic trap exploration: Amer. Assoc. Petrol. Geol. Reprint Series No. 26., 604 p.

Olbinski, J.S., 1983, Geology of the Buster Creek-Nehalem Valley area, Clatsop County, northwest Oregon: M.S. thesis, Oregon State University, Corvallis, 231 p.

Oles, K.F. and Enlows, H.E., 1971, Bedrock geology of the Mitchell quadrangle, Wheeler County, Oregon: Oregon Dept. Geol. and Min. Industries, Bull. 72, 62 p.

Oles, K.F, Johnson, J.G., Niem, A.R., and Niem, W.A., eds., 1980, Geologic field trips in western Oregon and southwestern Washington: Oregon Dept Geol. and Min. Industries, Bull. 101, 232 p.

Onasch, C.M., 1987, Temporal and spatial relations between folding, intrusion, metamorphism, and thrust faulting in the Riggins area, west-central Idaho; in Vallier, T.L. and Brooks, H.C., eds., Geology of the Blue Mountains region of Oregon, Idaho, and Washington: The Idaho Batholith and its border zone: U.S. Geol. Survey Prof. Paper 1436, p. 139-150.

Passega, P., 1957, Texture as a characteristic of clastic deposition: Amer. Assoc. Petrol. Geol., v. 41, p. 1952-1984.

Penoyer, P.E., 1977, Geology of the Saddle Mountain and Humbug Mountain area, Clatsop County, northwest Oregon: M.S. thesis, Oregon State University, Corvallis, 232 p.

Peterson, C.D., Scheidegger, K.F., Komar, P.D., and Niem, W.A., 1984, Sediment composition and hydrography in six high-gradient estuaries of the northwestern United States: Jour. Sed. Pet., v. 54, p. 86-97.

Peterson, C.D., Komar, P.D., and Scheidegger, K.F., 1985, Distribution geometry, and origin of heavy mineral placer deposits on Oregon beaches: Jour. Sed. Pet., v. 56, p. 67-77.

Peterson, C.D., Darienzo, M.E., and Parker, M.J., 1988, Coastal neotectonic field trip for Netarts Bay, Oregon: Oregon Geology, V. 50, p. 99-106.

Peterson, C.P., 1984, Geology of the Green Mountain-Young's River area, Clatsop County, northwest Oregon: M.S. thesis, Oregon State University, Corvallis, 215 p.

Pfaff, V.J., and Beeson, M.H., 1987, Miocene basalts of coastal Oregon and Washington: geochemical and geophysical evidence for Columbia Plateau origin [abs.]: Geol. Soc. Amer. abs. with programs, no. 136146.

Priest, G.R., Woller, N.M., Black, G.L., and Evans, S.H., 1982, Overview of the geology and geothermal resources of the central Oregon Cascades, in Priest, G.R., and Vogt, B.F., eds., Geology and Geothermal Resources of the Cascades, Oregon: Oregon Dept. Geol. and Min. Industries, Open file report O-82-7, p. 3-28.

Priest, G.R., 1989, Model for volcanic arc migration and uplift in the Cascades [abs.]: Geol. Soc. Amer. Abs. with Programs, 42nd Annual Meeting, Spokane, Washington, v. 21, p. 131.

Rarey, P.J., 1986, Geology of the Hamlet-North Fork of the Nehalem River area, southern Clatsop and northernmost Tillamook counties, northwest Oregon: M.S. thesis, Oregon State University, Corvallis, 488 p.

Rarey, P.J., Niem, A.R., and Murphy, T., 1984, Middle Pliocene Pomona flow and intrusives in the northwest Oregon Coast Range [abs.], in Oregon Academy of Sciences, Proceedings of the Oregon Academy of Sciences, meeting Feb. 25, Eugene, Oregon, v. 20, p. 51.

Rau, W.W., 1988, Washington State Department of Natural Resources, written communication.

Rau, W.W., 1989, Washington Department of Natural Resources, personal communication to R.E. Wells, U.S. Geol. Survey.

Reidel, S.P., in press, Stratigraphy of the Grande Ronde Basalt from the lower Salmon River and northern Hells Canyon area, Idaho, Oregon, and Washington, in Bonnichsen, B., ed., Cenozoic Geology of Idaho, p. 77-101.

Reidel, S.P., Tolan, T.L., Hooper, P.R., Beeson, M.H., Fecht, K.R., and Anderson, J.L., in prep, The Grande Ronde Basalt, Columbia River Basalt Group: stratigraphic descriptions and correlations in Washington, Oregon, and Idaho.

Reinech, H.E., and Singh, I.B., 1980, Depositional Sedimentary Environments: Springer-Verlag Pub. Co., New York, 549 p.

Royce, C.F., Jr., 1970, An Introduction to Sediment Analysis: Tempe, Arizona, 180 p.

Russell, J.C., 1893, A geological reconnaissance in central Washington: U.S. Geol. Survey Bull. 108, 108 p.

Scheidegger, K.F., Kulm, L.D., and Runge, E.J., 1971, Sediment sources and dispersal patterns of Oregon continental shelf sands: Jour. Sed. Pet., v. 41, p. 1112-1120.

Schenck, H.G., 1927, Marine Oligocene of Oregon: California Univ. Dept. Geol. Sci. Bull., v. 16, no. 12, p. 449-460.

Schlicker, H.G., Deacon, R.J., Beaulieu, J.D., and Olcott, G.W., 1972, Environmental geology of the coastal region of Tillamook and Clatsop Counties, Oregon: Oregon Dept Geol. and Min. Industries, Bull. 74, 164 p.

Schmidt, V., and McDonald, D.A., 1979, The role of secondary porosity in the course of sandstone diagenesis, in Scholle, P.A., and Schluger, P.R., eds., Aspects of diagenesis: SEPM Spec. Pub. No. 26, p. 175-209.

Schmincke, H.U., 1967, Stratigraphy and petrology of four upper Yakima Basalt flows in south-central Washington: Geol. Soc. Amer. Bull., v. 78, p. 1385-1422.

Scholle, A.S., 1979, A color illustration guide to constituents, textures, cements, and porosities of sandstones and associated Rocks: Amer. Assoc. Petrol. Geol. Mem. 28, 200 p.

Scholle, A.S., and Schluger, P.R., 1979, Aspects of diagenesis: SEPM Spec. Pub. No. 26, 443 p.

Shepard, F.P., 1979, Currents in submarine canyons and other types of sea valleys, in Geology of Continental Slopes: SEPM Spec. Pub. No. 27., 374 p.

Shepard, F.P., Dill, R.F., and Rad, U.V., 1982, Physiography and sedimentary processes of the La Jolla submarine fan and fan valley, California, in Tillman, R.W., and Ali, S.A., Deep water canyons, fans, facies: Models for stratigraphic trap exploration: Amer. Assoc. Pet. Geol. Reprint Series No. 26., 604 p.

Simpson R.W., and Cox, A.V., 1977, Paleomagnetic evidence for tectonic rotation of the Oregon Coast Range: Geology, v. 5, p. 585-589.

Smith, W.D., 1924, Oil and gas investigation of the Pacific Northwest: Economic Geology, v. 19, p. 455-465.

Smith, T.N., 1975, Stratigraphy and sedimentation of the Onion Peak area, Clatsop County, Oregon: M.S. thesis, Oregon State University, Corvallis, 190 p.

Snavely, P.D., Jr., and Vokes, H.E., 1949, The coastal area between Cape Kiwanda and Cape Foulweather, Oregon: U.S. Geol. Survey Oil and Gas Invest. Map OM-97, scale 1:62,500.

Snavely, P.D., Jr., and Wagner, H.C., 1963, Tertiary geology of western Oregon and Washington: Wash. Div. of Mines and Geology, Inves. Rep. 22, 25 p.

Snavely, P.D., Jr., and Wagner, H.C., 1964, Geologic sketch of northwestern Oregon: U.S. Geol. Survey Bull. 1181-M, p. M1-M17.

Snavely, P.D., Jr., Rau, W.W., and Wagner, H.C., 1964, Miocene stratigraphy of the Yaquina Bay area, Newport, Oregon: The Ore Bin, v. 26, no. 8, p. 133-151.

Snavely, P.D., Jr., MacLeod, N.S., and Rau, W.W., 1969 a,b, Geology of the Newport area, Oregon: The Ore Bin, v. 31, p. 25-48.

Snavely, P.D., Jr., MacLeod, N.S., and Wagner, H.C., 1973, Miocene tholeiitic basalts of coastal Oregon and Washington and their relations to coeval basalts of the Columbia Plateau: Geol. Soc. Amer. Bull., v. 84, p. 387-424.

Snavely, P.D., Jr., and Wagner, H.C., 1976, Geologic map of the Cape Foulweather and Euchre Mountain Quadrangles, Oregon: U.S. Geol. Survey Misc. Inv. Map I-868, scale 1:62,500

Snavely, P.D., Jr., MacLeod, N.S., Wagner, H.C., and Rau, W.W., 1976, Geologic Map of the Yaquina and Toledo quadrangles, Oregon: U.S. Geol. Survey Misc. Inv. Map I-867, scale 1:62:500.

Snavely, P.D., Jr., Pearl, J.E., and ander, D.L., 1977, Interim report on the petroleum potential and geologic hazards in the outer continental shelf-Oregon and Washington Tertiary province: U.S. Geol. Survey, Open File Report 77-282, 63p.

Snavely, P.D., Jr., Wagner, H.C., and Lander, D.L., 1980, Interpretation of the Cenozoic geologic history of the central Oregon continental margin: cross-section summary: Geol. Soc. Amer. Bull., v. 91, p. 143-146.

Snavely, P.D., Jr., 1987, Tertiary geologic framework, neotectonics, and petroleum potential of the Oregon-Washington continental margin; in Scholl, D.W., Grantz, A., and Vedder, F.G., eds., Geology and resource potential of the continental margin of western North America and adjacent ocean basins - Beaufort Sea to Baja California: Circum-Pacific Council for Energy and Mineral Resources, Earth Science Series, v. 6, p. 305-335.

Snavely, P.D., Jr., 1989, U.S. Geological Survey, written communication.

Snavely, P.D., Jr., 1989, U.S. Geological Survey, written communication to A.R. Niem, Oregon State University.

Stowe, D.A., 1986, Deep clastic seas; in Reading, H.G., ed., Sedimentary Environments and Facies: Blackwell Sci. Pub. Co., 576 p.

Swanson, D.A., Wright, T.L., Hooper, P.R., and Bentley, R.P., 1979, Revisions in stratigraphic nomenclature of the Columbia River Basalt Group: U.S. Geol. Survey Bull., 1457-G, 59 p.

Tankard, A.J., and Barwis, J.H., 1982, Wave-dominated deltaic sedimentation in the Devonian Bokkeveld Basin of South Africa: Jour. Sed. Pet., v. 52, p. 959-974.

Tillman, R.W., and Syed, A.A., eds., 1982, Deep Water Canyons, Fans and Facies,: Models for Stratigraphic Trap Exploration: Am. Assoc. Petrol. Geol., Reprint Series No. 26, 604 p.

Tissot, B.P., and Welte, D.H., 1978, Petroleum Formation and Occurence: Springer-Verlag Pub. Co., New York, 538 p.

Tolan, T., 1989, Westinghouse Co., Hanford, personal communication.

Tolson, P.M., 1976, Geology of the Seaside-Young's River Falls area, Clatsop County, Oregon: M.S. thesis, Oregon State University, Corvallis, 191 p.

Turner, D.L., 1970, Potassium-argon dating of Pacific Coast Miocene Foraminiferal stages, in Brandy, O.L., ed., Radiometric dating and paleontologic zonation: Geol. Soc. Amer. Spec. Paper 124, p. 91-129.

Vallier, T.L., and Brooks, H.C., 1987, The Idaho Batholith and its border zone: a regional perspective; in Vallier, T.L., and H.C. Brooks eds., Geology of the Blue Mountains Region of Oregon, Idaho, and Washington: The Idaho Batholith and its Border Zone: U.S. Geol. Survey Prof. Paper 1436, p.1-8.

Van Atta, R.O., 1971, Sedimentary petrology of some Tertiary formations, upper Nehalem River basin, Oregon: PhD. dissertation, Oregon State University, Corvallis, 245 p.

Van Atta, R.O., and Kelty, K.B., 1985, Scappoose Formation, Columbia County, Oregon: New evidence of age and relation to the Columbia River Basalt Group: Amer. Assoc. Petrol. Geol. Bull., v. 69, p. 688-698.

Vance, J.A., 1989, Detrital kyanite and zircon: provenance and sediment dispersal in the middle and late Eocene Puget and Cowlitz groups, SW Washington and NW Oregon [abs.]: Geol. Soc. Amer. Bull. Abs. with Programs, 42nd Annual Meeting, Spokane, Washington, v. 21, p. 153.

Vokes, H.E., Norbisrath, H., and Snavely, P.D., Jr., P.D., 1949, Geology of the Newport-Waldport area, Lincoln County, Oregon: U.S. Geol. Survey Oil and Gas Invest. Map 88, scale 1:62,500.

Walker, R.G., and Mutti, E., 1973, Turbidite facies and facies associations, in Middleton, G.V., and Bouma, A.H., eds., Turbidites and deep water sedimentation: SEPM Short Course, p. 119-157.

Walker, R.G., 1982, Deep water sandstone facies and ancient submarine fans - Models for exploration for stratigraphic traps, in Tillman, R.S., and Ali, S.A., eds., Deep water canyons, fans and facies: Models for stratigraphic trap exploration: Amer. Assoc. Petrol. Geol. Reprint Series No. 26., 604 p.

Walker, R.G., 1984, Facies Models, 2nd edition: Geological Association of Canada Pub., Toronto, Ontario, 317 p.

Warren, W.C., Norbisrath, H., and Grivetti, R.M., 1945, Geology of northwest Oregon west of Willamette River and north of latitude 45° 15′: U.S. Geol. Survey Oil and Gas Invest. Preliminary Map 42, Scale 1:148,000.

Warren, W.C., and Norbisrath, H., 1946, Stratigraphy of the upper Nehalem River Basin, northwest Oregon: Am. Assoc. Petrol. Geol. Bull., v. 30, p. 213-237.

Washburne, C.W., 1914, Reconnaissance of the geology and oil prospects of northwest Oregon: U.S. Geol. Survey Bull. 590, p. 60-69.

Waters, A.C., 1961, Stratigraphic and lithologic variations in the Columbia River Basalt: Amer. Jour. Sci., v. 259, p. 583-611.

Wells, F.G., and Peck, D.L., 1961, Geologic map west of the 121st meridian: U.S. Geol. Survey Misc. Geol. Invest. Map I-325, scale 1:500,000.

Wells, R.E., 1981, Geologic map of the eastern Willapa Hills, Cowlitz Lewis, Pacific, and Wahkiakum counties, Washington: U.S. Geol. Survey Open File Report 81-674, 1 map.

Wells, R.E., Niem, A.R., Macleod, N.S., Snavely, P.D., Jr., and Niem, W.A., 1983, Geologic map of the west half of the Vancouver (Wa.-Ore.) 1° X 2° quadrangle, Oregon: Oregon Dept of Geol. and Min. Industries, Open File Map O-83-6.

Wells, R.E., Engebretson, D.C., Snavely, P.D., Jr., and Coe, R.S., 1984, Cenozoic plate motions and the volcano-tectonic evolution of western Oregon and Washington: Tectonics, v. 3, p. 275-294.

Wells, R.E., and Coe, R.S., 1985, Paleomagnetism and geology of Eocene volcanic rocks of southwest Washington, implications for mechanisms of tectonic rotation: Jour. Geophys. Res., v. 90, p. 1925-1947

Wells, R.E., Niem, A.R., 1987, Geology of the Columbia River Basalt Group in the Astoria Basin, Oregon and Washington: Evidence for invasive flows [abs]: Geol. Soc. Amer. Abs. with Programs, no. 134238.

Wells, R.E., 1987, U.S., Geological Survey, written communication.

Wells, R.E., and Heller, P.L., 1988, The relative contribution of accretion, shear, and extension to Cenozoic tectonic rotation in the Pacific Northwest: Geol. Soc. Amer., v. 100, p. 325-337.

Wells, R.E., 1988 and 1989, U.S. Geological Survey, personal communication.

Wells, R.E., 1989, Geologic map of the Cape Dissappointment-Naselle River area, Pacific and Wahkiakum counties, Washington: U.S. Geol. Survey Misc. Inv. Series Map I-1832, scale 1: 62:500

Wells, R.E., and Snavely, P.D., Jr., 1989, Paleogene geologic history of the Oregon-Washington continental margin [abs.]: Geol. Soc. Amer. Abs. with Programs, v. 21, p. 157.

Wells, R.E., Simpson, R.W., Bentley, R.D., Beeson, M.H., Mangan, M.T., and Wright, T.L., in prep., Correlation of Miocene flows of the Columbia River Basalt Group from the central Columbia River Plateau to the coast of Oregon and Washington.

Wells, R.E., Simpson, R.W., Bentley, R.D., Beeson, M.H., Mangan, M.T., and Wright, T.L., in press, Correlation of Miocene flows of the Columbia River Basalt Group from the central Columbia River Plateau to the coast of Oregon and Washington, in Reidel, S.P., and Hooper, T.L., eds., Volcanism and tectonism in the Columbia River flood-basalt province: Boulder Colorado, Geol. Soc. Amer. Spec. Paper 239.

Welton, J.E., 1984, SEM Petrology Atlas; Methods in Exploration Series: Amer. Assoc. Petrol. Geol. Pub., 237 p.

Wermiel, 1987, Oregon Department of Geology and Mineral Industries, personal communication.

Whipple, J.W., Connor, J.J., Raup, O.B., and McGimsey, R.G., 1984, Preliminary report on the stratigraphy of the Belt Supergroup, Glacier National Park and adjacent Whitefish Range, Montana: in Montana Geological Society 1984 Field Conference and Symposium, p. 23-50.

Wilcox, R.E., Harding, T.P., and Seely, D.R., 1973, Basic wrench tectonics: Amer. Assoc. Petrol. Geol., v. 57, p. 74-96.

Winker, C.D., and Edwards, M.B., 1983, Unstable progradational clastic shelf margins, in Stanley, D.J., and Moore, G.T., The shelfbreak: critical interface on continental margins: SEPM Spec. Pub. No. 33, p. 139-158

Wright, L.D., 1976, Morphodynamics of a wave-dominated river mouth, in Proceedings of the 15th Coastal Engineering Conference, Amer. Soc. of Civil Eng., p. 1721-1755.

Wright, T.L., Grollier, M.J., and Swanson, D.A., 1973, Chemical variation related to the stratigraphy of the Columbia River Basalt: Geol. Soc. Amer. Bull. v. 84, p. 371-386.

Yeats, R.S., 1977, Structure, stratigraphy, plutonism, and volcanism of the central Cascades, Washington. Part I: Geological setting of the Skyomish Valley; in Geological Excursions in the Pacific Northwest: Geol. Soc. Amer. annual meeting, Seattle, p.265-275.

Zingula, R.P., 1968, Techique: New breakthrough in sample washing: Jour. of Paleon., v. 42, p. 1092.

APPENDICES

APPENDIX I

Bewley Creek Formation Measured Section A-A′, B-B′, and C-C′

Section A-A′

Bewley Creek formation

Initial Point (A): northwest quarter sec. 10, T. 3 S., R 10 W.. Section measured in northwest-trending logging road depicted in figure 18 approximately 20 m above the contact with the Smuggler Cove formation.

Terminal Point (A′): extreme northwest quarter sec. 10, T. 3 S., R. 10 W.. (Figure 18).

Thickness (m)	Total (m)	Description
18.0	67.7	Very fine- to fine-grained arkosic lithic micaceous well to very well-sorted sandstone. Moderately hematite cemented, light gray (N7) to moderate orange pink (5 YR 8/4). Locally leisegang banded. Sandstone parts along bedding, is slightly bioturbated with pelecypod molds. Moderately friable with common hematite stain along bedding planes. Locally spheroidally weathered. Swaley cross stratification present with common low angle truncation surfaces, troughs, rare swales. Probably a hummocky cross-stratified sequence.
1.0	49.7	Coarse-grained to gritty pumiceous sandstone, moderately to strongly hematite cemented. Massive.
4.8	48.7	Cover
3.2	43.9	Very coarse-grained arkosic-lithic sandstone. Lithology as above.
1.5	40.7	Cover
7.2	39.3	As above except includes large (>50 cm diameter) Teredo-bored stump within pebbly to very coarse-grained friable lithic-rich trough cross-bedded sandstone. Troughs up to 1 m across. Woody detritus is widely scattered throughout the deposit.

APPENDIX I (continued)

Thickness (m)	Total (m)	Description
6.8	32.1	Lithology as above but very coarse-grained to gritty with abundant woody debris. Abundant hematite cemented cross-bedded sandstone. Locally channelized with large sweeping cross beds up to 2 m across and 50 cm deep. Base of troughs include moderately to well-rounded pebbles of chert and volcanic rock fragments.
1.2	25.3	Coarse- to very coarse-grained arkosic micaceous, lithic-rich sandstone with with abundant pumice and silicic to mafic volcanic rock fragments. Massive.
11.0	24.1	Cover
1.6	13.1	As above with some coarse-grained sandstone and local manganese (?) concretions. Rare carbonaceous horizons.
1.5	11.5	Medium- to coarse-grained moderately sorted hematite cemented sandstone. trough cross-stratified with troughs 1-1.5 m across and approximately 20-30 cm deep. Predominantly composed of micaceous-arkosic volcaniclastic-rich friable sandstone.
8	10	Horizontally laminated fine-grained friable to slightly hematite cemented sandstone which thickens and thins along strike. Low angle trucation surfaces define swales that may represent a hummocky cross-stratified horizon. Sequence grades upward to horizontally laminated fine-grained sandstone.
2	2	Predominantly fine-grained micaceous-arkosic lithic-rich friable uncemented sandstone. Light gray (N7) to pinkish gray (5 YR 8/1). Hematite cement is locally concentrated along bedding planes. Dark gray manganese (?) concretions also occur locally and parallel bedding.

APPENDIX I (continued)

Section B-B′
Bewley Creek formation

Initial Point: (B) Northwest quarter of the northeast quarter of sec. 2, T. 3 S., R. 10 W. (Figure 18). Traverse started at contact between Smuggler Cove formation and Bewley Creek formation. Nature of contact is gradational.

Terminal Point: (B′) Southeast quarter of the southwest quarter of sec. 35, T. 2 S., R. 10 W. (Figure 18).

Thickness (m)	Total (m)	Description
3.0	167.5	Medium-scale trough cross-stratification common. Same lithology as below. Coarse-grained lithic-rich sandstone grades to leisegang banded medium-grained arkosic-lithic sandstone. Some carbonized wood fragments concentrated along bedding.
1.8	164.5	Channel truncates cross-bedded sandstones. Lithology as below. Large-scale sweeping cross strata grade to medium-scale trough cross-bedded coarse-grained lithic-rich pumiceous sandstone. General fining-upward sequence. Leisegang banding common.
1.5	162.7	Medium-grained to gritty pumiceous and basalt lithic rich sandstone. Extensively cross-bedded with small to medium-scale trough crossbeds up to 70 cm across. Very coarse-grained to pebbly at base of troughs. Sequence truncated by large channel-fill complex.
17.2	161.1	Cover
1.0	133.9	Tuffaceous siltstone overlain by horizontally laminated silty sandstone. Arkosic-micaceous with abrupt lower contact.
1.0	132.9	Cover
3.2	131.9	Swaley fine-grained arkosic sandstone, possibly amalgamated hummocky cross-stratified.
4.7	128.7	Not in place
0.3	124.0	Horizontally laminated siltstone.

APPENDIX I (continued)

Thickness (m)	Total (m)	Description
3.3	123.7	Swaley arkosic-micaceous lithic fine-grained sandstone. Moderately cemented with hematite, and includes some black manganese oxide (?) concretionary horizons (<30 cm thick). Sequence appears to be an amalgamated hummocky cross-stratified package with common synforms and rare antiformal hummocks.
3.4	120.4	Cover
1.3	117.0	Lithology as above; horizontally laminated sandstone.
9.3	113.7	Cover
1.7	94.4	Fine-grained micaceous-arkosic lithic-rich sandstone with common hematite cement. Slightly friable. Very pale orange (10 YR 8/2). Massive.
24.3	92.7	Cover
38.2	68.4	Medium-grained arkosic-micaceous, lithic rich sandstone with dark gray (N3) horizons stained with manganese oxide (?). Small faults cut exposure with small (<10 cm) offset. Rare hummocks and common swales present here with low angle (<15_o) truncation surfaces. May represent hummocky cross stratified sandstone sequence.
26.0	30.2	Cover
0.7	5.2	Silty sandstone, arkosic micaceous.
1.7	4.5	40 cm thick tuffaceous siltstone scoured by sandstone bed with lithology as in interval 2.8. Sandstone bed is 70 cm thick and faintly parallel laminated.
2.8	2.8	Massive sandstone (1.2 m thick) grading to subhorizontally laminated fine-grained sandstone with common organic-rich horizons of comminuted plant detritus. Thin (<30 cm) siltstone interbeds are common and scoured into by fine-grained sandstone. Exposure is cut by intra-formational faults of small offset (<15).

APPENDIX I (continued)

Section C-C′
Bewley Creek formation

Initial Point: (C) Southwest quarter of the northwest quarter of sec. 34, T. 2 S., R. 10 W. (Figure 18).

Terminal Point: (C) Southwest quarter of the northwest quarter of sec. 34, T. 2 S., R. 10 W. (Figure 18). Traverse ended at contact between Bewley Creek formation and the Sutton Creek member of the Nye Mudstone.

Thickness (m)	Total (m)	Description
Sutton Creek member		Dark gray (N3) silstone. Horizontally laminated to massive. Carbonaceous.
3.1	80.3	Cover
1.2	77.2	Sandy siltstone, dark gray (N3) mottled with yellow sulfur stain.
0.6	75.0	Medium-grained hematite cemented arkosic-micaceous sandstone grading to carbonaceous bioturbated fine- grained micaceous arkosic silty sandstone.
12.8	74.4	Cover
9.2	61.6	Loose unconsolidated medium- to coarse-grained well sorted sandstone. possibly includes minor pumice. Massive.
23.6	52.4	Cover
5.6	28.8	Mottled fine- to medium-grained arkosic-micaceous sandstone with mnor lithic fragments. Extensively bioturbated deposit with rare reinforced clay-lined burrows. Iron stain concentrated along fractures.
21.0	23.2	Cover
3.2	3.2	Very fine- to fine-grained silty mottled sandstone. Slightly iron stained to light brown (5 YR 6/2).

APPENDIX II
Angora Peak Member Measured Section D-D′ and E-E′

Section D-D′

Sea Cliff Cape Kiwanda Measured Section
Angora Peak member of the Astoria Formation

Initial Point (D): southwest quarter sec. 13, T. 4 S., R. 11 W.
Base of measured section starts at disconformable contact between the Angora Peak member and underlying Smuggler Cove formation exposed at low tide on the south side Cape Kiwanda.

Terminal Point (D′): southwest quarter sec. 13, T. 4 S., R. 11 W.
Top of measured section corresponds to the seaward tip of Cape Kiwanda.

Thickness (m)	Total (m)	Description
6.0	67.4	Sandstone: medium grained arkosic sandstone with subordinate basalt lithic fragments. Trough cross stratified with trough 1 m across or less. Deposit capped by tightly hematite-cemented sandstone.
11.0	61.4	Sandstone: Channel cuts into previous interval. Lithology changes to extremely basalt lithic-rich medium-grained sandstone with stringers and lenses of basalt cobbles that may represent channel lag deposit. Trace of large-scale trough cross stratification. Resistant calcite conretionary horizons are fairly common. Upsection basalt clasts become smaller grading to disseminated pebbles in medium-grained arkosic lithic sandstone.
3.7	60.4	Sandstone: fine to medium-grained extremely bioturbated interval with disseminated wood chunks. Faint horizontal lamination.
9.7	56.7	Sandstone: medium-grained, some silty sandstone, with abundant disseminated carbonaceous plant matter and Teredo-bored wood. Grades upward to extensively bioturbated zone bearing Rosselia burrows. Deposit includes carbonaceous clots (approx. 1 m across) that contain Tillamook basalt pebbles. Rare, discontinuous laminae (<4 cm thick) of siltstone are also present, but disrupted by bioturbation. Deposit coarsens upward to medium to coarse-grained.

APPENDIX II (continued)

Thickness (m)	Total (m)	Description
0.6	47.0	Cobble conglomerate: Scoured into previous interval. Deposit composed of normally graded basalt cobble and grit.
1.3	46.4	Sandstone: medium to coarse-grained sandstone, bioturbated with some discontinuous laminae of siltstone. Sandstone is dusky yellow green (5GY 5/2). Sandstone contain calcite concretions and is basalt lithic-rich. Rare pelecypod fossil molds and small cobbles of basalt are also present. Thin stringers of organic material define crude horizontal laminae.
0.6	45.1	Cobble and boulder conglomerate: Abrupt change to strongly hematite-cemented cobble and boulder-bearing horizon predominately composed of weathered rounded to subrounded basalt cobbles (5-19 cm diam.) with a hornblende gabbro (?) or amphibolite cobble, and both a two-mica granite boulder (30 cm diam.) and a sedimentary quartzite boulder (28 cm. diam.).
1.0	44.5	Sandstone: lithology as below, trough cross-stratified to horizontally laminated sandstone grading to homogenized burrowed bioturbated medium grained sandstone. Weathered to pale yellowish orange (10 YR 8/6)
5.0	43.5	Sandstone: medium to coarse-grained, well sorted, with rare stringers of basalt cobbles (5 to 15 cm diam.). Deposit is predominately trough cross-stratified.
1.3	38.5	Sandstone: scoured into previous interval and characterized by micaceous-arkosic horizontally laminated medium-grained sandstone that may represent wedge sets. Wedge sets dip seaward.
3.7	37.2	Sandstone: same as in interval 32.0 with local pods of sandstone rip-ups and basalt cobbles (8-11 cm diam) in trough cross-stratified sandstone. Predominately clean arkosic micaceous sandstone.
1.5	33.5	Sandstone: same as in interval 28.5.

APPENDIX II (continued)

Thickness (m)	Total (m)	Description
3.5	32.0	Sandstone: abrupt change from interval below to subhorizontally laminated sandstone occasionally cut by trough cross-stratified medium-grained sandstone. Horizontal laminae are very long and laterally continuous, and display some lateral thickening and thinning along strike. Troughs are well developed, predominately dip landward, and are filled with medium to very coarse-grained sand. At base of cross bed sets there are some load structures. Sandstone is very pale orange (10 YR 8/2).
2.4	28.5	Sandstone: same lithology as below but mottled and bioturbated.
3.0	26.1	Sandstone: well sorted, arkosic micaceous, hematite concretionary sandstone with abundant low angle cross-bedding and some discontinuous stringers and lenses (approximately 15 cm thick) of basalt cobble and pebble conglomerate which scour up to 30 cm down into underlying medium to coarse-grained sandstone. Trough forsets of sandstones are bidirectional, but predominately landward-directed.
2.0	23.1	Sandstone: as in interval 19.9, with thin (<5 cm) basalt pebble stringers. Pebbles up to 8 cm in diameter. Sandstone grades upward to micaceous carbonaceous interval.
1.2	21.1	Basalt: vertical dike of N_2 low Mg, low Ti Sentinel Bluff Unit of the Grande Ronde Basalt Sandstone baked up to 8 cm away from contact with the dike, and the dike is locally sheared in a fault plane.
2.4	19.9	Sandstone: Scoured into previous interval. Medium-grained, well sorted, hummocky cross-stratified to horizontally laminated and trough cross stratified arkosic-micaceous sandstone. Local calcite concretions. Light gray (N7) where fresh.

APPENDIX II (continued)

Thickness (m)	Total (m)	Description
1.2	17.5	Sandstone: well sorted, medium-grained arkosic micaceous sandstone with some stringers of basalt pebbles (2-5 cm diam). Deposit includes large conical-shaped (1 m across, 0.7 m deep) zone of disturbed bedding that may represent the burrow of a manta ray.
2.4	16.3	Sandstone: as in interval 11.8 m, but predominately medium to coarse-grained, subhorizontally to horizontally laminated sandstone with Teredo-bored wood. Thin (<5 cm) stringers of vesicular basalt pebbles are present, as are carbonaceous bundles which bear basalt pebbles. Sandstones are characterized interbedded trough cross stratified and horizontally laminated sandstone. Upward sedimentary structures change to interbedded carbonaceous bioturbated burrowed sandstones and hummocky cross-bedded sandstone with some convoluted bedding.
2.1	13.9	Sandstone: as below, with more abundant carbonaceous material.
1.5	11.8	Sandstone: Extensively bioturbated, moderately sorted, carbonaceous sandstone with common Rosselia burrows.
1	10.3	Sandstone: Scoured into previous interval. Coarse-grained, well sorted, horizontally laminated to structureless burrowed sandstone with abundant Rosselia burrows increasing in frequency upward. Moderately friable to locally hematite and calcite cemented. Predominately very pale orange (10YR 8/2).
4.0	9.3	Sandstone: Medium grained sandstone, extensively bioturbated, bearing many 4-6 cm vertical Rosselia burrows. Stringers of organic terrigenous organic matter are common, as are large (3-5 cm) coalified wood chunks.
1.5	5.3	Sandstone: fine grained arkosic-micaceous sandstone similar to interval at 2.5 m, but with common calcite and hematite cemented concretions. Trace of trough cross stratified medium grained sandstone which grades to an extremely micaceous horizontally laminated sandstone.

APPENDIX II (continued)

Thickness (m)	Total (m)	Description
1.3	3.8	as below, but coarsens to fine to medium-grained sandstone.
1.5	2.5	Sandstone: extremely carbonaceous, micacaceous, bioturbated, silty sandstone with thin (<1 cm) stringers of carbonaceous plant matter ranging up to 70 cm in length. Tererdo-bored wood fragments up to 8 cm long are fairly common. Deposit is predominately medium dark gray (N4), but is commonly stained to a dusky yellow (5Y 5/6). Fresh broken exposure gives off a sulfurous odor.
1	1	Sandstone: fine to medium-grained, micaceous, arkosic, with minor lithic content. moderately sorted, locally calcite cemented, bioturbated. Medium dark gray (N4) where fresh, weathers to moderate orange pink (5YR 8/4).

APPENDIX II (continued)

Section E-E′

Cape Lookout Highway Measured Section
Angora Peak member of the Astoria Formation

Initial Point (E): northeast quarter sec. 7, T. 3 S., R. 10 W.
700 meters northwest of the intersection of Cape Lookout Highway and Camp Merriwether access road. Measured above the approximately located contact with the underlying Smuggler Cove formation.

Terminal Point (E′): southwest quarter sec. 6, T. 3 S., R. 10 W.
Top of measured section is located at the contact between the Angora Peak member and the N_2 low magnesium-low titanium Winterwater flows of the Grande Ronde Basalt near the apex of the hill.

Thickness (m)	Total (m)	Description
14.2	433.4	Sandstone: lithology as below. Deposit of large chaotic jumble of sandstone blocks that range in size from 2 to 10 meters in length in contact with N_2 low magnesium low titanium Winterwater Unit of the Grande Ronde Basalt. Many sandstone blocks are near vertical, and between blocks is a structureless friable sandstone of similar composition and grainsize to sandstone in blocks.
8.5	419.2	Sandstone: fine-grained, well-sorted, micaceous, arkosic sandstone with rare thin interbeds composed of siltstone rip-ups deposited upon an undulatory surface that may represent the swale of a hummocky cross-stratified bed. Sandstone is iron-stained and weathered to grayish orange pink (5 YR 7/2). Rare MnO-cemented concretions are also present.
6.5	410.7	Sandstone: fine-grained, well-sorted, friable, arkosic-micaceous sandstone with some thin (3 mm) siltstone rip-ups deposited along laminae of hummocky cross-stratified sandstone. Between a set HCS sandstone is a lag of basalt pebbles that may signify a first order hummocky cross-stratification boundary. The pebbly interval includes a fossil hash composed of many articulate and inarticulate bivalves including Anadara sp. and possibly Chlamys sp..Pebbly and fossil-rich zone is 70-150 cm thick, and is scoured into sandstone below.

APPENDIX II (continued)

Thickness (m)	Total (m)	Description
33.2	404.3	Sandstone: fine to medium-grained well-sorted sandstone with 1 m thick interval characterized by interbedded sandy siltstone and fine grained sandstone. Most of the deposit is amalgamated hummocky cross-stratified sandstone with rare antiforms preserved, but is locally disturbed by bioturbated intervals. The sandstone is weathering spheroidally, and is commonly leisegang banded and fractured. The sandstone that is 10 meters from the top of this interval is fossiliferous and includes the unidentified bivalves.
2.4	371.1	Sandstone: very fine to fine-grained, silty, friable sandstone with rare thin (<4 cm) thick laminated mudstone interbeds between hummocky cross-stratified sandstone sequences. Most HCS is amalgamated with few antiforms preserved. Flecks of black carbonaceous plant matter are fairly common, and rare leaf imprints are present.Sandstone weathers to yellowish gray (5Y 8/1), however it is light gray (N7) where fresh). Some spheroidal weathering is present.
33.0	368.7	Cover: vegetation.
2.2	335.7	Basaltic grit: Laterally discontinuous beds of well rounded basalt granules and pebbles (3-7 mm diameter) that thicken and thin along strike from 4 cm to 18 cm. The botton contact of each grit bed is scoured into arkosic micaceous sandstone, and there are some load structures at the base of the grit beds. Near the top of the sequence the uppermost basalt grit bed grades back to arkosic micaceous, fine to medium grained sandstone.
2.2	333.5	Sandstone: lithology as in previous interval. Deposit includes several discontinuous lenses (23-64 cm thick) of fossil hash-bearing sandstone in a possibly hummocky cross-stratified sequence. Fossils include the bivalves Anadara sp., and Spisula (Mactromeris) sp. cf. S. (M.) albaria.
2.2	331.3	Sandstone: as in interval 326.5

APPENDIX II (continued)

Thickness (m)	Total (m)	Description
2.8	329.3	Cover: vegetation and stream.
9.3	326.5	Sandstone: lithology as previous interval. Local discontinuous calcite concretionary horizons form resistent ribs or shelves that range from 13 to 48 cm thick. The deposit is Hummocky cross stratified, with numerous swales and a few antiforms preserved. Predominately amalgamated sequence. Medium bluish gray (5B 5/1) where fresh. Deposit is extremely micaceous, with abundant large (< 2mm) mucovite mica flakes, and some concentrations of black flecks of carbonaceous plant matter. Fresh exposures have sulfurous odor. Where silty, sandstone is richer in organic matter.
5.1	317.2	Sandstone: well sorted, fine-grained, arkosic-micaceous sandstone, possible hummocky cross-stratified.
1.2	312.1	Cover: vegetation.
7.6	310.9	Sandstone: lithology as in interval 291.3, friable, subhorizontally laminated, and parts along bedding planes. Weathered exposures are very pale orange (10YR 8/2).
12.0	303.3	Cover: vegetation
47.0	291.3	Sandstone: well sorted, fine to medium grained, micaceous-arkosic sandstone. Structureless, with common iron stain along fracture planes.
3.3	244.3	Sandstone: As in interval 233.4, with 3 cm thick tuffaceous claystone bed.
7.6	241.0	Basalt dike: Pillowed and heavily altered brecciated basalt. Basalt is the N_2 high high magnesium Sentinel Bluff Unit of the Grande Ronde Basalt. Pillow rinds are most extensively weathered, with pillow cores remaining fairly fresh. Basalt is nonvesicular, and aphyric. Near upper contact with overlying sandstone the basalt is extremely brecciated, and partially mixed with sandstone as a pepperite.

APPENDIX II (continued)

Thickness (m)	Total (m)	Description
3.0	233.4	Sandstone: fine to medium-grained arkosic-micaceous laminated sandstone as a chaotic jumble of blocks in structureless matrix of loose and unconsolidated sand of similar grainsize and composition. Sandstone is invaded by fingers (< 1 m long) of brecciated basalt which may represent a pepperite dike.
43.0	230.4	Cover: colluvium and debris flow.
3.8	187.4	Siltstone: Medium dark gray (N4) sandy siltstone, micaceous, friable, chippy, iron stained. Weathers to moderate orange pink (5YR 8/4).
1.5	183.6	Sandstone: fine to medioum-grained, well sorted, arkosic, friable sandstone. Commonly iron-stained and bioturbated.
40.0	182.1	Cover: vegetation
5.5	142.1	Sandstone: fine-grained, well sorted, at base coarsening upward to medium grained micaceous-arkosic sandstone. Common low angle cross stratification that may represent hummocky cross stratification. Deposits includes fossil mold of Anadara sp.
5.2	136.6	Sandstone: as below but lacks organic matter.
4.0	131.4	Sandstone: very fine to fine-grained, very well sorted, micaceous, arkosic friable sandstone with disseminated small (<1 cm) flecks of carbonaceous plant matter. Exposure is mottled from extensive bioturbation, and is leisegang banded. Fresh surfaces are medium gray (N5), but weathered surfaces are commonly dusky yellow (5Y 6/4).
5.6	127.4	Cover: vegetation
7.6	121.8	Engineered fill
9.1	114.2	Cover: vegetation

APPENDIX II (continued)

Thickness (m)	Total (m)	Description
5.0	105.1	Sandstone: very fine to fine grained, micaceous-arkosic, friable, horizontally laminated to hummocky cross-stratified sandstone, with both hummocks and swales preserved. Weathered exposures are moderate orange pink (5YR 8/4).
5.0	100.1	Sandstone: medium-grained, friable, very micaceous, arkosic sandstone. Predominately bioturbated deposit with a trace of low-angle cross-stratification preserved.
7.2	95.1	Sandstone: as below but with large (1 mm diameter) muscovite mica flakes.
7.1	87.9	Sandstone: Muscovite mica-rich, arkosic, well-sorted fine-grained sandstone with disseminated flecks of carbonaceous plant detritus approximately 2 mm long. Exposure gives off a slight sulphurous odor and is mantled by a thin grayish yellow (5Y 7/2) weathering coat. Deposit is mottled due to moderate to extensive bioturbation.
2.1	80.8	Sandstone: same lith as below. Strongly leisegang banded, with trace of hummocky cross-stratification. Most of this interval is homogenized by extensive bioturbation.
6.1	78.7	Sandstone: fine to medium grained, arkosic micaceous, friable sandstone with local hematite stained and cemented horizons. Deposit is structureless, possibly due to bioturbation. Weathered exposures are moderate orange pink (5 YR 8/4) to light brown (5YR 6/4).
71.6	72.6	Cover: Predominately basalt and sandstone colluvium and vegetation.
1	1	Sandstone: very fine to fine-grained, arkosic, micaceous, friable sandstone. Hematite cement and stain is concentrated along bedding planes, and most sedimentary structures have been obliterated by bioturbation. Weathers to very pale yellow (10 YR 8/2).

APPENDIX III

Netarts Bay Member Measured Section F-F′

Netarts Bay member of the Astoria Formation
Measured Reference Section

Initial Point (F): Northwest quarter of the northwest quarter of sec. 11, T. 2 S., R. 10 W. (Figure 60). At contact with the Angora Peak member.

Terminal Point (F′): Northwest quarter of the southeast quarter of sec. 10, T. 2 S., R. 10 W. At contact with the Cannon Beach member.

Thickness (m)	Total (m)	Description
3.6	170.4	Massive fine- to medium-grained, pebbly sandstone. Loose, friable, unconsolidated with large (>1.5 meter in length) siltstone rip-ups or wall blocks suspended in sandstone matrix. Deposit is draped by horizontally laminated mudstone of Cannon Beach member that contains rare very thin (<2 cm) bedded turbidite (?) sandstone interbeds.
7.3	166.8	Horizontally laminated sandstone with rare siltstone interbeds. Sandstone is medium-grained, well-sorted, and includes large (> 7cm) siltstone rip-ups.
1.8	159.5	Cover
4.5	157.7	Sandstone, fine- to medium-grained, leisegang banded, predominantly horizontally laminated with some cut and fill structures. Grades upward to micaceous arkosic well-sorted sandstone and a 2 cm to 14 cm thick dark gray (N3) siltstone with wavy and starved ripple laminated sandstone. Siltstone is overlain by turbidite sandstone bed with T_{b-c} amalgamated sequences, and rare T_{a-e} interbeds. The mudstone within the upper part of the turbidite beds is bioturbated.
2.4	153.2	Massive medium- to coarse-grained pebbly sandstone with siltstone rip-ups and large pebbles in matrix support.
12.1	150.8	Cover

APPENDIX III (continued)

Thickness (m)	Total (m)	Description
6.1	138.7	Pebbly sandstone interbedded with massive sandstone. Locally contains blocks composed of similar material.
2.1	132.6	Chaotic zone composed of randomly oriented blocks (>30 cm diameter) of sandstone.
1.0	130.5	Vertical block (>2 m diameter) of siltstone with some thin-bedded turbidite sandstone interbeds.
6.2	129.5	Sequence of vertical beds adjacent to subhorizontal beds. Possible wall block of Netarts Bay strata. Block composed of thick-bedded turbidite sandstones (0.2-0.3 m thick). A thick (1.5-2 m) interbed of siltstone occurs in the middle of this turbidite sandstone package. Near the undisturbed strata a clastic dike (7 cm thick) injects the siltstone. Between the steeply-dipping strata and subhorizontal sandstones, there is a 1 m thick zone friable loose unconsolidated massive sandstone. Adjacent "undisturbed" sandstone is horizontally laminated, friable, fine- to medium-grained with some siltstone rip-ups.
9.1	123.2	Medium-grained arkosic micaceous horizontally laminated sandstone.
6.1	114.1	Thinly interbedded sandstone and siltstone overlain by pebbly mudstone at top of the sequence.
1.5	108.0	Light brown siltstone. Horizontally laminated with rare starved ripple laminated sandstone. Sandstone laminae <1 cm thick.
4.6	106.5	Interbedded light gray (N7) siltstone and fine-grained sandstone. Some mudstone rip-ups in matrix support. Overlain by penecontemporaneously deformed very fine- to fine-grained sandstone. Abrupt lower contact, normal grading. Turbidite sequence.

APPENDIX III (continued)

Thickness (m)	Total (m)	Description
1.5	109.9	Horizontally laminated fine-grained silty sandstone.
6.1	108.4	Cover
4.6	102.3	Possible channel wall adjacent to block described below. Carbonaceous, fossil-mold-bearing, bioturbated sandstone.
0.6	97.7	Massive pebbly medium- to coarse-grained sandstone scoured into block described below.
6.1	97.1	Large penecontemporaneously emplaced block of light gray (N7) fine- to medium-grained sandstone with faint horizontal lamination. Rare slump (?) structures present. Bedding more distinct upward, grading to horizontally laminated sandstone with organic-rich layers 1 mm to 1 cm thick. Possible Bouma T_{c-e} here. Block >4.5 m in diameter.
4.6	91.0	Sandstone, friable, unconsolidated, massive, pebbly with basalt and chert pebbles floating in sandstone matrix. Grades upward to very coarse- and coarse-grained sandstone. Crude stratification upward with some stringers of pebble-rich sandstone. Deposit includes sandy siltstone, deeply scoured by overlying massive, pebbly, sandstone bed. Grades upward to horiz. laminated medium- to fine-grained sandstone.
12.2	86.4	Cover
3.0	74.2	Possible channel wall block >5 m in diameter. Block composed of Bouma T_{c-e} sequences and includes thin (<1 cm thick) siltstone interbeds between turbidite sandstones. Block includes clastic dikes injected upward from massive fluidized sandstone interval of massive pebbly sandstone.

APPENDIX III (continued)

Thickness (m)	Total (m)	Description
1.5	71.2	Chaotic zone with 1.5 meter diameter clasts with lithology as below, suspended in massive fine- to medium-grained matrix. Large blocks are randomly oriented.
3.0	69.7	Sandstone, horizontally laminated micaceous-arkosic with abundant brown comminuted organic matter concentrated at top of each 10-15 cm thick sequence. Horiz. lam sandstone represents T_d interval, and plant matter occurs within the uppermost Bouma T_{d-e} interval. Common iron stain and leisegang banded.
20.0	66.7	Cover
3.0	46.7	Lithology as above but locally mottled, possibly bioturbated medium-grained sandstone.
1.0	43.7	Lithology as below with wood fragment 5 cm thick.
0.6	42.7	Cover
1.5	42.1	Fine-grained structureless, carbonaceous, micaceous arkosic sandstone. Moderately sorted with common leisegang banding.
22.8	40.6	Cover
1.0	17.8	Siltstone, horizontally laminated with thin 1 to 3 cm thick fine to medium-grained turbidite sandstone beds with ripple laminae (T_c) grading to horizontally laminated (T_d) interval.
0.4	16.8	Sandstone with erosional lower contact, horizontally laminated at base grading through ripple laminated fine-grained sandstone to siltstone.
0.6	16.4	Siltstone, very thin bedded (< 1 cm).

APPENDIX III (continued)

Thickness (m)	Total (m)	Description
0.9	15.8	Horizontally laminated ungraded to crudely graded fine- to medium-grained arkosic micaceous sandstone. Friable and iron stained very pale orange (10 YR 8/2) to light brown (5 YR 5/6). Leisegang banded. Local convolute bedding in fine-grained sandstone. Fines upward to siltstone.
1.2	14.9	Siltstone with thin ripple-laminated fine- to medium-grained sandstone 1 cm to 3 cm thick. Siltstone beds 3 to 6 cm thick.
4.6	13.7	Disrupted bedding with starved ripple-laminated sandstone beds (10 cm thick) interbedded with 17 to 30 cm thick micaceous siltstone interbeds. Blocks of siltstone are locally entrained in a structureless very fine-grained sandy matrix that may represent a clastic dike 60 cm thick.
1.5	9.1	Thinly interbedded sandstone, very fine-grained micaceous-arkosic; and light gray (N7) siltstone with mica concentrated along bedding planes. Siltstone interbeds approximately 1 cm thick, sandstone interbeds 10 cm thick. Sandstones have abrupt lower contacts, crude normal grading with Bouma T_{d-e} structures.
6.1	7.6	Loose, friable, medium-grained, structureless, light gray (N7) arkosic-micaceous, lithic sandstone. Massive.
1.5	1.5	Volcaniclastic pebbly very coarse- to coarse-grained sandstone in erosional contact with extremely bioturbated and fossiliferous sandstones of the Angora Peak member. Netarts Bay sandstone contains rip-ups of underlying sandstone. Clastic dike 1 m wide and 5 m in length composed of pebbly sandstone injects downward into Angora Peak member. Dike is structureless and extends upward into Netarts Bay strata approximately 3 meters.

APPENDIX III (continued)

Thickness (m)	Total (m)	Description
		Netarts Bay member sandstone is moderately to poorly sorted, friable to hematite cemented, with common stingers of basalt pebbles. Moderately to extremely friable.

APPENDIX IV

Checklist Of Fossils

Checklist of Fossils from the Smuggler Cove Formation

Samples:	CL-48Z	36-88	63-88	65-88
Foraminifera (Identified by H. Heitman, Unocal Corp.)				
Cyclammina sp.	X	X	X	-
Cyclammina clarki	-	-	-	X
Haplophragmoides sp.	-	X	-	X
Dentalina consorbina	-	-	-	X
Lenticulina simplex	-	-	-	X
Uvigerina obesa impolita	-	-	-	X
Sphaeroidina variabilis	-	-	-	X
Bathysiphon sp.	-	-	-	X
Rhabdammina sp.	-	-	-	X
Foraminifera, arenacious	-	-	X	-

Sample:	40-88
Pelecypods (identified by Ellen Moore, USGS, ret.)	
Unidentified Naticid	X
Unidentified mytilid	X

Sample:	63-88	65-88
Pollen (Identified by Kirk Waln, Unocal Corp.)		
Quercus sp. (Oak)	X	X

Fossil localities for the Smuggler Cove Formation

CL-48Z	T. 3 S., R. 10 W., Section 10, south 1/2, center
40-88	T. 3 S., R. 10 W., Section 10, northwest corner
36-88	T. 2 S., R. 9 W., Section 18, northwest corner
63-88	T. 4 S., R. 11 W., Section 13, southwest corner
65-88	T. 3 S., R. 10 W., Section 10, southeast corner

Checklist of Fossils from the Bewley Creek Formation

Samples:	CL-88	CL-140	CL-51Z	66-88	NNB-46Y
Pelecypods (Identified by Ellen Moore, USGS, ret.)					
Spisula (Mactromeris) sp.	X	-	-	X	-
Spisula (Mactromeris) sp. c.f. S. (M.) albaria (Conrad)	-	X	X	-	-
Lucinoma sp. cf. L. hannibali	X	-	-	-	X
Mytilid	-	X	-	-	-
Mytilid (?)	X	-	-	-	-
Solen (?) sp.	X	-	-	-	-
Venerid (?)	-	X	-	-	-
Anadara (Anadara) devincta (Conrad)	-	-	X	-	-
Crenella (?)	-	-	X	-	-
Chlamys (?)	-	-	X	-	-

APPENDIX IV (continued)

Samples:	CL-88	CL-140	CL-512	66-88	NNB-46Y
Vertipectin fucanus (Dall)	-	-	X	-	-
Panopea abrupta (Conrad)	-	X	X	-	-
Unidentified nuculanid	X	-	X	-	-
Unidentified venerid	X	-	-	-	-
Gastropods (Identified by Ellen Moore, USGS, ret.)					
Unidentified naticid	X	-	X	-	-
Epitonid (?)	X	-	-	-	-
Scaphopods (Identified by Ellen Moore, USGS, ret.)					
Dentalium sp.	X	-	X	-	-

Pollen (Identified by Kirk Waln, Unocal Corp.)

Samples:	NNB-45
Quercus sp. (Oak)	X
Fagus sp. (Beech)	X
Carya sp.	X
Betula sp. (Birch)	X

Fossil localities for the Bewley Creek Formation

CL-88	T. 2 S., R. 10 W., Section 35, southeast corner
NNB-45	T. 2 S., R. 10 W., Section 12, northeast corner
NNB-46Y	T. 2 S., R. 9 W., Section 6, southwest corner
CL-512	T. 3 S., R. 10 W., Section 4, southwest corner
CL-140	T. 3 S., R. 10 W., Section 9, center
66-88	T. 2 S., R. 10 W., Section 33, southeast corner

Checklist of Fossils from the Sutton Creek Member of the Nye Mudstone

Samples:	CL-145	CL-131
Foraminifera (Identified by W. Rau, Wash. Dept. Nat. Res., specified, and H. Heitman, Unocal Corp.)		
Bulimina pyrula	X	-
Bulimina cf. B. ovata (d'Orbigny) I.D.	by Rau X	-
Gyroidina cf. G. soldanii (d'Orbigny)	by Rau X	-
Trochammina sp.	X	-
Cibicides cf. C. elmaensis Rau var. A	by Rau -	X
Buccella mansfieldi oregonensis (Cushman, Stewart and Stewart)	by Rau -	X
Uvigerina sp.	by Rau -	X
Florilus costiferum (Cushman)	by Rau X	X
Bolivina cf. B. chehalisensis Rau	by Rau -	X
Cassidulina cf. C. crassipunctata (Cushman and Hobson)	by Rau -	X

APPENDIX IV (continued)

Fossil localities for the Sutton Creek member of the Nye Mudstone

CL-145 T. 2 S., R. 10 W., Section 34, west 1/2 center
CL-131 T. 3 S., R. 11 W., Section 1, southeast corner

Checklist of Fossils from the Angora Peak member of the Astoria Formation

Samples:	NNB-39	NNB-40	CL-74	20-88
Pelecypods (Identified by Ellen Moore, USGS, ret.)				
Anadara (Anadara) devincta (Conrad)	X	-	-	-
Anadara (Anadara) sp. cf. A. (A.) devincta (Conrad)	-	-	-	X
Anadara sp.	-	-	X	-
Clincardium (?) sp.	X	-	-	-
Katherinella (Katherinella) angustifrons (Conrad)	-	X	-	-
Katherinella (Katherinella) sp. cf. C. (C.) angustifrons (Conrad)	X	-	-	-
Katherinella sp. cf. K. angustifrons (Conrad)	X	-	-	-
Lucinoma (?) sp.	X	-	-	-
Panopea abrupta (Conrad)	X	-	-	-
Spisula (?) sp. cf. S. (M.) albaria (Conrad)	X	-	-	-
Spisula (Mactromeria) sp. cf. S. (M.) albaria (Conrad)	-	-	X	X
Chione (Securella) ensifera (Dall)	-	-	-	-
Chlamys(?)	-	-	-	-
Macoma arctata (Conrad)	-	-	-	-
Vertipectin sp. cf. V. fucanus (Dall)	-	-	-	-
Vertipectin (?) sp. cf. V. fucanus (Dall)	-	-	-	-
Unidentified pectinid	-	-	-	-
Unidentified nuculanid	X	-	-	-
Gastropods (Identified by Ellen Moore, USGS, ret.)				
Ficus modesta	X	-	-	-
Callcantharus sp. cf. C. carlsoni (Anderson and Martin)	-	-	-	-
Unidentified naticid	-	-	-	-
Scaphopods (Identified by Ellen Moore, USGS, ret.)				
Dentalium sp.	-	-	-	-

Samples:	SNB-105	3-88-8	57-88
Pelecypods (Identified by Ellen Moore, USGS, ret.)			
Lucinoma sp. cf. L. hannibali (Clark)	-	-	-
Anadara (Anadara) devincta (Conrad)	X	-	-
Anadara (Anadara) sp. cf. A. (A.) devincta (Conrad)	-	-	-
Anadara sp.	-	X	-

APPENDIX IV (continued)

Samples:	SNB-105	3-88-8	57-88
Clincardium (?) sp.	-	-	X
Katherinella (Katherinella) angustifrons (Conrad)	-	-	-
Katherinella (Katherinella) sp. cf. C. (C.) angustifrons (Conrad)	-	-	-
Katherinella sp. cf. K. angustifrons (Conrad)	-	-	-
Lucinoma (?) sp.	-	-	-
Panopea abrupta (Conrad)	-	-	-
Spisula (?) sp. cf. S. (M.) albaria (Conrad)	-	-	-
Spisula (Mactromeria) sp. cf. S. (M.) albaria (Conrad)	X	-	-
Chione (Securella) ensifera (Dall)	-	-	-
Chlamys(?)	-	X	-
Macoma arctata (Conrad)	-	-	-
Vertipectin sp. cf. V. fucanus (Dall)	-	-	-
Vertipectin (?) sp. cf. V. fucanus (Dall)	-	-	-
Unidentified pectinid	-	-	-
Unidentified nuculanid	X	-	-
Gastropods (Identified by Ellen Moore, USGS, ret.)			
Ficus modesta	-	-	-
Calicantharus sp. cf. C. carlsoni (Anderson and Martin)	-	-	-
Unidentified naticid	-	-	-
Scaphopods (Identified by Ellen Moore, USGS, ret.)			
Dentalium sp.	-	-	-

Samples:	58-88	59-88	61-88
Pelecypods (Identified by Ellen Moore, USGS, ret.)			
Lucinoma sp. cf. L. hannibali (Clark)	-	-	-
Anadara (Anadara) devincta (Conrad)	-	-	-
Anadara (Anadara) sp. cf. A. (A.) devincta (Conrad)	-	-	-
Anadara sp.	-	-	-
Clincardium (?) sp.	X	-	
Katherinella (Katherinella) angustifrons (Conrad)	-	X	-
Katherinella (Katherinella) sp. cf. C. (C.) angustifrons (Conrad)	-	-	X
Katherinella sp. cf. K. angustifrons (Conrad)	-	-	-
Lucinoma (?) sp.	-	-	-
Panopea abrupta (Conrad)	-	-	-
Spisula (?) sp. cf. S. (M.) albaria (Conrad)	-	-	-
Spisula (Mactromeria) sp. cf. S. (M.) albaria (Conrad)	-	-	-

APPENDIX IV (continued)

Samples:	58-88	59-88	61-88
Chione (Securella) ensifera (Dall)	-	X	-
Chlamys(?)	-	-	-
Macoma arctata (Conrad)	-	X	-
Vertipectin sp. cf. V. fucanus (Dall)	-	X	-
Vertipectin (?) sp. cf. V. fucanus (Dall)	-	-	X
Unidentified pectinid	-	X	-
Unidentified nuculanid	-	-	-

Gastropods (Identified by Ellen Moore, USGS, ret.)

Ficus modesta	-	-	-
Calicantharus sp. cf. C. carlsoni (Anderson and Martin)	-	-	-
Unidentified naticid	-	-	-

Scaphopods (Identified by Ellen Moore, USGS, ret.)

Dentalium	-	-	-

Pollen (Identified by Kirk Waln)

Samples:	3-88-5	3-88-7
Quercus sp. (Oak)	X	X
Fagus sp. (Beech)	X	-
Carya sp. (Hickory)	X	X
Betula sp. (Birch)	X	X
Momipites sp.	-	X
Deflandrea phosphoritica	-	X

Fossil localities for the Angora Peak member of the Astoria Formation

NNB-39	T. 2 S., R. 10 W., Section 11, northwest corner
NNB-40	T. 2 S., R. 10 W., Section 11, northwest corner
CL-74	T. 3 S., R. 10 W., Section 6, southwest corner
20-88	T. 3 S., R. 11 W., Section 1, northwest corner
SNB-105	T. 2 S., R. 10 W., Section 27, northwest corner
3-88-5	T. 3 S., R. 10 W., Section 6, southeast corner
3-88-7	T. 3 S., R. 10 W., Section 6, southwest corner
3-88-8	T. 3 S., R. 10 W., Section 1, southeast corner
28-88	T. 2 S., R. 10 W., Section 22, northwest corner
57-88	T. 1 S., R. 10 W., Section 15, northwest corner
58-88	T. 1 S., R. 10 W., Section 15, southwest corner
59-88	T. 1 S., R. 10 W., Section 15, southwest corner
61-88	T. 3 S., R. 10 W., Section 33, southwest corner

Checklist of Fossils from the Netarts Bay member of the Astoria Formation

Pelecypods (Identified by Ellen Moore, USGS, ret.)

Samples:	28-88	26-88
Anadara (Anadara) sp. cf. A. (A.) devincta (Conrad)	X	-
Spisula (Mactromeria) sp. cf. S. (M.) albaria (Conrad)	-	X

APPENDIX IV (continued)

Samples:	28-88	26-88
Unidentified pectinid	X	X

Samples:	NNB-32X	SNB-107	34-88
Pollen (Identified by Kirk Waln)			
Quercus sp. (Oak)	X	X	X
Reworked Eocene Dinoflagellates	-	X	-

Fossil localities for the Netarts Bay member of the Astoria Formation

NNB-32X	T. 2 S., R. 10 W., Section 2, southeast corner
SNB-107	T. 2 S., R. 10 W., Section 28, center
28-88	T. 2 S., R. 10 W., Section 22, northwest corner
34-88	T. 2 S., R. 10 W., Section 30, southwest corner

Checklist of Fossils from the Cannon Beach member of the Astoria Formation

Samples:	NNB-6a	0-18	NNB-30
Foraminifera (Identified by W. Rau, Wash. Dept. Nat. Res., specified, and H. Heitman, Unocal Corp.)			
Florilus cosiferum (Cushman)I.D. by Rau	X	-	-
Bulmina cf. B. ovata d'Orbigny by Rau	X	-	-
Globigerina sp. by Rau	X	-	-
Suggrunda sp. by Rau	X	-	-
Florilus cf. F. inclsum (Cushman)by Rau	X	-	-
Nonionella miocenica Cushman by Rau	X	-	-
Bulimina pyrula	X	X	-
Angulogerina astoriensis	X	-	-
Bolivina cf. vaughani	X	-	-
Bolvina marginata	X	-	-
Bulimina sp.	X	-	-
Buliminella elegantissima	X	-	-
Cassidulina sp.	X	-	-
Eponides sp.	X	-	-
Frondicularia advena	X	-	-
Lenticulina sp.	X	-	-
Suggrunda eckisi	X	-	-
Uvigerina obesa impolita	X	-	-
Fissurina sp.	X	-	-
Epistominella sp.	X	-	-
Globigerina sp.	X	-	-
Haplophragmoides sp.	-	-	X

Samples:	NNB-4	NNB-6A	NNB-9B	NNB-30	M-117	46-88	50-88
Pollen (Identified by Kirk Waln)							
Carya sp. (Hickory)	X	X	-	X	X	-	X
Quercus sp. (Oak)	X	X	X	X	X	X	X
Betula sp. (Birch)	X	X	-	X	-	-	X
Ulmus sp. (Elm)	-	X	-	-	-	-	-
Fagus sp. (Beech)	-	-	-	X	X	-	X

APPENDIX IV (continued)

Samples:	51-88	60-88	71-88
Pollen (Identified by Kirk Waln)			
Carya sp. (Hickory)	X	-	X
Quercus sp. (Oak)	X	X	X
Betula sp. (Birch)	X	-	X
Fagus sp. (Beech)	X	-	X

Fossil localities for the Cannon Beach member of the Astoria Formation

NNB-4	T. 2 S., R. 10 W., Section 9, northeast corner
NNB-6a	T. 2 S., R. 10 W., Section 4, northwest corner
NNB-9b	T. 2 S., R. 10 W., Section 4, center
O-18	T. 1 S., R. 10 W., Section 33, northeast corner
NNB-30	T. 2 S., R. 10 W., Section 3, northwest corner
M-117	T. 1 S., R. 10 W., Section 16, southeast corner
46-88	T. 1 S., R. 10 W., Section 17, northwest corner
50-88	T. 1 S., R. 10 W., Section 17, northwest corner
51-88	T. 1 S., R. 10 W., Section 17, northwest corner
60-88	T. 2 S., R. 10 W., Section 16, northeast corner
71-88	T. 1 S., R. 10 W., Section 18, northwest corner

Checklist of Fossils from Sedimentary Interbeds within Grande Ronde Basalt

Sample:	13-88
Pelecypods (Identified by Ellen Moore, USGS, ret.)	
Oyster	X
Gastropods (Identified by Ellen Moore, USGS, ret.)	
Cerithid (?)	X

Fossil locality for the sedimentary interbed within the Grande Ronde Basalt

13-88	T. 1 S., R. 11 W., Section 24, southeast corner
26-88	T. 2 S., R. 10 W., Section 32, east 1/2, center

Checklist of Fossils from Well ONG CZ#1

Depth in feet:	300	600	1650	3740	3770	3950	6030
Pollen (Identified by Kirk Waln)							
Quercus sp. (Oak)	X	X	X	X	X	X	X
Fagus sp. (Beech)	X	X	X	-	X	-	-
Ulmus sp. (Elm)	-	X	X	-	-	-	-
Carya sp. (Hickory)	-	X	-	-	-	-	-
Alnus sp. (Alder)	-	X	-	-	-	-	-
Ephedra sp.	-	X	-	-	-	-	-
Tuberculodinium vancampoae	-	X	-	-	-	-	-
Momipites sp.	-	-	X	-	-	X	X
Betula sp. (Birch)	-	-	X	X	-	X	X

APPENDIX IV (continued)

Depth in feet:	300	600	1650	3740	3770	3950	6030
Pterocarya sp.	-	-	-	X	-	-	-
Bombacaceae	-	-	-	-	X	-	-
Spinidinium densispinatum	-	-	-	-	X	-	-
Cordoshaeridium funiculatum	-	-	-	-	X	-	-
Plicapollis sp.	-	-	-	-	-	-	-

Foraminifera (Identified by H. Heitman, Unocal corp)

Depth in feet:	300	600	1650	3740	3770
Bolivina marginata	X	-	X	-	-
Bulimina inflata aligata	X	-	-	-	-
Bulimina sp.	-	-	X	-	-
Bulimina pyrula	-	-	-	-	X
Buliminella subfusiformis	X	-	-	-	-
Cassidulina laevigata carinata	X	X	-	-	-
Cibicides floridanus	X	-	X	-	-
Gyroidina soldanii	X	X	-	-	X
Lenticulina sp.	X	-	-	-	-
Cyclammina clarki	X	X	X	X	X
Haplophragmoides sp.	X	X	X	X	X
Haplophragmoides trullissata	-	X	X	X	X
Nodosaria	-	X	-	-	-
Quinqueloculina sp.	-	X	-	-	-
Uvigerina cf. gallowayi	-	X	-	-	X
Uvigerina auberiana	-	X	-	-	-
Melonis pompiliodes	-	X	-	-	-
Rhabdammina sp.	-	X	-	-	-
Bathysiphon sp.	-	-	X	X	-
Suggrunda eckisi	-	-	-	-	X
Arenaceous Foraminifera	-	-	-	X	-

Checklist of Fossils from Well REC CZ#1

Pollen (Identified by Kirk Waln, Unocal Corp.)

Depth in feet:	3920	3980	5480	5555
Quercus sp. (Oak)	X	X	X	X
Betula sp. (Birch)	X	X	X	X
Momipites sp.	X	X	-	X
Fagus sp. (Beech)	X	X	-	-
Spinidinium densispinatum	-	X	-	-
Spiniferites sp.	-	-	X	X
Areospaeridium diktyoplokus	-	X	-	-
Castanea sp.	-	-	X	X

APPENDIX IV (continued)

Foraminifera (Identified by Hal Heitman, Unocal Corp.)

Depth in feet:	3920	3980	5480	5555
Lenticulina sp.	X	-	X	-
Uvigerina sp.	X	-	-	-
Uvigerina beccarii	-	-	-	-
Ammodiscus sp.	X	-	-	-
Bathysiphon sp.	-	-	-	-
Cyclammina clarki	X	X	-	-
Haplophragmoides sp.	X	X	X	X
Trochammina sp.	X	X	-	-
Martinottiella communis	X	-	-	-
Anomalina glabrata	-	X	-	-
Bulimina sp.	-	X	-	-
Quinqueloculina sp.	-	X	-	-
Pseudonodosaria sp.	-	X	-	-
Bathysiphon sp.	-	-	-	-
Guttulina sp.	-	-	-	X
Arenaceous Foraminifera	-	X	-	-

APPENDIX V

Modal Analyses of Sandstones

Bewley Creek formation

	38-88	CL-55	CL-59	CL-65	SNB-101
Porosity	6	18	7	0	11
Matrix	15	-	7	3	10
Cement	8	15	14	6	10
Clay Rim	5	13	5	2	6
Hematite	3	2	9	4	3
Calcite	-	-	-	26	5
Chlorite	-	-	-	-	-
Siderite	-	-	-	-	-
Zeolite	-	-	-	-	-
Detrital Grains*	79	67	72	65	66
Quartz and Chert	39	36	26	37	37
Mono xl. Quartz	22	27	19	28	23
Poly xl. Quartz	13	7	5	6	6
Hydroth. Quartz	-	-	-	-	-
Chert	4	2	2	3	3
Feldspar	19	30	21	35	26
Orthoclase	5	13	7	8	9
Microcline	2	3	5	2	3
Twinned Plag.	6	5	3	6	3
Untwinned Plag.	6	9	6	19	10
Mica	tr	1	2	2	3
Biotite	-	1	1	1	2
Muscovite	tr	-	1	1	1
Chlorite	-	-	-	-	-
Lithic Fragments	38	30	49	24	35
Felsic Volcanic	9	-	7	-	2
Mafic Volcanic	21	18	30	17	23
Quartzite	2	2	2	tr	2
Schist	-	1	-	1	tr
Phillite	1	2	1	2	2
Granitic	3	5	1	3	3
Sandstone	-	tr	1	1	tr
Siltstone	-	1	1	-	tr
Chalcedony	-	-	-	tr	tr
Pumice	2	1	6	-	2
Heavy Minerals	2	3	1	2	2
Opaques	2	-	1	-	
Glauconite	-	-	-	-	-

* Grain percentages are renormalized to 100% detrital grains.

APPENDIX V (continued)

	Sutton Creek member of the Nye Mudstone		
	CL-56	21-88	SNB-102
Porosity	23	1	15
Matrix	3	-	9
Cement	9	23	8
Clay Rim	3	-	5
Hematite	6	10	3
Calcite	-	13	-
Chlorite	-	-	-
Siderite	-	-	-
Zeolite	-	-	-
Detrital Grains*	65	76	68
Quartz and Chert	33	36	28
Mono xl. Quartz	25	19	19
Poly xl. Quartz	5	10	6
Hydroth. Quartz	-	-	-
Chert	3	7	2
Feldspar	35	24	22
Orthoclase	11	7	8
Microcline	3	2	3
Twinned Plag.	3	6	4
Untwinned Plag.	18	9	8
Mica	3	-	3
Biotite	2	-	2
Muscovite	1	-	1
Chlorite	-	-	-
Lithic Fragments	28	31	45
Felsic Volcanic	-	11	5
Mafic Volcanic	5	13	31
Quartzite	2	1	1
Schist	-	-	tr
Phillite	1	-	1
Granitic	4	2	3
Sandstone	-	-	tr
Siltstone	16	4	tr
Chalcedony	-	-	tr
Pumice	-	-	2
Heavy Minerals	1	-	tr
Opaques	-	-	-
Glauconite	-	9	-

* Grain percentages are renormalized to 100% detrital grains.

APPENDIX V (continued)

Angora Peak member of the Astoria Formation

	20-88	NNB-31	NNB-31A	NNB-46	52-88	53-88
Porosity	tr	7	1	4	18	1
Matrix	-	-	5	12	4	-
Cement	34	19	34	33	10	20
Clay Rim	1	14	5	15	3	10
Hematite	1	1	1	18	7	10
Calcite	31	-	27	-	-	-
Chlorite	-	-	-	-	-	-
Siderite	-	-	-	-	-	-
Zeolite	1	4	1	-	-	-
Detrital Grains*	66	74	60	51	68	79
Quartz and Chert	45	29	35	32	37	28
Mono xl. Quartz	36	17	27	26	24	13
Poly xl. Quartz	4	9	6	6	9	8
Hydroth. Quartz	-	-	-	-	-	1
Chert	5	3	2	-	4	6
Feldspar	27	38	37	46	43	27
Orthoclase	10	17	12	22	16	9
Microcline	1	1	1	2	3	2
Twinned Plag.	8	7	14	7	12	7
Untwinned Plag.	8	13	10	15	12	9
Mica	1	7	3	6	-	1
Biotite	1	5	1	4	-	1
Muscovite	tr	2	2	2	-	-
Chlorite	-	-	-	-	-	-
Lithic Fragments	20	23	22	11	15	40
Felsic Volcanic	-	-	-	-	2	-
Mafic Volcanic	17	15	20	8	10	37
Quartzite	tr	2	tr	-	1	tr
Schist	1	tr	-	-	tr	-
Phillite	1	1	-	2	tr	tr
Granitic	1	1	1	1	tr	3
Sandstone	-	-	-	tr	tr	tr
Siltstone	-	4	1	tr	1	-
Chalcedony	-	-	tr	-	-	-
Pumice	-	-	-	-	1	-
Heavy Minerals	4	2	3	3	3	-
Opaques	3	1	-	2	1	4
Glauconite	-	-	-	-	-	-

* Grain percentages are renormalized to 100% detrital grains.

APPENDIX V (continued)

Angora Peak member of the Astoria Formation (Cont.)

	56-88	K-148
Porosity	tr	1
Matrix	-	-
Cement	32	23
Clay Rim	-	4
Hematite	-	2
Calcite	32	17
Chlorite	-	-
Siderite	-	-
Zeolite	-	-
Detrital Grains*	68	76
Quartz and Chert	46	21
Mono xl. Quartz	35	9
Poly xl. Quartz	7	8
Hydroth. Quartz	-	1
Chert	4	3
Feldspar	31	33
Orthoclase	7	8
Microcline	3	3
Twinned Plag.	8	13
Untwinned Plag.	13	9
Mica	tr	1
Biotite	-	tr
Muscovite	tr	1
Chlorite	-	-
Lithic Fragments	21	43
Felsic Volcanic	1	-
Mafic Volcanic	13	41
Quartzite	1	tr
Schist	tr	tr
Phillite	-	tr
Granitic	5	1
Sandstone	1	-
Siltstone	-	1
Chalcedony	-	-
Pumice	-	-
Heavy Minerals	1	-
Opaques	1	2
Glauconite	-	-

* Grain percentages are renormalized to 100% detrital grains.

APPENDIX V (continued)

Netarts Bay member of the Astoria Formation

	NNB-11	NNB-12	NNB-29	35-88	NNB-40Z
Porosity	17	9	1	3	-
Matrix	-	-	48	22	-
Cement	8	19	tr	5	34
Clay Rim	4	11	tr	4	6
Hematite	4	6	tr	1	2
Calcite	-	-	-	-	25
Chlorite	-	-	-	-	-
Siderite	-	-	-	-	-
Zeolite	-	2	tr	tr	1
Detrital Grains*	75	72	51	70	66
Quartz and Chert	37	36	46	44	47
Mono xl. Quartz	23	22	33	24	38
Poly xl. Quartz	13	11	9	17	6
Hydroth. Quartz	-	tr	-	-	-
Chert	1	3	4	3	3
Feldspar	31	37	34	27	42
Orthoclase	9	14	9	9	8
Microcline	5	4	7	1	4
Twinned Plag.	7	5	3	8	13
Untwinned Plag.	10	14	15	9	17
Mica	2	4	tr	3	tr
Biotite	1	2	-	1	-
Muscovite	1	2	tr	2	tr
Chlorite	-	-	-	-	-
Lithic Fragments	29	21	18	21	6
Felsic Volcanic	-	-	tr	1	-
Mafic Volcanic	17	10	8	14	5
Quartzite	3	tr	4	2	1
Schist	1	2	-	1	-
Phillite	tr	1	-	1	-
Granitic	5	5	-	1	tr
Sandstone	-	-	-	1	-
Siltstone	3	3	6	-	-
Heavy Minerals	1	2	1	1	2
Opaques	-	-	1	4	2
Glauconite	-	-	-	-	1

* Grain percentages are renormalized to 100% detrital grains.

APPENDIX V (continued)

	Cannon Beach member of the Astoria Formation				
	NNB-10	O-18	O-30Z	42-88	46-88
Porosity	7	13	6	28	9
Matrix	11	1	6	5	-
Cement	16	12	9	5	15
Clay Rim	13	8	7	2	13
Hematite	3	3	2	3	1
Calcite	-	-	-	-	-
Chlorite	-	-	-	-	1
Siderite	-	-	-	-	-
Zeolite	-	1	-	-	tr
Detrital Grains*	66	74	79	62	76
Quartz and Chert	31	35	35	48	36
Mono xl. Quartz	17	24	25	31	18
Poly xl. Quartz	11	7	8	10	8
Hydroth. Quartz	-	tr	-	1	7
Chert	3	4	2	6	3
Feldspar	46	39	37	27	38
Orthoclase	22	13	15	2	14
Microcline	7	4	4	2	4
Twinned Plag.	4	7	6	12	8
Untwinned Plag.	13	15	12	11	12
Mica	3	4	tr	1	2
Biotite	1	2	-	1	1
Muscovite	2	2	tr	-	1
Chlorite	-	-	-	-	-
Lithic Fragments	16	20	21	23	24
Felsic Volcanic	-	tr	-	-	-
Mafic Volcanic	7	10	11	18	13
Quartzite	2	1	2	2	2
Schist	1	3	2	-	2
Phillite	1	1	1	tr	1
Granitic	1	1	2	3	2
Sandstone	-	-	-	-	tr
Siltstone	4	4	3	-	4
Heavy Minerals	4	1	6	1	tr
Opaques	-	1	1	-	-
Glauconite	-	-	-	-	-

* Grain percentages are renormalized to 100% detrital grains.

APPENDIX V (continued)

	Grand Ronde Basalt Interflow Sand	Sandstone of Whale Cove	
	17-88	CL-85	0-108
Porosity	tr	12	13
Matrix	-	-	-
Cement	36	20	6
Clay Rim	1	16	5
Hematite	2	2	tr
Calcite	32	-	-
Chlorite	tr	1	1
Siderite	-	-	-
Zeolite	1	1	-
Detrital Grains*	64	68	81
Quartz and Chert	36	40	32
Mono xl. Quartz	27	22	19
Poly xl. Quartz	6	14	11
Hydroth. Quartz	-	3	2
Chert	3	1	tr
Feldspar	30	30	34
Orthoclase	13	15	19
Microcline	3	1	2
Twinned Plag.	7	4	6
Untwinned Plag.	7	10	7
Mica	5	8	11
Biotite	3	5	8
Muscovite	2	3	3
Chlorite	-	-	-
Lithic Fragments	28	16	16
Felsic Volcanic	tr	-	-
Mafic Volcanic	25	11	7
Quartzite	1	1	3
Schist	tr	3	2
Phillite	1	1	1
Granitic	-	-	2
Sandstone	-	-	-
Siltstone	2	-	1
Pumice	-	-	-
Heavy Minerals	1	1	3
Opaques	tr	5	2
Glauconite	-	-	2

* Grain percentages are renormalized to 100% detrital grains.

APPENDIX VI

Statistical Parameters from Sieve Analysis of Sandstones

Samples	Folk and Ward SKI	Md phi	Mz phi	Sl phi	Kg	Sand %	Silt and Clay %	Coarsest 1% Microns	Median Microns
BEWLEY CREEK FORMATION									
37-88	0.29	2.60	2.73	0.87	0.91	89.11	10.89	420	165
38-88	0.50	0.80	1.08	1.18	1.29	94.32	5.68	1150	575
39-88	0.10	3.20	3.24	0.95	1.36	81.73	18.27	485	180
40-88	0.20	3.25	3.32	0.67	1.02	92.74	7.26	270	150
41-88	0.67	1.90	2.36	1.29	1.46	86.74	13.26	540	270
CL-49	0.44	1.60	1.83	0.96	2.08	93.66	6.34	840	330
CL-50	0.31	3.10	3.21	0.67	1.31	84.80	15.20	268	117
CL-51	0.43	1.75	1.98	0.99	1.34	92.82	7.18	740	299
CL-53	0.44	1.95	2.11	0.70	0.95	96.59	3.41	430	250
CL-59	0.29	0.95	1.18	1.47	1.35	93.16	6.82	2150	510
CL-65	0.37	1.25	1.45	1.17	1.66	92.92	7.08	1375	460
SNB-101	0.33	2.58	2.74	0.97	0.92	85.91	14.09	352	167
SUTTON CREEK MEMBER OF THE NYE MUDSTONE									
CL-56	0.25	1.70	1.75	0.63	1.57	97.52	2.48	575	309
CL-80	0.31	1.80	1.94	0.91	1.65	94.44	5.56	870	287
ASTORIA FORMATION									
Angora Peak member of the Astoria Formation									
NNB-31	0.28	3.18	3.29	0.63	1.37	87.71	12.29	202	117
52-88	0.48	1.90	2.04	0.59	1.43	96.71	3.29	460	270
64-88	0.35	2.27	2.37	0.76	1.31	92.62	7.38	575	205
CL-73	0.18	3.10	3.10	0.51	1.52	92.07	7.93	230	118
CL-74	0.11	3.10	3.09	0.40	1.59	94.20	5.80	232	118
CL-84	0.12	3.12	3.17	0.67	1.44	95.01	4.99	310	115
M-116	0.17	2.58	2.59	0.78	1.39	91.77	2.23	408	167
Netarts Bay member of the Astoria Formation									
NNB-11	0.22	1.65	1.80	1.11	1.30	95.32	4.68	1750	317
NNB-29	0.54	1.90	2.20	0.96	1.03	90.99	9.01	468	268
35-88	0.00	1.75	1.81	1.35	1.29	94.66	5.34	2820	300
Cannon Beach member of the Astoria Formation									
NNB-11Z	0.28	1.55	1.68	1.03	1.63	94.66	5.34	1030	340
0-17	0.52	1.95	2.24	1.00	1.19	90.68	9.32	535	260
0-18	0.05	2.70	2.63	0.82	1.03	91.98	8.02	406	154
0-30Z	0.35	1.51	1.67	0.94	1.91	94.63	5.37	1300	340
42-88	0.02	2.70	2.36	0.70	1.21	94.05	5.95	380	154
46-88	0.50	1.90	2.11	0.78	1.39	94.82	5.18	540	270

SKI - Skewness
Md - Median
Mz - Mean
Sl - Standard Deviation
Kg - Kurtosis

APPENDIX VI (continued)

Statistical Parameters from Sieve Analysis of Sandstones

Samples	Folk and Ward SKI	Md phi	Mz phi	SI phi	Kg	Sand %	Silt and Clay %	Coarsest 1% Microns	Median Microns
GRANDE RONDE BASALT SEDIMENTARY INTERBED									
Grand Ronde Interflow Sandstone									
17-88	0.20	3.18	3.22	0.47	1.15	92.06	7.94	256	110
SANDSTONE OF WHALE COVE									
CL-87	0.20	3.65	3.71	0.79	1.07	68.15	31.85	250	80
CM-91	0.10	3.20	3.24	0.73	1.16	85.91	14.09	318	140
O-108	0.06	2.60	2.58	0.75	1.33	93.98	6.02	435	165
O-109	0.35	2.15	2.27	0.79	1.40	92.91	7.09	485	235

APPENDIX VII

Heavy Mineral Analyses of Sandstones

Bewley Creek formation

Sample Number	37-88	39-88	40-88	CL-50	CL-59	SNB-101
Non-opaque grains (=100%)						
Amphibole	61	62	56	70	59	60
Hornblende	57	62	53	69	56	57
Green	40	56	28	46	39	44
Blue-green	8	1	17	11	10	8
Brown	9	5	8	12	7	5
Basaltic	-	tr	-	-	tr	-
Tremolite-Actinolite	4	tr	3	1	3	3
Glaucophane	-	-	tr	tr	-	-
Orthopyroxene	4	tr	7	3	2	-
Hypersthene	-	-	-	tr	2	-
Enstatite	4	tr	7	3	tr	-
Clinopyroxine	2	-	-	3	3	-
Diopside	-	-	-	-	1	-
Augite	2	-	-	3	2	-
Micas	11	-	13	3	3	4
Green Biotite	8	-	2	-	-	1
Brown Biotite	3	-	11	3	3	3
Chlorite	-	-	tr	tr	-	-
Epidote Group	13	20	5	8	19	13
Clear epidote	10	5	3	3	9	8
Green epidote	3	13	-	-	3	-
Zoisite	tr	2	2	3	5	5
Clinozoisite	-	-	-	2	2	-
Garnet	-	5	7	3	10	9
Clear	-	2	7	1	-	3
Pink	-	3	-	2	5	6
Red	-	-	-	-	5	-
Tourmaline	2	5	2	5	tr	3
Elbaite	1	3	1	5	tr	-
Schorlite	1	2	1	-	-	3
Apatite	2	-	tr	tr	2	-
Kyanite	-	-	-	-	-	-
Monazite	-	1	3	1	-	tr
Rutile	1	tr	tr	2	-	1
Sillimanite	-	-	-	-	-	-
Sphene	-	-	-	-	-	-
Staurolite	tr	-	-	-	-	-
Zircon	4	7	3	1	1	10
Opaque grains (leucoxine, magnetite, hematite, limonite, and ilmenite as % total of sample)	15	45	40	35	18	32

APPENDIX VII (continued)

	Sutton Creek member of the Nye Mudstone			Angora Peak member of the Astoria Formation				
Sample Number	CL-56	CL-80	52-88	CL-73	CL-74	CL-84	M-116	64-88
Non-opaque grains (=100%)								
Amphibole	60	66	59	75	55	57	59	75
Hornblende	60	66	56	73	55	56	59	75
Green	36	42	25	34	33	36	34	30
Blue-green	18	16	20	18	9	11	19	22
Brown	6	8	11	16	5	9	6	18
Basaltic	-	tr	-	4	8	tr	tr	5
Tremolite-Actinolite	-	tr	3	2	-	tr	tr	tr
Glaucophane	-	-	-	-	tr	1	-	-
Orthopyroxene	6	4	3	1	4	9	4	8
Hypersthene	4	4	-	-	4	-	1	7
Enstatite	2	tr	3	1	-	9	3	1
Clinopyroxine	1	tr	4	-	3	2	1	tr
Diopside	-	-	1	-	-	-	-	-
Augite	1	tr	3	-	3	2	1	tr
Micas	1	tr	2	tr	7	2	tr	3
Green Biotite	-	tr	-	-	3	tr	-	-
Brown Biotite	1	tr	2	tr	4	2	tr	3
Chlorite	-	tr	-	tr	-	-		-
Epidote Group	16	23	15	23	27	25	29	11
Clear epidote	6	9	6	9	7	4	7	3
Green epidote	5	10	4	7	7	8	9	2
Zoisite	-	tr	-	2	4	4	5	tr
Clinozoisite	5	4	5	5	9	9	8	6
Garnet	2	2	3	2	1	1	1	2
Clear	1	1	2	1	1	1	1	1
Pink	-	1	-	1	-	-	-	1
Red	1	-	1	tr	-	-	tr	tr
Tourmaline	1	1	1	tr	3	2	1	tr
Elbaite	1	-	-	tr	2	1	tr	tr
Schorlite	tr	1	1	tr	1	1	1	tr
Apatite	tr	-	-	-	tr	-	-	-
Kyanite	1	1	1	-	-	tr	tr	1
Monazite	tr	tr	tr	-	-	-	tr	-
Rutile	-	tr	-	tr	tr	-	tr	tr
Sillimanite	-	-	-	-	-	tr	-	-
Sphene	-	-	-	-	-	-	-	-
Staurolite	tr	-	tr	-	tr	-	-	-
Zircon	2	3	2	tr	tr	tr	5	tr
Opaque grains (leucoxine, magnetite, hematite, limonite, and ilmenite as % total of sample)	18	30	33	55	27	15	23	37

APPENDIX VII (continued)

	Netarts Bay member of the Astoria Formation		
Sample Number	NNB-11	NNB-29	35-88
Non-opaque grains (=100%)			
Amphibole	2	tr	tr
Hornblende	2	tr	-
Green	2	tr	-
Blue-green	-	-	-
Brown	-	-	-
Basaltic	-	tr	-
Tremolite-Actinolite	-	-	-
Glaucophane	tr	-	-
Orthopyroxene	2	-	-
Hypersthene	2	-	-
Enstatite	-	-	-
Clinopyroxine	-	-	-
Diopside	-	-	-
Augite	-	-	-
Micas	15	24	52
Green Biotite	tr	8	25
Brown Biotite	15	16	27
Chlorite	-	tr	-
Epidote Group	29	22	26
Clear epidote	7	-	-
Green epidote	13	12	12
Zoisite	tr	tr	-
Clinozoisite	9	10	14
Garnet	14	16	12
Clear	14	4	12
Pink	-	12	-
Red	-	-	-
Tourmaline	11	4	1
Elbaite	6	3	1
Schorlite	5	1	tr
Apatite	-	-	-
Kyanite	tr	4	-
Monazite	tr	-	-
Rutile	tr	tr	-
Sillimanite	-	-	-
Sphene	-	-	-
Staurolite	-	-	-
Zircon	27	30	9
Opaque grains (leucoxine, magnetite, hematite, limonite, and ilmenite as % total of sample)	45	75	23

APPENDIX VII (continued)

	Grande Ronde Basalt Sandstone Interbed	Cannon Beach member of the Astoria Formation			
Sample Number	17-88	NNB-112	0-18	0-302	46-88
Non-opaque grains (=100%)					
Amphibole	63	7	6	-	tr
Hornblende	62	7	6	-	tr
Green	39	7	6	-	-
Blue-green	19	-	-	-	-
Brown	4	-	tr	-	-
Basaltic	tr	-	-	-	-
Tremolite-Actinolite	1	-	tr	-	-
Glaucophane	-	-	tr	-	-
Orthopyroxene	3	tr	2	3	-
Hypersthene	3	-	-	3	-
Enstatite	-	tr	2	tr	-
Clinopyroxine	-	-	-	-	-
Diopside	-	-	-	-	-
Augite	-	-	-	-	-
Micas	2	4	10	27	28
Green Biotite	2	2	4	15	11
Brown Biotite	tr	2	6	12	17
Chlorite	-	-	tr	tr	-
Epidote Group	22	23	37	31	24
Clear epidote	5	5	7	16	2
Green epidote	12	18	12	9	14
Zoisite	tr	-	3	-	tr
Clinozoisite	5	tr	15	6	8
Garnet	4	44	25	30	22
Clear	4	22	15	9	14
Pink	-	-	7	18	8
Red	-	22	3	3	-
Tourmaline	3	tr	4	tr	5
Elbaite	3	tr	2	-	-
Schorlite	-	tr	2	tr	5
Apatite	-	-	-	-	tr
Kyanite	-	tr	2	tr	6
Monazite	-	-	-	tr	-
Rutile	-	1	tr	tr	3
Sillimanite	-	-	-	-	-
Sphene	-	-	-	-	-
Staurolite	-	-	-	-	tr
Zircon	3	22	14	9	12
Opaque grains (leucoxine, magnetite, hematite, limonite, and ilmenite as % total of sample)	20	55	48	67	62

APPENDIX VII (continued)

Sample Number	Sandstone of Whale Cove CL-87	CM-91	O-108	O-109
Non-opaque grains (=100%)				
Amphibole	31	48	66	18
Hornblende	27	48	64	14
Green	27	41	57	13
Blue-green	-	7	6	1
Brown	-	tr	1	-
Basaltic	-	-	tr	-
Tremolite-Actinolite	4	-	2	4
Glaucophane	tr	-	-	-
Orthopyroxene	5	7	2	-
Hypersthene	-	-	-	-
Enstatite	5	7	2	-
Clinopyroxine	-	4	1	-
Diopside	-	-	-	-
Augite	-	4	1	-
Micas	24	4	1	-
Brown Biotite	23	4	1	-
Green Biotite	1	-	-	-
Chlorite	tr	-	-	-
Epidote Group	27	33	24	63
Clear epidote	20	14	5	19
Green epidote	-	10	15	38
Zoisite	-	4	1	-
Clinozoisite	7	5	3	6
Garnet	2	-	1	1
Clear	2	-	1	1
Pink	-	-	-	-
Red	-	-	-	-
Tourmaline	7	2	1	2
Elbaite	-	-	-	2
Schorlite	7	2	1	-
Apatite	-	tr	-	-
Kyanite	4	tr	1	4
Monazite	-	-	-	-
Rutile	-	-	tr	tr
Sillimanite	-	-	tr	-
Sphene	-	-	-	-
Staurolite	-	-	tr	-
Zircon	1	2	3	12
Opaque grains (leucoxine, magnetite, hematite, limonite, and ilmenite as % total of sample)	25	32	15	20

APPENDIX IIX

Source Rock Analyses

ROCK EVAL PYROLYSIS

EPR NO.	DEPTH (FT.) Sample #	GRP SORC	ANAL DATE YYMMDD	ANAL METH	S1 (MG/GRM)	S2 (MG/GRM)	S3 (MG/GRM)	HYDROGEN INDEX	OXYGEN INDEX	TRANSF. RATIO	TEMP. (CENT.)	TOC (PCT) R-E	COMMENTS
110902	NNB-64 1	GJRM	890222	REV3	.07	.84	1.14	62	84	.08	424	1.35	INSTRUMENT #1 (LECO)
110913	36-88	GJRM	890222	REV3	.01	.36	.38	39	41	.03	427	.91	INSTRUMENT #1 (LECO)
110924	CL-48	GJRM	890222	REV3	.03	.11	.71	25	161	.21	443	.44	INSTRUMENT #1 (LECO)
110935	51-88	GJRM	890222	REV3	.05	.54	1.01	40	74	.09	424	1.35	INSTRUMENT #1 (LECO)
110946	60-88	GJRM	890222	REV3	.04	.61	1.40	51	118	.06	425	1.18	INSTRUMENT #1 (LECO)
110957	63-88	GJRM	890222	REV3	.06	.99	.67	116	78	.06	424	.85	INSTRUMENT #1 (LECO)
110968	65-88	GJRM	890222	REV3	.02	.58	.14	68	16	.03	422	.85	INSTRUMENT #1 (LECO)
110979	M-117	GJRM	890222	REV3	.02	.35	.67	27	52	.06	414	1.28	INSTRUMENT #1 (LECO)
110990	CL-144	GJRM	890222	REV3	.04	.44	.47	45	48	.08	408	.97	INSTRUMENT #1 (LECO)
111001	CL-145	GJRM	890222	REV3	.02	.41	.67	32	52	.05	419	1.27	INSTRUMENT #1 (LECO)

Data Provided by Exxon Research Labs

APPENDIX IIX (continued)

VITRINITE SUMMARY

SAMPLE FILE NAME	DEPTH/SAMPLE NUMBER	NO. OF OBSERVATIONS	MIN. %Ro.	MAX. %Ro.	AVG. %Ro.	STD. DEV.
E-765-01	110902	75	0.34	0.62	0.45	0.06
	POPULATION NO. 1	75	0.34	0.62	0.45	0.06 +
E-765-02	110913	75	0.37	0.62	0.48	0.05
	POPULATION NO. 1	75	0.37	0.62	0.48	0.05 +
E-765-10	110924	20	0.49	1.97	0.96	0.33
	POPULATION NO. 1	4	0.49	0.60	0.55	0.05 +
	POPULATION NO. 2	11	0.74	1.06	0.93	0.10
	POPULATION NO. 3	4	1.18	1.24	1.22	0.03
	POPULATION NO. 4	1	1.97	1.97	1.97	0.00
E-765-03	110935	75	0.33	0.64	0.43	0.05
	POPULATION NO. 1	75	0.33	0.64	0.43	0.05 +
E-765-04	110946	75	0.35	0.63	0.46	0.06
	POPULATION NO. 1	75	0.35	0.63	0.46	0.06 +
E-765-05	110957	38	0.30	1.46	0.63	0.33
	POPULATION NO. 1	22	0.30	0.49	0.38	0.06 +
	POPULATION NO. 2	11	0.70	1.01	0.84	0.09
	POPULATION NO. 3	5	1.12	1.46	1.25	0.14
E-765-06	110968	35	0.33	1.81	0.56	0.31
	POPULATION NO. 1	27	0.33	0.53	0.42	0.05 +
	POPULATION NO. 2	4	0.62	0.77	0.67	0.07
	POPULATION NO. 3	3	1.14	1.21	1.17	0.04
	POPULATION NO. 4	1	1.81	1.81	1.81	0.00
E-765-07	110979	75	0.36	1.17	0.49	0.13
	POPULATION NO. 1	72	0.36	0.59	0.47	0.05 +
	POPULATION NO. 2	1	0.70	0.70	0.70	0.00
	POPULATION NO. 3	2	1.15	1.17	1.16	0.01
E-765-08	110990	80	0.32	0.96	0.41	0.08
	POPULATION NO. 1	79	0.32	0.60	0.41	0.05 +
	POPULATION NO. 2	1	0.96	0.96	0.96	0.00
E-765-09	111001	75	0.35	0.62	0.46	0.06
	POPULATION NO. 1	75	0.35	0.62	0.46	0.06 +

APPENDIX IX

Major and Minor Element Geochemistry of Selected Igneous Rock Samples

APPENDIX IX-A
Major and Minor Element Geochemistry of Samples Collected During this study

Run 1189, Mike J. Parker, OSU

	MJP K1	MJP 488	MJP 588	MJP 3088	MJP 3288A	MJP 4388	MJP 4488	MJP 7188	MJP 7289	MJP 7289B
Date	30JL89	30JL89	01AG89	01AG89	01AG89	01AG89	31JL89	30JL89	31JL89	01AG89
UNNORMALIZED RESULTS (WEIGHT %):										
SIO2	57.94	56.73	57.40	55.86	55.63	56.56	58.65	57.15	56.26	56.37
AL2O3	14.42	13.79	14.25	14.40	14.36	13.48	14.57	14.75	14.15	13.34
TIO2	1.868	2.077	2.142	1.882	1.799	2.124	2.141	1.998	1.818	2.079
FEO*	11.15	12.26	10.34	10.60	10.82	12.26	9.90	10.51	10.72	12.01
MNO	0.204	0.285	0.174	0.183	0.187	0.184	0.186	0.182	0.225	0.209
CAO	7.40	7.22	6.78	8.43	8.35	6.85	6.81	8.20	7.73	7.16
MGO	4.00	3.82	3.08	4.57	4.45	3.28	3.30	4.21	4.37	3.40
K2O	1.00	1.46	1.67	0.83	0.83	1.62	1.65	0.86	1.22	1.32
NA2O	3.08	3.19	3.56	3.50	3.53	3.42	3.45	3.29	3.31	3.53
P2O5	0.315	0.371	0.363	0.259	0.250	0.368	0.360	0.294	0.319	0.365
TOTAL	101.38	101.20	99.76	100.51	100.21	100.15	101.02	101.44	100.12	99.78
NORMALIZED RESULTS (WEIGHT %):										
SIO2	57.15	56.06	57.54	55.57	55.52	56.48	58.06	56.34	56.19	56.49
AL2O3	14.22	13.63	14.28	14.33	14.33	13.46	14.42	14.54	14.13	13.37
TIO2	1.843	2.052	2.147	1.872	1.795	2.121	2.119	1.970	1.816	2.084
FEO*	11.00	12.11	10.36	10.55	10.80	12.24	9.80	10.36	10.71	12.04
MNO	0.201	0.282	0.174	0.182	0.187	0.184	0.184	0.179	0.225	0.209
CAO	7.30	7.13	6.80	8.39	8.33	6.84	6.74	8.08	7.72	7.18
MGO	3.95	3.77	3.09	4.55	4.44	3.28	3.27	4.15	4.36	3.41
K2O	0.99	1.44	1.67	0.83	0.83	1.62	1.63	0.85	1.22	1.32
NA2O	3.04	3.15	3.57	3.48	3.52	3.42	3.42	3.24	3.31	3.54
P2O5	0.311	0.367	0.364	0.258	0.249	0.367	0.356	0.290	0.319	0.366
TRACE ELEMENTS (PPM):										
NI	7	2	1	10	10	0	3	0	8	0
CR	16	16	11	21	19	18	10	9	16	14
SC	32	32	36	35	33	35	40	33	33	36
V	314	352	350	319	311	351	351	338	300	348
BA	662	613	632	456	419	619	626	438	539	597
RB	33	44	48	34	34	46	45	31	37	49
SR	316	315	324	344	344	309	320	355	317	314
ZR	165	174	183	162	157	178	181	165	159	175
Y	35	40	43	35	31	39	41	32	33	39
NB	12.5	13.8	13.3	11.9	11.2	16.1	16.2	12.5	12.1	14.0
GA	20	23	24	23	25	22	24	20	20	22
CU	8	0	0	19	20	0	5	10	6	0
ZN	114	125	133	106	102	123	127	108	108	123
PB	10	10	10	7	11	16	10	9	11	11
LA	19	17	23	17	13	16	6	1	15	14
CE	47	53	50	44	29	55	51	26	60	40
TH	3	6	6	4	4	6	5	2	5	7

Total Fe is expressed as FeO;
Major elements are normalized on a volatile-free basis.

APPENDIX IX-A (continued)

Run 1189, Mike J. Parker, OSU

	MJP 7389	MJP 7489	MJP 7589	MJP 8089A	MJP 8089B	MJP 8089C	MJP 8089E	MJP-CL 76A	MJP CL 152	MJP CL 159
Date	30JL89	30JL89	30JL89	01AG89	30JL89	31JL89	01AG89	02AG89	31JL89	31JL89
	UNNORMALIZED RESULTS (WEIGHT %):									UNNORMAI
SIO2	58.30	56.24	58.14	76.21	54.20	56.65	45.72	56.62	56.51	58.27
AL2O3	14.14	14.31	14.35	13.95	20.36	20.09	21.40	13.76	14.59	14.37
TIO2	2.092	2.018	2.151	0.097	4.030	2.638	0.742	2.102	1.854	2.125
FEO*	11.03	10.92	10.73	0.48	5.62	5.81	11.00	11.40	10.48	11.12
MNO	0.211	0.190	0.186	0.008	0.104	0.064	0.209	0.211	0.189	0.199
CAO	7.16	8.08	6.81	1.09	5.56	5.37	11.97	7.26	8.35	6.91
MGO	3.63	4.19	3.71	0.00	2.08	0.84	6.28	3.52	4.53	3.60
K2O	1.23	0.94	1.62	5.12	2.52	2.62	0.20	1.52	1.00	1.63
NA2O	3.33	3.35	3.13	3.52	4.30	6.00	1.76	3.30	3.21	3.18
P2O5	0.384	0.284	0.365	0.037	0.736	1.190	0.163	0.363	0.260	0.368
TOTAL	101.51	100.52	101.19	100.51	99.51	101.27	99.44	100.06	100.97	101.77
	NORMALIZED RESULTS (WEIGHT %):									NORMALI:
SIO2	57.43	55.95	57.46	75.82	54.47	55.94	45.98	56.59	55.97	57.26
AL2O3	13.93	14.24	14.18	13.88	20.46	19.84	21.52	13.75	14.45	14.12
TIO2	2.061	2.008	2.126	0.097	4.050	2.605	0.746	2.101	1.836	2.088
FEO*	10.87	10.86	10.60	0.48	5.65	5.74	11.06	11.39	10.38	10.93
MNO	0.208	0.189	0.184	0.008	0.105	0.063	0.210	0.211	0.187	0.196
CAO	7.05	8.04	6.73	1.08	5.59	5.30	12.04	7.26	8.27	6.79
MGO	3.58	4.17	3.67	0.00	2.09	0.83	6.32	3.52	4.49	3.54
K2O	1.21	0.94	1.60	5.09	2.53	2.59	0.20	1.52	0.99	1.60
NA2O	3.28	3.33	3.09	3.50	4.32	5.92	1.77	3.30	3.18	3.12
P2O5	0.378	0.283	0.361	0.037	0.740	1.175	0.164	0.363	0.257	0.362
	TRACE ELEMENTS (PPM):									
NI	1	10	1	10	34	9	7	0	7	3
CR	10	12	13	0	147	0	19	16	20	11
SC	33	34	33	1	26	8	39	35	35	37
V	349	320	364	0	331	115	338	349	319	366
BA	620	450	604	729	517	803	119	592	417	622
RB	50	32	44	142	58	57	4	45	32	45
SR	317	352	300	276	720	972	532	309	342	302
ZR	177	165	172	52	307	419	43	173	159	173
Y	43	34	38	6	63	71	16	38	33	38
NB	15.1	12.0	14.6	6.2	83.3	119.0	2.0	15.7	11.2	15.1
GA	24	24	20	14	24	24	19	22	20	25
CU	0	16	0	3	33	0	129	0	20	0
ZN	127	112	128	12	142	139	76	121	109	127
PB	11	7	6	46	6	9	1	10	8	10
LA	27	27	23	9	62	100	6	18	11	14
CE	62	52	51	25	118	190	12	51	42	60
TH	5	3	5	3	9	10	0	5	5	5

Total Fe is expressed as FeO;
Major elements are normalized on a volatile-free basis.

APPENDIX IX-A (continued)

	MJPONG 4580	MJP CFW	MJPSNB 132	MJPSNB 151	MJPSNB 156	MJPSNB 161	MJPSNB 162
Date	01AG89	31JL89	31JL89	31JL89	31JL89	02AG89	01AG89
LIZED RESULTS (WEIGHT %):							
SIO2	49.26	52.52	57.24	56.64	57.16	56.72	53.22
AL2O3	15.04	13.46	13.82	14.76	14.24	13.94	13.76
TIO2	3.426	3.123	2.092	1.864	2.028	2.153	3.130
FEO*	10.84	13.00	11.63	10.19	11.39	11.68	14.08
MNO	0.197	0.239	0.221	0.181	0.203	0.185	0.241
CAO	10.74	8.30	7.30	8.30	7.44	7.08	8.29
MGO	4.65	4.17	3.61	4.69	3.98	3.30	4.03
K2O	0.81	0.94	1.33	1.10	1.43	1.51	1.27
NA2O	3.28	2.85	3.33	3.21	3.12	3.39	2.69
P2O5	0.442	0.679	0.365	0.261	0.319	0.368	0.629
TOTAL	98.68	99.28	100.94	101.20	101.31	100.33	101.34
ED RESULTS (WEIGHT %):							
SIO2	49.92	52.90	56.71	55.97	56.42	56.54	52.52
AL2O3	15.24	13.56	13.69	14.59	14.06	13.89	13.58
TIO2	3.472	3.146	2.073	1.842	2.002	2.146	3.089
FEO*	10.98	13.09	11.52	10.07	11.24	11.64	13.89
MNO	0.200	0.241	0.219	0.179	0.200	0.184	0.238
CAO	10.88	8.36	7.23	8.20	7.34	7.06	8.18
MGO	4.71	4.20	3.58	4.63	3.93	3.29	3.98
K2O	0.82	0.95	1.32	1.09	1.41	1.51	1.25
NA2O	3.32	2.87	3.30	3.17	3.08	3.38	2.65
P2O5	0.448	0.684	0.362	0.258	0.315	0.367	0.621
TRACE ELEMENTS (PPM):							
NI	57	8	0	7	0	3	10
CR	96	15	15	18	15	13	21
SC	33	39	31	37	39	38	38
V	328	393	359	322	365	377	424
BA	236	541	557	436	552	638	543
RB	13	30	51	32	39	40	32
SR	450	326	311	336	302	321	312
ZR	223	173	172	155	165	179	173
Y	33	41	38	33	38	42	44
NB	41.2	14.0	13.8	12.8	14.1	15.8	16.1
GA	25	20	22	21	21	23	20
CU	48	10	1	18	0	1	12
ZN	12ϐ	155	122	105	127	125	139
PB	3	8	9	12	9	10	8
LA	24	15	27	2	19	25	30
CE	67	49	50	43	46	58	64
TH	4	5	2	6	3	8	5

Total Fe is expressed as FeO;
Major elements are normalized on a volatile-free basis.

APPENDIX IX-A (continued)

	MJPSNB 162	MJPSNB 162R
Date	01AG89	01AG89
UNNORMALIZED RESULTS (WEIGHT %):		
SIO2	53.22	52.33
AL2O3	13.76	13.48
TIO2	3.130	3.112
FEO*	14.08	14.46
MNO	0.241	0.237
CAO	8.29	8.22
MGO	4.03	3.84
K2O	1.27	1.27
NA2O	2.69	2.82
P2O5	0.629	0.629
TOTAL	101.34	100.40
NORMALIZED RESULTS (WEIGHT %):		
SIO2	52.52	52.12
AL2O3	13.58	13.43
TIO2	3.089	3.100
FEO*	13.89	14.40
MNO	0.238	0.236
CAO	8.18	8.19
MGO	3.98	3.82
K2O	1.25	1.26
NA2O	2.65	2.81
P2O5	0.621	0.627
TRACE ELEMENTS (PPM):		
NI	10	5
CR	21	21
SC	38	39
V	424	435
BA	543	552
RB	32	35
SR	312	314
ZR	173	177
Y	44	45
NB	16.1	16.3
GA	20	23
CU	12	11
ZN	139	144
PB	8	7
LA	30	27
CE	64	49
TH	5	6

Total Fe is expressed as FeO;
Major elements are normalized on a volatile-free basis.

APPENDIX IX (continued)

APPENDIX IX-B

Geochemical Data of Samples Run on the Washington State University, Pullman, Rugaku X-Ray Fluorescence Machine Normalized to the Older Phillips XRF Machine Using Values Listed in Table 1

SAMPLE	73.89	74.89	75.89	80.89a	80.89b	80.89c	80.89e	CL-76a	CL-152	CL-159
SIO2	56.57	55.29	56.6	72.38	54.02	55.29	46.92	55.85	55.31	56.42
AI203	14.9	15.11	15.07	14.86	19.34	18.92	20.06	14.78	15.25	15.03
TIO2	2.16	2.11	2.22	.359	3.99	2.66	.95	2.2	1.95	2.19
FeO	10.96	10.95	10.71	1.2	6.06	6.14	11.14	11.45	10.5	11.02
MNO	.21	.197	.194	.066	.136	.106	.213	.214	.196	.203
CAO	7.09	7.99	6.8	1.66	5.76	5.5	11.63	7.25	8.2	6.85
MGO	3.78	4.32	3.87	.53	2.43	1.28	6.28	3.73	4.61	3.75
K20	1.16	.91	1.53	4.77	2.39	2.44	.226	1.45	.96	1.53
Na20	2.53	2.54	2.47	2.59	2.83	3.29	2.09	2.53	2.5	2.48
P205	.35	.276	.3388	.0796	.642	.99	.181	.34	.255	.339

SAMPLE	ONG-4580	CFW	SNB-132	SNB-151	SNB-156	SNB-161	SNB-162	SNB-162	SNB-162R
SIO2	50.11	52.67	55.95	55.31	55.7	55.6	52.34	52.34	52.01
AL203	15.79	14.65	14.73	14.35	14.99	14.87	14.66	14.66	14.56
TIO2	3.46	3.15	2.17	1.96	2.11	2.23	3.1	3.11	3.12
FEO	11.07	13.05	11.57	10.21	11.31	11.69	13.8	13.8	14.26
MNO	.203	.235	10.22	.19	.206	.194	.233	.233	.232
CAO	10.58	8.28	7.25	8.14	7.35	7.1	8.12	8.12	8.13
MGO	4.81	4.35	3.79	4.74	4.11	3.52	4.15	4.15	4.01
K20	.81	.92	1.26	1.05	1.35	1.44	1.2	1.2	1.21
NA20	2.54	2.41	2.53	2.49	2.47	2.56	2.34	2.35	2.39
P205	.408	.597	.339	.256	.302	.343	.547	.547	.551

SAMPLE	K1	4.88	5.88	30.88	32.88A	43.88	44.88	71.88	72.89	72.89B
SIO2	56.32	55.39	56.66	54.97	54.92	55.75	57.11	55.63	55.5	55.76
AL203	15.09	14.7	15.14	15.17	15.17	14.58	15.23	15.31	15.03	14.52
TIO2	1.96	2.16	2.24	1.99	1.92	2.22	2.21	2.08	1.94	2.18
FEO	11.09	12.13	10.48	10.66	10.9	12.25	9.96	10.48	10.81	12.06
MNO	.206	.265	.187	.193	.196	.194	.194	.19	.224	.213
CAO	7.32	7.16	6.87	8.31	8.26	6.9	6.81	8.03	7.7	7.21
MGO	4.12	3.96	3.34	4.67	4.57	3.51	3.5	4.3	4.49	3.63
K20	.96	1.39	1.59	.811	.811	1.54	1.55	.83	1.17	1.26
NA20	2.46	2.49	2.62	2.58	2.6	2.57	2.57	2.52	2.53	2.6
P205	.298	.343	.341	.278	.249	.343	.3348	.282	.305	.343

APPENDIX IX (continued)

APPENDIX IX-C

Geochemical Analyses of Basalt Sampled from the Tillamook Embayment by P.D Snavely Jr., and R. Wells of the U.S. Geological Survey

Geochemical Data (recalculated water-free) from Snavely et at., 1973

Sample #	MR69-148	MR69-147	MR69-145	SR61-20	MR68-33	MR69-144	MR68-31
SiO_2	54.8	55.1	55.7	55.8	55.9	56.1	56.2
Al_2O_3	14.7	14.7	14.3	14.3	13.9	13.8	13.6
Fe_2O_3	2.2	2.2	2.5	2.8	1.9	1.7	2.2
FeO	9.2	8.7	8.9	9.8	10.4	10.5	9.5
MgO	4.3	4.6	4.1	3.3	3.6	3.5	3.8
CaO	7.8	8.2	7.5	6.8	7.2	7.0	7.7
Na_2O	3.6	3.4	3.5	3.2	3.2	3.6	3.0
K_2O	0.84	0.88	1.1	1.6	1.3	1.1	1.5
TiO_2	2.0	1.8	1.8	2.0	2.0	2.0	2.1
P_2O_5	0.32	0.28	0.30	0.40	0.42	0.40	0.35
MnO	0.26	0.21	0.22	0.20	0.17	0.24	0.17

Sample #	SR62-64	STIL62-1A	SR61-22	SR61-22
SiO_2	56.2	56.3	56.8	56.9
Al_2O_3	13.9	14.2	14.3	14.6
Fe_2O_3	4.0	2.7	2.1	1.6
FeO	8.9	9.4	9.4	9.8
MgO	3.1	3.4	3.5	3.5
CaO	6.5	6.7	6.8	6.8
Na_2O	3.3	3.4	3.3	3.3
K_2O	1.5	1.4	1.4	1.4
TiO_2	2.0	1.9	1.8	1.9
P_2O_5	0.38	0.37	0.37	0.39
MnO	0.18	0.18	0.19	0.20

Unpublished Geochemical Data Furnished by R. Wells of the USGS

Sample #	W83-80	W83-81	W83-82	W83-83	W83-84
SiO_2	53.7	55.3	55.3	54.6	54.5
Al_2O_3	13.9	13.4	13.5	13.1	13.0
Fe_2O_3	12.1	13.0	12.9	13.6	13.6
FeO					
MgO	4.44	3.51	3.61	3.44	3.31
CaO	8.15	6.85	7.19	7.10	7.09
Na_2O	3.19	3.05	3.13	3.00	3.12
K_2O	0.77	1.67	1.46	1.41	1.56
TiO_2	1.87	1.98	1.93	2.05	2.10
P_2O_5	0.27	0.33	0.33	0.37	0.37
MnO	0.18	0.19	0.19	0.21	0.24

APPENDIX X

Basalt Magnetic Polarities

SITE NUMBER	GEOCHEMICAL TYPE	UNIT NAME	POLARITY: NORM/REV
CFW	Frenchman Sp.	Ginkgo	N weak
SNB-162	Frenchman Sp.	Ginkgo	float
4-88	Low Mg Low Ti	Grouse Creek	R
7-88		Grouse Creek	R
85-89		Grouse Creek	R
83-89		Grouse Creek	R
CL-152	High Mg	Sentinal Bluff	R weak
MR69-145	High Mg	Sentinal Bluff	
30-88	High Mg	Sentinel Bluff	N
32-88A	High Mg	Sentinel Bluff	N
71-88	High Mg	Sentinel Bluff	R
72-89	High Mg	Sentinel Bluff	N
74-89	High Mg	Sentinel Bluff	N weak
MR69-147	High Mg	Sentinel Bluff	
MR69-148	High Mg	Sentinel Bluff	
SNB-151	High Mg	Sentinel Bluff	N weak
W83-80	High Mg	Sentinel Bluff	N
17-88A		Sentinal Bluff	N
CL-75		Sentinel Bluff	N
12-88		Sentinel Bluff	N
16-88		Sentinel Bluff	N
32-88		Sentinel Bluff	N
5-88	Low Mg Low Ti	Winterwater	N
43-88	Low Mg Low Ti	Winterwater	N
44-88	Low Mg Low Ti	Winterwater	N
72-89B	Low Mg Low Ti	Winterwater	N
73-89	Low Mg Low Ti	Winterwater	N
75-89	Low Mg Low Ti	Winterwater	N weak
CL-159	Low Mg Low Ti	Winterwater	N
CL-76A	Low Mg Low Ti	Winterwater	N
K-1	Low Mg Low Ti	Winterwater	N
MR68-31	Low Mg Low Ti	Winterwater	
MR69-144	Low Mg Low Ti	Winterwater	
SNB-132	Low Mg Low Ti	Winterwater	N
SNB-156	Low Mg Low Ti	Winterwater	N
SNB-161	Low Mg Low Ti	Winterwater	N
SR61-20	Low Mg Low Ti	Winterwater	
SR61-21	Low Mg Low Ti	Winterwater	
SR61-22	Low Mg Low Ti	Winterwater	
SR62-64	Low Mg Low Ti	Winterwater	
STIL62-1A	Low Mg Low Ti	Winterwater	
W83-81	Low Mg Low Ti	Winterwater	N
W83-82	Low Mg Low Ti	Winterwater	N
W83-83	Low Mg Low Ti	Winterwater	
W83-84	Low Mg Low Ti	Winterwater	
CL-137		Winterwater	N
70-88		Winterwater	N
CL-130		Winterwater	N
CL-126		Winterwater	N
67-88		Winterwater	N
CL-77		Winterwater	R
CL-158		Winterwater	N
CL-57		Winterwater	N
CL-125		Winterwater	N
CL-76A		Winterwater	N
CL-135		Winterwater	N
CL-71		Winterwater	N
SNB-122		Winterwater	N
CL-134		Winterwater	N
CL-127		Winterwater	N
CL-136		Winterwater	N
CL-138		Winterwater	N
CL-154		Winterwater	R
CL-157		Winterwater	N
CL-71		Winterwater	N
CL-123		Winterwater	N
CL-133		Winterwater	N
68-88		Winterwater	N
33-88		Winterwater	N
0-26		Winterwater	N
6-88		Winterwater	N
72-89D		Winterwater	N
72-89E		Winterwater	N

APPENDIX X (continued)

Paleomagnetic Data of Wells et al. (In press)

Unit local name	flow no. (this paper)	Site	Lat.	Long.	d/s	Treat.	n/nt	k	a_{95}	Ic	Dc
GRANDE RONDE BASALT											
High MgO N2											
Short Beach-Cape Meares*	C018	SS132	45.47	236.03	11/190	200	8/8	86	6.0	80.3	14.0
Short Beach-Cape Meares*	C017	SS151	45.47	236.03	11/190	200	8/8	35	9.5	69.0	26.8
Cannon Beach**	C016	SR7	45.96	236.07	15/180	300	6/7	63	8.5	50.8	11.2
Low MgO N2											
flows of Winterwater?											
Cape Lookout	C015	DB3	45.36	236.03	9/205	-	6	31	12.2	22.7	356.8
Cape Lookout	C014	DB4	45.35	236.03	9/205	-	6	134	5.8	21.1	344.0
Cape Lookout	C013	DB5	45.35	236.03	9/205	-	6	144	5.6	13.9	345.4
Cape Lookout	C012	DB6	45.35	236.03	9/205	-	5	48	11.2	30.5	336.6
Depoe Bay	C011	DB8	44.80	235.94	16/180	-	6	111	6.4	22.5	354.4
N. Cape Lookout	C010	SS125	45.38	236.05	15/160	200	6/6	174	5.1	30.5	344.1
normal direction											
Cape Falcon Sill*	C09	SR8	45.77	236.06	15/180	400	8/8	697	2.1	47.5	21.5
Mt. Hebo Sill*	C08	SR9	45.21	236.24	15/180	200	8/8	844	1.9	64.3	357.5
east direction											
Barth falls Quarry	C07	V033	46.06	236.32	15/180	100	8/8	18	13.6	85.0	86.5
Fishhawk Falls	C06	V001	45.96	236.50	15/180	300	8/8	199	3.9	80.0	155.2
Jencks Rd. Quarry**	C05	SR10	45.18	236.11	15/180	300	4/8	40	14.7	29.7	114.6
Siletz R. Quarry**	C04	SR11	44.88	236.00	15/180	300	7/8	220	4.1	62.3	132.0
Low MgO R2											
straight up direction											
Maxwell Pt.,	C03A	DB1	45.46	236.03	4/181	-	4	85	10.0	-80.4	274.6
Oceanside	C03	DB2	44.46	236.03	4/181	-	5	80	8.6	-80.7	245.0

APPENDIX XI

Checklist of Sample Localities

SITE	LOCATION
K-1	SE SW SEC. 13, T. 4 S., R. 11 W.
4-88	SE NW SEC. 28, T. 1 S., R. 10 W.
5-88	SE SW SEC. 21, T. 1 S., R. 10 W.
6-88	NW SW SEC. 21, T. 1 S., R. 10 W.
NNB-6A	SW NW SEC. 4, T. 2 S., R. 10 W.
7-88	NW NE SEC. 28, T. 1 S., R. 10 W.
NNB-10	SW SE SEC. 3, T. 2 S., R. 10 W.
NNB-11	NE SE SEC. 3, T. 2 S., R. 10 W.
NNB-11Z	SW SE SEC. 3, T. 2 S., R. 10 W.
NNB-12	NE NE SEC. 10, T. 2 S., R. 10 W.
12-88	SE NE SEC. 14, T. 1 S., R. 10 W.
16-88	NE NE SEC. 12, T. 1 S., R. 11 W.
17-88	SE SE SEC. 13, T. 1 S., R. 11 W.
17-88A	SE SE SEC. 13, T. 1 S., R. 11 W.
O-17	SE NE SEC. 34, T. 1 S., R. 10 W.
O-18	NW NE SEC. 33, T. 1 S., R. 10 W.
21-88	SW SE SEC. 1, T. 3 S., R. 11 W.
20-88	NW SW SEC. 1, T. 3 S., R. 11 W.
O-26	SE SW SEC. 19, T. 1 S., R. 10 W.
NNB-29	NW SE SEC. 2, T. 2 S., R. 10 W.
O-30Z	NW SE SEC. 34, T. 1 S., R. 10 W.
30-88	SE SE SEC. 24, T. 1 S., R. 11 W.
NNB-31	NW NE SEC. 1, T. 2 S., R. 10 W.
NNB-31A	NW NE SEC. 1, T. 2 S., R. 10 W.
32-88	SE SE SEC. 24, T. 1 S., R. 11 W.
32-88A	SE SE SEC. 24, T. 1 S., R. 11 W.
33-88	NW NE SEC. 30, T. 1 S., R. 10 W.
35-88	NE NW SEC. 1, T. 2 S., R. 9 W.
36-88	SE NW SEC. 18, T. 2 S., R. 10 W.
37-88	SW NW SEC. 10, T. 3 S., R. 10 W.
38-88	NW NW SEC. 10, T. 3 S., R. 10 W.
39-88	NE NE SEC. 9, T. 3 S., R. 10 W.
NNB-40Z	SW NW SEC. 11, T. 2 S., R. 10 W.
40-88	SW SW SEC. 3, T. 3 S., R. 10 W.
41-88	NE SW SEC. 3, T. 2 S., R. 10 W.
42-88	SW NE SEC. 28, T. 1 S., R. 10 W.
43-88	NE NE SEC. 29, T. 1 S., R. 10 W.
44-88	NW NW SEC. 29, T. 1 S., R. 10 W.
NNB-46	SW NW SEC. 7, T. 2 S., R. 9 W.
46-88	SW NW SEC. 17, T. 1 S., R. 10 W.
CL-48Z	SW SE SEC. 10, T. 3 S., R. 10 W.
CL-49	NE SW SEC. 9, T. 3 S., R. 10 W.
CL-50	SW SE SEC. 5, T. 3 S., R. 10 W.
CL-51	NW SW SEC. 4, T. 3 S., R. 10 W.
51-88	SW NW SEC. 17, T. 1 S., R. 10 W.
52-88	NE NW SEC. 8, T. 1 S., R. 10 W.
CL-53	SW NW SEC. 10, T. 3 S., R. 10 W.
53-88	SE NW SEC. 8, T. 1 S., R. 10 W.

APPENDIX XI (continued)

SITE	LOCATION
CL-55	NE SE SEC. 3.,T. 3 S., R. 10 W.
56-88	SE NE SEC. 16, T. 1 S., R. 10 W.
CL-56	SE NW SEC. 5, T. 3 S., R. 10 W.
CL-57	NW SW SEC. 6, T. 3 S., R. 10 W.
CL-59	NW SE SEC. 3, T. 3 S., R. 10 W.
60-88	NE NE SEC. 16, T. 2 S., R. 10 W.
63-88	SE SW SEC. 13, T. 4 S., R. 11 W.
64-88	SE SW SEC. 13, T. 4 S., R. 11 W.
65-88	SW SE SEC. 10, T. 3 S., R. 10 W.
CL-65	SE NW SEC. 3, T. 3 S., R. 10 W.
67-88	NE SE SEC. 36, T. 2 S., R. 11 W.
68-88	NE SE SEC. 36, T. 2 S., R. 11 W.
70-88	SW NE SEC. 1, T. 3 S., R. 10 W.
71-88	NW NW SEC. 18, T. 1 S., R. 10 W.
CL-71	SW NE SEC. 1, T. 3 S., R. 10 W.
72-89	Cape Lookout
72-89B	Cape Lookout
72-89D	Cape Lookout
72-89E	Cape Lookout
CL-73	NE SW SEC. 6, T. 3 S., R. 10 W.
73-89	Cape lookout
CL-74	NE SW SEC. 6, T. 3 S., R. 10 W.
74-89	NW NW SEC. 18, T. 1 S., R. 10 W.
CL-75	SE SW SEC. 6, T. 3 S., R. 10 W.
75-89	SW SE SEC. 17, T. 1 S., R. 10 W.
CL-76A	NE SE SEC. 6, T. 3 S., R. 10 W.
CL-77	NW SE SEC. 6, T. 3 S., R. 10 W.
80-89A	SE SW SEC. 13, T. 4 S., R. 11 W.
80-89B	SE SW SEC. 13, T. 4 S., R. 11 W.
80-89C	SE SW SEC. 13, T. 4 S., R. 11 W.
80-89E	SE SW SEC. 13, T. 4 S., R. 11 W.
CL-80	NE SW SEC. 33, T. 2 S., R. 10 W.
83-89	NE NE SEC. 24, T. 1 S., R. 10 W.
CL-84	NE SE SEC. 32, T. 2 S., R. 10 W.
CL-85	NE NE SEC. 31, T. 2 S., R. 10 W.
85-89	SE NW SEC. 31, T. 2 S., R. 10 W.
CL-87	NW NW SEC. 29, T. 2 S., R. 10 W.
CM-91	NW SE SEC. 20, T. 1 S., R. 10 W.
SNB-101	SW SW SEC. 25, T. 2 S., R. 10 W.
SNB-102	SW SW SEC. 23, T. 2 S., R. 10 W.
O-108	NW NE SEC. 30, T. 1 S., R. 10 W.
O-109	SE SE SEC. 19, T. 1 S., R. 10 W.
M-116	SE SE SEC. 8, T. 1 S., R. 10 W.
M-117	SE SE SEC. 17, T. 1 S., R. 10 W.
SNB-122	NE NW SEC. 31, T. 2 S., R. 10 W.
CL-125	SW SE SEC. 36, T. 2 S., R. 11 W.
CL-126	SE SW SEC. 36, T. 2 S., R. 11 W.
CL-127	SE NE SEC. 36, T. 2 S., R. 11 W.
CL-130	NW SE SEC. 36, T. 2 S., R. 11 W.
SNB-132	SW SE SEC. 19, T. 2 S., R. 11 W.

APPENDIX XI (continued)

SITE	LOCATION
CL-133	SW SW SEC. 32, T. 2 S., R. 10 W.
CL-134	SW NW SEC. 31, T. 2 S., R. 10 W.
CL-135	SE SE SEC. 36, T. 2 S., R. 11 W.
CL-136	NE NE SEC. 1, T. 3 S., R. 10 W.
CL-137	NE NE SEC. 1, T. 3 S., R. 10 W.
CL-138	SW NE SEC. 1, T. 3 S., R. 10 W.
CL-144	SE SE SEC. 33, T. 2 S., R. 10 W.
CL-145	SW NW SEC. 34, T. 2 S., R. 10 W.
K-148	SE SW SEC. 13, T. 4 S., R. 11 W.
SNB-151	NW SW SEC. 28, T. 2 S., R. 10 W.
CL-152	SE NE SEC. 29, T. 2 S., R. 10 W.
CL-154	SE SE SEC. 29, T. 2 S., R. 10 W.
SNB-156	NE NE SEC. 32, T. 2 S., R. 10 W.
CL-157	SW NE SEC. 32, T. 2 S., R. 10 W.
CL-158	NE SE SEC. 32, T. 2 S., R. 10 W.
CL-159	NW SW SEC. 32, T. 2 S., R. 10 W.
SNB-161	NE SE SEC. 19, T. 2 S., R. 10 W.
SNB-162	SW NW SEC. 29, T. 2 S., R. 10 W.
CFW	SE SE SEC. 19, T. 1 S., R. 10 W.